

UNIVERSITY OF
BIRMINGHAM

PARTICULATE MATTER CHARACTERIZATION AND CONTROL IN PREMIXED COMPRESSION IGNITION ENGINES

By

Yasser Al Qahtani

A thesis submitted to

The University of Birmingham

For the degree of

DOCTOR OF PHILISOPHY

The University of Birmingham

School of Engineering

January 2017

UNIVERSITY OF
BIRMINGHAM

University of Birmingham Research Archive

e-theses repository

This unpublished thesis/dissertation is copyright of the author and/or third parties. The intellectual property rights of the author or third parties in respect of this work are as defined by The Copyright Designs and Patents Act 1988 or as modified by any successor legislation.

Any use made of information contained in this thesis/dissertation must be in accordance with that legislation and must be properly acknowledged. Further distribution or reproduction in any format is prohibited without the permission of the copyright holder.

ABSTRACT

Diesel engines are broadly used as power units with high fuel efficiency. Conversely, they are considered as the main contributors to air pollutions as they emit high NO_x and particulate Matter (PM) emissions and thus have an adverse impact on the environment and human health. As more stringent regulations for emissions are introduced, low temperature combustion (LTC) strategy with high volatile fuels demonstrated the potential to reduce the PM, NO_x emissions by operating engines under a premixed compression ignition (PCI) condition.

This study presents the effect of dieseline fuel or G75 (75% by volume of gasoline blended with 25% by volume of diesel) and naphtha fuel on the particle size and number distribtuion and chemical characterization of PM emissions. The EGR cooler was deactivated for the case of G75 and naphtha fuels for the purpose of introducing hot EGR to increase the gas temperature that helps to oxidize soot also to help the fuel vaporization for better mixing. The investigations were carried out at diesel engine running on a PCI mode and at steady state.

The experimental results showed that the deactivation of the EGR cooler to introduce hot EGR for both fuels, G75 and naphtha, was proven as a good technique in significantly reducing the total particle number and mass concentrations by about 99% and the mean diameter to a smaller size ~ 10 nm. Advancing the injection timing and with the usage of a large amount of EGR of the G75 fuel significantly reduced the particle numbers' concentration. When the single injection was used, it was found that the total particle numbers' concentration and smoke of both fuels G75 and naphtha, reduced significantly by about 99%. G75 fuel produced the lowest emission of NO_x (0.27 g/kWh) compared to diesel

fuel at low and medium loads. Also, the total carbon (TC) was reduced by more than 54% for G75 and naphtha fuels compared to diesel fuel.

The double injection strategy was more flexible than the single injection. It reduced the total particle numbers' concentration and smoke by about 99.80%. At low and medium loads, G75 fuel produced the lowest emission of NO_x (0.22 g/kWh) compared to diesel and naphtha fuels. It is found that double injection of both G75 and naphtha fuels effectively reduced the total PAH compounds by more than 90% compared to single injected diesel engine. G75 fuel produced very low concentration of alkanes and cycloalkanes compared to diesel and naphtha fuels at both injection strategies. However, the single injection of G75 fuel is considered as the lowest producer of cycloalkanes compared to double injection.

This thesis is dedicated to my parents, brothers and sisters for their great support along the way

ACKNOWLEDGMENTS

Finally, the long journey to complete this research work is over. Despite the challenges, pain and restless nights, the journey has become thoroughly enjoyable and one of the major accomplishments that I will be proud of for the rest of my life. First and above all, I thank God, who granted me the strength and health to complete my research work successfully.

In deep gratitude and appreciation, I would like to thank my supervisor Professor Hongming Xu for offering me the great chance to do a PhD. His enthusiasm and continuous support created the most motivated and attainable research work environment.

Many individuals are involved in the success and completion of this thesis. First and foremost, I would like to thank my friend Soheil Zeraati Rezaei. It wouldn't be an exaggeration to say that without his continuous help, the journey would have been more difficult. He was more than a friend, as we used to share our thoughts, even our pains. I would like to give honour and thanks to him. Also, I would like to thank Dr Jose Herreros for his valuable help and academic feedback.

Special thanks to Saudi Aramco for sponsoring my advanced degree program. I would like to thank at Saudi Aramco both Professor Gautam Kalghatgi and Dr Amer for their help and support. Many thanks go to Dr Akbar Ghafourian and Dr Haider Butt for their guidance and assistance during my annual review. Many thanks go to my colleagues, Dr Salim Alam and Dr Arumugam Sakunthalai Ramadhas for their help and support. I would like to thank Carl Hingley, Peter Thornton, Lee Gauntlett, Jack Garrod, Simon, Chongming Wang, Tawfiq Badawy, Thomas Lattimore, Dr Ahmed Al Shehabi and anyone else whose name I missed out, for their technical support, for friendship and making my life easier.

I would like to thank my friends, Medhat, Mahboob and Malekering for their company in our outdoor adventures during our spare time.

This thesis was copy-edited for the conventions of language, spelling and grammar by Oxbridge Editing Proofreading Service.

TABLE OF CONTENTS

CHAPTER 1 INTRODUCTION **1**

1.1 Background **1**

1.1.1 Global Energy Demand 1

1.2 Toxicity of Diesel Engine Compounds in Exhaust System **3**

1.2.1 Carbon Monoxide (CO) 4

1.2.2 Nitrogen Oxides (NO_x) 5

1.2.3 Hydrocarbons (HCs) 5

1.2.4 Particulate Matter (PM) 6

1.3 Environmental Effects of Emissions **7**

1.3.1 Air Quality and Pollutants 7

1.3.2 Global Warming 7

1.4 Emission Legislation **8**

1.5 Towards High Efficiency and Low Emissions of CI Engines **10**

1.5.1 Historical Background 10

1.5.2 Clean Diesel Engines 11

1.6 Objectives and Approaches **12**

1.7 Thesis Outline **13**

CHAPTER 2 LITERATURE REVIEW **15**

2.1 Particulate Matter (PM) **15**

2.2 Fundamentals of Soot Formation 20

2.2.1 Soot Formation Process 21

2.2.1.1 Soot Oxidation Process 22

2.2.1.2 Fuel Pyrolysis 23

2.2.1.4 Soot Surface Growth 25

2.2.1.5 Soot Coagulation and Agglomeration 26

2.3 Particulate Matter Measurement 27

2.3.1 Particulate Matter Measurement Techniques 28

2.3.1.1 Particulate Matter Measurement Conventionally 28

2.3.1.2 Particulate Matter Measurement Individually 30

2.4 Diesel Particulate Matter Composition 32

2.4.1 Soluble Organic Fractions of Diesel PM 32

2.4.2 Polycyclic Aromatic Hydrocarbons (PAHs) 34

2.4.3 Solid Fractions of PM 38

2.4.4 Sulphate Fractions of PM 38

2.5 Low Temperature Combustion Diesel Engines 39

2.5.1 Introduction 39

2.5.2 Premixed Compression Ignition (PCI) Combustion 41

2.5.3 NOx Emissions from PCI Combustion 42

2.5.4 Particulate Matter (PM) Emissions from PCI Combustion 43

2.5.5 Effect of Injection Strategies on PM emissions 45

22.5.6 Fuel Auto-Ignition Quality and Volatility in a PCI Engine 46

2.5.7 Dieseline Fuelled Premixed or Partially Premixed CI engines 48

2.5.8 Gasoline Compression Ignition (GCI) engines 49

2.6 Summary 52

CHAPTER 3 EXPERIMENT SETUP 53

33.1 Engine Test Cell 53

3.1.1 Engine 54

3.1.2 Dynamometer 55

3.1.3 Engine Control 55

3.1.4 Fuel Metering 56

3.1.6 Pressure Data Acquisition 59

3.2 Exhaust Measurement Instruments 60

3.2.1 Engine Exhaust Gas Emissions' Measurement 60

3.2.2 Smoke Meter 61

3.2.3 DMS500 62
3.2.4 Diluter 64
3.2.5 Filter Paper and Sample Extraction 66
3.2.6 Sample Extraction 67
3.2.6.1 Extraction Method for Trace Metals 67
3.2.6.2 Extraction Method for GC-MS 67
3.3 Analytical Measurement Instruments 68
3.3.1 Elemental Carbon (EC) and Organic Carbon (OC) 68
3.3.2 Inductively Coupled Plasma-Optical Emission Spectrometry (ICP-OES). 69
3.3.3 Gas Chromatography – Mass Spectrometry (GC-MS) 69
3.3.4 GC X GC-ToF-MS 71
3.3.5 Transmission Electron Microscopy (TEM) 72
3.4 Data Processing 75
3.4.1 Heat Release Rate Analysis 75
3.4.2 Brake Thermal Efficiency Calculation 75
33.4.3 Data Uncertainty 76
3.5 Summary 77
CHAPTER 4 EFFECT OF EGR TEMPERATURE, INJECTION PRESSURE AND TIMING ON PM OF DIESEL AND DIESELINE FUELLED PCI 78
4.1 Introduction 78
4.1.1 Research Objective 80
4.2 Experimental Set-up 80
4.2.1 The Engine and Test Conditions 80
4.2.2 Sampling and Analysis 81
4.3 Particle Size and Number Distribution of Diesel and G75 Fuels 83
4.3.1 The Effect of EGR Temperature on Particle Size and Number Distribution of Diesel Fuel 83
4.3.2 The Effect of the EGR Ratio on PM of Diesel and G75 Fuels 85

4.3.3 Effect of Injection Pressure and Timing 89
4.3.3.1 Effect of Injection Pressure and Timing at a Load of 1.37 bar BMEP..... 90
4.3.3.2 Effect of Injection Pressure and Timing at a Load of 2.98 bar BMEP..... 99
4.4 Chemical Characterization of Diesel and G75 PM..... 102
4.4.1 Elemental, Organic and Total Carbon 102
4.5 Summary 104
CHAPTER 5 PM CHARACTERISTICS OF DIESELINE AND NAPHTHA FUELLED PCI WITH SINGLE INJECTION..... 106
5.1 Introduction 106
5.1.1 Research Objective 107
5.1.2 Test Conditions 108
5.2 Combustion Performance 109
5.2.1 Heat Release Rate Analysis 109
5.2.2 Ignition Delay 113
5.2.3 Brake Thermal Efficiency..... 114
5.2.4 Regulated Emissions..... 116
5.3 Effect of Engine Load on Particle Size Distribution 118
5.3.1 Particle Size-Number Distribution..... 119
5.3.2 Particle Size-Surface Area Distribution..... 124
5.3.3 Total Particle Mass and Particle Number 128
5.3.4 Effect of Ignition Delay on PN 129
5.4 Chemical Characterization of PM 131
5.4.1 Metal Concentration in PM..... 131
5.4.2 OC, EC and TC in PM..... 136
5.4.3 Poly Aromatic Hydrocarbons (PAHs) in PM 137
5.5 Summary 145
CHAPTER 6 PM CHARACTERISTICS OF DIESELINE AND NAPHTHA FUELLED PCI WITH DOUBLE INJECTION..... 148

6.1 Introduction 148

6.1.1 Research Objective 149
6.1.2 The Engine and Test Conditions 149
6.2 Combustion Performance 151

6.2.1 Heat Release Rate Analysis 151
6.2.2 Regulated Emissions 156
6.3 Particle Size-number Distribution with Double Injection 158

6.3.1 Effect of Engine Load on Particle Size-Number Distribution 158
6.3.2 Metal Concentration in Particulates with Double Injection 162
6.3.3 PAHs' Concentrations with Double Injection 165
6.4 Single Injection versus Double Injection 170

6.4.1 Heat Release Analysis 170
6.4.2 Regulated Emissions 175
6.4.3 Total Particle Number Concentrations 177
6.4.4 PAHs' Concentration 179
6.4.5 C-alkanes and C-cycloalkanes' Concentrations 180
6.5 Summary 192

CHAPTER 7 SUMMARY, CONCLUSIONS AND FUTURE WORK 195

7.1 Introduction 195

7.2 Summary and Conclusions 195

7.3 Future Work 199

7.3.1 PM Morphology 199
7.3.2 PM Emissions after a DOC 200
7.3.3 PM Emissions at Higher Load 200
7.3.4 G75 and Naphtha Fuels' Spray Characteristics 200
LIST OF REFERENCES 201

LIST OF ABBREVATIONS

AHR50	50% of cumulative apparent heat release
ATDC	After Top Dead Centre
IMEP	Indicated Mean Effective Pressure
BMEP	Brake Mean Effective Pressure
BSNOX	Brake Specific Nitrogen Oxides
BSHC	Brake Specific Hydrocarbon
BSCO	Brake Specific Carbon Monoxide
BTDC	Before Top Dead Centre
BTE	Brake Thermal Efficiency
CAD	Crank Angle Degree
CN	Cetane Number
CO	Carbon Monoxide
dQ	Change of Heat Release
dv	Change of In-cylinder Volume
dp	Change of In-cylinder Pressure
dθ	Change of Crank Angle Degree
DOC	Diesel Oxidation Catalyst
DAQ	Data Acquisition
DMS	Differential Mobility Sizer
DPF	Diesel Particulate Filter
EC	Elemental Carbon
ECU	Engine Control Unit
EU	European Union
EOI	End Of Injection
EPA	Environmental Protection Agency
FID	Flame Ionization Detector
FSN	Filter Smoke Number
GCI	Gasoline Compression Ignition
HC	Hydrocarbon

HCCI	Homogenous Charge Compression Ignition
ICE	Internal Combustion Engine
IMEP	Indicated Mean Effective Pressure
LTC	Low Temperature Combustion
MPRR	Maximum Pressure Rise Rate
$\dot{m}_f$	Fuel Mass Flow Rate
NO	Nitrogen Oxide
NO2	Nitrogen Dioxide
NOX	Nitrogen Oxides
OC	Organic Carbon
OH	Hydroxyl
PCI	Premixed Compression Ignition
PPCI	Partially Premixed Compression Ignition
PCCI	Premixed Charge Compression Ignition
P	Power
PAHs	Polyaromatic Hydrocarbons
PM	Particulate Matter
PN	Particulate Number
Q_{HV}	Lower Fuel Heating Value
RON	Research Octane Number
RCCI	Reactivity Controlled Compression Ignition
SI	Spark Ignition
SOC	Start Of Combustion
SOI	Start Of Injection
SOF	Soluble Organic Fraction
SVOF	Semi-Volatile Organic Fraction
TC	Total Carbon
TDC	Top Dead Centre
UBHC	Unburned Hydrocarbon
VNT	Variable Nozzle Turbine
η_f	Thermal Efficiency
γ	Specific Heat Ratio

LIST OF FIGURES

Figure 1.1: World energy consumption trend (World Energy Outlook, 2007) 2
Figure 1.2: Crude oil products' consumption (World Energy Outlook, 2010) 3
Figure 2.1: Typical particle composition for a diesel engine (Kittelson, 1998) 15
Figure 2.2: Particles' classification on the dimensions basis (Frenklach et al., 1994) 16
Figure 2.3: A typical diesel particle size distribution (Kittelson, 1998) 17
Figure 2.4: Substructure of carbon particle (Smith, 1981; Vander Wal et al., 1999) 21
Figure 2.5: Schematic diagram of the steps in the soot formation process (Bockhorn, 2013) 22
Figure 2.6: Particle morphology from SEM (Scanning Electron Microscopy) (captured under engine mode of 1800 rpm, 30 Nm): (a) Diesel magnification of 10000; (b) Diesel magnification of 65000 (Yanfei Li et al ,2012). 26
Figure 2.6: PM compositions at different engine operating conditions (Horiuchi et al., 1990) 33
Figure 2.7: Priority list of PAHs (Ravindra et al., 2008). * (not included in priority list); B2 (probable human carcinogen); D (not listed as human carcinogens) 35
Figure 2.8: Local equivalence ratio versus local temperature with different combustion mechanisms (Soloiu et al., 2013) 41
Figure 3.1: Overview of engine test cell 53
Figure 3.2: Schematic drawing of the engine test cell 54
Figure 3.3: Refinery process diagram (Gary and Handwerk, 1984) 58
Figure 3.4: (a) Charger amplifier (b) Kistler pressure sensor 59
Figure 3.5: Combustion DMS500 (differential mobility sizer) 62
Figure 3.6: Two stage-dilution system of DMS500 (DMS500 user manual, version 4.03, pg.19) 63
Figure 3.7: DMS500 classifier (DMS500 user manual, version 4.03, pg.119) 64
Figure 3.8: Schematic drawing of the diluter 65
Figure 3.9: Sample probes 65
Figure 3.10: Filter papers with deposits for diesel, G75 and naphtha fuels 66
Figure 3.11: Naphtha fuel chromatogram: x-axis is for the retention time of each peak in minutes, y-axis is for the detector response 71
Figure 3.12: Transmission Electron Microscopy (TEM) (Ford, B et al, 2011). 72
Figure 3.13: TEM image for (a) coal ash soot, (b) diesel soot, (c) primary particle for coal ash, (d) primary particle for diesel (Chen, Y et al , 2005) 73
Figure 3.14 shows a schematic for particle geometry and sizes (Seong, H et al ,2012). 74
Figure 4.1: Liquid fuel on the piston bowl (Vegburner Website) 79
Figure 4.2: Schematic of the experimental set-up without DOC 82
Figure 4.3: The effect of hot EGR on particle size and number distribtuon of diesel fuel at two loads: (a) at 1.37 bar BMEP, (b) at 2.98 bar BMEP 84
Figure 4.4: The effect of EGR ratio on Particle number and size distribution of diesel and G75 fuels at two loads 1.37 and 2.98 bar BMEP: (a, b) diesel, (c, d) G75 88

Figure 4.5: The effect of EGR ratio on nucleation, accumulation and CMD of diesel and G75 fuels at two loads 1.37 & 2.98 bar BMEP: (a) Diesel and (b) G75 89
Figure 4.6: The effect of injection timing on the particle size number distribution for diesel and G75 fuels, two loads: 1.37 and 2.98 bar BMEP and at different injection pressures : (a) and (b), for diesel (c), (d),(e),(f),(g) and (h) for G75..... 95
Figure 4.7: The effect of injection pressure of diesel on the particle number concentration .. 97
Figure 4.8: The effect of injection timings of diesel and G75 on the particle number concentration and CMD for 1.37 and 2.98 bar BMEP at injection pressures: (a) 150 bar; (b) 250 bar; (c) 350 bar 98
Figure 4.9: Hydrocarbons emissions (a) at 1.37 bar BMEP, (b) at 2.98 bar BMEP 101
Figure 4.10: Elemental carbon (EC), organic carbon (OC) and total carbon (TC) concentration of diesel and G75 fuels at both loads with their EC/OC ratio 103
Figure 5.1: In-cylinder pressure and heat release rate of diesel, G75 and naphtha fuels with single injection versus crank angle: (a) 1.5, (b) 3, (c) 6, (d)12 bar BMEP..... 111
Figure 5.2:Maximum incyline pressure and heat release rate of diesel, G75 and naphtha fuels with single injection versus engine loads. 112
Figure 5.3: The ignition delay (a), the combustion duration (b) of three fuels at four different loads..... 113
Figure 5.4: The brake thermal efficiency (a) and maximum pressure rise rate (b) 115
Figure 5.5: BSNOx (a), Smoke (b), BSHC (c), BSCO (d) emissions at four loads with single injection 116
Figure 5.6: Particle size- number distributions at four loads(a) 1.50, (b) 3 , (c) 6, (d) 12 bar BMEP 120
Figure 5.7: (a) Total particle number concentration and CMD (b) nucleation and accumulation mode particles 123
Figure 5.8: Particle size-surface area distribution at loads (a) 1.50, (b) 3, (c) 6, (d) 12 bar BMEP 127
Figure 5.9: Comparison between total particle number concentration and total particle mass at four different loads 128
Figure 5.10: Comparison between total particle number concentration and Ignition delay at four different loads (a) all fuels (b) G75 and naphtha fuels 130
Figure 5.11: Concentrations of trace metals in diesel, G75 and naphtha particulates at four different loads (a) Cu, (b) Ca, (c) Cr, (d) Fe, (e) Zn, (f) Pb, (g) Ni..... 133
Figure 5.12: Elemental carbon EC, organic carbon OC, total carbon TC and OC/EC ratios of diesel, G75 and Naphtha fuels at two loads: (a) 1.50 bar BMEP, (b) 3bar BMEP 136
Figure 5.13: The concentrations of identified 16 PAHs for diesel, G75 and naphtha fuels at four loads (a) 1.50 , (b)3 , (c) 6, (d) 12 bar BMEP..... 141
Figure 6.1: In-cylinder and heat release rate of diesel, G75 and naphtha fuels with double injection vs. crank angle: (a) 1.5 ,(b) 3 , (c) 6 bar BMEP 153
Figure 6.2: Maximum incyline pressure and heat release rate of diesel, G75 and naphtha fuels with double injection versus engine loads..... 153
Figure 6.3: Ignition delay (a) combustion duration (b) for diesel, G75 and naphtha fuels at three different loads with double injection..... 155

Figure 6.4: The brake thermal efficiency (a) and maximum pressure rise rate (b) of three fuels at three loads 155
Figure 6.5: The emissions of three fuels at three loads: (a) Smoke, (b) BSNOx (c) BSCO, (d) BSHC 157
Figure 6.6: The particle size-number distribution of diesel, G75 and naphtha fuels with double injection at three loads: (a) 1.50 bar BMEP, (b) 3 bar BMEP (c) 6 bar BMEP 160
Figure 6.7: The particle number concentrations of diesel, G75 and naphtha fuels with double injection at three loads: (a) total PN, (b) total PN of nucleation and accumulation modes ... 161
Figure 6.8: Concentrations of trace metals in diesel, G75 and naphtha particulates at three different loads with double injection (a) Fe, (b) Pb, (c) Zn, (d) Ca, (e) Cu, (f) Cr, (g) Ni 164
Figure 6.9: Concentrations of PAH compounds in diesel, G75 and naphtha particulates at three different loads with double injection (a) 1.50 bar BMEP, (b) 3 bar BMEP, (c) 6 bar BMEP 168
Figure 6.10: In-cylinder pressure and heat release rate comparision between single and double injections of (a) diesel fuel , (b) G75 fuel , and (c) and naphtha fuel at 6 bar BMEP 172
Figure 6.11: Maximum heat release rate and in-cylinder pressure comparision between single and double injections of (a) diesel fuel , (b) G75 fuel , and (c) and naphtha fuel at 6 bar BMEP 173
Figure 6.12: The comparison between single and double injection of three fuels at three loads: (a) ignition delay, (b) combustion duration, (c) BTE and (d) MPRR 174
Figure 6.13: The comparison between single and double injection of three fuels at three loads: (a) smoke, (b) $BSNO_x$, (c) BSCO, and (d) BSHC 176
Figure 6.14: The comparison between single and double injection of total particle number and CMD of three fuels at three loads (a) PN, (b) CMD 178
Figure 6.15: The comparison of PAHs concentration between single and double injection of three fuels at three loads 180
Figure 6.16: A two dimensional separation (a) G75 contour plot in 3D (b) G75 contour plot, (c) diesel fuel contour plot*, (d) engine oil contour plot* (*Alam[b], et al., 2016) 184
Figure 6.17: C-Alkanes distribution with carbon number (a) single injection, and (b) double injection 186
Figure 6.18: C-Cycloalkanes distribution with carbon number (a) single injection, and (b) double injection 188
Figure 6.19: Total concentration at single and double injections: (a) C-alkanes, (b) C-cycloalkanes 189

LIST OF TABLES

Table 1.1: European emission standards for passenger cars (Engeljehringer, 2013; Merkisz and Pielecha, 2015).....9
Table 2.1: Diesel particle sizing instruments (Kittelson et al., 1999; Burtscher, 2001).....31
Table 2.2: Priority list of PAHs with carcinogenic classification (Ravindra et al., 2008).....36
Table 3.1: Puma engine specifications.....55
Table 3.2: Fuel properties (~ represents an estimation value).....57
Table 3.3: Specification of AVL smoke meter 415SG002.....61
Table 3.4: Total particle number (PN) concentrations' uncertainties.....76
Table 4.1: Test conditions.....82
Table 4.2: Test conditions of EGR variation.....85
Table 5.1: Test conditions at four different loads for diesel, G75 and naphtha fuels.....108
Table 5.2: the chemical properties of 16 PAHs identified in this study (Matar, S., & Hatch, L. F. 2001).....139
Table 5.3: PAHs concentrations in particulates of diesel, G75 and naphtha fuels at four different loads with single injection * The concentration increased compared to diesel fuel 143
Table 6.1: Test conditions at four different loads for diesel, G75 and naphtha fuels with double injection.....150
Table 6.2: PAHs concentrations in particulates of diesel, G75 and naphtha fuels at three different loads with double injection, * The concentration increased compared to diesel fuel 169
Table 6.3: C-alkanes and Cycloalkanes concentrations in particulates of diesel, G75 and naphtha fuels at 6 bar BMEP loads with single and double injections. 190

LIST OF PUBLICATIONS

Investigation of Different Injection Pressures and Timings for a Dieseline RON(75) Fuelled PCI Engine- Particulate Matter Emissions Characterization. Yasser Al Qahtani, Soheil Zeraati Rezaei, Hongming Xu. Prepared for Applied Energy Journal

Particle Size- Number Distribution of Dieseline and Naphtha fuelled PCI engine with single and double injection strategies. Yasser Al Qahtani, Soheil Zeraati Rezaei, Hongming Xu. Prepared for Fuel Journal

Chemical Composition of Particulate Matter of Dieseline and Naphtha fuelled PCI engine. Yasser Al Qahtani, Soheil Zeraati Rezaei, Hongming Xu. Prepared for Atmospheric Environment Journal

CHAPTER 1

INTRODUCTION

1.1 Background

1.1.1 Global Energy Demand

Energy is considered as the key mover of the growth of economy around the world. Future energy growth mainly depends on the available sources that are affordable and environmentally friendly.The primary sources of energy like coal and petroleum oil are converted into secondary sources of energy like steam and electricity. Crude oil is considered as the most plentifully available source of energy in the world and its products are mainly used in the transport sector. Crude oil price is volatile and it depends on the market. The developed countries consume around 43 million barrels per day (MBD) while developing countries consume around 22 (MBD) (Energy Outlook, 2007). Coal is considered as the second main source of energy in the world and it is mainly used for electric power generation. In recent years, natural gas has had the highest rate of energy source growth and its efficiency makes it a choice for power generation. Hydroelectricity is considered as a major use of hydro energy around the world. Renewable energy has become very popular and its prices and regularity policies are playing a significant role in the renewable energy developments (Ramadhas, 2016). Oil industries around the world are main players in driving the world economy growth of both developed and developing countries. Figure 1.1 shows the energy

outlook projection up to 2030 and it demonstrates that crude oil will be in high demand and considered as the primary source of energy in future. It has been expected that crude oil consumption demand will increase by 1.6% from 75MBD in 2000 to 120 MBD in 2030 according to the Intergovernmental Panel on Climate Change (IPCC) assessment (Biofuel, 2003; Ramadhas, 2016). The global energy demand projection demonstrated that over 60 % of oil production is consumed in transportation as shown in Figure 1.2 and it is expected that oil-based fuel will continue to be the main source of fuel in the transport sector in future (World Energy Outlook, 2010).

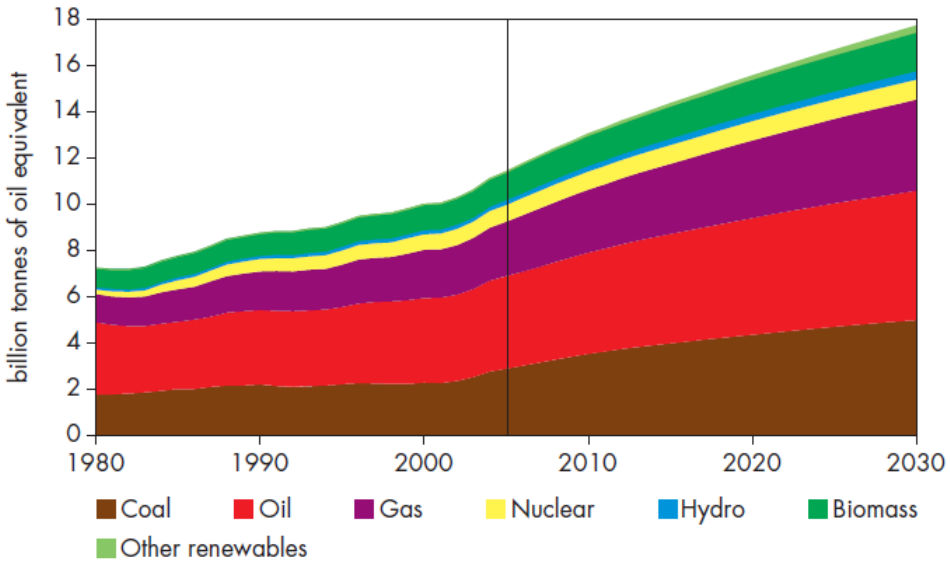


Figure 1.1: World energy consumption trend (World Energy Outlook, 2007)

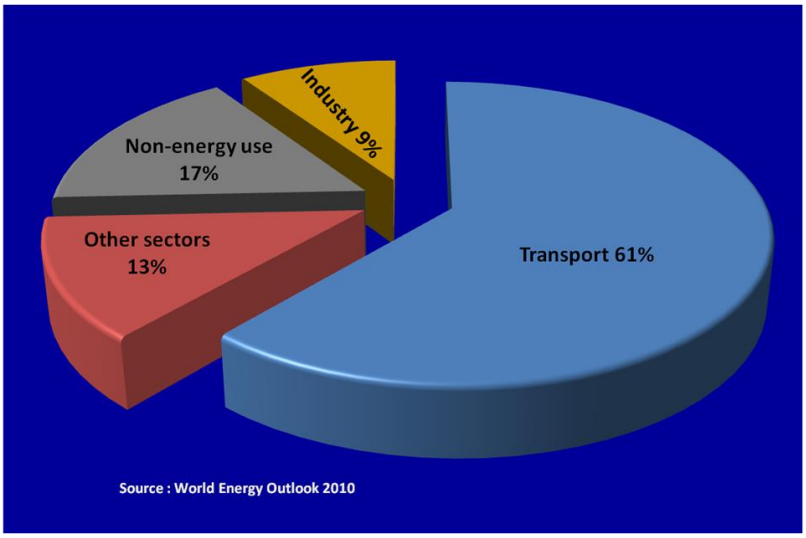


Figure 1.2: Crude oil products' consumption (World Energy Outlook, 2010)

1.2 Toxicity of Diesel Engine Compounds in Exhaust System

Diesel engine combustion products are considered as one of the major source of toxic gases to which people living either in rural or urban areas are exposed. Most of the patients who visit primary care clinics are living in urban areas and they are significantly exposed to diesel exhaust gas emissions, since they live close to busy highways and streets. In Europe and Japan, there is a high rate of chronic respiratory diseases as reported by epidemiologic surveyors, due to close exposure to diesel exhaust gas emissions. The National Institute for Occupational Safety and Health (NIOSH) approximates that millions of people are occupationally exposed to diesel exhaust gas emissions in their workplaces (Krivoshto, 2008; Kagawa, 2002).

For many years, the toxic characteristics of engine-out emissions e.g. nitrogen dioxide (NO_2), nitric oxide (NO), carbon monoxide (CO), hydrocarbon (HCs), and sulfure dioxide (SO_2)

found in diesel engines have been extensively studied and well understood. Recently, a lot of research has been conducted to fully understand and study diesel particulate matter (DPM); which is considered as one of the major diesel emissions that has a significant effect on human health. The research on the effect of DPM on human health is still in its initial stage, since there are many questions waiting to be answered. All public health organizations have defined DPM as a mixture of carbonaceous fraction (soot), ash fraction, organic fraction and sulphate fraction and its regulations have been implemented by various health organizations (Eastwood, 2008; Rosenbaum et al, 1999; Majewski and Khair, 2006).

1.2.1 Carbon Monoxide (CO)

Carbon monoxide is an odourless, colourless and extremely toxic gas. The exposure of humans to only 1% concentration of CO can be deadly (Penney, 1996). The presence of CO in the blood is based on the affinity of CO to blood haemoglobin (Hb). Haemoglobin is considered as the blood component that fixes oxygen molecules in the lungs in the form of HbO_2 and delivers them to the tissues, organs and cells in the human body. The affinity of CO to haemoglobin is 200 times stronger than O_2. The presence of CO in the lungs forms carboxyhaemoglobin (HbCO). The HbCO lessens the oxygen's capacity to be carried by the blood and this will result in impaired distribution of oxygen by the haemoglobin. The CO symptoms are dizziness, headache and can cause coma or death (Majewski and Khair, 2006).

1.2.2 Nitrogen Oxides (NO_x)

Nitrogen oxides (NOx) consist mainly of nitrogen dioxide (NO_2) and nitric oxide (NO). They are formed when oxygen (O_2) is combined with nitrogen (N_2). The lifespan of nitrogen dioxide (NO_2) and nitric oxide (NO) in the atmosphere varies from one to seven days. Nitric oxide (NO) is colourless, odourless and non-toxic and it is considered as a precursor of higher toxicity compounds. It oxidises rapidly in the atmosphere to form nitrogen dioxide; also, it forms ozone via a photochemical reaction between NO and hydrocarbons (HCs) in the atmosphere. Nitric oxide (NO) can cause throat, eye and nose irritations and also pulmonary oedema.

Nitrogen dioxide (NO_2) is an extremely toxic gas and it is a reddish-brown colour with a strong, irritating odour. It is dangerous to be exposed to 100 ppm concentration of NO_2 and it is fatal at 200 ppm. It may cause coughing, chest pain, eye irritation, lung inflammation, pulmonary oedema, hemoptysis and dyspnea (Majewski and Khair, 2006; Eastwood, 2008; Hilborn and Still, 1990; Peterson et al., 2003).

1.2.3 Hydrocarbons (HCs)

The emitted hydrocarbons from a diesel engine exhaust are a mixture of various hydrocarbon compounds. Some of them are derived from fuel and others from lubricating oil. Their

toxicity depends on the chemical formula. Hydrocarbons with longer carbon chains are toxic and have irritating odours. Some of them, like benzene are carcinogenic; while the other derivatives like aldehydes and formaldehydes are toxic and carcinogenic (EPA, 2001). The exposure of the human body to hydrocarbons can cause cardiac, neurologic, pulmonary, dermatologic, hepatic, lung inflammation and chronic cough. (Krivoshto, 2008; Levine et al., 2009).

Another pollutant that is emitted from diesel engines is carbon dioxide (CO_2), which is regulated in many countries. Some other unregulated pollutants are ammonia and sulphur compounds. They are toxic to human health and can cause dermal toxicity and some eye irritation (U.S. EPA, 1991).

1.2.4 Particulate Matter (PM)

Particulate matter (PM) is proposed as the main cause of some chronic respiratory disorders like asthma, cardiovascular issues, lung cancer and even death. Particulates vary in their size from nanometres to micrometres and their toxicity is generally dependent on their size. When the smaller size particles are inhaled by humans, they can deeply penetrate the lungs' bronchi and even into the blood stream. The smaller the size of particles, the more dangerous they are to human health (Kagawa, 2002).

1.3 Environmental Effects of Emissions

1.3.1 Air Quality and Pollutants

Air pollutants have an adverse effect on the environment by interfering with climate, animal species and plants' physiology. They can originate from man-made sources, like emissions from internal combustion engines; and natural sources, like wind erosion or volcanic eruptions. Some pollution sources could be initiated from both natural and man-made origins such as fires. Pollutants in the atmosphere could be transformed to harmful products due to their chemical reaction in the atmosphere. Some of the products could be secondary air pollutants which are more harmful to the environment and human health, such as ozone (Sher, 1998).

1.3.2 Global Warming

The gradual heating of the earth's atmosphere is called global warming. Over the past century, scientists have documented the rise of the temperature of the earth's surface, the ocean and the atmosphere; it has been noticed that the temperature has risen by 0.8°C, as reported by the Environmental Protection Agency. It is proposed that over the next 100 years, the temperature may rise from 1.133 to 6.42°C (Bradford, 2014). There are still disagreements among scientists about whether global warming is caused by human activities. More evidence

suggests that global warming is caused by anthropogenic climate forcing agents. These agents are accumulated, suspended substances in the atmosphere originating from the increase of combusted fossil fuels and other human activities (Houghton et al., 2001). Certain types of gases in the atmosphere are introduced by human activities and more of them, equals more warming. The atmospheric gases are responsible for the greenhouse effect, which are also called “greenhouse gases”. They include carbon dioxide (CO_2), nitrous oxide (N_2O), methane (CH_4) and water vapour. Carbon dioxide (CO_2) is considered as the most important and predominant gas (Majewski and Khair, 2006). According to the Oceanography Scripps Institution, scientists reported that in May 2013, the level of CO_2 in atmosphere was as high as 400 ppm. This level has not been that high since the Pliocene era, three to five million years ago. The effect of global warming is evident in many places in the world. For example, according to the U.S. Geological Survey (USGS), in Montana's Glacier National Park there were once about 150 glaciers and now only 25 remain larger than 25 acres. Scientists also suggest that the increase of global warming will make more hurricanes intense as has been observed in the past years (Bradford, 2014).

1.4 Emission Legislation

In 1992, the European Union (EU) introduced emission regulations and standards and these were finalized with acceptable limits for engine exhaust emissions for diesel and petrol engines, as shown in Table 1.1. In January 2005, Euro 4 was applied for diesel light commercial vehicle emissions such as NOx and PM and they were limited to 0.25 and 0.025 g/km respectively. In September 2009, Euro 5 was introduced and implemented and the

emissions of NOx and PM were reduced to 28% and 80%, respectively. The Environmental Protection Agency (EPA) reported that the continuous reduction in engine-out emissions, along with engine development, do not guarantee the decrease of emissions' risks; however, more stringent regulations on NOx, PM, CO and HC will be applied, such as Euro6+ to be implemented in 2017.

Table 1.1: European emission standards for passenger cars (Engeljehringer, 2013; Merkisz and Pielecha, 2015).

		Euro 1	**Euro 2**	**Euro 3**	**Euro 4**	**Euro 5**	**Euro 5+**	**Euro 6**	**Euro 6+**
		1992	**1996**	**2000**	**2005**	**2009**	**2011**	**2014**	**2017**
Gasoline	**CO (mg/km)**	2720	2200						
	HC+ NOx(mg/km)	970	500	200	100	100	100	100	
	NO_x (mg/km)			150	80	60	60	60	
	PM (DI) (mg/km)					5	4.5	4.5	
	PN(km^{-1})							$6x10^{12}$	$6x10^{11}$
Diesel	**CO (mg/km)**	2720	1000	640	500	500	500	500	
	HC+ NOx(mg/km)	970	700	560	300	230	230	170	
	NO_x (mg/km)			500	250	180	180	80	
	PM (mg/km)	140	80	50	25	5	4.5	4.5	
	PN(km^{-1})						$6x10^{11}$	$6x10^{11}$	

1.5 Towards High Efficiency and Low Emissions of CI Engines

1.5.1 Historical Background

Internal combustion engines (ICEs) are very old technologies which were discovered more than a hundred years ago. Otto invented the four-stroke cycle, but surprisingly he was not aware of thermodynamics. Thermodynamics was firstly applied to ICEs by Rudolf Diesel. He tried to build a highly efficient engine by implementing the Carnot cycle, but unfortunately his idea did not generate enough work. To build a highly efficient engine, Rudolf discovered that fuel type is the key element and that was between 1892 and 1897. He managed to produce a diesel engine with brake efficiency of 30.2%, which was higher than Otto's engine at that time (Pulkrabek, 2004). The brake efficiency of CI engines has gone through a stable evolvement from 30% to 44% (Wayne, 2007). When emission regulations became more stringent in the middle of the 1990s, there was a necessity to introduce a CI engine with a new concept of combustion. The new concept should work as CI engine for efficiency and as a SI engine in terms of pollution levels, if it is equipped with a three-way catalyst. In 1979, Onishi invented the HCCI concept for two–stroke engine (Onishi et al., 1979) and in 1983 the HCCI concept was studied in a four-stroke cycle by (Foster and Najt, 1983). Continuous works and investigations have been conducted to fully understand the HCCI combustion process.

1.5.2 Clean Diesel Engines

Diesel engines offer high efficiency compared to gasoline engines. They emit significant amounts of NO_x and PM and these are considered as their drawbacks. Therefore, the concept of low temperature combustion (LTC) has been evolved in order to attain a comparable efficiency to diesel engines and comparable emissions to spark ignition (SI) engines equipped with a three-way catalyst (Atkinson et al., 2010; Benajes et al., 2012). In HCCI combustion, a lean mixture of air and fuel is compressed and auto-ignites throughout the combustion chamber near the top dead centre (TDC). The nature of the mixture in the auto-ignition in HCCI made it a challenge to control the injection timing at full load range (Kalghatgi et al., 2010). Therefore, at the first decades of the 21st century, an intermediate combustion process was well studied.

A premixed or partially premixed compression ignition (PPCI) or (PCI) engine is considered as an intermediate process. During the compression stroke, fuel is injected in the PCI. To some extent and before the start of combustion, fuel is mixed with air. With this mode of combustion, a very low amount of soot and NO_x can be attained, even at high load 15 bar IMEP (Noehre et al., 2006). The injection timing of fuel in PCI can be controlled and this gives an advantage of controlling the start of combustion. In order to achieve PPCI or PCI combustion and have low soot and NO_x emissions, it is required to use high level of EGR and advance the injection timing of the fuel with a high volatility and low cetane number (CN) (Lu et al., 2011). Fuels with low CN and high volatilities can increase ignition delay and this helps to provide sufficient time for fuel and air to have a better mixing. A study has been conducted by (Kalghatgi et al., 2007) and it has been concluded that gasoline fuelled PCI can attain low smoke, low NO_x and provide a long ignition delay in order for the mixture to be

better mixed. At the University of Birmingham, a researcher (Dr Fan Zhang) investigated dieseline-fuelled PCI. The study concerned understanding the effect of operating conditions on the combustion performance and emissions of dieseline G50 (50% of gasoline fuel blended in 50% of diesel fuel) compared to a conventional diesel engine. This work is an extension of his work, but the investigation focuses on the particle size distributions (number and surface area) and chemical characterizations (EC,OC,PAHs, alkanes and cycloalkanes concentrations) of a diesel and low CN fuels (CN~30) running on PCI mode. The low CN fuels are dieseline (higher ratio, G75) and naphtha. The investigation of particle size distributions, especially the chemical characterization of PM running on PCI mode with low CN fuels (dieseline and naphtha) is considered as a new study since no such data available in a research portfolio. Due to the limited resources, the PM morphology study is recommended as a future work.

1.6 Objectives and Approaches

The main objective is to investigate the particle size distributions and chemical characterization of PM for low octane fuels running in a premixed compression ignition engine. The main objectives are:

- Investigate the effect of EGR temperature of both diesel and G75 fuels.
- Conduct a screening test to study the effect of injection pressure and timing of diesel and G75 fuels on particle number concentration and total carbon of PM. The screening test will identify the interesting points that should have a further investigation in terms of particle size distributions and chemical characterization of PM.
- Prepare a low processed fuel (naphtha fuel) and blend it in a way that should have a similar specification of G75 for sake of comparison with G75 and diesel fuels.

- Investigate the effect of single and double injection strategies on the particle size distributions and chemical characterization of diesel, G75 and naphtha PM.

1.7 Thesis Outline

This thesis covers seven chapters with different aspects. Chapters 1and 2 contain a review of the world's energy demand and the effect of engine-out emissions on the environment and human health. Also, the soot fundamentals, soot formation process and PM measurement techniques are presented. Furthermore there is a review of low temperature combustion and the latest research and challenges in gasoline compression ignition (GCI) engines and premixed compression ignition (PCI) are discussed. In Chapter 3, there is an introduction to the engine test cell set-up with the measurement equipment, such as the HORIBA, smoke meter, DMS500 and diluter. Also, the analytical equipment: EC/OC, ICP-OES, GC-MS and GCXGC-ToF-MS are presented. In Chapter 4, a screening test was conducted for diesel and G75 fuels at two loads. The tests covered the effect of EGR temperature, the injection pressure and timing on the particle size and number distribtuions and chemical characterization of PM. In Chapter 5, it focuses on the effect of single injection using three different fuels: diesel, G75 and naphtha on the combustion performance, regulated emissions, particle size- distributions (number, surface area and mass), the effect of ignition delay on PM, the effect of single injection on the EC, OC, TC, trace metals and PAHs' concentration at four different loads (low-medium, and high). In Chapter 6, an investigation is presented concerning the effect of double injection on particle size-number distribution, combustion performance, regulated emissions, PAHs and trace metals' concentrations for three fuels at

low and medium loads. Also, it discusses the comparison between single injection and double injection in terms of combustion performance, regulated emissions, total particle number concentration, PAHs, alkanes and cycloalkanes' concentration. In Chapter 7, the main conclusions of the research and suggestions for future research work are presented.

CHAPTER 2

LITERATURE REVIEW

2.1 Particulate Matter (PM)

Particulate Matter is considered as one of the main issues concerning diesel engines' emissions that are related to human health; and it is mainly composed of elemental carbon (soot) with organic fraction, sulphate fraction, nitrate fraction and ash fraction adsorbed into its surface. The organic fraction or soluble organic fractions (SOF), is originally formed by unburned fuel and lubricating oil. Sometimes they form during the combustion process and the catalyst's reactions. It usually includes aldehydes, alkanes, alkenes and aromatics. In a diesel particulate matter, the fraction of soot or insoluble organic fraction (SOL) is more than 50%. For the other fractions their distribution varies between 1-20% as shown in Figure 2.1 (Ullman, 1989; Kittelson, 1998; Eastwood, 2008).

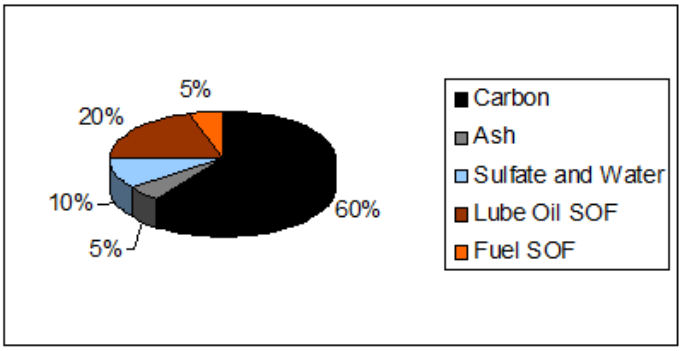


Figure 2.1: Typical particle composition for a diesel engine (Kittelson, 1998)

Most authors have divided PM into the following categories, based on the aerodynamic diameter, as shown in Figure 2.2. Aerodynamic diameter could be described as a sphere diameter (density 1 g/cm^3) with the same settling velocity of a given any density or shape of a particle in laminar air flow:

- PM_{10} (particles with aerodynamic diameters less than 10 µm or 10000 nm)
- $PM_{2.5}$ (fine particles with aerodynamic diameters less than 2.5µm or 2500 nm)
- Ultra-fine particles (with aerodynamic diameters less than 0.1 µm or 100 nm)
- Nano particles (with diameters less than 0.05 µm or 50 nm)

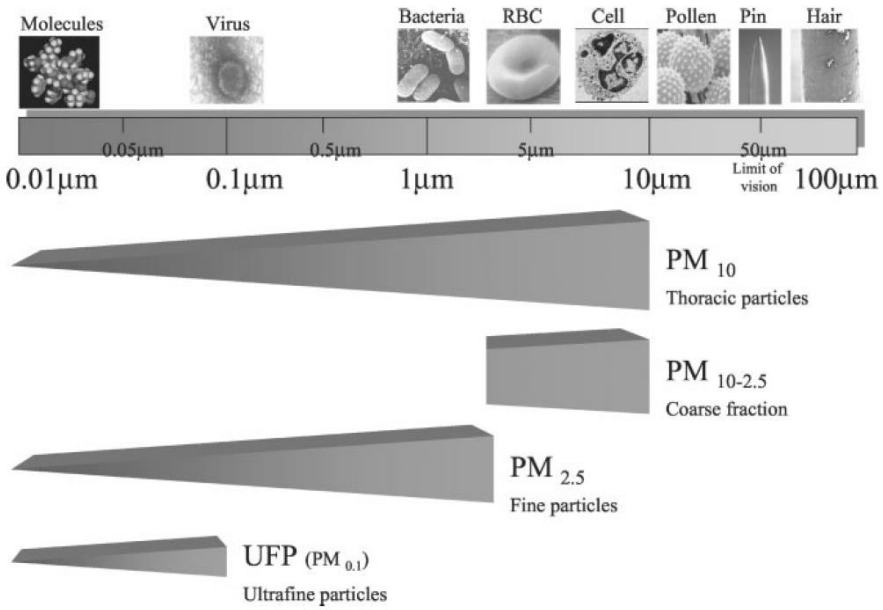


Figure 2.2: Particles' classification on the dimensions basis (Frenklach et al., 1994)

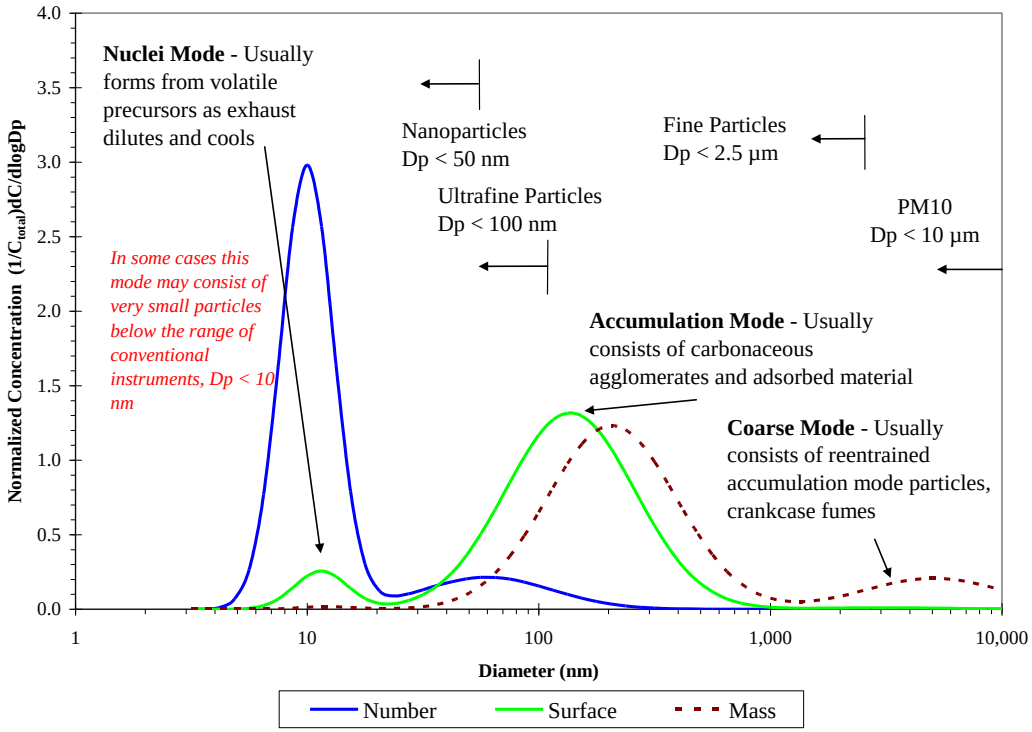


Figure 2.3: A typical diesel particle size distribution (Kittelson, 1998)

The particle size distribution of a typical diesel is presented in Figure 2.3 in logarithmic scale, which is used for particle aerodynamic diameters. The particles formation starts with nucleation followed by nuclei particles agglomeration. The nucleation of particles happens inside the engine's cylinder forming carbon and ash and in the dilution tunnel forming water, sulfuric acids and hydrocarbons through heterogeneous and homogenous nucleation mechanisms (Majewski and Khair, 2006; Merkisz and Pielecha, 2015). As shown in Figure 2.3, particle size distribution has bimodal distribution corresponding to three different modes: nucleation mode, accumulation mode and coarse mode. The particles with size below 50 nm are positioned in nucleation mode region. The original diameter of a nuclei particle is about 1 nm and it has been noticed that the extreme concentration of the nuclei particles happens at 10 to 20 nm (Abdul-Khalek et al., 1999). Nucleation mode depends on sampling techniques and engine technology. The total PM mass constitutes up to 10 in nucleation mode, but 99% of the

total particle number. It contains mostly volatile condensate e.g. hydrocarbons, sulfuric acids and some solid particles. The particles with diameter between 50 to 1000 nm are in accumulation mode. The maximum concentration of particles in accumulation mode occurs between 100 and 200 nm. Accumulation mode particles are composed of solid particles (carbon, ash) mixed with adsorbed materials (hydrocarbons, sulphuric acids) and condensate. For coarse mode, it has particles with a diameter above 1000 nm or 1 µm; with the total PM mass encompassing 5 % to 20 % and has almost no involvement with the particle numbers. The deposited materials in the exhaust system, engine cylinder walls and sampling system are considered as the main source of generating coarse particles (Kittelson et al., 2002).

The physical characteristics of particulate matter are the shape, dimension and composition. The size distribution of the particles that are emitted by internal combustion engines is characterized in the same way as population (Hind, 2012). The mean or average is the total sum of the particles divided by the number of the particles; while the median is the size of the particle from which half of the particles are smaller and the other half is larger. The most encountered particle size is called the mode. The geometric mean is mostly used to characterize aerosol particles and it is the nth root of the product n values (Eastwood, 2008).

Particle size distribution has a normal distribution and it is categorized in many types. Volume distribution $v(D_p)$, mass distribution $m(D_p)$, surface area distribution $s(D_p)$ and number distribution $n(D_p)$ are considered as the main categories of interest (Seinfeld, J. H, 1986). To explain $n(D_p)$, count the particles number as a function of diameters in a gas unit's volume; $n(D_p)dD_p$ could be defined as the particle number within the size range from D_p *to* $D_p + dD_p$.

The total number *N* of particles of unit volume of gas is given by:

$$N = \int_0^{\infty} n(Dp)dDp \qquad 2.1$$

Where $n(D_p)$ is the particles number within a unit volume of gas as a diameter fraction and it is measured as $\mu m^{-1}\ cm^{-3}$; while *N* is the total number of particles per gas unit volume and it is cm^{-3}. Particle sizes extend into orders of magnitude and because of this the number of particles $n(D_p)$ will be as a function of the logarithm of the particle diameter $n(log\ D_p)$. Then, the number of particles within a size range is from $logD_p$ *to* $logD_p + d\ logD_p$ is $n(logD_p)d\ logD_p$. So, the total number *N* of particles of unit volume of gas is given by:

$$N = \int_{-\infty}^{\infty} n(logDp)d\ logDp \qquad 2.2$$

Considering the same aerosol, the number of particles within the range dD_p is equal to $d\ logD_p$ and it does not depend on how the distribution is expressed. Writing the total particle number as *dN gives* the following:

$$dN = \ n(Dp)dDp = n(logDp)d\ logDp \qquad 2.3$$

Or

$$n(logDp) = \frac{dN}{d\ logDp} \qquad 2.4$$

The expression of *dN / d logDp* appears on many graphs of particle size number distribution and the advantage is that it shows the area under the curve of any size range is proportional to the number of particles within that range. This is also true for the other distributions i.e. mass, volume and surface area (Eastwood, 2008).

The particle volume concentration is measured in V(μm^3/cm^3) and it is given by the following:

$$V = \sum_i \frac{\pi}{6} D_i^3 PN_i \qquad 2.5$$

The particle surface area concentration is measured in S(μm^2/cm^3) and it is given by the following:

$$A = \sum_i \pi \ D_i^2 PN_i \qquad 2.6$$

The particle mass concentration is measured in M(μg /cm^3) and it is given by the following :

$$M = \sum_i \frac{\pi}{6} \rho \ D_i^3 PN_i \qquad 2.7$$

Where D_i is the particle diameter in nanometres (nm) or micrometres (μm) at a given particle number PN_i. The density ρ here is in unity and it is 1 g/cm^3 .

2.2 Fundamentals of Soot Formation

Soot is a harmful pollutant and it is considered as an indication of low combustion efficiency. In general, soot can be defined as a solid substance containing mostly carbon atoms, with a carbon to hydrogen ratio 10:1. In fuel-rich regions and at elevated temperature, the unburned fuel starts nucleating from a vapour phase to solid phase forming soot. Some hydrocarbon or other molecules can be either adsorbed or condensed on soot and this depends on the surrounding environment. The main compositions of particulate are soot or carbonaceous fraction (typically more 50% in a diesel particulate), soluble organic fraction. Other fractions

are worn metals, bound water and sulphate (Tree and Svensson, 2007; Choi et al., 1994; Ullman, 1989; Kittelson, 1998). Some studies show that soot particles are in a chain-like structure and they contain up to 4000 smaller spherical particles called spherules. Spherules are composed of concentric lamellate arranged around the centre. This arrangement is similar to the structure of carbon black. The atoms of carbon are bonded together in hexagonal faced cantered arrays called platelets. The spacing between the platelets is 0.355 nm and there are about 2 to 5 platelets per crystallite. Thousands of crystallites constitute a spherule as shown in Figure 2.4 (Smith, 1981; Vander Wal et al., 1999; Amann and Siegla, 1981; Heywood, 1988).

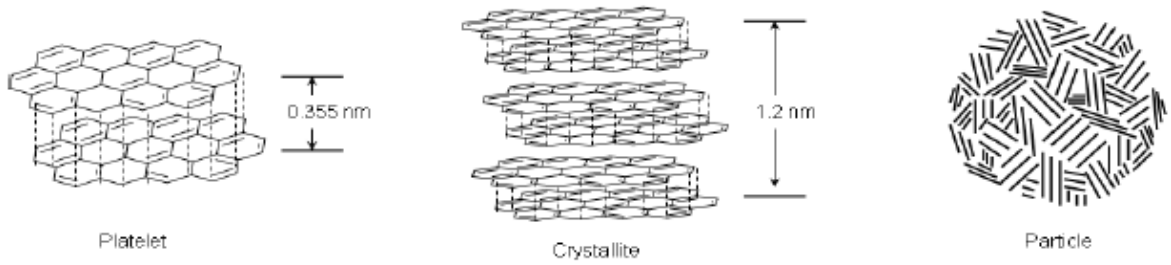


Figure 2.4: Substructure of carbon particle (Smith, 1981; Vander Wal et al., 1999)

2.2.1 Soot Formation Process

Solid particles are mainly developed or transformed from vapour or liquid phase. The development process should undergo as following: pyrolysis, nucleation, surface growth, coalescence, agglomeration and oxidation (Bockhorn, 2013; Tree and Svensson, 2007). The soot formation process is demonstrated in Figure 2.5. At each step, two processes occur simultaneously: oxidation and formation. Both processes are continually competing and they

depend on the operation conditions, fuel composition, in-cylinder pressure, temperature and oxygen content.

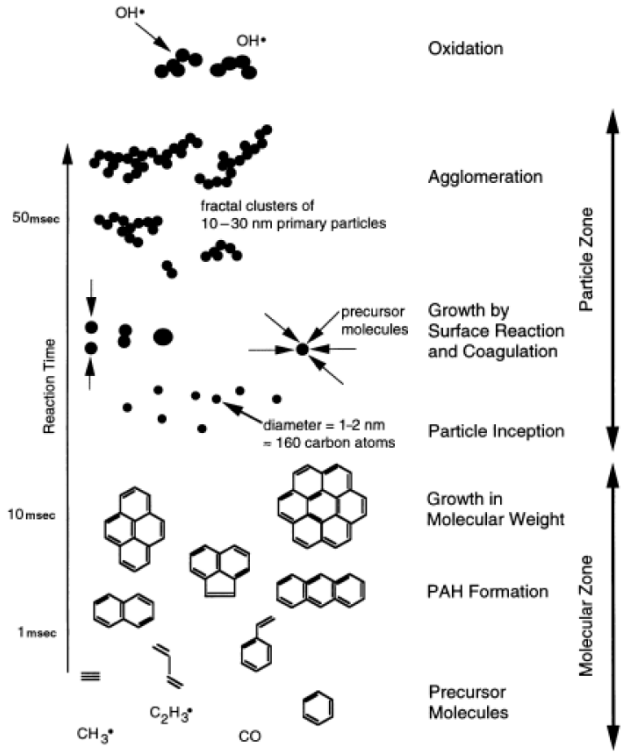


Figure 2.5: Schematic diagram of the steps in the soot formation process (Bockhorn, 2013)

2.2.1.1 Soot Oxidation Process

Carbon monoxide (CO) is a combustion product and it is a result of the oxidation of carbon. The oxidation of carbon means the carbon will not grow into solid particles even in a fuel-rich region. The oxidation process can happen in all the steps of the soot formation process and that depends mainly on the mixture and temperature (higher than 1300 K) Glassman (1989). The process of oxidation of small particles undergoes two stages: absorption and desorption.

The first stage is absorption of oxygen to the particulate surface. The second stage is the separation of oxygen with some fuel component from the particulate surface or it is called desorption (Glassman, 1998). Smith has stated that soot's graphite structure causes high resistance to oxidation (Smith, 1981). The more the particles agglomerate, there is a reduction of specific areas and as a result, less soot oxidizes. Hydroxyl radical (OH) is considered the main factor of soot oxidation in either fuel-rich regions or stoichiometric conditions. In lean conditions, both OH and O_2 are most likely to dominate the soot oxidation (Bartok and Sarofim, 1991).

2.2.1.2 Fuel Pyrolysis

In the presence of high temperature and the absence of oxygen, the endothermic reaction that alters the molecular structure of the fuel without oxidation is called pyrolysis. Pyrolysis produces building blocks for soot or soot precursors. In parallel to the soot formation process, oxidation occurs at any step. The rate of fuel pyrolysis and oxidation depends on the temperature. Increasing the temperature will increase the rate, but oxidation rate will be quicker. This clarifies why in diffusion flames (absence of oxygen) more soot forms with an increase of temperature; while less soot formed in premixed flames (oxygen presence) with an increase of temperature (Glassman, 1998).

Fuels pyrolysis produce soot precursors such as polycyclic aromatic hydrocarbons (PAH) and acetylene. In laminar diffusion flames, typical pyrolysis products are CH_4, C_2H_2, C_2H_4, C_3H_6 and benzene (Tree and Svensson, 2007). Wang and Frenklach say that the formation of PAH is caused by the polymerisation of acetylene, which is considered the main soot precursor.

Non-aromatic species such as phenyl or acetylene could produce aromatic rings through polycyclisation of the molecules (Wang and Frenklach, 1997).

There are three possible ways that non-aromatic species produce aromatic rings. According to Wang and Frenklach (1997), a first way of benzene formation is:

$$n\text{-}C_4H_5 + C_2H_2 \longrightarrow n\text{-}C_6H_5 \text{ (phenyl ring)} \quad (2.8)$$

$$n\text{-}C_4H_5 + C_2H_2 \longrightarrow n\text{-}C_6H_7 \text{ (benzene + hydrogen atom)} \quad (2.9)$$

According to Miller and Melius (1992), a second way of benzene formation is:

$$C_3H_3 + C_3H_3 \longrightarrow C_3H_5 \text{ (phenyl + hydrogen atom)} \quad (2.10)$$

$$C_3H_3 + C_3H_3 \longrightarrow C_6H_6 \text{ (benzene)} \quad (2.11)$$

The third way according to Pfefferle et al. (1994):

$$C_4H_4 + C_3H_3 \longrightarrow C_7H_7 \text{ (toluene)} \quad (2.12)$$

Nucleation (soot particle inception or nuclei) is developed from the transformation of particles from vapour phase to solid phase. The smallest detectable diameter of nuclei is in the range 1.50-2 nm. The addition of radicals of small molecules like hydrocarbons, aliphatic to larger aromatics' molecules is the process of particle inception and with temperatures variation in the range (1300 -1600K). The particle nuclei could provide sites or places for surface growth and that later could contribute to the addition of the total soot mass (Agarwal et al., 2011). The

first aromatic rings are likely formed by two propynyl radicals, C_3H_3. Then, alkyl groups are added to the aromatic ring forming PAH structure. In the presence of soot precursors in the vapour phase and acetylene, the PAH's structure grows and develops particle nuclei. The soot formation is slow down by the ring rupture as noted by Haynes and Wagner (1981). There are three possible soot nucleation routes as stated by Bryce et al. (1999):

- The ring structures that are formed by the cyclization of chain molecules e.g. the formation of a benzene ring via acetylene molecules combination
- The formation of polycyclic by aromatic rings dehydrogenation at low temperature (direct path route)
- At higher temperature, break up and racialization of rings (Agarwal et al., 2011).

2.2.1.4 Soot Surface Growth

The surface growth is defined as mass addition to the nucleated particle. The processes of nucleation and surface growth are simultaneous since the difference between the commencement of surface growth and the end of nucleation is not clear. The surface of the soot particles is reactively hot and ready to accept hydrocarbons in the gas phase, which in turn, remain the particle number constant and increase at the same time the total mass. The particle surface growth will continue growing as long as the particles are escaping from reaction zone to less reactive and cooler zones (Agarwal et al., 2011; Haynes and Wagner, 1981). Small particles have more reactive radicals than larger particles and because of that the surface growth rates of small particles are higher than of larger particles (Bartok and Sarofim, 1991).

2.2.1.5 Soot Coagulation and Agglomeration

Coagulation or Coalescence is the process when two spherical shaped particles collide and form one spherically shaped particle holding the combined mass, with a decrease in the particles' number. Agglomeration is a long chain of primary particles that are formed by the combination of the individual particles while maintaining their shapes as shown in Figure 2.6. The agglomerated particles or long chain structure of particles consists of spherical shaped primary particles and their sizes depend on some factors: operation conditions, fuel composition, in-cylinder pressure, temperature, oxygen content and the technique of sampling and measuring the particles. Many researchers estimated the primary particle size in diesel engines, and it was reported by (Lee et al., 2001), the primary particle size was found at the exhaust system in the range 20 to 30 Bruce has found the primary particle size to be from 30 nm to 70 nm by using a sampling probe and scattering technique (Bruce et al., 1991). Tree and Foster have found that particle size varied from 30 nm to 50 nm; while Pinson has found the particle size to be between 40 nm and 65 nm by using in-cylinder light scattering experiments (Tree and Foster, 1994; Pinson et al., 1994). The size of the agglomerated soot at the end of combustion was found in the range 100 nm and 2 μm as reported by (Ladommatos and Zhao, 1994; Desantes et al., 2005).

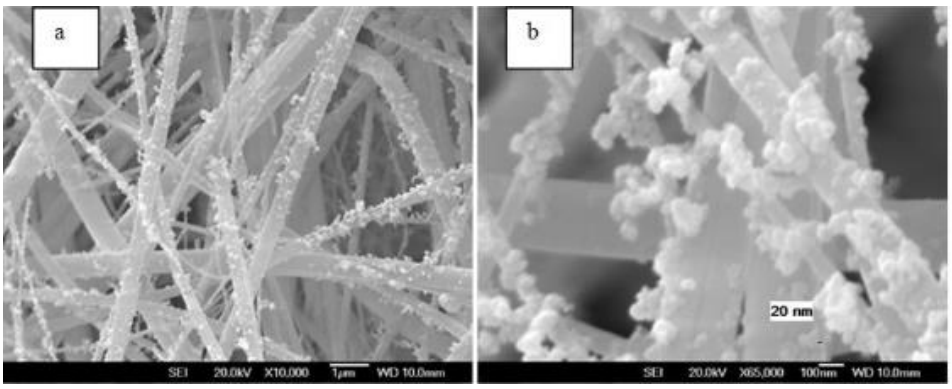


Figure 2.6: Particle morphology from SEM (Scanning Electron Microscopy) (captured under engine mode of 1800 rpm, 30 Nm): (a) Diesel magnification of 10000; (b) Diesel magnification of 65000 (Yanfei Li et al ,2012).

2.3 Particulate Matter Measurement

Diesel particulate matter (DPM) is an intricate mixture and its composition is characterized by commonly changing physical properties and chemical composition. DPM properties depend on engine technology, fuel type, operating conditions, exhaust after-treatment system, sampling method, sampling location and the time. Particulates undergo transformation in the atmosphere, dilution tunnel or sampling line, or measuring equipment. An example of transformation is particle coalescence, evaporation or condensation of volatile materials. Also, transformation in a sample train or measurement apparatus could lead to artifacts forming.

Many measurement techniques have been developed or embraced from different fields to measure DPM. The measurement techniques could be for the purpose of quality (e.g. accuracy, cost and repeatability), health effects and suitability for the purpose of emissions' legislation and emissions' research. The critical particle measurement parameters are: particle mass, size, volume, surface area, number concentration and particle composition (Kittelson et al., 1999; Majewski and Khair, 2006). Though particle mass is the most common parameter used to regulate PM emissions from diesel engines, recent medical research has demonstrated that particles of smaller sizes have a more significant effect on human health than particles with larger diameters; for example: one million particles of PM0.1 and one particle of PM10. The former is more risky to human health. Advanced diesel engines produce less particle mass than old engines, but they emit larger particle numbers and because of that research has been pushed forward to study particle measurements from mass to number (Abdul-Khalek et al., 1998).

2.3.1 Particulate Matter Measurement Techniques

Particulate measurement techniques could be divided into two techniques: particulate measured conventionally and particulate measured individually.

2.3.1.1 Particulate Matter Measurement Conventionally

2.3.1.1.1 Particulate Matter Sample Collection

The raw exhaust gas enters the dilution tunnel. There are many designs of dilution tunnels but there are basically two categories: full flow and partial flow. Full-flow dilution is to dilute all the exhaust gas and then take a proportional flow sample. Partial-flow dilution is to take a proportional flow sample and then dilute it (Eastwood, 2008). The tunnel must deliver the dilution in a repeatable and controllable manner, avoiding water condensation, reducing particle concentration to the apparatus and it should be similar to real-world emissions. The air that is used for dilution should be conditioned to dispose of any humidity and dirt. The conditioned air is mixed with raw exhaust gas and the temperature of the air should be sufficient to cool the raw exhaust gas to a temperature $\leq 52°C$.

A diluted sample of exhaust gas is drawn from the dilution tunnel and collected in a filter e.g. quartz, fibre glass, membranes. The filter should be preconditioned and cleaned, free from dirt or any suspended materials, if this is necessary, as some filters are already preconditioned. The filters then are weighed in a conditioned atmosphere with controlled relative humidity and temperature using a highly accurate balance. The deposited and weighed filter is ready for further analysis. After calculating the total particulate mass, the final results are presented in gram per kilometre (g/km) or grams per kilowatt-hour (g/KWh). This depends on the test

procedures. The equivalent units in the U.S. system are gram per mile (g/mi) and gram per brake horsepower-hour (g/bhp-he) (Majewski and Khair, 2006).

2.3.1.1.2 Particulate Matter Chemical Composition

The deposited or loaded filter is subjected to analysis using chemical and physical methods to define the DPM composition such as: soluble organic fractions (SOF), sulphates and poly aromatic hydrocarbons (PAHs). The DPM composition could be characterized or measured by either extraction by gasification or by solvents. By gasification, or thermogravimetric analysis (TGA), the deposited filter is subjected to two heat treatments in inert and oxidizing atmospheres. The first atmosphere evaporates soluble organic fractions and sulphates by using inert gas e.g N_2, He, Ar; while the second atmosphere oxides the carbonaceous fraction and what remains is the ash fraction. Using extraction by solvents, the deposited filter is extracted by dichloromethane (DCM), which is considered as the most common solvent used and it is recommended by the Environmental Protection Agency EPA. There are other solvents which could be used for extractions such as toluene, benzene/methanol and benzene/ethanol mixtures. Some solvents could result in different share of compounds. Toluene, for example, extracts heavy PAHs compared to DCM. An alcohol addition to the solvent mixture could extract sulphates (Perez et al., 1980).

After extraction the filter or SOF can be analysed for PAHs. The solvent is removed with inert gas at low temperature and then tested for PAHs using gas chromatography (GC), mass spectrometry and high performance liquid chromatography (HPLC). Ion chromatography calibrated with standard potassium sulphate solution K_2SO_4 could be used to determine the

sulphate fraction in the deposits on the filter. Another method of soluble organic fraction extraction is called vacuum evaporation. The organic fraction is obtained by evaporation, but in this procedure it is called volatile organic fraction (VOF). The disadvantage of this method is that the water sulphate also evaporates and present with VOF (Majewski and Khair, 2006).

The disadvantage of conventionally measuring particulate matter is the time delay from the sample collection until the time of the sample measurement results since the chances of the samples' properties changing are high.

2.3.1.2 Particulate Matter Measurement Individually

This technique is used to analyse or measure the particle sizes and numbers through the equipment. It is also called the *in situ* technique. The particle diameter presented in the measurement is the equivalent diameter of a spherical shaped particle and also it portrayed the size in aerosol. The particle size distribution could be presented in number distribution, mass distribution, volume distribution and surface area distribution. Several techniques for this particle size measurement could be categorised as the following (Kittelson et al., 1999; Burtscher, 2001):

- Aerodynamic diameter methods: accelerated particles' inertia is utilized. This method is used in many types of cascade impactors. One of the common impactors used in this group is called an electric low pressure impactor (ELPI).
- Diffusion batteries: this method determines the mobility diameters by the measurement of diffusion properties of the particles.

- Electrical mobility analyzers: this method determines the mobility diameters by the charged particle mobility measurement in the electrical field. The scanning mobility particle sizer (SMPS), the differential mobility spectrometer (DMS) and the engine exhaust particle sizer (EEPS) belong to this group. Table 2.1 summarizes the diesel particle sizing instruments using the aforementioned three methods.

Table 2.1: Diesel particle sizing instruments (Kittelson et al., 1999; Burtscher, 2001)

Method	**Instrument**	**Size range**
Aerodynamic Cascade impactors	Micro-orifice uniform deposit impactor (MOUDI)	0.056-10µm
	Nano MOUDI	0.010-10µm
	Electrical low pressure impactor ELPI	0.032-10µm
Electrical mobility analyzers	Electrical aerosol analyser EAA	0.003-1µm
	Differential mobility particle sizer DMPS	0.01-0.5µm
	Scanning mobility sizer SMPS	0.010-0.7µm
	Nano -differential mobility analyser (nano-DMA)	3-50nm
Diffusion batteries	Electrical diffusion battery EDB	5-300nm

There are other techniques that are used to measure particulate matter individually such as laser induced incandescence LII, light scattering. Also, particulate matter could be measured collectively e.g. flame ionisation; smoke (Eastwood, 2008).

2.4 Diesel Particulate Matter Composition

2.4.1 Soluble Organic Fractions of Diesel PM

Soluble organic fractions are extracted via a solvent that isolates organic fractions from the particulate; and the organic fractions are normally formed when the hydrocarbons adsorbed on the carbon particles surface or present in fine droplets' form. Fractions are sometimes referred to as volatile organic fractions (VOF) and this depends on the extraction technique. Most of the SOF at the diesel exhaust exists in vapour form, especially at a high exhaust temperature and high load. The SOFs become liquid when the exhaust temperature is cooled to below 52°C (Majewski and Khair, 2006).

The fractions of organic materials in the total DPM varies between engines. If the DPM has a high SOF content, it is called wet particulate; while low SOF content in the DPM is called dry particulate. In dry particulate, the SOF content in the DPM is 10% or less; while in wet particulate the SOF content is more than 50%. Figure 2.6, shows a measured SOF content in PM emissions emitted from a turbocharged 2.8-L DI diesel engine run at different speeds and loads at steady state condition with 0.38% wt of sulphur in the fuel. PM emissions are represented by the circles' size. The measurements show that SOF content is in excess of 50% when the measurements are taken at an exhaust temperature up to 200 °C. At high engine loads above 70% and an exhaust temperature of 400°C or more, the SOF content in PM drops; while at light loads and low temperature the SOF content is highest (Horiuchi et al., 1990).

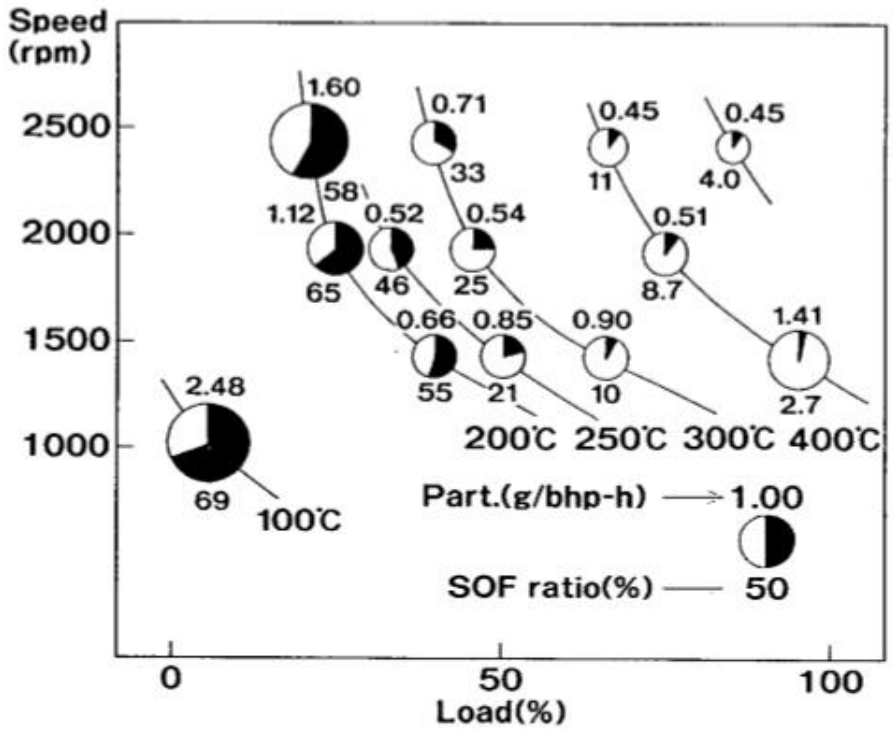


Figure 2.6: PM compositions at different engine operating conditions (Horiuchi et al., 1990)

The SOF is normally derived from diesel engine lube oil with a small fraction of hydrocarbons of the higher end boiling point of diesel fuel. Diesel fuel normally consists of hydrocarbons with a boiling range equal to aliphatic hydrocarbons with C12 to C20 of carbon atoms in their molecules. This is also true for diesel lube oil, as it has several compounds with a boiling point comparable to normal aliphatic hydrocarbons with carbon atoms ranging between C18 and C36. It has been believed that the major contributor to nucleation mode SOF is the engine lube oil. Some experiments demonstrated that the volatility of nucleation mode particles was noticed to be alike to C24 through to C32 normal alkanes, which indicates the origin of lube oil (Kittelson et al., 2002). Another study on light duty diesel engines demonstrated that the lube oil derived SOF has variability, as the contribution varies between 19% and 88% of the total PM (Cartellieri and Tritthart, 1984).

2.4.2 Polycyclic Aromatic Hydrocarbons (PAHs)

Polycyclic aromatic hydrocarbons (PAHs) are complex organic molecules that contain hydrogen and carbon atoms and two or up to six benzene rings joined in several more or less grouped forms (Rhead and Hardy, 2003). PAHs' presence indicates incomplete combustion and unburned lubricating oil (Richter and Howard, 2000). The special attraction or attention given to PAHs is due to their carcinogenic charisma and mutagenic as some of the carcinogenic PAHs were found attached or adsorbed to the surface of particulate matter. PAH emissions are considered as unregulated emissions, but their significant adverse effect on human health should be given high priority (Agarwal et al., 2015; Ravindra et al., 2008; Riddle et al., 2007). Figure 2.8 shows the high priority toxic PAHs. Some of compounds are tagged with B2 (probable human carcinogen); while some compounds are tagged with D (not listen as human carcinogens).

The classifications of carcinogenic PAHs with respect to agencies are presented in Table 2.2. The molecular structure of PAHs plays a significant role in the toxicity of these compounds. For example, two PAHs isomers with different molecular structures have different degrees of toxicity. In recent decades, it has been reported that diesel particulates contain various types of PAHs and because of that diesel particulates are considered as the main factor that have an adverse effect on human health (Agarwal et al., 2015). The Environmental Protection Agency (EPA) has listed 16 PAHs that are based on carcinogenic, probable carcinogenic and molecular structure as shown in Figure 2.7. Some of the compounds are tagged with B2 (probable human carcinogen); while some compounds are tagged with D (not listen as human carcinogens).

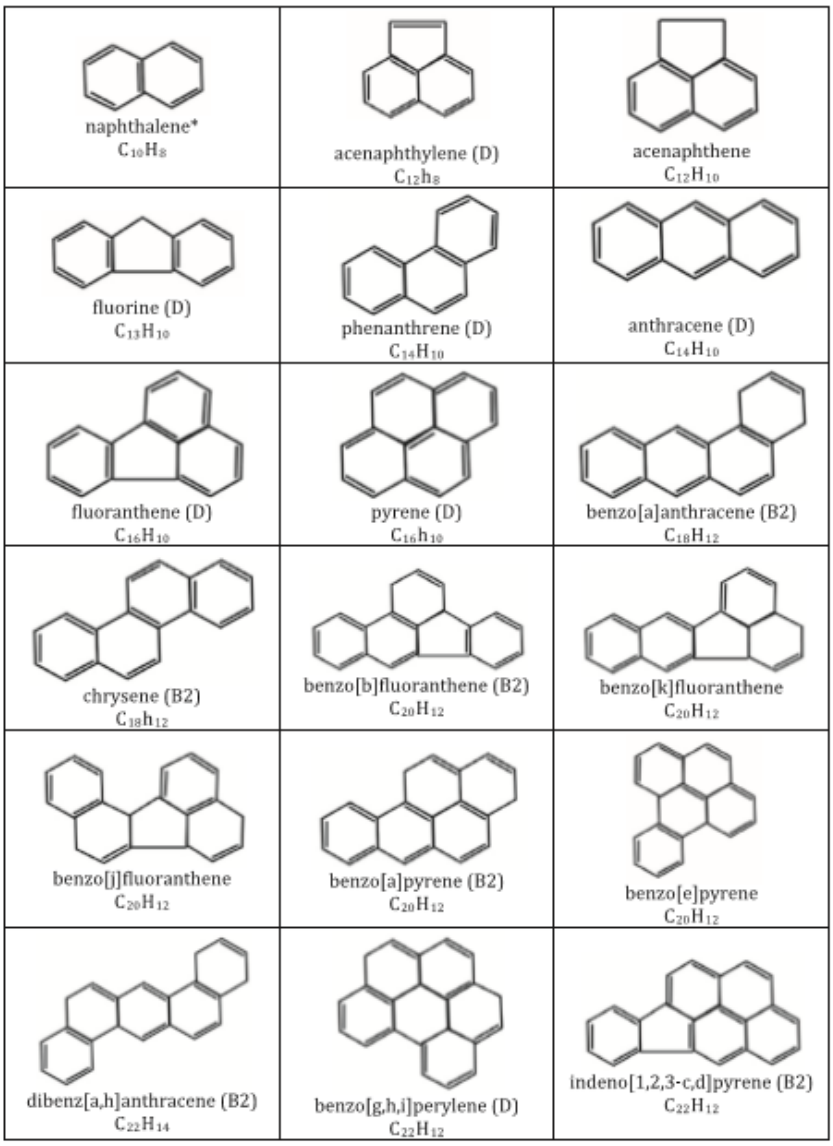


Figure 2.7: Priority list of PAHs (Ravindra et al., 2008). * (not included in priority list); B2 (probable human carcinogen); D (not listed as human carcinogens)

Table 2.2: Priority list of PAHs with carcinogenic classification (Ravindra et al., 2008)

Agency	PAH Compound(s)	Carcinogenic Classification
U.S. Department of Health and Human Services (HHS)	• benz(a)anthracene, • benzo(b)fluoranthene, • benzo(a)pyrene, • dibenz (a, h) anthracene, and • indeno (1,2,3-c, d) pyrene.	Known animal carcinogens
International Agency for Research on Cancer (IARC)	• benz(a)anthracene and • benzo(a)pyrene.	Probably carcinogenic to humans
	• benzo(a)fluoranthene, • benzo(k)fluoranthene, and • ideno (1,2,3-c, d) pyrene.	Possibly carcinogenic to humans
	• anthracene, • benzo (g, h, i) perylene, • benzo(e)pyrene, • chrysene, • fluoranthene, • fluorene, • phenanthrene, and • pyrene.	Not classifiable as to their carcinogenicity to humans
U.S. Environmental Protection Agency (EPA)	• benz(a)anthracene, • benzo(a)pyrene, • benzo(b)fluoranthene, • benzo(k)fluoranthene, • chrysene, • dibenz (a, h) anthracene, and • indeno (1,2,3-c, d) pyrene.	Probable human carcinogens
	• acenaphthylene, • anthracene, • benzo (g, h, i) perylene, • fluoranthene, • fluorene, • phenanthrene, and pyrene.	Not classifiable as to human carcinogenicity

A study has been conducted on a heavy duty DI diesel engine and it has been found that from a collected particulate sample of diesel and biodiesel, that diesel emits high particulate PAH compounds at low load conditions, compared to biodiesel. Most of the larger PAHs such as chrysene, benzo(k)flouranthene, benzo(b)flouranthene and benzo(a)flouranthene have been oxidized by a diesel oxidation catalyst (DOC). Also, it has been reported that flouranthene was present in the particulate though it was not present in diesel. This is evidence that flouranthene has been synthesized inside the combustion chamber (Li et al., 2008). It is reported that the pyro-synthesis process converts PAHs with low molecular weight to larger molecular weight PAHs; in addition to the lube oil contribution (Ravindra et al., 2008). Agarwal, A, et al., have assessed the toxicity emissions and health hazard of diesel and biodiesel fuels. The study covered organic carbon (OC), elemental carbon (EC) content, PAHs and particle size distributions (surface area and number), and it was reported that the toxicity of diesel is higher than that of biodiesel (Agarwal[a] et al., 2013).

Ultra-low sulphur diesel (ULSD) and Low sulphur diesel (LSD) have been studied and it was reported that ULSD emits PAH emissions lower than LSD by 8.6% (Lu et al., 2012). In the atmosphere, the primary diesel emissions could be transformed physically and chemically as reported by Zielinksa. He concluded that primary diesel exhaust emissions react with ozone, sunlight, NO_x radicals and OH radicals. Primary diesel exhaust monocyclic aromatics react with OH radicals forming several aromatic compounds such as nitro-PAHs, phenols, aromatics aldehydes (Zielinska, 2005). The incomplete combustion forms nitro PAHs inside the engine, which are considered as PAHs' precursors. The OH^- and NO_3^- radical reactions with PAHs could form Nitro-PAHs (Miet et al., 2009).

Heeb et al., 2008 reported that nitro PAHs contribute to the genotoxicity and mutagenicity of diesel particulates. Normally, some fraction of the percentage of the total PM contains PAHs,

as reported by some studies. It shows that the concentration of PAHs in diesel PM is around 0.5% of the total PM emissions. The concentration of a particular PAH varies and depends on engine technology. It varies from 0 to 260 µg/mile; while it is from 1 to more than 10 mg/mile for the total PAHs. In volumetric units, a particular PAH varies from 0 to 100 $\mu g/m^3$ and sometimes reaches 150 $\mu g/m^3$(Majewski and Khair, 2006).

2.4.3 Solid Fractions of PM

Solid fractions emitted from diesel engines are composed of carbon and metallic ash. The carbon fraction primarily consists of elemental carbon, or inorganic carbon. The elemental carbon is not bound with any other elements and it is spread soot or carbon black. The heterogeneous combustion process is responsible for the formation of carbon fractions. The premixed and diffusion flames are a motivated environment for the formation of solid particles' precursors. Metallic ash is also a component of solid fractions of PM. It is a mixture of phosphates, sulphates, oxides of zinc (Zn), calcium (Ca), magnesium (Mg) and other metals that are formed from the engine oil additives inside the combustion chamber or formed by engine wear like oxides of iron (Fe), chromium (Cr), and aluminium (Al) (Majewski and Khair, 2006).

2.4.4 Sulphate Fractions of PM

Sulphate fraction includes water soluble sulphates or SO_4^- ion, but the primary composition is sulphuric acid H_2SO_4. Sulphate particulates are formed during the interaction between water

H_2O and sulphuric acid H_2SO_4. Sulphate particulates are normally formed when the molar ratio of H_2O: H_2SO_4 is 8:3. They exist in the exhaust gas as nuclei particles and they are separated from carbon particles. Nuclei sulphate particles are normally composed of 3000 H_2SO_4 molecules and 8000 H_2O molecules. Sulphate particulates' formations mainly depend on the sulphuric acid H_2SO_4 and water H_2O vapour pressure. These two parameters are functions of: the sulphur level in fuel, the air/fuel ratio, the dilution tunnel's temperature and relative humidity and the fuel's sulphur conversion to SO_3 (Baumgard and Johnson, 1996; Eastwood, 2008).

2.5 Low Temperature Combustion Diesel Engines

2.5.1 Introduction

Among the types of internal combustion, diesel engines offer the advantage of higher thermal efficiency, CO_2 emissions and fuel consumption reductions. Therefore, diesel engines are considered as the common powertrain option for the transportation sector. The disadvantage or drawback of conventional diesel engines is the high level of particulate matter PM and NO_x emissions. Many researchers have shown that there is a correlation of respiratory and cardiovascular issues with suspended ultra-fine particles in the atmosphere (Atkinson et al., 2010; Pope III and Dockery, 2006; Benajes et al., 2012).

Due to high diesel engine emissions, stringent regulations are forcing the auto industries to reduce emissions. Soot in diesel engines forms inside the cylinder in regions with high temperature and local richness. By using exhaust gas recirculation (EGR), the adiabatic flame

temperature could be reduced and that could help in enhancing fuel-air mixture before the start of the combustion (SOC), therefore, low temperature combustion (LTC) is attained (Benajes et al., 2012; Colban, 2007). Premixed charge compression ignition (PCCI) combustion or premixed compression ignition (PCI) combustion and homogenous charge compression ignition (HCCI) combustion are common terms for Low temperature combustion (LTC) (Lilik and Boehman., 2011).

The decoupling of the combustion phasing from the injection timing, where the combustion is dominated by the kinetic chemical reactions, is known as HCCI; while the combustion phasing of PCI is coupled with injection timing. In HCCI, air and fuel are premixed in such a way that as the combustion starts the mixture is almost homogenous with equivalence ratio ϕ lower than 1 everywhere. In a PCI engine, the air-fuel mixture is premixed between the fuel injection and the start of combustion with the existence of regions with an equivalence ratio greater than unity. Figure 2.9 demonstrates the local equivalence ratio ϕ versus local temperature or flame temperature. It is noticed that at local temperature above 2200 K and a lean mixture zone, NO_x forms; while soot forms in a rich mixture zone with a local temperature above 1800 K. It is noticed that conventional diesel combustion intersects soot and NO_x formation zones; while PCCI or PCI and HCCI combustion mechanisms avoid soot and NOx zones and reduce them simultaneously. (Benajes et al., 2012; Soloiu et al., 2013).

In HCCI, controlling the ignition timing is a challenge in the full load range since the charge has an auto-ignition nature. The PCI has the advantage of controlling the combustion phasing by controlling ignition timing via the injection timing control (Kalghatgi et al., 2010).

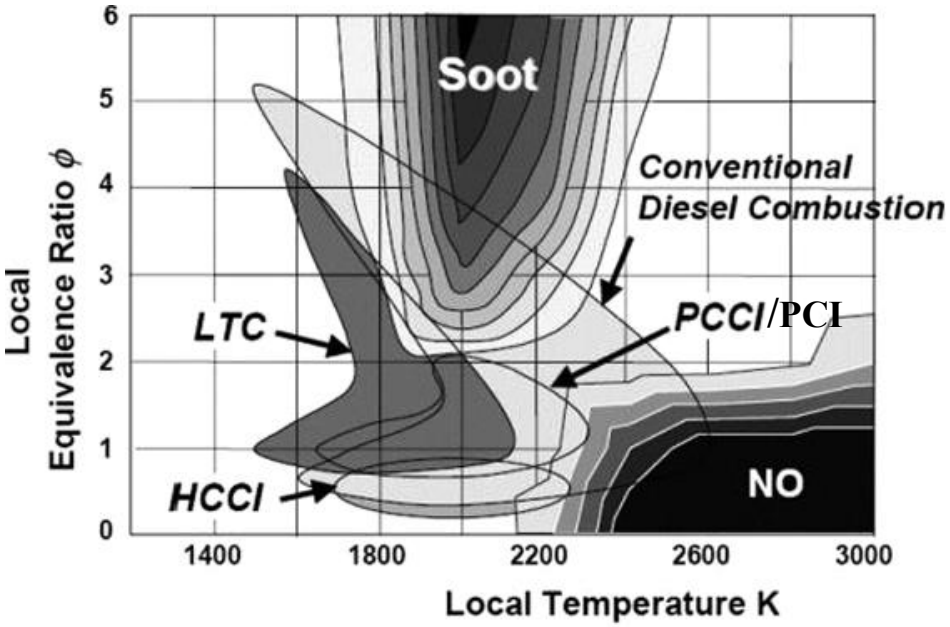


Figure 2.8: Local equivalence ratio versus local temperature with different combustion mechanisms (Soloiu et al., 2013)

2.5.2 Premixed Compression Ignition (PCI) Combustion

Premixed compression ignition (PCI) combustion has evolved from HCCI combustion, to control the start of combustion (SOC). Charge homogeneity in HCCI offers an uncontrollable start of combustion since the charge in the cylinder combusts simultaneously throughout the cylinder generating noise. The PCI process has been introduced to solve such a problem. The charge is not fully homogenous; in other words, it increases the ignition delay via charge motion enhancement, high EGR, reduced compression ratio and higher injection pressure (Imtenan et al., 2014).

The process of PCI combustion starts by injecting the fuel inside the cylinder through three ways: port fuel injection, advance direct injection and late direct injection. Port fuel and advance direct injections increase the hydrocarbon (HC) and carbon monoxide (CO) since these injections create fuel-wall impingement and incomplete fuel evaporation. However,

EGR and narrow spray angle injectors could reduce the fuel-wall impingement (Boot et al., 2010; Han et al., 2009; Fang et al., 2008, Imtenan et al., 2014).

Researchers have conducted several experiments to increase high load limits in PCI and reduce emissions. They reported that fuel properties, fuel additives, multiple injections, variable valve timings and fuel -air mixture enhancement can increase load and reduce emissions (Kawamoto et al., 2004; Imtenan et al., 2014; Kook and Bae, 2004; Fang et al., 2009).

A new approach of PCI has been introduced which starts by using a split injections strategy: early direct injection followed by late direct injection (pulsed at compression stroke). This strategy governs the ignition onset. The early injection stratifies with air inside the cylinder and as the piston reaches near top centre TDC (compression stroke), it creates HCCI like conditions. When the late direct injection happens before TDC, the area of fuel rich from the late direct injection burns before the lean fuel mixture. This variability of fuel-air mixture avoids an instant ignition of the whole charge and provides combustion phase control. Also, usage of high EGR provides longer ignition delay, which in turn, promotes or enhances fuel-air mixing. This results in fewer pockets of fuel–rich, followed by low temperature combustion that reduces the soot and NO_x level (Imtenan et al., 2014; Inagaki et al., 2006).

2.5.3 NOx Emissions from PCI Combustion

The emission of NOx is reduced by a premixed or leaner mixture with EGR moderation usage. The EGR obstructs the oxygen (O_2) flow rate into the cylinder which results in a reduction of the local temperature or flame temperature. Also, it increases ignition delay,

which in turn delays the start of combustion (SOC) and lowers the rise of pressure and temperature during combustion (Agarwal et al., 2015). Different blends of fuels with a lower cetane number (CN), higher volatility and higher auto-ignition resistance than diesel fuels, have been tested in PCI combustion mode. The fuels were 20% and 40% of n-butanol blended with diesel. It is reported that at higher injection pressure and along with EGR usage, the air-fuel mixture has been enhanced and there was sufficient ignition delay before the combustion commencement. This resulted in lower NO_x and the longer ignition delay is attributed to the lower CN of n-butanol (Valentino et al., 2012).

At the University of Birmingham, it is has been found that using a lower cetane number (CN) fuel such as gasoline blended in diesel in a ratio of 50:50,, named as dieseline fuel, has produced very low NOx (0.40 g/kWh) by using a large amount of EGR (Zhang et al., 2012). Late direct injection can also elongate the ignition delay to reach PCI combustion. It is reported that with injection retardation along with EGR usage, the NO_x level decreased (Jacobs and Assanis, 2007; Bittle et al., 2010).

2.5.4 Particulate Matter (PM) Emissions from PCI Combustion

Attaining PCI combustion reduces the formation of larger soot aggregate (accumulation mode particles) emissions and NO_x simultaneously. It is reported by Kittelson that the reduction of larger particles reduces the available sites on the surface area of the particles where the volatile materials can condense heterogeneously once the exhaust cools down. The reduction of sites forces volatile materials to condense or nucleate into smaller particles (Kittelson, 1998).

In LTC combustion, the formation of soot happens downstream in the jet head, in contrast to conventional diesel jets where it occurs in the upstream soot producing core (Dec, 1997; Imtenan et al., 2014). This shift of soot formation is attributed to the dilution of charge and mixing enhancement between injection end and ignition of the second stage (Idicheria and Pickett, 2005). Some researchers reported that the emitted PM from PCI combustion has lower PM mass compared to conventional diesel combustion, but it has a high number of particles (depends on EGR ratio, injection pressure) (Payri et al., 2011; Raatz and Mueller, 2001; Kolodziej et al., 2007).

In PCI combustion, it is reported that by late injection of fuel and with 48% of EGR, PM emissions decreased (Han et al., 2009). It was also observed by Alriksson and Denbratt that soot decreased rapidly with 50% of EGR then soot (Alriksson and Denbratt, 2006). In a heavy duty optical diesel engine with late injection, a study of the effect of spray aiming soot emissions has been conducted. Fuel vapour concentration was measured by Toluene (fuel tracer) fluorescence and the measured PAH fluorescence, combined with formaldehyde and OH to evaluate mixing, combustion and pollutants' formation. It has been observed the spray pattern with angle 152 degree created a wall impingement, since the fuel was injected towards the piston bowl's centre. It was also observed that near the piston bowl's floor the interaction of jet-jet generated regions of rich fuel and these regions are considered as the main sources of poly aromatic hydrocarbons (PAHs, soot precursor). It is concluded that a narrow injection of 124° or 160° can avoid fuel wall impingement and generated rich regions. (Genzale et al., 2009).

2.5.5 Effect of Injection Strategies on PM emissions

It has been discussed that attaining PCI combustion needs a low combustion temperature with low oxygen concentration, with the introduction of EGR and fuel advancing, or by retarding injection timings. It is reported by Jacobs and Assanis that a great low soot (0.03FSN) when the experiment was conducted with injected fuel at 25° BTDC with an air-fuel ratio lower than stoichiometric (14.7). Although the air-fuel ratio was lower than 14.7, which is considered as a rich mixture, the soot decreased. This gives an indication that in PCI combustion, net release of soot has little sensitivity to local equivalence ratio ϕ (Jacobs and Assanis, 2007). It is also reported that by advancing injection timing with extensive EGR PM emissions decreased by 50% compared to conventional diesel combustion. The soluble organic fractions (SOF) increased with the small size of the PM (Parks et al., 2010).

Advancing injection timing controls local equivalence ratio and ignition delay. So, increasing the injection delay with a higher value of equivalence ratio should reduce PM emissions with advancing injection timing. An opposite observation was reported by (Benajes et al., 2012). They conducted a PN emissions' study in PCI combustion with advancing injection timing. They observed that with advancing injection timing, PM emissions increased drastically. PM emissions were an increment of 185% when the injection timing advanced from -30° ATDC to -33°, although the injected fuel occurred before the start of the combustion in PCI mode. The drastic increase of PM was attributed to deposition of the fuel on the piston bowl's surface. As the fuel was injected in advance, the trajectory of the fuel was at a higher point and it crossed the surface of the piston bowl. This trajectory of fuel caused the liquid fuel spray to increase; hence more fuel was deposited on the piston bowl's surface.

Dual fuel injection strategies have been investigated and a study was conducted by (Singh et al., 2007). At low load condition, where fuel is premixed well, the first injected fuel was at 22° BTDC. A cool flame heat release occurred at early injection timing followed by second stage combustion. The formation of soot was low since the fuel was premixed well and there were less fuel-rich pockets. The second injected fuel was at 15° BTDC. Mixed controlled combustion happened since at late injection timing this combustion behaves like conventional diesel combustion. This resulted in less soot. At the University of Birmingham, a study was conducted on a light duty 2.2 litre, four cylinder diesel engine, fuelled with dieseline (50% gasoline/50% diesel). The split injections were investigated and it was concluded that the large sized particles had been reduced: the smoke number by 90% and the particles' mean diameter was reduced by 23.8 nm (Rezaei et al., 2013).

22.5.6 Fuel Auto-Ignition Quality and Volatility in a PCI Engine

Diesel fuel's auto-ignition quality is determined by its cetane number (CN). The higher the cetane number, the quick the combustion starts; and it is measured by comparing the ignition characteristics of a fuel with reference fuels in a cooperative fuel research (CFR) engine, using standard method ASTM D613. Volatility or distillation characteristics are the tendency of fuel to vaporize and are related to fuel vapour pressure; and they are also important for the fuel performance and safety. The volatility of the fuel is determined by the distillation at atmospheric pressure using standard method ASTM D86 (Kalghatgi, 2014).

Conventional diesel fuel has a high auto-ignition quality and low volatility. This property is not favoured in PCI combustion since the fuel combusts quickly as there is not sufficient time

for the air and fuel to be well mixed. Also, this property puts a limitation on the operating range. However, conventional diesel fuels can be run in PCI at low loads only if the used fuels have a cetane number (CN) ranging from 40 to 60 with low ignition delays (IDs). Over this range, there is a small difference in IDs and also only a small effect from the CN on the combustion phase, unless the operating conditions change e.g. higher EGR ratio or lower compression ratio (CR).

Fuels with high volatilities and lower CN have the potential to run a diesel engine in the PCI combustion mode (Kalghatgi, 2014). A fuel with CN of 24 has been carried out in a single cylinder research diesel engine running at different engine speeds and loads. It was reported that the emitted smoke was almost zero and it was also concluded that in terms of smoke reduction, the effect of fuel auto-ignition is more significant than fuel volatility in PCI combustion and in the case of low CN (Kalghatgi et al., 2010; Hildingsson et al., 2010).

An investigation in optical diesel engine running in a PCI combustion was carried out and studied the effect of fuels' volatility on early injection. The fuels' volatility was varied, while the auto-ignition quality was preserved as constant. It was concluded that a fuel with higher volatility and at an injection timing earlier than 30° BTDC produces fewer smoke emissions and less fuel wall impingement (Cheng et al., 2010).Four different fuels: D1, n-heptane, F1 and D2 with CNs (56, 54, 44.5 and 39.6 respectively) with different volatilities and with diesel auto-ignition range have been tested in PCI combustion mode at a speed of 1200 rpm, with no EGR, at load 4 IMEP and injection pressure 650 bar. It was concluded that fuel D1 has lower smoke since it has higher ignition delay and this allows the fuel to be better mixed with air. Fuels F1 and n-heptane have the lowest smoke emissions or negligible smoke emissions. They are more volatile than D1 and D2 and this would provide better mixing with air. Also these two fuels F1 and n-heptane have no aromatics and this give an indication that

the aromatics' level can affect NOx or soot formation (Kalghatgi et al., 2010; Hildingsson et al., 2010).

2.5.7 Dieseline Fuelled Premixed or Partially Premixed CI engines

As discussed previously, there are several ways to reach PCI combustion, such as advancing injection timing, increasing the EGR level, reducing the compression ratio, increasing the injection pressure. There is one more way relating to the alteration of fuel properties. It has been proven that fuels with higher volatilities, lower cetane number (CN < 30) and research octane number (RON > 60) are suitable for PCI combustion (Kalghatgi et al., 2007; Risberg et al., 2006).

Gasoline and diesel are the most commonly used fuels and available in markets abundantly. The concept of blending gasoline fuel into diesel is called "dieseline". It was given this name by Professor Hongming Xu at the University of Birmingham. The idea behind blending gasoline into diesel is to alter fuel properties. Gasoline has a high octane number (~ 90 – 100) and this property does not ignite fuel eagerly. Diesel fuel has a high cetane number CN (~ 50 – 60) and this property ignites fuel easily. Dieseline has a mixture of both fuels and so is favourable in PCI combustion since the properties have been changed.

Researchers at the University of Birmingham have conducted experiments on a 2.2 litre, four cylinder, fuelled with dieseline, light duty diesel engine run in the PCI combustion mode and they investigated the effect of the dieseline fuel (50 % gasoline: 50% diesel) on PM emissions. It was concluded that running the engine at 1800 rpm with load 3 bar BMEP and increasing EGR up to 50%, the particle size distribution had a bimodal shape; the total

particle number concentration was reduced by 95%; and the count median diameter (CMD) reduced by 50 %.

Advancing injection timing can reduce particle number PN effectively. It was stated that advancing the injection timing from 23° to 28° BTDC with an EGR ratio 50%, the larger sized particles (accumulation mode) were reduced compared to conventional diesel combustion. In contrast, the number of small sized particles (nucleation mode) was increased as a result of fuel impingement on the walls of the cylinders; but the general observation was the total particle number concentration was reduced by 99% and even the smoke decreased to almost zero (Zhang et al.,2012). Prikhodko et al. have investigated the effect of dieseline on PM emissions by using a light duty diesel engine operating with diesel direct injection and gasoline port fuel injection, or as it is called, dual fuel or Reactivity Controlled Compression Ignition (RCCI). It is reported that the particle size distribution was bimodal and PM mass emissions were low, similar to dieseline fuelled PPCI where the fuels were blended offline. Therefore, it produces fewer larger sized particles and the particle number concentrations were also lower, as much as two orders of magnitude, compared to conventional diesel combustion (Prikhodko et al., 2010, 2011).

In this thesis, the particle size number distribution and chemical compositions will be investigated deeper and wider in dieseline fuelled PCI (offline blending).

2.5.8 Gasoline Compression Ignition (GCI) engines

Gasoline compression ignition (GCI) offers the possibility of reducing PM and NO_x emissions with low fuel consumption and its achievement is extremely dependent on the injection of

gasoline or gasoline-like fuels near top dead centre (TDC). In other words, it is PCI combustion but with low octane fuels. Low octane fuel has a higher auto-ignition quality and higher volatility. The effect of the fuel's properties has been studied in gasoline PCI or GCI at 4 and 10 bar IMEP with EGR sweeps. The fuels used are diesel and four gasolines with different ON (91, 84, 78 and 74). It is stated that at low load, diesel fuel demonstrated a high smoke number, 2 FSN, when using 50% EGR, compared to the other four gasolines; while the four gasolines showed a similar trend of soot (almost zero) and NO_x, but at high load, 10 bar IMEP, all fuels demonstrated a similar trend of NO_x emissions. It is also concluded by Gautam that the best fuels for gasoline fuelled PCI or GCI are fuels with an octane number between 75 and 85, as long as the layout of the engine is kept constant (Hildingsson et al., 2009, 2010).

In Gautam's GCI or gasoline PCI concept, as a function of fuel ignitability rather than volatility and as the combustion starts after the injection end, as long as the ignition delay and combustion phasing of fuels are matched, regardless of fuel composition and volatility, the emissions of soot and NO_x are the same. Also, Gautam concluded that increasing aromatic content in fuel will increase the operating range (upper load limit); since aromatic fuels are more resistant to auto-ignition compared to paraffinic fuels, as the temperature is kept constant while increasing the pressure (Kalghatgi, 2005; Kalghatgi et al., 2010). Researchers at Lund University stated that the gasoline PCI concept is that NO_x and soot could be avoided simultaneously as long as the fuel has a gasoline boiling range and a correct combination of EGR and lambda ʎ, though the combustion could start during injection (Kalghatgi, 2005; Hildingsson et al., 2010). A study was conducted on gasoline PPCI or GCI in a single cylinder Scania D12 running at 1200 rpm, CR 14, up to 14 bar IMEP, single injection and 25% EGR. It is concluded that the engine produced 46% indicated efficiency and emitted smoke 0.36 FSN and 1.21 g/kWh of NO_x (Risberg et al., 2006).

Double or triple injection strategies can produce acceptable efficiency with low smoke and NO_x at high loads, by reducing the peak pressure rise rate. A recent study was carried out about characterizing gasoline PCI performance and showed that gasoline PCI could be operated near 18 bar IMEP via a triple injection strategy. It is reported that triple injection reduced NOx and PM emissions and low specific fuel consumption (180 g/kWh) with less pressure rise rate < 10 bar per crank angle degree (Ra et al., 2011, 2012). Another study conducted by Delphi Corporation investigated gasoline PCI at 6 bar IMEP with triple injection strategy and it is reported that triple injection reduced NOx, smoke and fuel consumption compared to single and double injections (Sellnau et al., 2011). Many recent studies have been conducted using multiple injection strategy at medium and high loads using gasoline PCI, as seen in the referenced papers (Manente et al., 2009; Hanson et al., 2009; Sellnau et al., 2011, 2012).

Many researched have been investigated the effect of operating conditions like speed, loads and injections on smoke and NOx. A study was carried out using gasoline PCI or GCI operating at different speeds and loads from 2 bar to 18 bar IMEP and it is reported that the smoke was decreased less than 0.01 FSN and NOx less than 0.2 g/kWh (Sellnau et al., 2012). Another study was conducted on a GCI combustion engine running at different speeds, loads and injection timings to investigate PM emissions. It is reported that at low load conditions (5.5 bar IMEP) PM emissions consisted of 30 % of soot aggregates with an average diameter of 40 nm (elemental carbon to organic carbon ratio is 55:43 by weight) and 70% of organic particles. At high load conditions (14 bar IMEP) all particles were mainly soot aggregates > 98% with an average diameter of 25 nm (Zelenyuk et al., 2014).

In this thesis, the particle size number distribution and chemical compositions will be investigated deeper and wider in gasoline-like fuel used with PCI/PPCI or GCI.

2.6 Summary

This chapter discusses PM compositions, the fundamentals of soot formation and processes and its measurement techniques. Also, it reviews the latest conducted studies and the progress in research in the area of low temperature combustion (LTC), namely, PCI engines. The focus on PCI is about utilizing the low octane fuels and the effect of operating conditions on NOx and soot emissions is investigated. This review introduces a strong motivation to investigate the utilization of low octane fuels like dieseline.

CHAPTER 3

EXPERIMENT SETUP

33.1 Engine Test Cell

The engine test cell was re-commissioned by the author and the author's colleague Soheil Zeraati Rezaei. This chapter discusses the equipment that has been used to conduct all the experiments. It covers the engine specifications, engine dynamometer and emission equipment. Figure 3.1 demonstrates an overview of the test cell.

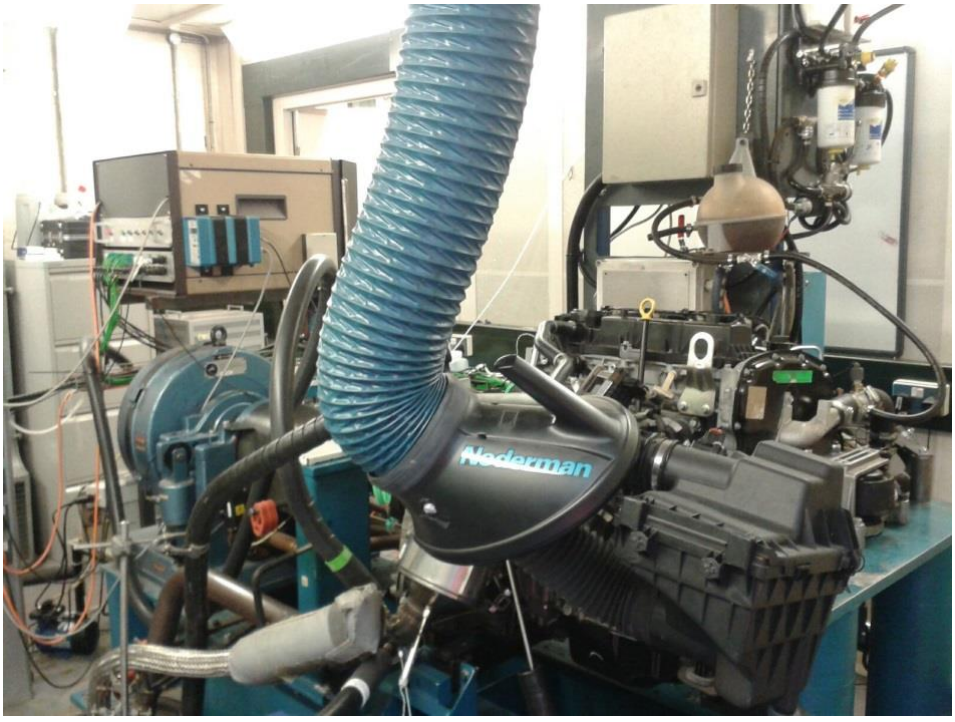


Figure 3.1: Overview of engine test cell

3.1.1 Engine

The experiments have been conducted using a 2.2 L, four cylinder Ford Puma engine, equipped with a variable nozzle turbocharger (VNT) and common rail direct injection, and controlled by an open engine control unit (ECU). The engine coolant temperature was adjusted by a thermal controller and it was between 90 ±1 °C. The EGR cooler was deactivated to introduce hot EGR to increase the intake manifold temperature for G75 and naphtha fuels; but for diesel, cold EGR was introduced as discussed in section 5.1. Engine combustion air temperature was at room temperature of 25°C. The compression ratio of the engine is preserved as it is introduced to the auto market: 15.5:1. The tests were conducted at steady state. A schematic drawing of the engine test cell is presented in Figure 3.2. The engine specifications are presented in Table 3.1.

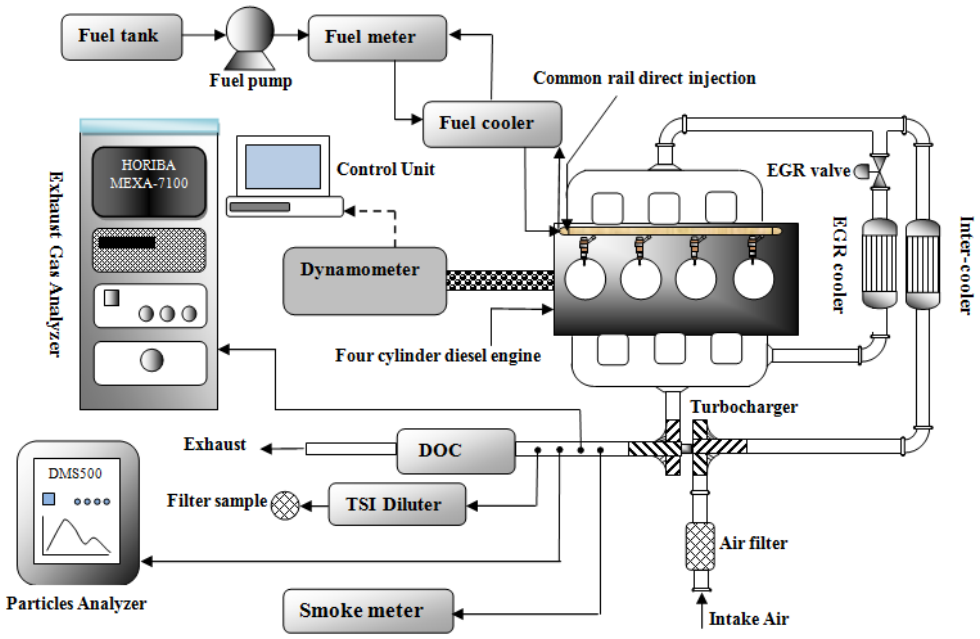


Figure 3.2: Schematic drawing of the engine test cell

Table 3.1: Puma engine specifications

Bore	86 mm
Stroke	94.6mm
Injection System	Common Rail system
Engine Capacity	2198 cc
Compression ratio	15.5

3.1.2 Dynamometer

An eddy current dynamometer was used which was manufactured by Froude Consine Ltd. It has a closed loop cooling system using laboratory water. The dynamometer controller has two modes: speed and torque modes. By settling the speed manually, the engine speed will accelerate to the settled speed if the fuel flow rate is increased by using the open engine control unit (ECU). By increasing the fuel flow rate further, the engine torque will increase. In this study, the speed was fixed at 1800 rpm, while the torque was varied based on the designed test matrix. A full description of the dynamometer can be found in our colleague Zhang Jun's PhD thesis (Zhang, J. 2011).

3.1.3 Engine Control

The engine controller was an open engine control unit (ECU) produced by the Pi-Innovo company. It has ATI VISION which can control accurately and independently the operating parameters of the engine. It can control the injection timing, pressure and duration. The injection pulses could be up to six in each engine cycle. It can also control the EGR valve position and VNT angles. (Pi-Innovov generic user guide, 2013).

3.1.4 Fuel Metering

Fuel metering or consumption was measured by using an AVL733S while the fuel cooling system was an AVL752. The measuring duration for repeatable fuel consumption was set to 180 seconds for diesel, G75 and naphtha fuels. The longer duration of fuel consumption measurement is very helpful for G75 and naphtha fuels, since they have higher vapour pressure and lower boiling points compared to diesel fuel.

3.1.5 Test Fuels

Three types of fuels have been used in the experiments. They are diesel fuel, dieseline fuel and naphtha fuel. The diesel fuel was European standard diesel (EN590), while the dieseline fuel was a blend of gasoline with research octane number RON 95 (ULG95) in diesel fuel. The ratio of gasoline fuel to diesel fuel was 75:25 by volume and it has been named as G75 fuel. The diesel and gasoline fuels were provided by Shell Global Solutions, UK. The naphtha fuel was provided by CORYTON Advanced Fuels Company, UK. Naphtha is a generic term used in refinery plants. It is the overhead liquid product or cut obtained from the atmospheric distillation unit as shown in Figure 3.3.

Naphtha is also obtained from other processes like catalytic, hydrocracking, cracking and coking processes. Naphtha's composition varies and depends on the crude oil type and the processing unit, whether it is obtained from an atmospheric distillation unit or other units. There are two types of naphtha: light naphtha and heavy naphtha and they differ based on

their boiling range. In this study, light naphtha has been used in the experiments. In the following chapters the term, naphtha, will be used instead of light naphtha. Table 3.2 presents the fuel properties of the tested fuels. For G75 and naphtha fuels, a lubricant of Infineum R655 was added (300 ppm by volume).

Table 3.2: Fuel properties (~ represents an estimation value)

Property	**Unit**	**Diesel**	**Dieseline (G75)**	**Naphtha**
Density @15°C	Kg/m^3	845	768	742
Viscosity@40°C	mm^2/s	2.9	/	0.6612
Sulphur Content	mg/kg	Max 10	7.1	<0.1
Residue	%(v/v)	/	1.4	/
RON		/	~75	74.5
Derived Cetane Number DCN		51	30	27
Lubricity	µm	460	365	/
Distillation (IPB)	°C	150	37.2	39
Distillation (FPB)	°C	352	326.4	192.5
Aromatics	%,(v/v)	/	32.8	18
Net calorific value	MJ/kg	42.5	43.01	43.86

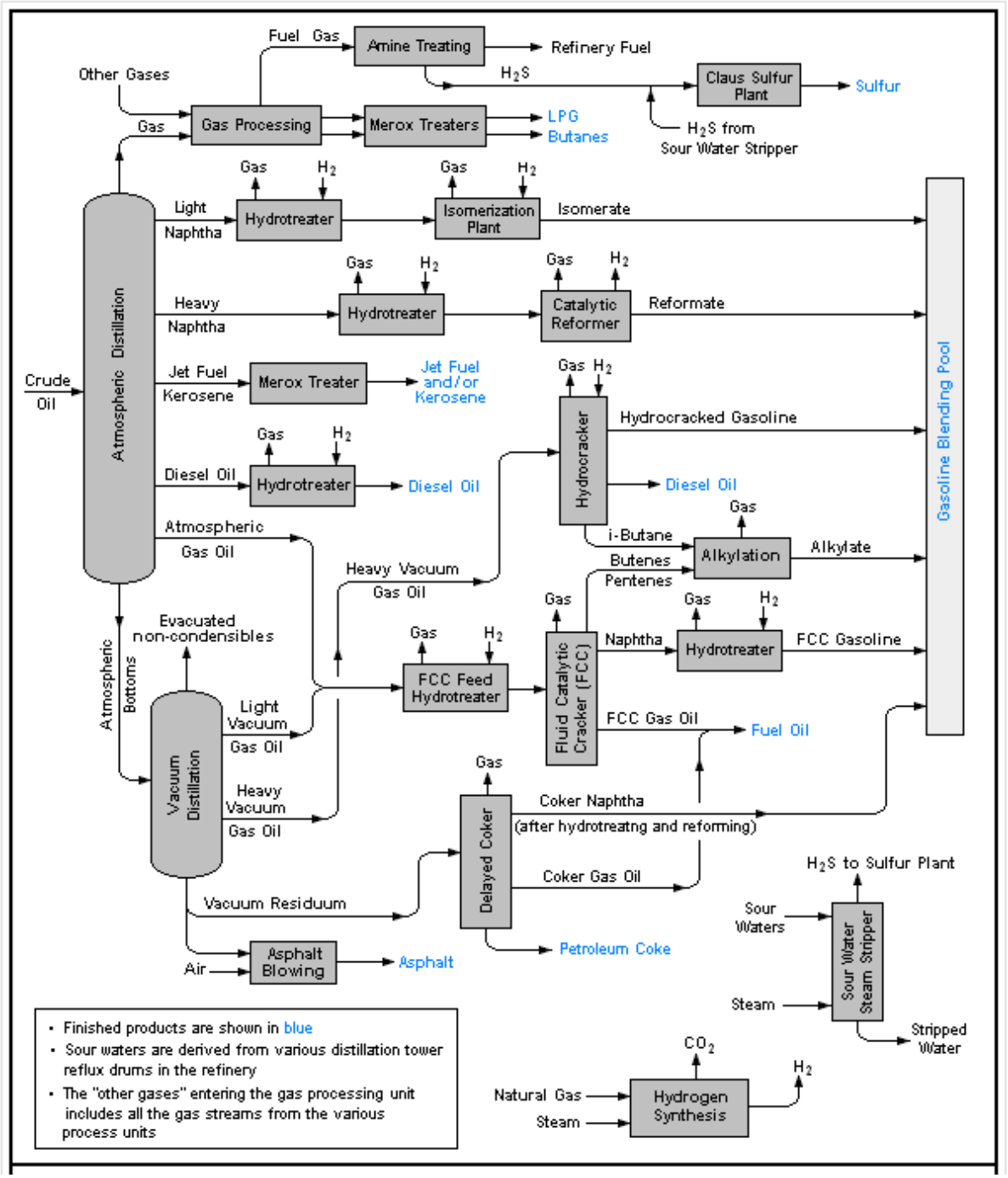


Figure 3.3: Refinery process diagram (Gary and Handwerk, 1984)

3.1.6 Pressure Data Acquisition

A Kistler quartz pressure sensor (type 6056A42) as shown in Figure 3.4 (a) with glow plug adaptor (type 6542Q18X2) was installed in the first cylinder for in-cylinder pressure measurement. A shaft encoder from AMI Elektronik (type A500/016) was aligned with the engine crank shaft via stainless steel flexible beam coupling. The charge amplifier (type 5011B10Y50) as shown in Figure 3.4 (b) converts the produced electrical charge by the pressure sensor to proportional voltage signals. Then, the signal can be recorded via a National Instrument PC16251 at every crank angle. The shaft encoder generates two different pulses. One pulse is generated to identify every crank angle degree and the other pulse is generated every revolution combined with a camshaft pulse to trigger in-cylinder pressure measurement. The acquired pressure data was averaged for 200 cycles. The detailed specifications of the Kistler pressure sensor, PC16251 and shaft encoder can be found in Zhang Jun's PhD thesis (Zhang, J. 2011).



(a) (b)

Figure 3.4: (a) Charger amplifier (b) Kistler pressure sensor

3.2 Exhaust Measurement Instruments

3.2.1 Engine Exhaust Gas Emissions' Measurement

The gaseous emissions e.g. O_2, CO, HC, NO_X, and EGR ratio (by measuring the concentrations of CO_2 in the intake and exhaust simultaneously) were measured by using A MEXA-700EGR analyser. A solenoid valve system (SVS) receives calibration gases and then sends them to the analyser rack (ANR) and oven unit (OVN) respectively. In the ANR, there are analysers for each gas. The exhaust gas is sampled from the engine via a heated line at 190°C in order to prevent the condensation of water and HCs. The hydrocarbon concentrations are measured by using the flame ionization detection (FID) method where the HCs are passed to hydrogen flame. In the hydrogen flame, heat energy generates ions and the ions are proportional to the carbon atoms number in the sample.

The concentration of carbon monoxide (CO) is measured by using a non-dispersive infrared (NDIR) method. A molecule has different atoms and at specific wavelengths absorbs infrared energy. At constant pressure, the concentration of CO is proportional to the degree of absorption. The concentration of NO_x is measured by the chemiluminescence (CLD) method. In this method, NO is oxidized to NO_2 in a reactor when it is mixed with O_3. Part of the produced NO_2 is in an excited state and it emits or releases energy in the form of light once it returns to the ground state. Thus, the amount of light can be used to measure the concentration. The concentration of O_2 is measured by using a magneto-pneumatic detection (MPD) method. In this method, the gas flows through a magnetic field; oxygen has a greater

response compared to other gases and the change of pressure is as shown by the O_2 concentration.

3.2.2 Smoke Meter

The smoke or soot concentration in an engine's exhaust was measured by using an AVL smoke meter 415SG002 (specification is presented in Table 3.3). The principle of the smoke meter is as the following: a sample of gas exhaust is taken via a probe, passes through an exhaust gas line and is sucked through a filter paper. A reflectometer is used to measure the blackening of the filter paper and the output as a filter smoke number (FSN). The range of FSN is from (0 to 10). Zero means a clean filter or unloaded while 10 means fully loaded (filter is black).

Table 3.3: Specification of AVL smoke meter 415SG002

Measurement Range	FSN:0-10 Soot conenctration:0-32000 mg/m3 Pollution level :0-100%
Resolution	0.001 FSN, 0.01 mg/m3 , 0.01%
Repeatability	$\sigma \leq \pm$(0.005FSN+3% of measurement value
Exhaust Gas Back Pressure	-100 –400 mbar
Permissible exhaust temperature at sampling point	600 °C

3.2.3 DMS500

The particle number-size distribution was measured by using a combustion DMS500 (differential mobility sizer) as shown in Figure 3.5. The DMS500 dilution system undergoes two stages as shown in Figure 3.6: the first stage is the dilution ratio, where the exhaust gas is sampled at 150 °C through a heated line and diluted by cleaned compressed air (3-6 bar) to avoid the condensation of particles in the sample line and then diluted with a fixed dilution ratio 5:1. In the second stage the dilution ratio was varied via a rotary disk to keep the particle concentration at a suitable range.



Figure 3.5: Combustion DMS500 (differential mobility sizer)

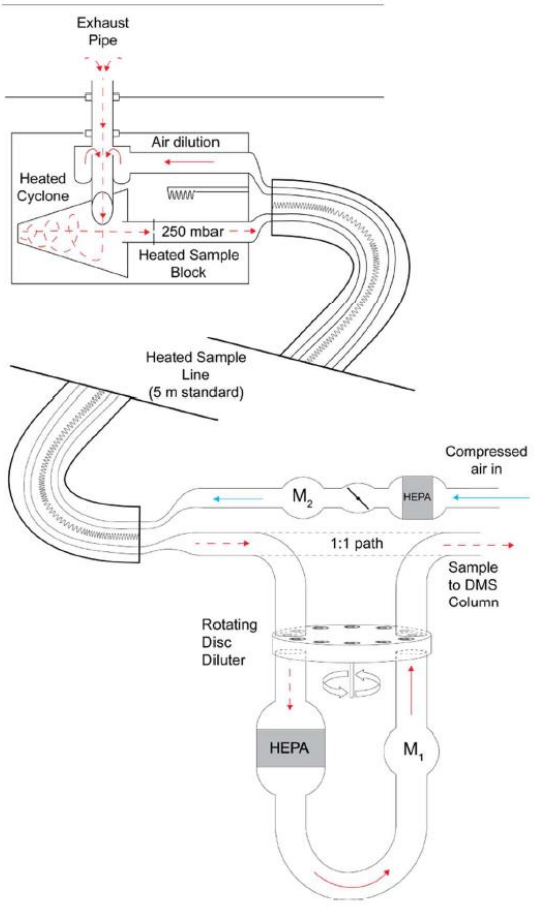


Figure 3.6: Two stage-dilution system of DMS500 (DMS500 user manual, version 4.03, pg.19)

The classifier as shown in Figure 3.7 separates the charged particles according to their electrical mobility and operates at 0.25 bar absolute for the (5-1000 nm range) with an external vacuum pump. Before the particles enter the classifier, they are positively charged. Then, they flow within a particle-free sheath flow. The high voltage is applied to the central electrode. The charged particles are deflected by the high voltages towards the electrometer rings. Particles with lower drag and higher charge will be deflected more and land on the electrometer rings and will remain there until cleaning takes place (DMS500 user manual, 2015).

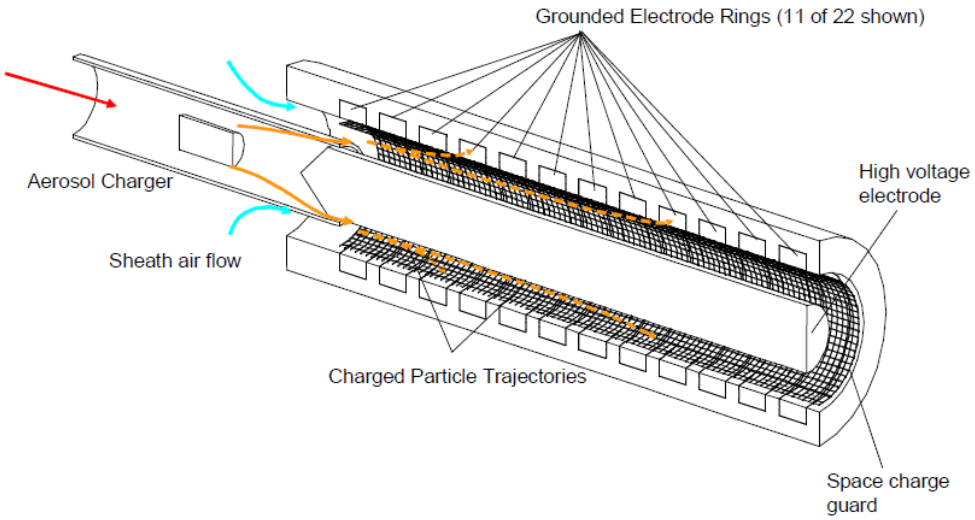


Figure 3.7: DMS500 classifier (DMS500 user manual, version 4.03, pg.119)

3.2.4 Diluter

A TSI diluter model 3302A with a dilution ratio variation was used to conduct the experiments. The diluter was modified by using two HEPA filters and a moisture trap in order to obtain cleaned compressed air as shown in Figure 3.8. The undiluted exhaust gas is drawn via a heated line at a temperature of 190 °C and with an isokinetic sample probe with multi-holes as shown in Figure 3.9. The number of holes in a given row and the number of rows in the sample probe have an effect on the mass flow rate distribution between the holes as reported by (Zhang et al., 2013). It was found that reducing both the number of holes in each row and the number of rows of the sample probe reduced the measurement errors from 45 % to 10 %. It was reported that bends or non-straight sections before the sample collection may create inhomogeneity of the particle concentration cross section of the exhaust

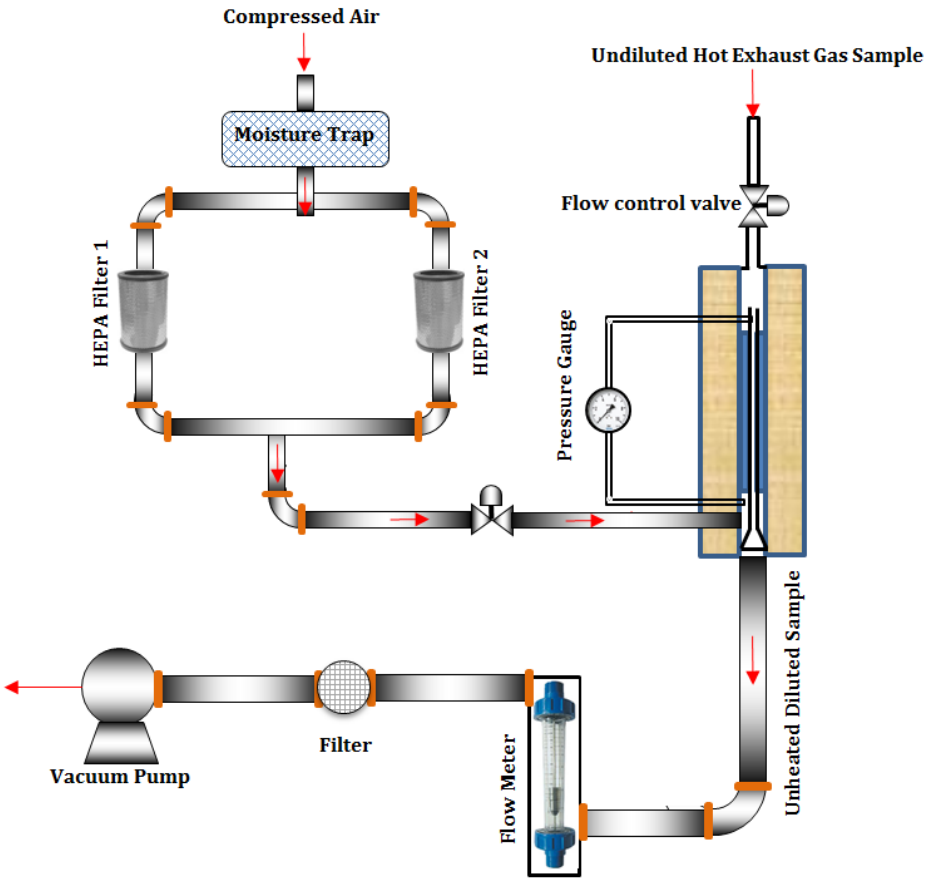


Figure 3.8: Schematic drawing of the diluter



Figure 3.9: Sample probes

pipe; so a multi-holes sample probe is recommended (Giechaskiel et al., 2012). The undiluted hot exhaust gas is then diluted with cleaned compressed air at ambient temperature. The dilution ratio (DR) is adjusted by the nitric oxide (NO) measurement before and after the dilution system. A vacuum pump was used to create a flow rate, which was fixed at 10 l/min.

3.2.5 Filter Paper and Sample Extraction

The diluted emitted particulates from the diesel engine were collected through two types of filters: a glass microfiber filter (GF/F, 47 mm, Whatman and 450 µm of thickness) and quartz filter substrates (Whatman, 47 mm, and 450 µm of thickness). Glass microfiber filters were only used for the screen tests that are discussed in Chapter 4. The samples were collected using a filter holder assembly which was downstream of a modified TSI diluter (model 3302A), at a temperature lower than 52°C and for a predetermined time and dilution ratio, which are discussed in Chapters 4, 5 and 6. Figure 3.10 presents the quartz filter papers used for diesel, G75 and naphtha fuels.



Figure 3.10: Filter papers with deposits for diesel, G75 and naphtha fuels

3.2.6 Sample Extraction

Before loading, the filter papers (quartz filter) were first preheated to 500°C to remove any contaminations like ash or organic species. After the collection, the filter papers containing the deposits were wrapped in aluminium foil to avoid light exposure and were prepared for extractions and offline analyses.

3.2.6.1 Extraction Method for Trace Metals

Trace metals were extracted from the loaded filter papers by using the USEPA, MESW-846, and 3015A methods; where the metals are extracted using a hot plate digestion method. One square centimetre of the filter paper with the deposits was put into an inter bottle and 15 ml of concentrated HNO_3 (high purity) was added into the bottle. In less than 5 min, the temperature of each sample was increased to 175°C and maintained at 175°C for about 4 min. After digestion, the extracts were taken and filtered via the Whatman 541, 22µm in thickness. The extracts were then diluted to 20ml with distilled water and transferred to inert bottles. Then, the sample extracts were ready for analyses in the ICP-OES as discussed in section 3.3.2.

3.2.6.2 Extraction Method for GC-MS

The filter papers with deposits were placed in laboratory glass containers cleaned with dichloromethane (DCM purity 100%). For quantification, the filter papers were spiked with 50µl of 1ng/µl of deuterated internal standards. Then, 15 ml of DCM was added into the glass

containers and ultra-sonicated in a water bath for 20 min at 20°C to homogenize the samples. The extracts were passed through pipettes with glass wool and sodium sulphate anhydrous in order to remove moisture and particles respectively. The extracts were then concentrated under nitrogen flow to 2ml. The extracts were transferred to amber vials and 50 µl of nonane was injected into them. Finally, the extracts were concentrated to 50 µl and prepared for both GC-MS and GCXGC-ToF-MS analyses as discussed in sections 3.3.3 and 3.3.4 (Alam[a] et al., 2016).

3.3 Analytical Measurement Instruments

3.3.1 Elemental Carbon (EC) and Organic Carbon (OC)

Sunset Lab Inc equipment was used for measuring total carbon (TC), organic carbon (OC) and elemental carbon (EC). It is a National Institute for Occupational Safety and Health (NIOSH) recognized method. It works on the principal of placing a punched standard sized ($1cm^2$) sample from the collected filter in an oven, which has been already purged with helium gas. The oven temperature increases from 0°C to 850 °C by stepped temperature ramps and increases thermally desorbing pyrolysis products and organic compounds (OC) into a manganese dioxide (MnO_2) oxidizing oven. Quantitatively, the flow of the carbon fragments through the MnO_2 oxidizing oven converts to CO_2 gas. Along with the helium stream, the CO_2 gas is swept out of the MnO_2 oxidizing oven and mixed with hydrogen gas and then the mixtures quantitatively convert to methane after flowing through a heated nickel catalyst. A flame ionization detector (FID) is used to measure the methane. Once the initial

temperature ramp is finished, the oven is cooled down to 600°C and the flow stream is switched to an oxidizing helium/ O_2 carrier gas mixture. Any elemental carbon kept in the filter is oxidized off into the oxidizing oven and then EC in the same manner as OC is detected (Sun lab user manual).

3.3.2 Inductively Coupled Plasma-Optical Emission Spectrometry (ICP-OES).

An ICP-OES technique is used to detect the trace metals and it has two parts: inductively coupled plasma and optical emission spectrometry. The extracted sample is first pumped by a peristaltic pump and delivered to a nebulizer. In the nebulizer, the sample is atomized and taken inside the plasma flame. In torching, a coil produces radio frequency and that ignites argon gas. The plasma flame is created by argon gas and its temperature is between 7000-10000°C. The molecules are atomized and excited to a higher state by hot plasma. A light (considered as the metal characteristic) is emitted by the excited atoms whey thy return to a ground state. The light and wavelength are then measured by a detector in OES. The intensity of the light is an indication of metal concentration, while the type of metal could be measured by the type of emitted wavelength (ICP-OES manual, 2013).

3.3.3 Gas Chromatography – Mass Spectrometry (GC-MS)

GC-MS combines both techniques of gas chromatography and mass spectrometry. GC separates all the chemical mixtures in a sample into pure chemicals while MS identifies and quantifies the chemicals. GC has a column that separates chemical mixtures based on their

volatility and they are carried by helium gas. Chemicals with high volatility travel more quickly than low volatile components.

An Agilent Technologies 6890 gas Chromatography (GC) equipped with an Agilent HP-5 mass spectrometry (MS) was used for the PAH analysis. It has a non-polar capillary column with the following dimensions (30 m, 0.25 mm ID, 0.25 µm film thickness - 5% phenylpolysiloxane). It was used in tandem with a 5973N mass spectrometer (MS). An Agilent 7683 auto-liquid sampler was used to inject 1 µL (split-less injection) of the extracted sample at 300^{o}C. The initial temperature of the PAH was 120^{o}C and then the temperature was kept for 2 minutes and ramped up at 4^{o}C/min until it reached 300^{o}C and then kept for 10 minutes. Helium gas with flow rate 1mL/min was used as a carrier gas. To quantify the analytes of the sample in single ion monitoring (SIM) mode, the detector was set and it covered the masses that ranged from 122 to 305 atomic mass units. The mass spectrometer (MS) source and quadrupole temperatures were 230^{o}C and 150^{o}C respectively. The time for sample analysis was 15 minutes (Alam^{c} et al, 2014). The MSDS Chemstation software was used to check the produced chromatogram of each sample. The samples then were quantified against calibration graphs of PAH internal standard. Figure 3.11 presents a chromatogram of one of the samples. It has peaks corresponding to various PAH compounds. For any given analyte, the amount of time that the analyte stays on the column is called retention time; while the areas under the peaks are proportional to the concentrations of the compounds.

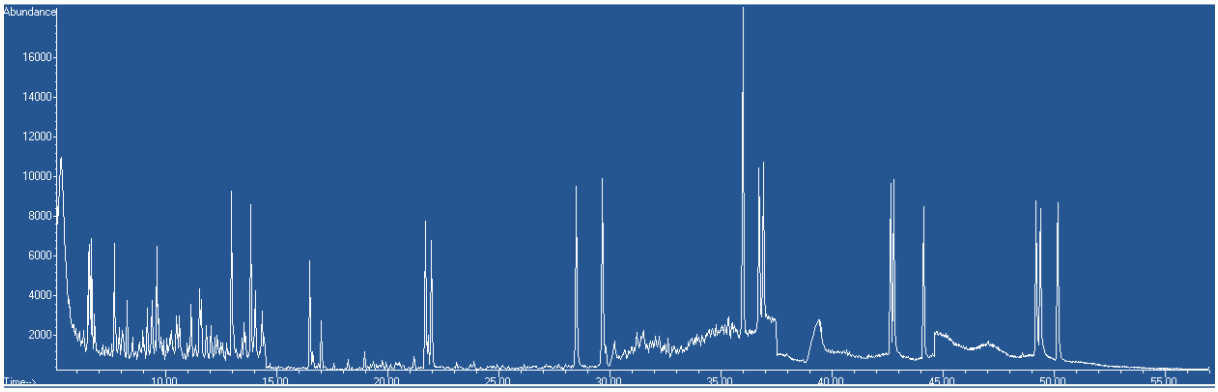


Figure 3.11: Naphtha fuel chromatogram: x-axis is for the retention time of each peak in minutes, y-axis is for the detector response

3.3.4 GC X GC-ToF-MS

Gas chromatogram (GC) - time of flight (ToF) - mass spectrometry (MS) has two columns or dimensions and a modulator. The first column is non polar, longer, with thicker film and wider bore. It separates chemical mixtures' volatilities; while the second column is very short, narrow and it is for polarity. The modulator is thermal in nature and its function is to trap and release consecutive portions of the first column or first dimension effluent and inject it into the second column or second dimension of different selectivity where it is separated and detected. A quantity of 1 µL of the extracted sample was injected at 300°C in a split ratio 100:1. The carrier gas was helium and it was at a constant flow rate 1 ml /min. The primary oven was at an initial temperature of 120°C which was held for 2 minutes.

Then, the temperature was ramped up at 2°C/min until it reached 210°C. Subsequently, the temperature increased at 1.5°C/min to 325°C. For the secondary oven, the initial temperature was 120°C and was held for 2 minutes. Then, the temperature was ramped up at 3°C/min until it reached 200°C. The temperature then increased at 2°C/min to 325°C. In order to ensure that

all species passed via the column, the temperature was ramped up at 1°C intervals to 330 °C. The ion source temperature was 280°C; while the temperature of the transfer line was 330°C (Alam[a] et al, 2016).

3.3.5 Transmission Electron Microscopy (TEM)

Transmission electron microscopy (TEM) has three important systems. First, the electron gun produces the beam electron where the beam is focused onto the object via condenser system as shown in Figure 3.12. Second, the image-producing system which consists of movable specimen stage, objective lenses, and intermediate and projector lenses. In image-producing, a real and highly magnified image is formed as shown in Figure 3.13. The third system is the image –recording which produces an observable image to human eye by converting the electron image. In image-recording system, there are fluorescent screen to view and focus the image and a digital camera for everlasting records. In addition, a vacuum system which contains pumps, gauges, valves, and power supplies are required (Ford, B et al, 2011).

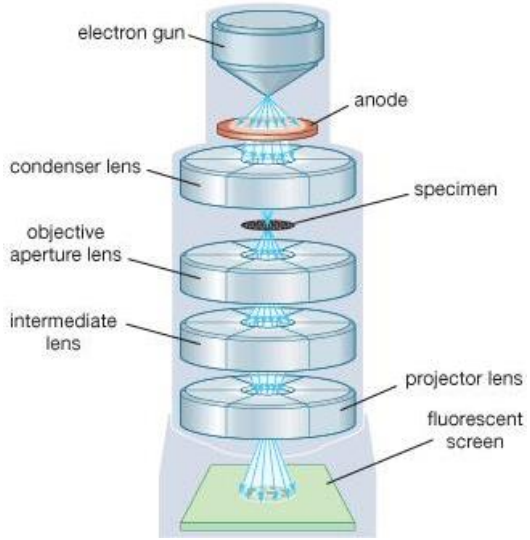


Figure 3.12: Transmission Electron Microscopy (TEM) (Ford, B et al, 2011).

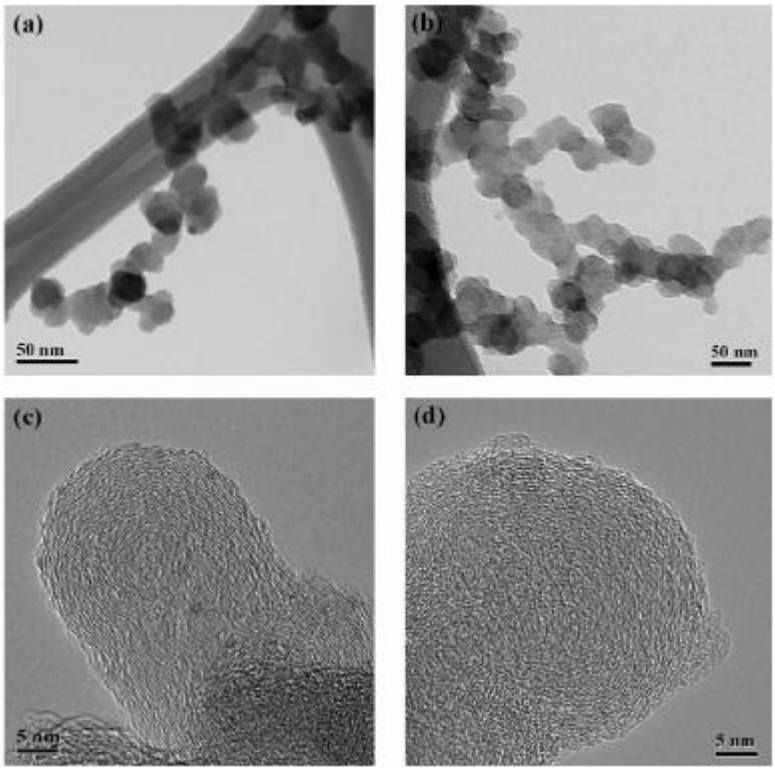


Figure 3.13: TEM image for (a) coal ash soot, (b) diesel soot, (c) primary particle for coal ash, (d) primary particle for diesel (Chen, Y et al , 2005)

The collected samples could be analysed to study their morphology by using TEM with high resolution. The detailed of the particles morphological properties like sizes and fractal geometry can be analysed by a custom image processing / data acquisition system (Yazicioglu et al, 2001). With this system, the primary particle number density (n), the primary particle diameter (d_p), fractal dimension (D_f) and the radius of gyration (R_g) could be examined and quantified.

The following equation could define the radius of gyration of a single aggregate:

$$R_g = \sqrt{\frac{1}{n}\sum_{i=1}^{n} r_i^2} \qquad 3.1$$

For an individual primary particle, the distance from the centroid of associated aggregate to the centre is r_i. Within a single aggregate particle, n is the number of primary particles. Figure 3.14 shows a schematic for particle geometry and sizes.

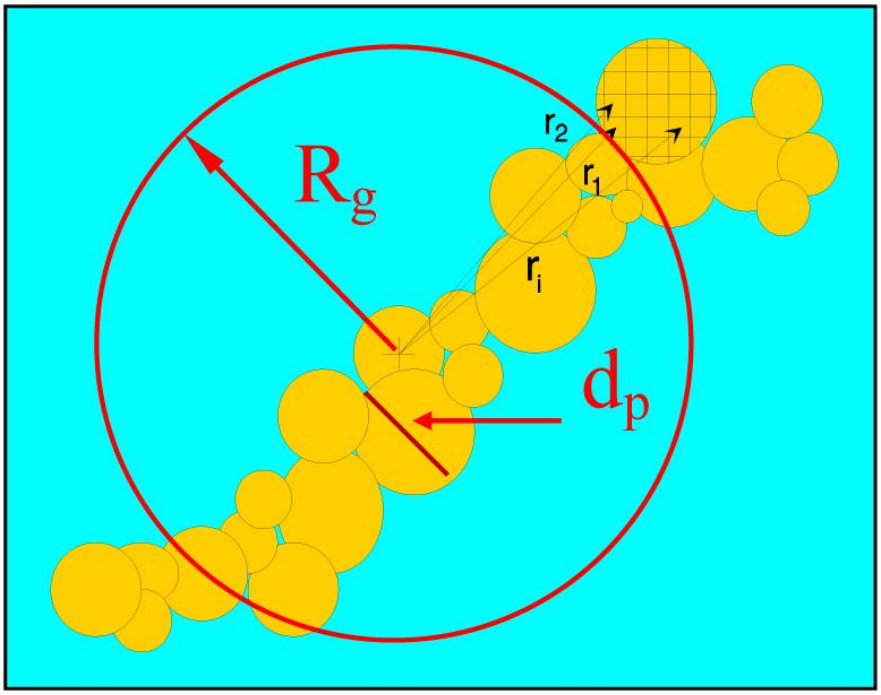


Figure 3.14 shows a schematic for particle geometry and sizes (Seong, H et al ,2012).

The number (n) of primary particles could be determined by the following equation:

$$n = (\frac{A_a}{A_P})^{1.09} \qquad 3.2$$

The projected area of an aggregate is A_a while the projected area of a primary particle is A_p, and α is 1.09. Also, the number of primary particles can be determined by:

$$n = K_f(\frac{R_g}{d_P})^{D_f} \qquad 3.3$$

Where $d_p$is the average primary particle diameter, K_f is the prefactor, and D_f is the fractal dimension. The fractal analysis offers exclusive information about particle geometry, since it can statistically standardize the complex shape of aggregate particles emitted from engines

(Chen, Y et al , 2005). The aforementioned method is for studying the particulate matter morphology. Due to the limited resources at my research program, it is proposed to study the PM morphology in future work.

3.4 Data Processing

3.4.1 Heat Release Rate Analysis

The following equation was used to calculate the heat release rate (Heywood, 1988):

$$\frac{dQ}{d\theta} = \frac{\gamma}{\gamma-1} P \frac{dv}{d\theta} + \frac{1}{\gamma-1} V \frac{dp}{d\theta} \qquad 3.4$$

Where θ is the crank angle degree; γ is specific heat ratio ($\frac{Cp}{Cv}$); P and V are the instantaneous pressure and volume of the engine cylinder respectively.

3.4.2 Brake Thermal Efficiency Calculation

The following equations was to calculate the brake thermal efficiency (BTE) (Heywood, 1988):

$$\eta_{f\,(\%)} = \frac{P\ (kw) X\ 3.6}{\dot{m}_f\ X\ Q_{HV}} \qquad 3.5$$

$$Brake\ Power\ P = 2\pi\ N\ T \qquad 3.6$$

Where η_f is the brake thermal efficiency; $\dot{m}_f$ the fuel mass flow rate (kg/h); Q_{HV} the lower heating value of the fuel (MJ/kg); P is brake power (kW); N is engine speed (rps) and N is engine torque (n.m).

33.4.3 Data Uncertainty

To assess the error bar or parameters' variability, t distribution can be used as the following:

$$Error\ bar = \pm Z_{\alpha/2} \frac{\sigma}{\sqrt{n}} \qquad 3.4$$

Where σ is representing the standard deviation of the sample; n is the sample size; α is the confidence level and Z is the confidence coefficient. Table 3.4 presents an example of the uncertainties of the total particle number concentrations for diesel, G75 and naphtha fuels at all loads for both injection strategies: single and double.

Table 3.4: Total particle number (PN) concentrations' uncertainties

		Diesel Fuel			**G75 Fuel**			**Naphtha Fuel**		
Injection	**Load (bar BMEP)**	**Total PN Conc***	**Error (±)**	**Error (%)**	**Total PN Conc***	**Error (±)**	**Error (%)**	**Total PN Conc***	**Error (±)**	**Error (%)**
Single injection	1.5	$8.25x10^{14}$	$2.25x10^{12}$	0.27	$1.16\ x10^{13}$	$1.11x10^{11}$	0.96	$9.88x10^{13}$	$4.70x10^{12}$	4.76
	3	$6.37x10^{14}$	$5.55x10^{12}$	0.87	$2.40\ x10^{12}$	$3.12x10^{10}$	1.3	$2.98x10^{12}$	$1.06x10^{11}$	3.57
	6	$3.24x10^{14}$	$2.62x10^{12}$	0.81	$7.31\ x10^{12}$	$2.32x10^{11}$	3.17	$8.49x10^{12}$	$5.48x10^{09}$	0.06
	12	$5.27x10^{14}$	$1.89x10^{13}$	3.58	$2.03\ x10^{14}$	$3.10x10^{12}$	1.52	$2.70x10^{14}$	$2.29x10^{11}$	0.08
Double injection	1.5	$1.03x10^{15}$	$6.11x10^{12}$	0.59	$3.32\ x10^{13}$	$1.45x10^{11}$	0.63	$7.46x10^{13}$	$4.28x10^{11}$	0.57
	3	$1.16x10^{15}$	$1.48x10^{12}$	0.13	$1.81\ x10^{12}$	$6.36x10^{09}$	0.35	$3.00x10^{13}$	$2.94x10^{11}$	0.98
	6	$1.96x10^{15}$	$9.58x10^{13}$	0.39	$3.58\ x10^{12}$	$6.68x10^{10}$	1.86	$2.97x10^{12}$	$2.29x10^{05}$	0.77

3.5 Summary

This chapter describes the engine test cell and all the equipment involved in conducting the experiments. The engine used was a 2.2L, four cylinder Ford Puma engine, equipped with common rail direct injection and EGR cooler modification deactivated for only G75 and naphtha fuels. Also, the engine parts and control unit were briefly discussed, providing references. Furthermore, the tested fuels with their properties were presented. This chapter also gives a detailed description of the engine emissions' measurement equipment used, such as the Horiba gas analyser and the smoke meter. The DMS500 was used to study the particle size distribution; the particle size-number distribution, the particle size-surface area distribution and mass distribution in the aerosol air. For analytical measurement equipment, ICP-OES, GC-MS, EC/OC and 2D GC-TOF-MS were used to analyse the chemical compositions of the filter papers with deposits collected from the diesel engine run on diesel, G75 and naphtha fuels. The PM morphology analysis was discussed and it was proposed to be conducted as future work.

CHAPTER 4

EFFECT OF EGR TEMPERATURE, INJECTION PRESSURE AND TIMING ON PM OF DIESEL AND DIESELINE FUELLED PCI

4.1 Introduction

In low temperature combustion, premixing fuel and air has the potential to reduce the formation of larger agglomerate soot particles, since the local equivalence ratio ϕ is decreased. The particles' surface area has sites to embrace any heterogeneously condensed volatile materials as the exhaust gas temperature cools down. The reduction in the number of larger particles means that the surface area of these particles is reduced. In other words, the volatile materials will not find enough surface area to condense on, so they could easily nucleate and form small particles (Kolodziej, et al., 2013). The increase in small particles and the decrease in larger particles have been observed when the engine was running on PCI mode, as reported by Kittelson (1998) and Benajes et al. (2010).

Several research studies were conducted about PM emitted from diesel engines, concluding that LTC emits a lower particle number and mass compared to conventional diesel combustion. It may have higher particle numbers and soluble organic fraction (SOF), however; this depends on the EGR ratio and injection pressure and timing (Payri, et al., 2011; Raatz and Mueller, 2001; Akihama, et al., 2001; Kolodziej, et al., 2007). It is reported that by advancing injection timing with extensive EGR, PM emissions decreased by 50% compared to conventional diesel combustion. The soluble organic fractions (SOF) increased with a

small size of PM (Parks, et al., 2010). Advancing the injection timing provides sufficient time for the air and fuel to mix more effectively. This better mixing of air and fuel helps to reduce PM emissions. There was an opposite observation, however, reported by Benajes, et al. (2012). They conducted a PN emissions study in PCI combustion with advancing injection timing, and observed that with advancing injection timing, PM emissions increased drastically. PM emissions saw an increase of 185% when the injection timing advanced from -30° ATDC to -33°, although the injected fuel occurred before the start of the combustion in PCI mode. When the fuel was injected in advance and at low in-cylinder pressure, the penetration of injected fuel took longer to reach the piston bowl surface and formed a film of liquid fuel (fuel impingement) as shown in Figure 4.1. As a result, the liquid fuel left the chamber as unburned fuel, which could lead to the increase of small particles.

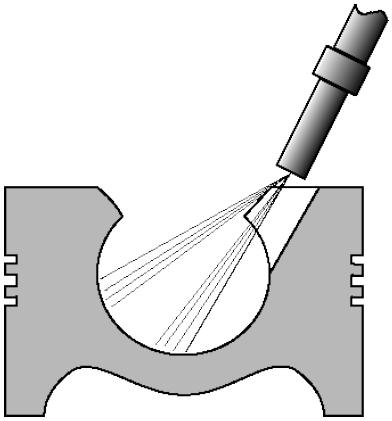


Figure 4.1: Liquid fuel on the piston bowl (Vegburner Website)

Fuel with higher auto-ignition resistance and volatility demonstrated an improvement in mixing with the surrounding air. The fuel's volatility promotes fast evaporation, while the high resistance of auto-ignition gives enough time for the charge to be sufficiently mixed before ignition starts. This property favours gasoline – or gasoline-like fuels with a low cetane

number – over diesel fuel. This chapter investigates the effect of EGR temperature, injection pressure, and timing on the particle number concentration of diesel and dieseline fuelled PCI.

4.1.1 Research Objective

This study is a screen test about the effect of engine load, injection pressure, injection timing, and EGR temperature on the particle size and number distribution, elemental carbon (EC), organic carbon (OC), and EC/OC ratio of both diesel and G75 fuels. The presented data were collected or logged at conditions comparable to diesel fuel in terms of particle number (PN), engine out emissions, and brake thermal efficiency.

4.2 Experimental Set-up

4.2.1 The Engine and Test Conditions

The tests were conducted on a 2.2L, four-cylinder Ford Puma engine, equipped with common rail direct injection, variable nozzle turbocharger (VGT), and controlled by an open engine control unit (ECU). The EGR cooler was deactivated to introduce hot EGR in order to increase the intake manifold temperature for the G75 fuel, but for diesel cold EGR was introduced, as discussed in section 4.3.1. The compression ratio of the engine was preserved at its default of 15.50:1 and the engine was not equipped with a diesel oxidation catalyst (DOC).

A schematic of the set-up is shown in Figure 4.2; the engine specification list is presented in Table 3.1 in section 3.1.1. In addition, the properties of the tested fuels, diesel and G75, are listed in Table 3.2 in section 3.1.5. The tests were conducted at two different loads: 1.37 and 2.98 bar BMEP, with an EGR ratio 52% and 45% respectively. They were taken at different

injection pressure and timings, and at a constant speed of 1800 rpm with fixed ($\lambda \sim 1.20$) as shown in Table 4.1. Also, hot EGR was introduced in order to increase the intake temperature for the case of the dieseline fuel. The loads were averaged since they were not stable at each test condition, where the variation was ±0.50 N.m.

The gaseous emissions (e.g. O_2, CO, HC, NO_X, and EGR ratio) were measured using a MEXA-700 EGR analyser, as discussed in section 3.2.1. The particle number-size distribution was measured by using combustion DMS500, as discussed in section 3.2.3.

4.2.2 Sampling and Analysis

At a steady state condition, the exhaust gas sample was drawn from the exhaust pipe – heated to 190°C to prevent any condensation in the line – to downstream of the modified TSI diluter model 3302A, with a dilution ratio of 100:1 and flow rate of 10 l/min. It was reported that a high dilution ratio reduced the volatile particles' saturation ratio in the exhaust gas, resulting in a reduction in the number of volatile particles in the cooled exhaust gas (Abdul-Khalek, et al., 1999). The diluted emitted particulates from the diesel engine were collected on a glass microfibre filter (GF/F, 47mm, Whatman) at a temperature lower than 52°C for 20 minutes. The typical weight of a blank glass fibre filter is between 0.1243 g and 0.1245 g. The collected samples were wrapped with aluminium foil to prevent exposure to light and prepared for offline analysis of the concentrations of elemental carbon (EC) and organic carbon (OC), as discussed in section 4.4.

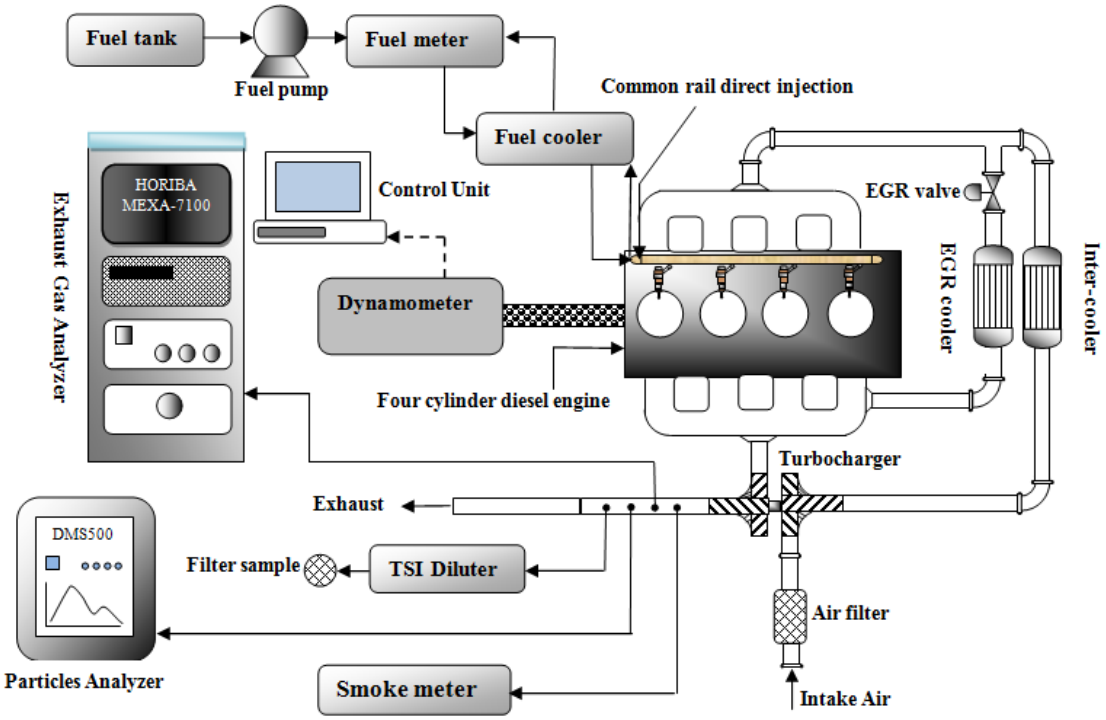


Figure 4.2: Schematic of the experimental set-up without DOC

Table 4.1: Test conditions

Condition	**1.37 bar BMEP, EGR 52% , 1800 rpm, λ ~ 1.20**									**Fuel**
Inj. P (bar)	150	250	350	500	700	900				
Inj. Timing (°bTDC)	13	10.5	11	7	6.5	6				**Diesel**
HC(ppm)	585	591	552	814	945	1104				
Inj. P (bar)	150			250			350			
Inj. Timing (°bTDC)	20	30	40	20	30	40	28	30	40	**G75**
HC(ppm)	9369	2966	2644	2928	4908	9963	4183	4257	10984	
	2.98 bar BMEP, EGR 45% , 1800 rpm, λ ~ 1.20									
Inj. P (bar)	150	250	350	500	700	900	1400			
Inj. Timing (°bTDC)	16.5	11	9.5	8.5	8	7.5	5.8			**Diesel**
HC(ppm)	363	637	690	587	797	963	1537			
Inj. P (bar)	150			250			350			
Inj. Timing (°bTDC)	32.5	42.5	52.5	32.5	42.5	52.5	32.5	42.5	52.5	**G75**
HC(ppm)	2470	1864	4642	2526	4819	9091	2183	7908	10896	

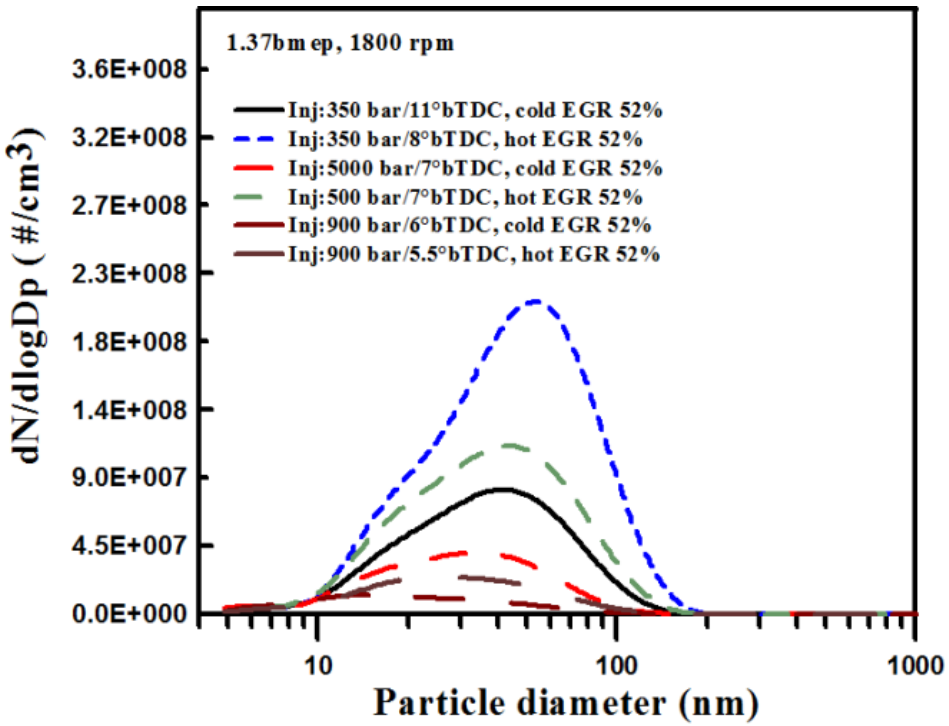
4.3 Particle Size and Number Distribution of Diesel and G75 Fuels

4.3.1 The Effect of EGR Temperature on Particle Size and Number Distribution of Diesel Fuel

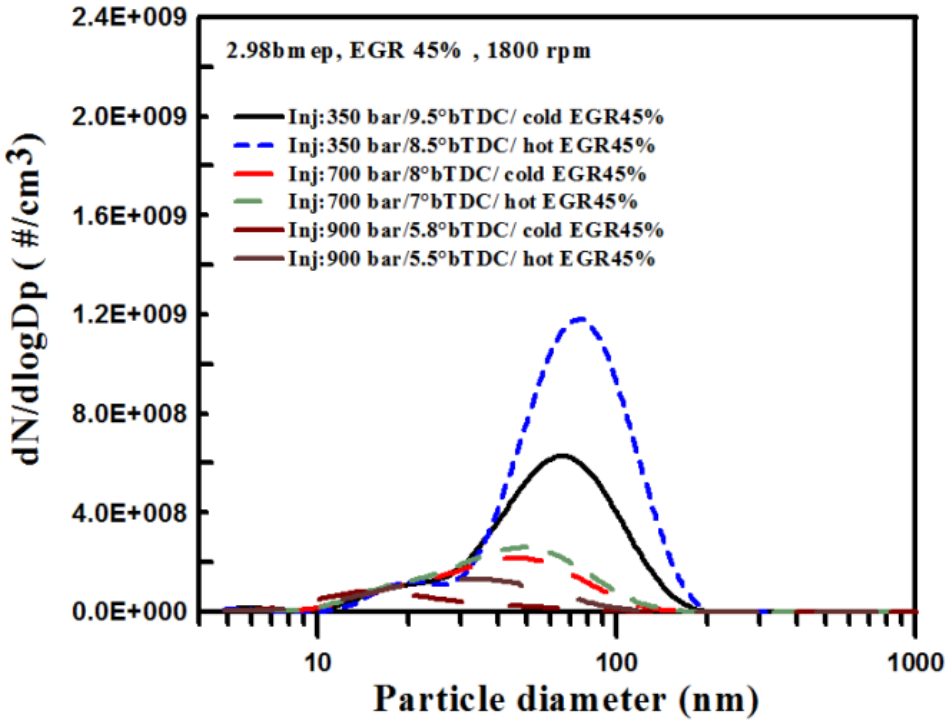
The recirculation of exhaust gas to the engine intake will increase the inlet temperature; there will also be a heat capacity increase since CO_2 and H_2O are present, but the oxygen availability will be reduced (Hountalas, et al., 2008). This section presents a screen test about the effect of hot EGR (deactivated EGR cooler) and cold EGR on particle size and number distribution of diesel fuel, operated at two different loads of 1.37 and 2.98, bar BMEP, with different injection pressures as shown in Figure 4.3 (a, b). The speed and λ were fixed at 1800 rpm and 1.20 respectively. The EGR ratios were 52% for load 1.37 bar BEMP, and 24% for 2.98 bar BMEP.

It has been observed that for both loads and at different injection pressures, the hot EGR increased the particle number concentration and particle size to larger sizes compared to the cooled EGR conditions. The increase in EGR temperature increased the gas temperature, which resulted in a reduction in the amount of air and oxygen in the cylinder (known as thermal throttling). The lack of oxygen cannot be compensated for and so this halts the soot oxidation process earlier and results in an increase in emitted soot. A similar observation of soot increase under higher EGR temperature is reported by Hountalas, et al. (2008).

It is also suggested that the short ignition delay for the diesel fuel since it has high cetane number. With the increase of the gas temperature, and the injection timing being near the top dead centre, meaning that the mixture did not have time to mix sufficiently, resulting in an increase of soot



(a)



(b)

Figure 4.3: The effect of hot EGR on particle size and number distribtuon of diesel fuel at two loads: (a) at 1.37 bar BMEP, (b) at 2.98 bar BMEP

The cold EGR was not efficient for G75 fuel since the engine could not be started. Therefore, all data presented for G75 fuel was with the usage of hot EGR, while for diesel fuel it was with usage of cold EGR.

4.3.2 The Effect of the EGR Ratio on PM of Diesel and G75 Fuels

The EGR is considered as one of the effective strategies that ultimately reduce NOx emissions in diesel engines; conversely, the addition of EGR results in a soot emissions increase (Labecki and Ganippa, 2012). This section presents a screen test of the effect of EGR ratios on particle size and number distribution of diesel and G75 fuels for two loads, 1.37 and 2.98 bar BMEP, with injection timings varied as presented in Figures 4.4 and 4.5. The operating conditions are listed in Table 4.2.

Table 4.2: Test conditions of EGR variation

Condition	**1.37 bar BMEP, 1800 rpm, λ ~ 1.20**			
Inj. P (bar)	500			**Diesel**
EGR Ratio (%)	40	52	60	
Inj. Timing (°bTDC)	7	7	9	
Inj. P (bar)	250			
EGR Ratio (%)	45	52	60	**G75**
Inj. Timing (°bTDC)	30			
Condition	**2.98 bar BMEP, 1800 rpm, λ ~ 1.20**			
Inj. P (bar)	700			**Diesel**
EGR Ratio (%)	40	45	50	
Inj. Timing (°bTDC)	7.5	8	9	
Inj. P (bar)	250			
EGR Ratio (%)	40	45	48	**G75**

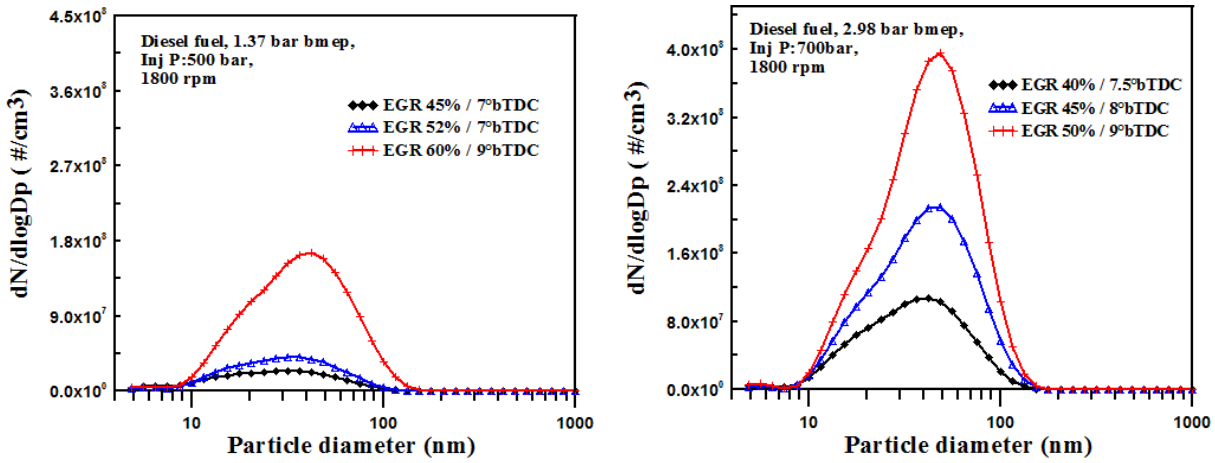
The cold EGR was used for diesel fuel since it is very efficient in reducing particle numbers compared to hot EGR, as discussed in section 4.3.1. For G75 fuel, hot EGR was used, since the engine could not start with cold EGR.

At low load 1.37 bar BMEP for diesel fuel, the increase of the EGR ratio from 40% to 60% shifts the peak of high particle number concentration upwards and increases the maximum detectable large particle size range. The particle number concentration for accumulation significantly increased from 8.20E06 cm^{-3} to 6.10E07 cm^{-3} and CMD from 44 nm to 49 nm, while the particle number concentration of the nucleation mode increased from 9.91E06 cm^{-3} to 4.20E07 cm^{-3}, and CMD from 16nm to 20nm as shown in Figures 4.4 and 4.5. The increase of particle number concentration and CMD with the increase of EGR ratio is attributed to the decrease in oxygen concentration that contributes to the combustion. Therefore, increasing EGR levels decreased the oxygen level, which affects the soot process as the pyrolytic reaction overcomes the soot oxidation reaction. This creates an environment of soot agglomeration, surface growth, and condensation of volatile fractions on the particulate surface.

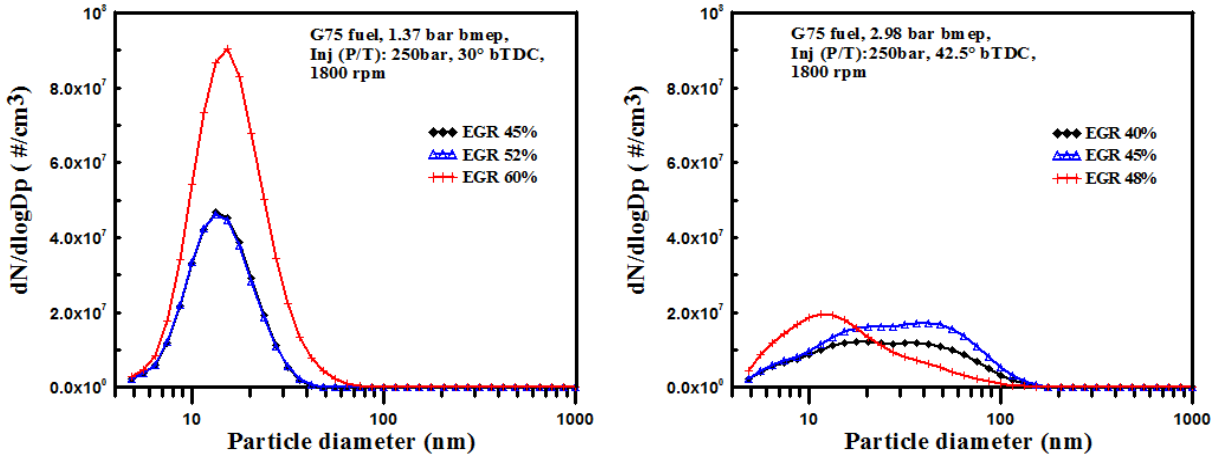
When the load increased to 2.98 bar BMEP and EGR ratios increased from 40% to 50%, at injection pressure of 700 bar as shown in Figure 4.4 (b), the peak of high particle number concentration shifts upwards with a similar maximum detectable larger particle size, but the high particle number concentration is considered higher than the low load 1.37 bar BMEP. The nucleation and accumulation mode particles, as well as CMD, increased as shown in Figure 4.5 (a). When the load and EGR ratio were increased, the fuel quantity increased and the EGR acted as preheater of the intake air, since at the entry of the intake manifold, the temperature of the exhaust gas was more than the temperature of the atmosphere. Therefore, a short ignition delay occurred and resulted in an increase of the PN.

For G75 at 1.37 bar BMEP and at injection pressure of 250 bar, increasing the EGR ratio from 45% to 60%, as shown in Figure 4.4(b), generated more pronounced nucleation mode particles with low CMD, as shown Figure 4.5 (b). This observation occurred with G50 fuelled PCI when the EGR ratio was increased to around 60% as reported by Zhang, et al. (2012). The increase of the concentration of small particles at EGR 60% could be attributed to the replacement of fresh air when the EGR level was increased, and to the reduction of oxygen concentration (soot oxidizer) that contributes to the combustion. Also, it is proposed that fuel impingement on the cylinder walls can result in the emission of unburned hydrocarbons along with PM (Shi and Reitz, 2010)

At load 2.98 bar BMEP and at injection pressure of 250 bar, as shown in Figure 4.4(d), increasing the EGR ratio from 40% to 48% produced little increase in the particle number concentration, with a decrease of larger particle sizes as shown in Figure 4.5 (b). When the fuel was injected at 30 °bTDC, the quantity was a little higher compared to the case of 1.50 bar BMEP; this could be explained by the fact that the temperature inside the chamber was high in order to shorten the time for fuel to be fully mixed with air, which led to an increase of small particle emissions.

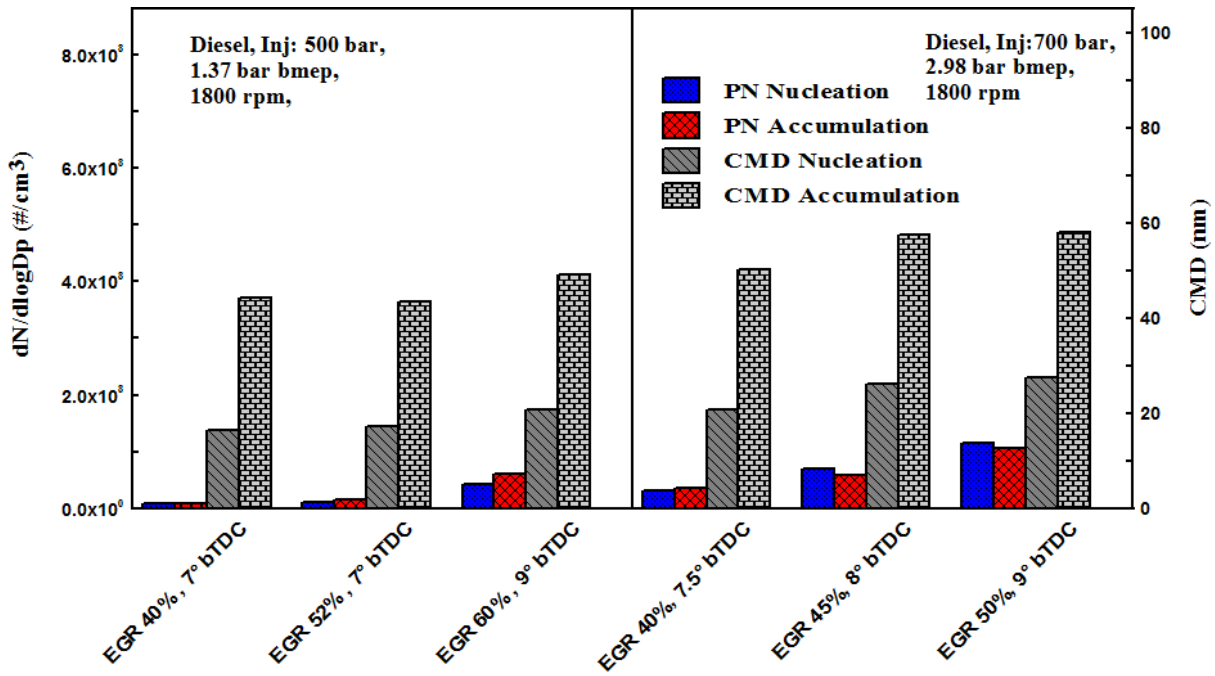


(a) (b)

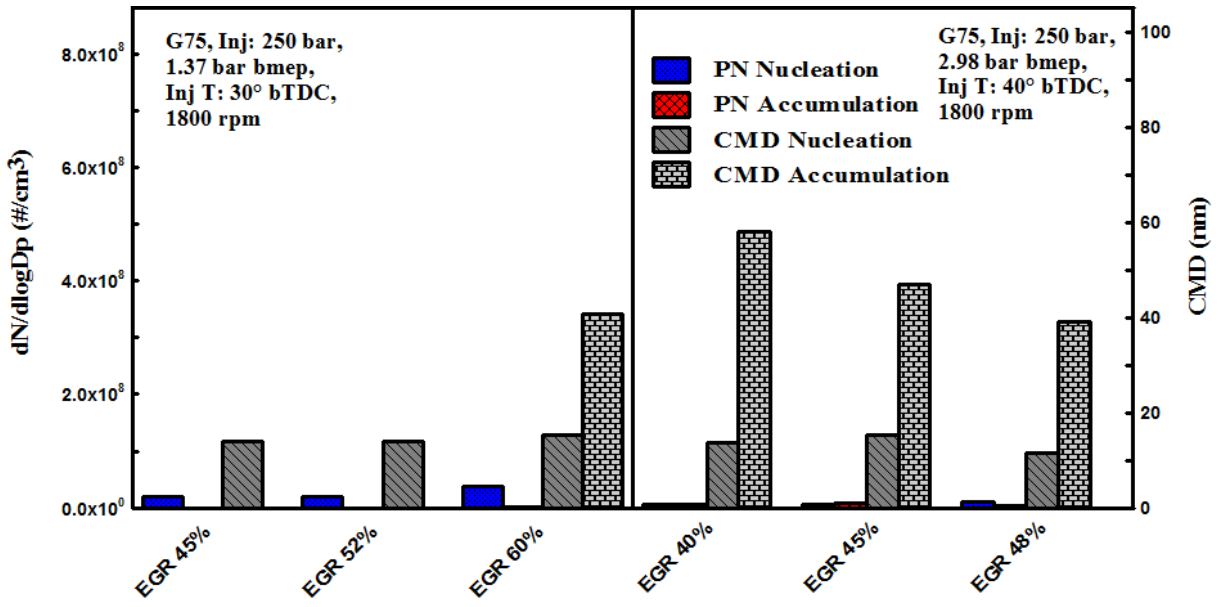


(c) (d)

Figure 4.4: The effect of EGR ratio on Particle number and size distribution of diesel and G75 fuels at two loads 1.37 and 2.98 bar BMEP: (a, b) diesel, (c, d) G75



(a)



(b)

Figure 4.5: The effect of EGR ratio on nucleation, accumulation and CMD of diesel and G75 fuels at two loads 1.37 & 2.98 bar BMEP: (a) Diesel and (b) G75

4.3.3 Effect of Injection Pressure and Timing

Particle size–number distributions were measured per unit volume at two engine loads 1.37 and 2.98 bar BMEP, while maintaining EGR ratios at 52% and 45% respectively. Fuel injection pressures were varied for diesel (150, 250, 350, 500, 700, 900, and 1400 bar) and for dieseline G75 (150, 250, and 350 bar) and all test conditions were at a constant speed of 1800 rpm with lambda ~1.20. The EGR valve cooler was deactivated for the G75 tests in order to introduce hot EGR to the intake, where the temperature was ~135 C° for 1.37 bar BMEP and ~150 C° for 2.98 bar BMEP. The injection timings were varied. The measurements were obtained after thermal stabilization of each test condition. The start of injection was varied from 52.5 to 5° bTDC. Figures 4.6, 4.7 and 4.8 illustrate the distribution of the particle size-number and the variation of particle number concentration for nucleation and accumulation modes for both diesel and G75 fuels at different operating conditions. Diesel figures have

been separated from G75 figures to maximize the visibility of the peaks of G75. Additionally, the y-scales have been adjusted differently for the sake of maximizing the peaks' visibility.

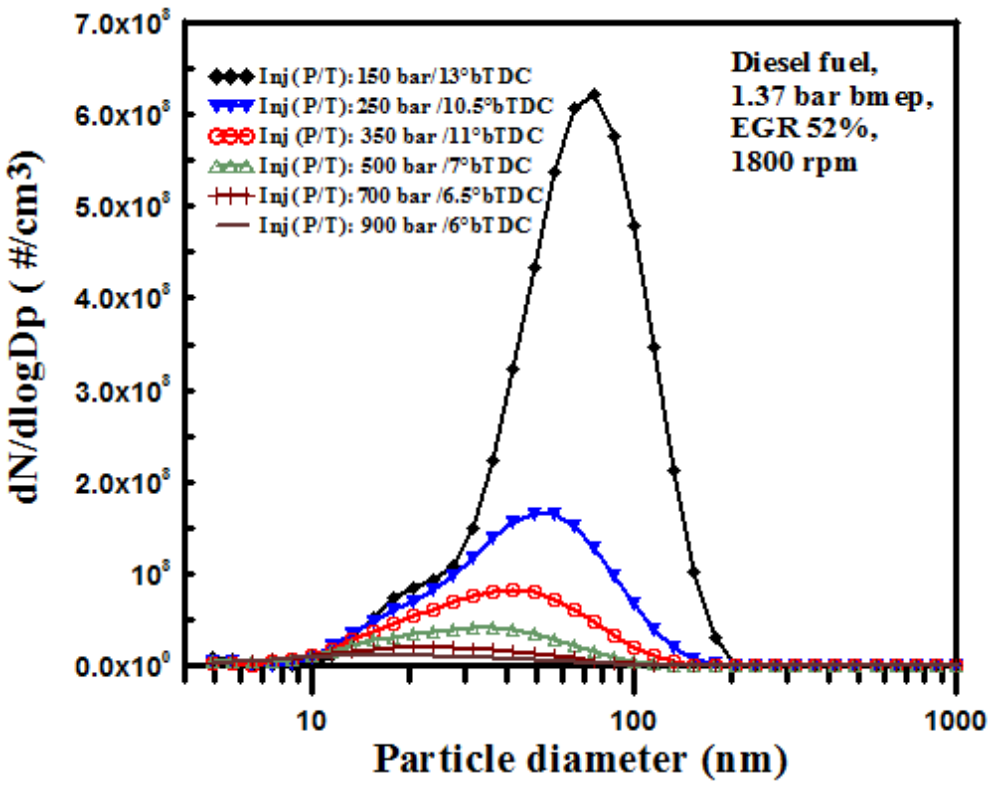
4.3.3.1 Effect of Injection Pressure and Timing at a Load of 1.37 bar BMEP

At low load 1.37 bar BMEP and for diesel fuel, when increasing injection pressure from 150 bar to 900 bar while maintaining EGR at 52 %, as shown in Figures 4.6 (a) and (b), the particle size-number distributions were in bimodal distribution and the peaks of the high particle number concentration of a larger size shifted towards smaller-sized particles. Larger-sized particles are mainly solid carbonaceous soot, while smaller-sized particles can be composed of solid particles and condensed/nucleated volatile materials (Filippo and Maricq, 2008). Increasing the injection pressure improves fuel atomization as the fuel droplet sizes reduced, resulting in better mixing of fuel and air. Therefore, the increase in injection pressure reduced the particle number concentration of both nucleation and accumulation by 90% and 98.50% respectively, as shown Figure 4.7.

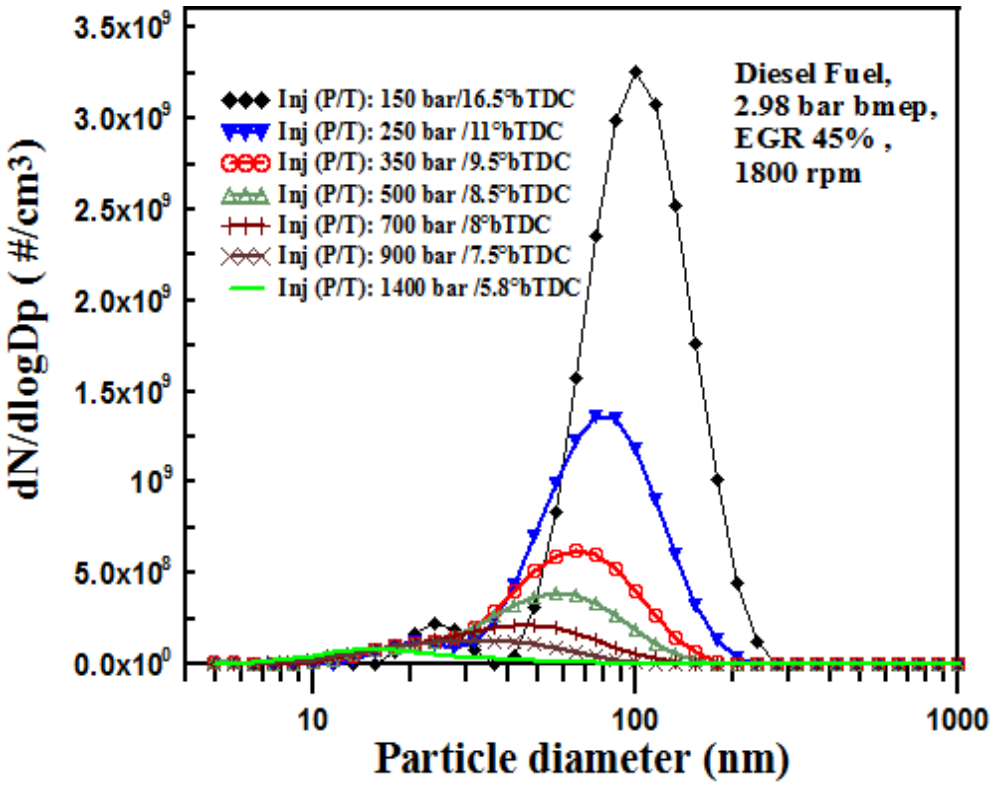
For the G75 fuel, the peaks of the high particle number concentration were mainly positioned in the small particle size region when the injection pressure was increased. The increase in injection pressure reduced the fuel droplet size; there are two factors that participate in this reduction. The first factor is evaporation, while the second factor is atomization. When the dieseline is injected, gasoline is more volatile than diesel fuel; therefore, the rate of vaporization is higher than diesel fuel. Atomization, however, reduces the droplet size to smaller than diesel (Payri, et al., 2012). The longer ignition delay with atomized fuel can help to generate a better mixing of fuel with the surrounding air.

At a low injection pressure of 150 bar, as shown in Figure 4.6(c), advancing injection timing from 20 to 40° bTDC reduced the particle number concentration. This reduction is attributed

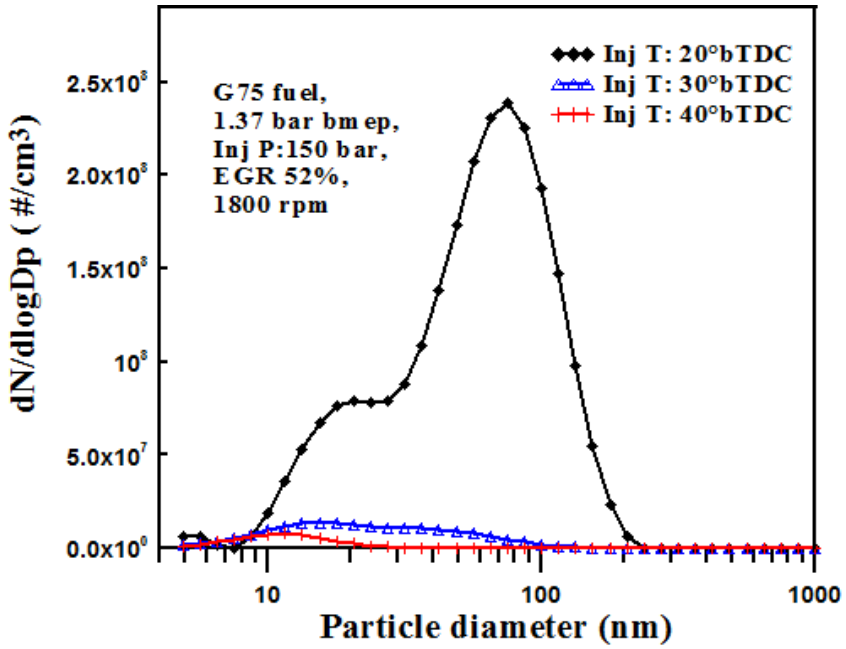
to the fuel injection being earlier with low quantity, which in turn increased the available time for fuel droplets to mix with the surrounding air. Consequently, this enhanced the combustion process and promoted soot oxidation over soot formation, resulting in a significant reduction in PN emissions. The concentration of both nucleation and accumulation modes reduced significantly by 95.30 % and 99.96 % respectively compared to diesel fuel at injection pressure of 150 bar. Also, the CMD in the nucleation mode reduced from 27 nm to 11 nm, and in the accumulation mode from 75 nm to 47 nm.



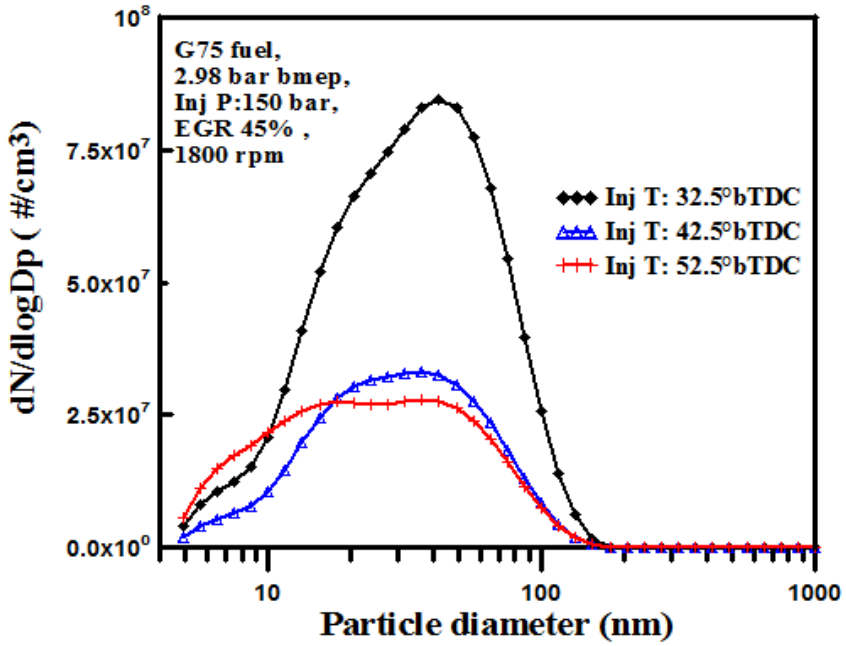
(a)


Diesel Fuel,
2.98 bar bmep,
EGR 45% ,
1800 rpm
Inj (P/T): 150 bar/16.5°bTDC
Inj (P/T): 250 bar /11°bTDC
Inj (P/T): 350 bar /9.5°bTDC
Inj (P/T): 500 bar /8.5°bTDC
Inj (P/T): 700 bar /8°bTDC
Inj (P/T): 900 bar /7.5°bTDC
Inj (P/T): 1400 bar /5.8°bTDC
dN/dlogDp (#/cm3)
Particle diameter (nm)

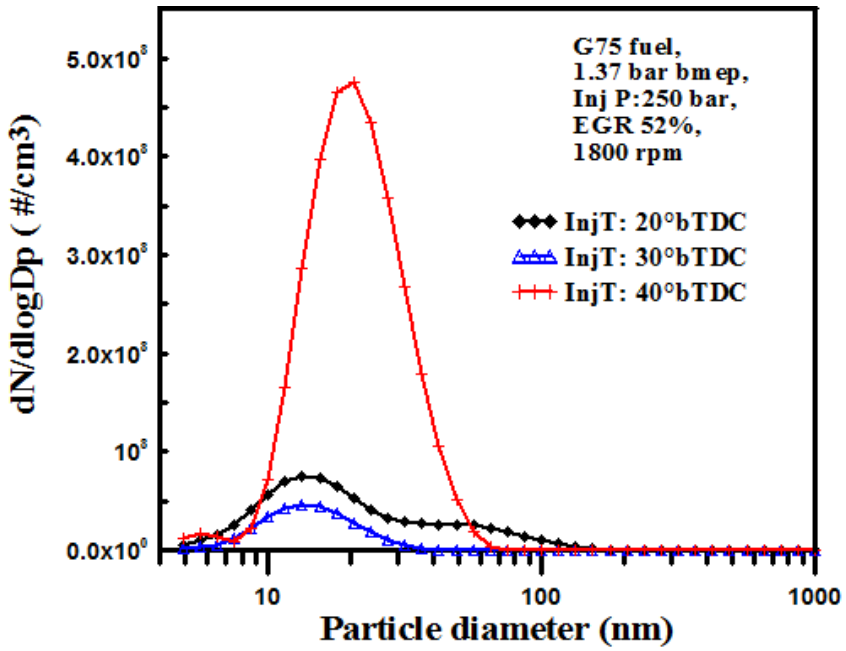
(b)


G75 fuel,
1.37 bar bmep,
Inj P:150 bar,
EGR 52%,
1800 rpm
Inj T: 20°bTDC
Inj T: 30°bTDC
Inj T: 40°bTDC
dN/dlogDp (#/cm3)
Particle diameter (nm)

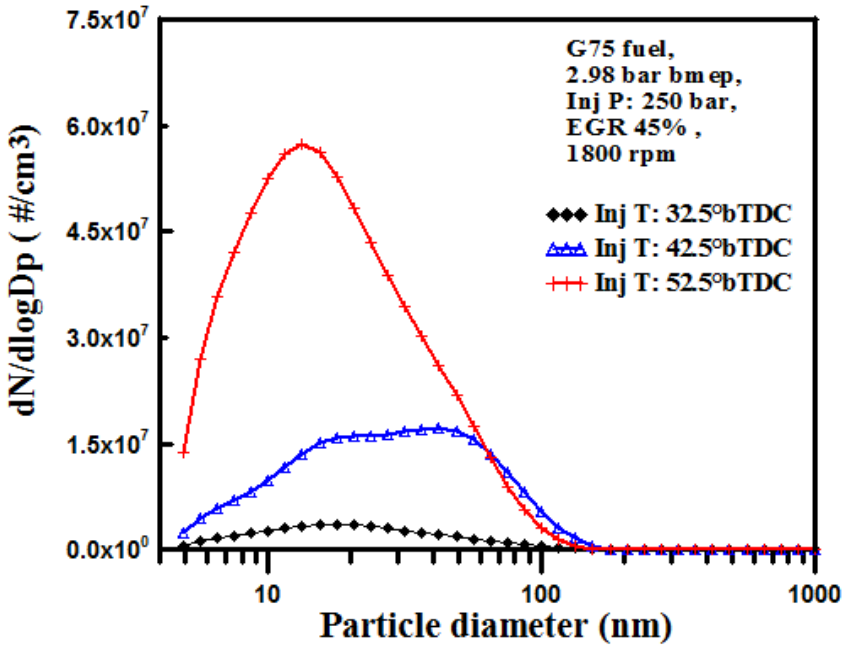
(c)


G75 fuel,
2.98 bar bmep,
Inj P:150 bar,
EGR 45% ,
1800 rpm
Inj T: 32.5°bTDC
Inj T: 42.5°bTDC
Inj T: 52.5°bTDC
dN/dlogDp (#/cm3)
Particle diameter (nm)

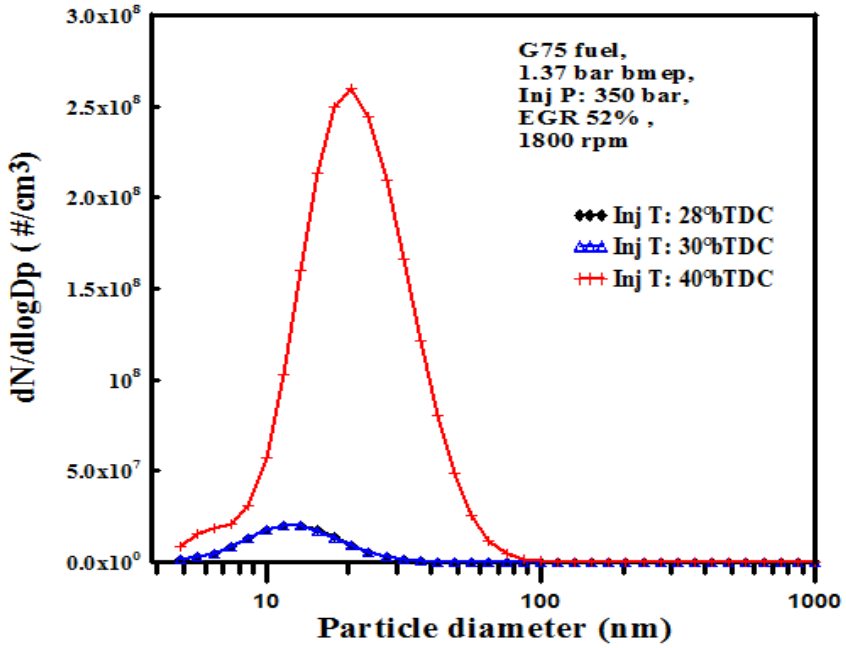
(d)


G75 fuel,
1.37 bar bmep,
Inj P:250 bar,
EGR 52%,
1800 rpm
InjT: 20°bTDC
InjT: 30°bTDC
InjT: 40°bTDC
dN/dlogDp (#/cm3)
Particle diameter (nm)

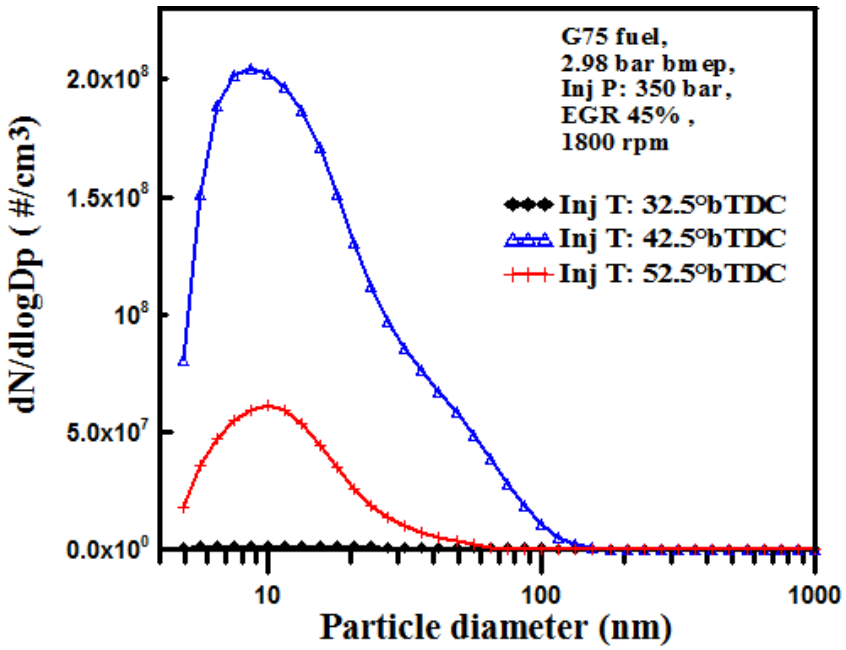
(e)


G75 fuel,
2.98 bar bmep,
Inj P: 250 bar,
EGR 45% ,
1800 rpm
Inj T: 32.5°bTDC
Inj T: 42.5°bTDC
Inj T: 52.5°bTDC
dN/dlogDp (#/cm3)
7.5x10^7
6.0x10^7
4.5x10^7
3.0x10^7
1.5x10^7
0.0x10^0
10
100
1000
Particle diameter (nm)

(f)


G75 fuel,
1.37 bar bmep,
Inj P: 350 bar,
EGR 52% ,
1800 rpm
Inj T: 28°bTDC
Inj T: 30°bTDC
Inj T: 40°bTDC
dN/dlogDp (#/cm3)
3.0x10^8
2.5x10^8
2.0x10^8
1.5x10^8
10^8
5.0x10^7
0.0x10^0
10
100
1000
Particle diameter (nm)

(g)



(h)

Figure 4.6: The effect of injection timing on the particle size number distribution for diesel and G75 fuels, two loads: 1.37 and 2.98 bar BMEP and at different injection pressures : (a) and (b), for diesel (c), (d),(e),(f),(g) and (h) for G75

At injection pressure of 250 bar and 20° bTDC, the particle size-number distribution is in bimodal distribution and the peak of the high particle number concentration is positioned in the small sized particles' region, as shown in Figure 4.6 (e). Compared with diesel fuel at an injection pressure of 250 bar, there was no large reduction in the concentration of particle number in the nucleation mode, as it was found to be around 8.34 E07 cm^{-3} for diesel and 5.37 E07 cm^{-3} for G75, as shown in Figure 4.8 (b). There is no specific explanation for that, but it could be explained by anomalies in equipment.

Advancing the injection from 20° bTDC to 30° bTDC further reduced the particle number concentration of the nucleation mode to around 41%, with no large particles in the accumulation mode as they were reduced more when the injection timing was further

advanced to 40° bTDC. This case is similar to that of injection pressure of 150 bar, but with opposite trend for the nucleation mode as the particle number concentration increased significantly. The sudden increase of concentration of small particles at 40° bTDC could be attributed to the fuel penetration being longer, which can generate fuel impingement on the cylinder wall. Since the volatility of G75 fuel is higher than that of diesel fuel, the fuel film formed on the cylinder wall or top land of the piston continuously vaporizes during the combustion stroke, which creates a diffusive combustion generating high PN and high hydrocarbon emissions, as shown in Figure 4.9 (a). A similar observation was reported by Benajes, et al. (2012) where the particle number concentration drastically increased when the injection timing was advanced.

At an injection pressure of 350 bar, as shown in Figure 4.6 (g), it was observed that the trend was almost similar to the experiment with injection pressure of 250 bar. Advancing the injection timing to 40° bTDC reduced the particle number concentration in the accumulation mode by 98.75% compared to diesel fuel; there was a significant increase in the number of nucleation mode particles. This significant increase in small particles in the nucleation mode could be related to the fuel impingement discussed earlier, which could produce UBHCs along with PM, as shown in Figure 4.9 (a). In order to be comparable with G75 fuel at low load 1.37 bar BMEP, the injection pressure of the diesel fuel should be increased to 900 bar to reduce the particle number concentrations of the nucleation and accumulation modes by 90% and 98% respectively. For G75 fuel, with a low injection pressure and at advanced injection timing 40° bTDC, the particle number concentrations of the nucleation and accumulation modes could be reduced by 95% and 99% respectively.

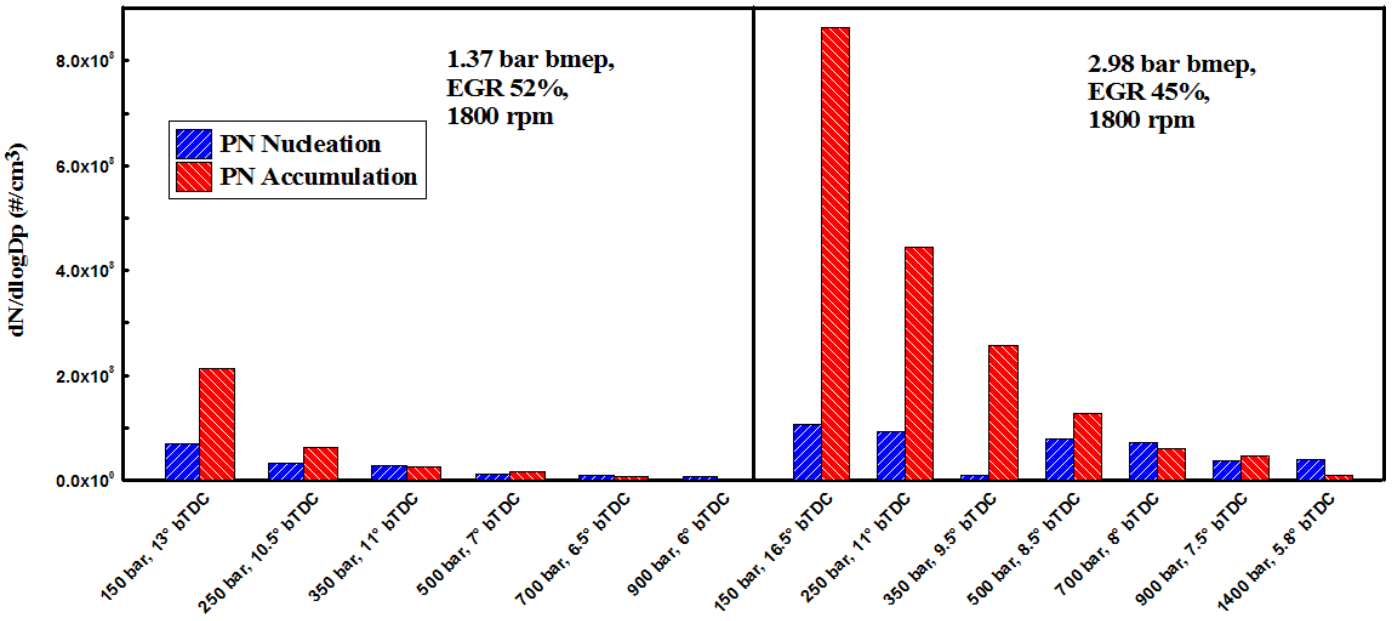
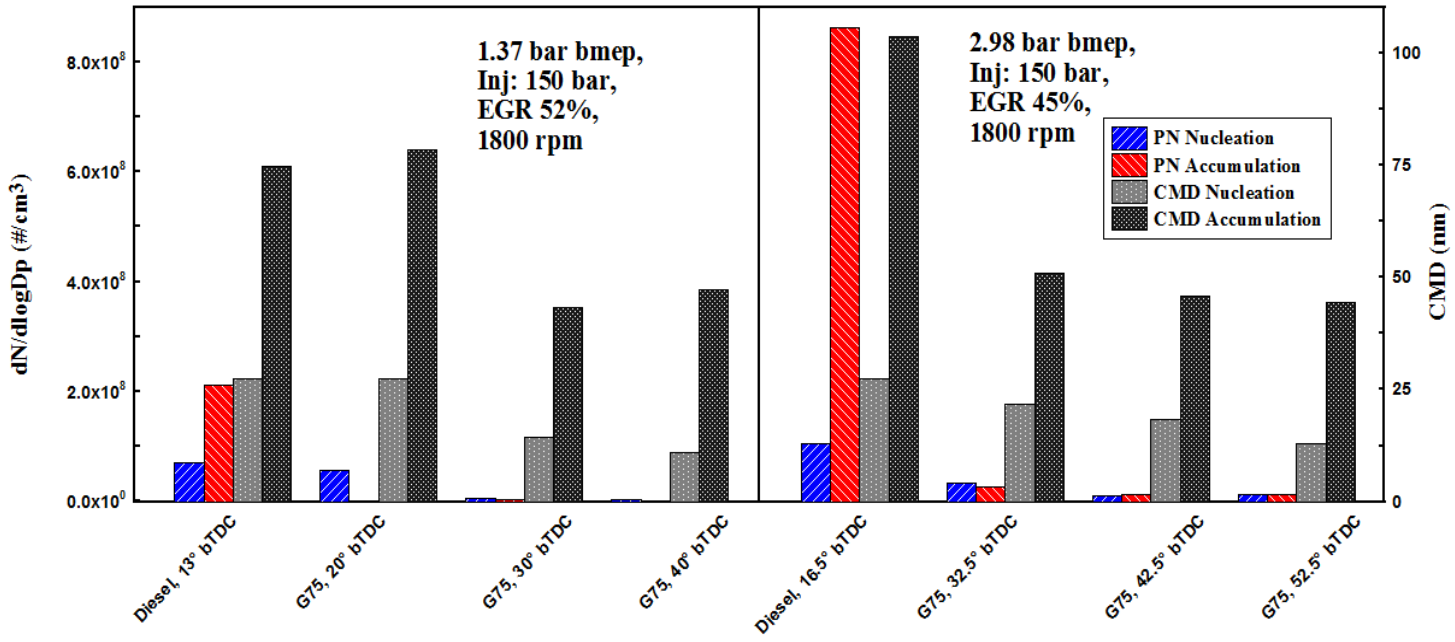
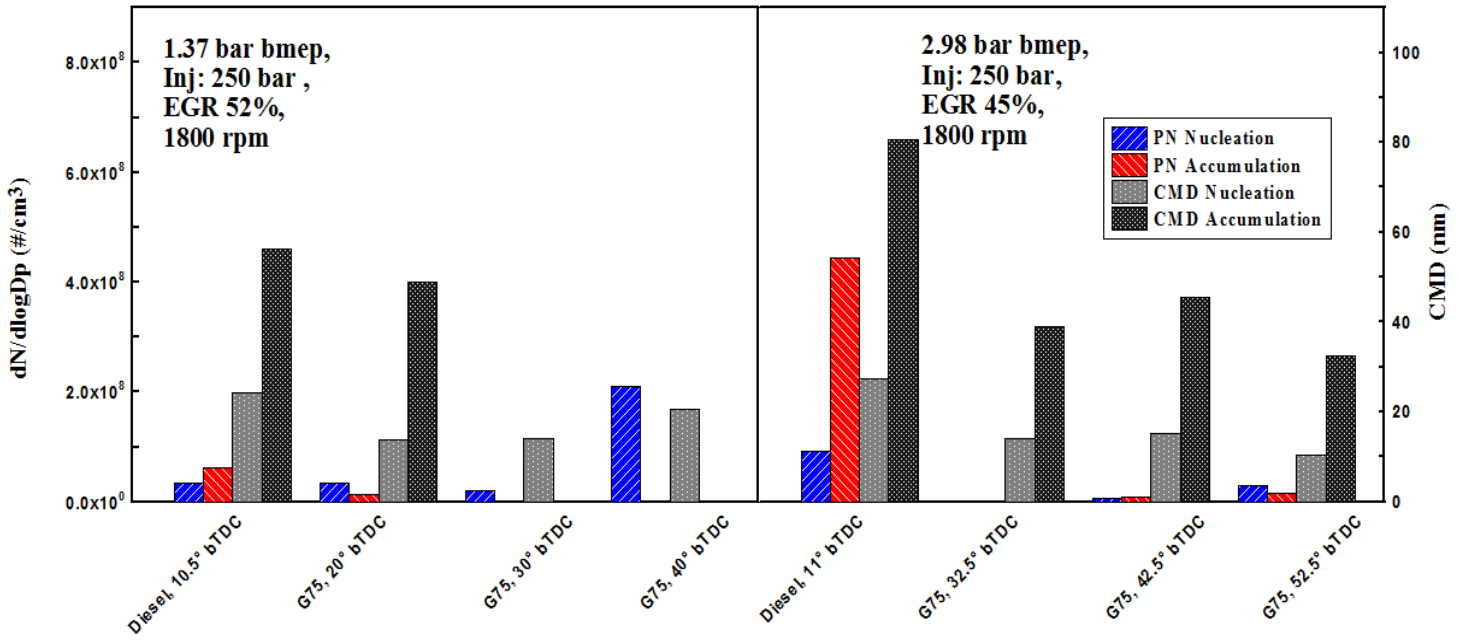


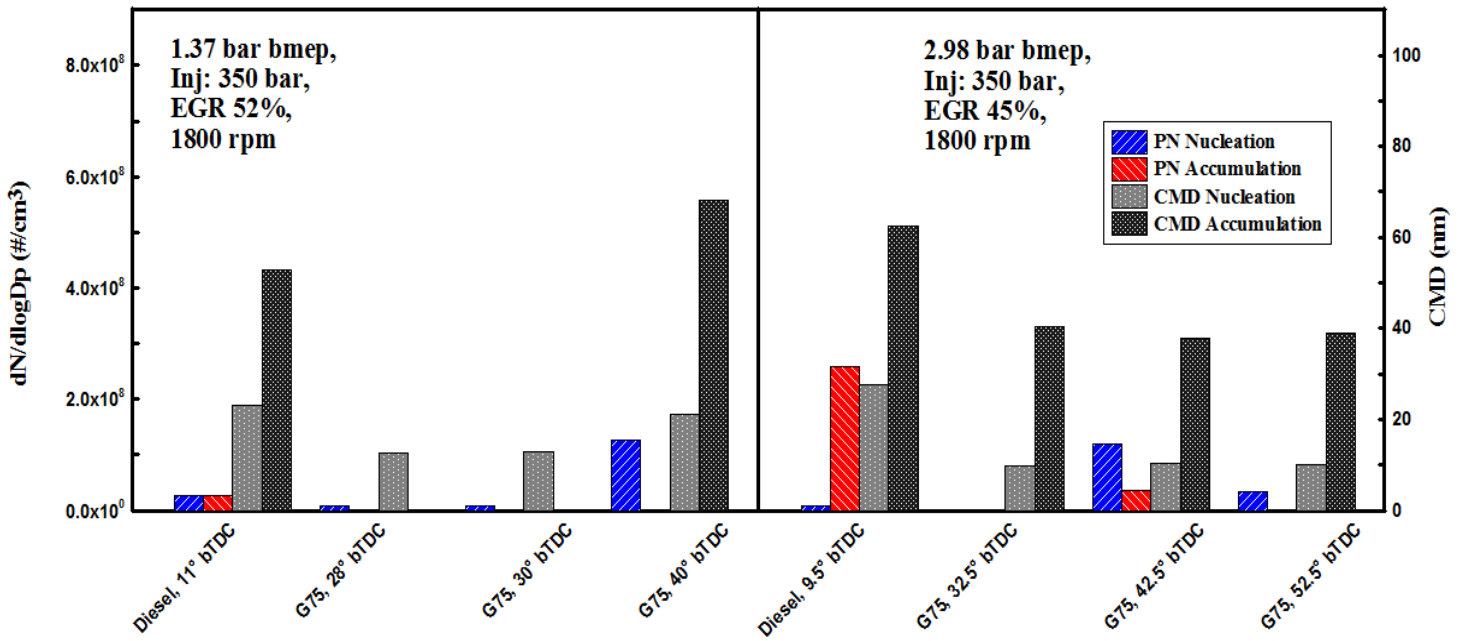
Figure 4.7: The effect of injection pressure of diesel on the particle number concentration



(a)



(b)



(c)

Figure 4.8: The effect of injection timings of diesel and G75 on the particle number concentration and CMD for 1.37 and 2.98 bar BMEP at injection pressures: (a) 150 bar; (b) 250 bar; (c) 350 bar

4.3.3.2 Effect of Injection Pressure and Timing at a Load of 2.98 bar BMEP

At a load of 2.98 BMEP and for diesel fuel, increasing the injection pressure from 150 bar to 1400 bar while maintaining EGR at 45%, the peak of the high particle number concentration shifted towards small sized particles due to better fuel atomization. Compared with a low load of 1.37 BMEP, the particle number concentrations and CMD of nucleation and accumulation were higher. With increasing engine loads, the air-fuel ratio decreased and created fuel-rich regions inside the combustion chamber, due to the injection of higher fuel quantities. These fuel-rich zones with lower local oxygen concentrations were subjected to a higher temperature, which set the reaction pathway onto a pyrolytic reaction, which in turn prevailed over the oxidation reaction and produced a motivated environment for soot formation and agglomeration.

For G75 at a low injection pressure of 150 bar and at 32.5° bTDC, as shown in Figure 4.6 (d), the particle number concentration of the nucleation mode with CMD 20 nm and accumulation with CMD 55 nm decreased by 66.80% and 96.85%, compared to diesel at an injection pressure of 150 bar. The EGR level was lower than in the case of load 1.37 bar BMEP, meaning that oxygen levels increased a little, helping the soot oxidation process. Moreover, the burning rate during combustion was slow, which provided time for the soot to be oxidized, leading to low emissions of PN. When the injection timing was advanced to 52.5° bTDC, the peaks of the high particle number concentration reduced and shifted towards small-sized particle regions. This is similar to the experiment at load 1.37 bar BMEP when the injection timing was advanced. The available time for fuel droplets to mix with the surrounding air was increased, providing an enhancement in the combustion process. Therefore, the particle number concentration of the nucleation mode and accumulation mode

decreased by 87% and 98%. Also, the CMD in the nucleation and accumulation modes reduced from 27 nm to 13 nm and 104 nm to 44 nm respectively compared to diesel fuel, as shown in Figure 4.8 (a).

When the injection pressure increased to 250 bar at 32.5° bTDC, as shown in Figure 4.6 (f), there was a significant reduction of the number of nucleation mode and accumulation mode particles – 98% and 99.70% respectively – and CMD reduced to a smaller size (~15 nm) compared to diesel fuel, as shown in Figure 4.8 (b). The fuel was injected inside the chamber in small-sized droplets at a temperature that helped to vaporize the gasoline fraction quickly, premixed well before the combustion started. The same observation was made when the injection pressure increased to 350, where the particle number concentration reduced by over 90% compared to diesel Figure 4.8 (c).

When the injection timing of G75 was advanced from 32.5 to 52.5° bTDC at an injection pressure of 250, the particle number concentration increased from 1.68E06 cm-3 to 2.74E07 cm^{-3} for nucleation mode particles and from 1.04E06 cm-3 to 1.70cm^{-3} for accumulation mode particles. The same observation was made at injection pressure of 350 bar. Even at low load 1.37 bar BMEP, a similar result was observed where the nucleation mode particles increased significantly when the fuel was further advanced. This increase in the number of small particles was attributed to fuel wall impingement. Furthermore, hydrocarbons were at a high level when the injection timing was advanced, as shown in Figure 4.9 (b). It could be said, therefore, that the increase of particle number in the nucleation mode mostly originates from unburned hydrocarbons.

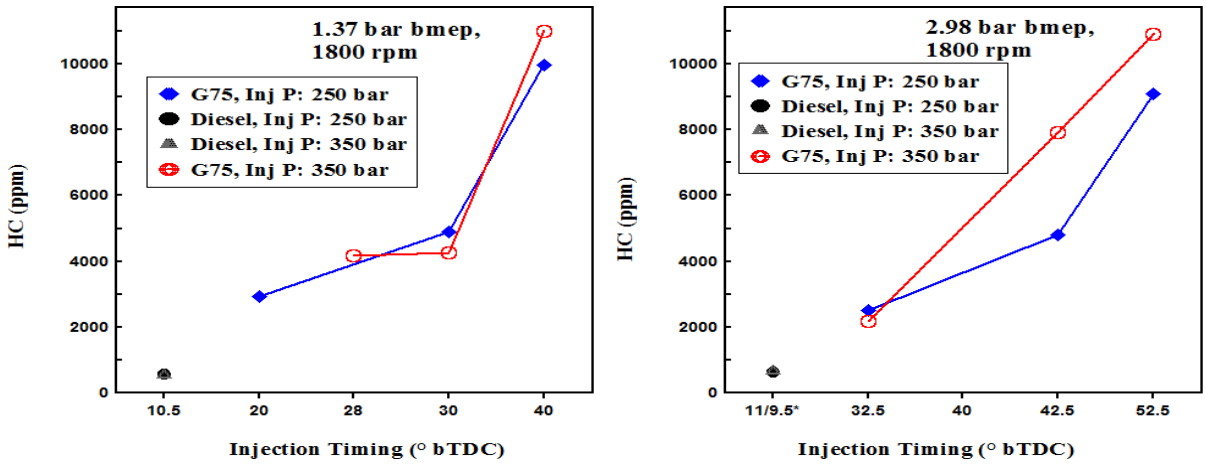


Figure 4.9: Hydrocarbons emissions (a) at 1.37 bar BMEP, (b) at 2.98 bar BMEP

* Left injection timing is at injection pressure 250 bar, right at 350 bar

G75 fuel demonstrated a large reduction in small particles in the nucleation mode and in large particles in the accumulation mode when the fuel had injection pressure of 250 bar and the injection timing was at 32.5° bTDC, compared to the other conditions of the G75 and diesel fuels. The decrease in particle number concentration could be attributed to the increase of injection pressure which atomizes fuel; furthermore, the fuel was injected near TDC, where in-cylinder pressure and temperature are high, in order to decrease the fuel's droplet size, which causes a better mixing of air and fuel (Agarwal[a], et al., 2013). In general, G75 fuel demonstrated itself to be a good fuel with the potential to reduce the particle number concentration and CMD.

4.4 Chemical Characterization of Diesel and G75 PM

4.4.1 Elemental, Organic and Total Carbon

Elemental carbon (EC) is a solid carbon formed through the pyrolytic reaction of unburned hydrocarbons in the combustion chamber under high temperature and pressure, in fuel-rich regions and at a low level of oxygen concentration. The hydrogen atoms are fragmented from the hydrocarbon chains, and the core carbon or (EC) remains. Organic carbon (OC) is a volatile organic material and usually condenses over solid carbon when a motivated environment is created, and when the materials' condensation participates in the growth of the particle. Both OC and EC are major components of the emitted exhaust gas from CI engines. The organic materials are carcinogenic and harmful to humans. They are composed of hundreds of organic compounds, such as polyaromatic hydrocarbons (PAHs) (Gangwar, et al., 2012 and Dwivedi, et al., 2006).

The concentrations of EC, OC, and total carbon (TC), as well as the OC/EC ratio of the two operating loads (1.37 and 2.98 bar BMEP) at different injection pressures and timings for diesel and G75 fuels, are presented in Figure 4.10. It has been noted that G75 demonstrated very low OC, EC and TC compared to diesel at both loads. This significant decrease may derive from the better mixing of the fuel with the surrounding air. At low load 1.37 bar BMEP for diesel and at 350 bar, it was found that EC, OC, and TC were low compared to load 2.98 bar BMEP. This is attributed to the lower combustion temperature preventing the extensive pyrolytic reaction from taking place, resulting in a reduction in organic carbon formation. Increasing the load creates a favourable environment for the formation of EC and OC since

the combustion temperature is sufficiently high; the OC/EC ratio decreased when the load is increased.

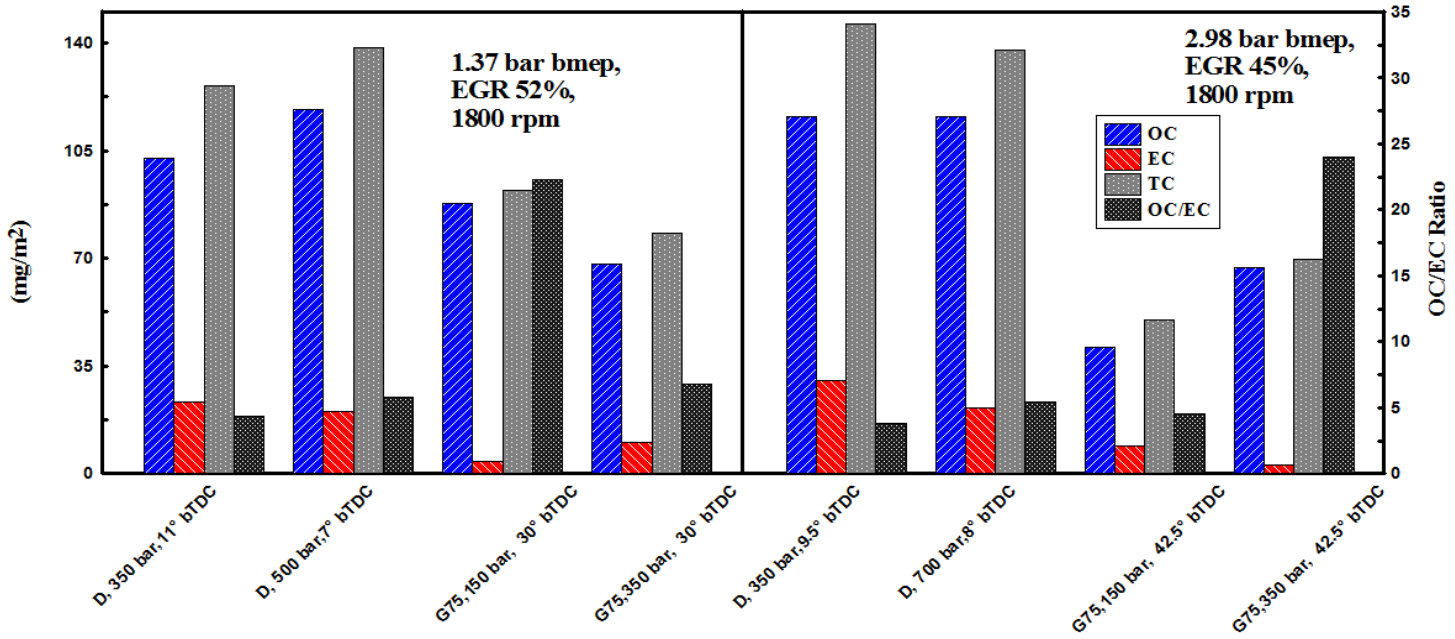


Figure 4.10: Elemental carbon (EC), organic carbon (OC) and total carbon (TC) concentration of diesel and G75 fuels at both loads with their EC/OC ratio

As the load increased, the combustion temperature increased, resulting in the re-burning of the organic species formed in the pyrolysis process and a subsequent reduction in OC production. Despite the fact that G75 has low EC, OC, and TC for both loads compared to diesel fuel, it shows opposite trends for the OC/EC ratio as it increased when the load was increased. This is due to fuel impingement in the cylinder wall and the piston top land crevice, where the temperature is lower in order to oxidize the fuel completely, as reported by Agarwal, et al. (2015). This also results in an increase in unburned hydrocarbons that can participate in the nucleation mode.

4.5 Summary

This study was conducted in order to investigate the effect of injection pressure and timing on the particle size and number distribtuion and chemical characterization of the PM of diesel and G75 fuels. The investigation was carried out on a Ford Puma four-cylinder common rail direct injection diesel engine, not equipped with DOC, with EGR cooler modification (deactivating the EGR cooler) and at a constant speed of 1800 rpm. The fuel injection pressure and timings have been investigated and the following observations were made:

- Using hot EGR for diesel fuel emits higher PN compared to when cold EGR was used at both loads. PN emissions were increased by around 90% compared to cold EGR. The increase in EGR temperature increased the gas temperature, which may have resulted in a reduction in the amount of oxygen in the cylinder (thermal throttling). Therefore, the soot oxidation process ceased earlier, leading to an increase in PN emissions.
- The engine was not capable of starting when the cold EGR was used for G75, and therefore hot EGR was used. The particle number concentrations (PN) significantly decreased by around 99% compared to diesel fuel. It was hypothesized that the preheated intake temperature via hot EGR led to the quick vaporization of gasoline fractions in diesel, and mixed well with the surrounding air.

- At load 1.37 bar BMEP, advancing the injection timing of the G75 fuel (e.g. Inj T: 40° BTDC, Inj P: 150 bar) significantly reduced the particle number concentration of both nucleation and accumulation by around 99% compared to diesel fuel. A similar observation of the reduction of PN emissions was made at load 2.98 bar BMEP, at injection timing of 32.5° BTDC, and injection pressure of 250 bar compared to diesel

fuel. G75 fuel has a longer ignition delay and was tried with an early fuel injection that provided enough time for the fuel to be sufficiently mixed with air before the start of ignition. Consequently, this enhanced the combustion process and promoted soot oxidation over soot formation, resulting in a significant reduction in PN emissions.

- In order to reduce PN emissions for diesel fuel by 99%, the injection pressure should be increased to 1400 bar with EGR 45%, injection timing at 5.8° bTDC, and at a load of 2.98 bar BMEP. Increasing the injection pressure reduced the fuel droplet sizes, providing for a better mixing of the fuel with air.
- Increasing the EGR ratio for diesel fuel when using cold EGR, and G75 fuel with hot EGR, increased PN emissions by more than 95%. This was attributed to the decrease in oxygen levels, which affects the soot oxidation process. Additionally, the lower temperature accompanied by an increase in the EGR percentage led to more PN emissions.
- G75 demonstrated very low EC, OC, and TC compared to diesel fuel. The OC, EC, and TC of G75 was reduced by 47%, 94% and 57% respectively compared to diesel fuel, but in some cases there was a high OC/EC of more than 100%. This could be due to high emissions of unburned fuel in some operating conditions, as previously discussed.

In general, G75 fuel demonstrated a high potential to reduce PN emissions with very low injection pressure compared to diesel.

CHAPTER 5

PM CHARACTERISTICS OF DIESELINE AND NAPHTHA FUELLED PCI WITH SINGLE INJECTION

5.1 Introduction

In premixed compression ignition (PCI) engines, if the final fuel injection, which controls combustion phasing, is sufficiently completed before combustion starts (long ignition delay), soot formation can be avoided and NOx can be controlled by introducing large amounts of EGR (Imtenan, et al., 2014). It has been reported that by running a diesel engine in PCI with single injection at 25° bTDC injection timing, soot can be reduced below FSN 0.03 (Jacobs and Assanis, 2007). It has also been reported that with a single injection strategy and an EGR ratio of 48%, PM emissions decreased (Han, et al., 2009). It was also found that soot emissions decreased rapidly when the EGR ratio was 50% (Alriksson and Denbratt, 2006).

The alteration of fuel properties is considered to be another way to attain PCI combustion. Fuels with higher volatilities, lower cetane numbers (CN < 30), and moderately high research octane numbers (RON > 60) are suitable for PCI combustion (Kalghatgi, et al., 2007; Risberg, et al., 2006). A study of different fuel volatilities has been conducted on an optical diesel engine running in PCI combustion mode, and found that a fuel with higher volatility produces fewer smoke emissions and less fuel wall impingement at an injection timing earlier than 30° BTDC (Cheng, et al., 2010).

At the University of Birmingham, it was reported that using a lower cetane number (CN) fuel such as gasoline, blended with diesel in a ratio of (50:50) to make dieseline fuel, produced very low NOx (0.06 g/kWh) with single injection at 28°bTDC and an EGR rate of 50%. Moreover, the larger-sized particles (accumulation mode) were reduced compared to conventional diesel combustion. In contrast, the number of smaller-sized particles (nucleation mode) was increased as a result of fuel impingement on the walls of the cylinders; the general observation, however, was that the total particle number concentration was reduced by 99% and that even smoke decreased to almost zero (Zhang, et al., 2012).

This chapter discusses the effect of single injection on combustion performance and on the particle size distributions and chemical characterization of the particulate matter (PM) of a diesel-, G75-, and naphtha-fuelled premixed compression ignition (PCI) engine. Furthermore, elemental carbons (EC), organic carbon (OC), EC/OC ratio, trace metals, and polyaromatic hydrocarbons (PAHs) are considered.

5.1.1 Research Objective

Using a single injection strategy, the study investigated the effect of load variation on the particle size distributions and chemical characterization of the PM of a diesel-, G75-, and naphtha-fuelled PCI engine. The pertinent points were collected in conditions comparable to diesel fuel in terms of BTE, NO_x, soot, and PN.

5.1.2 Test Conditions

The engine set-up and its specification is presented in Figure 3.2 and Table 3.1 in Chapter 3. The tested fuels were three fuels (diesel, G75, and naphtha) and their properties are presented in Table 3.2 in Chapter 3. The tests were conducted at four different loads (1.50, 3, 6, and 12 bar BMEP) with a constant speed of 1800 rpm and fixed ($\lambda \sim 1.25$). The logged data and filter papers were collected at steady state and before DOC as presented in Table 5.1.

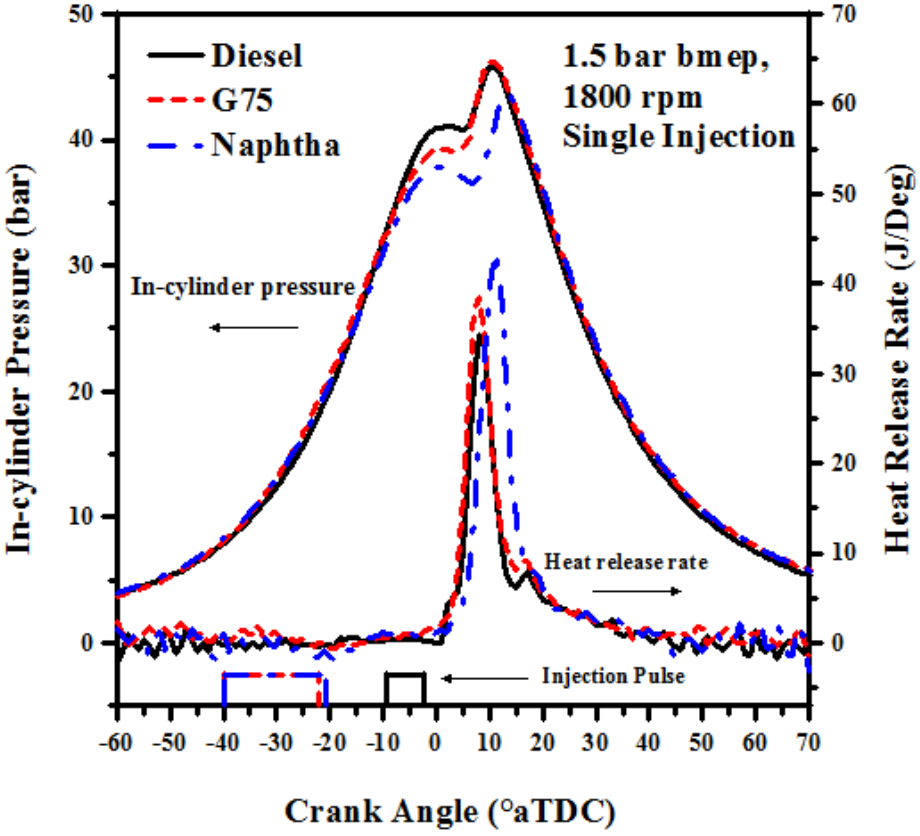
Table 5.1: Test conditions at four different loads for diesel, G75 and naphtha fuels

Speed (rpm)	**1800**				**Fuel**
Load (bar BMEP)	**1.50**	**3**	**6**	**12**	
Injection Pressure (bar)	500	700	1200	1200	
Injection Timing (°bTDC)	9.5	8	3	3	
EGR Ratio (%)	60	49	28	16.8	**Diesel**
NOx (g.kWh^{-1})	0.41	0.48	0.82	1.40	
Smoke (FSN)	0.37	0.46	0.49	1.42	
BTE (%)	24.28	34.56	38.87	40.63	
Injection Pressure (bar)	150	350	500	1000	
Injection Timing (°bTDC)	40	32.5	26	5	
EGR Ratio (%)	51	43	29.5	16.4	**G75**
NOx (g.kWh^{-1})	0.27	0.41	0.38	1.80	
Smoke (FSN)	0.003	0.006	0.02	0.85	
BTE (%)	22.92	32.86	37.99	39.69	
Injection Pressure (bar)	150	350	500	1000	
Injection Timing (°bTDC)	40	32.5	26	5	
EGR Ratio (%)	44.50	31.40	29.50	29.50	**Naphtha**
NOx (g.kWh^{-1})	0.37	0.50	0.32	1.60	
Smoke (FSN)	0.014	0.007	0.012	0.411	
BTE (%)	22.35	31.91	35.76	39.62	

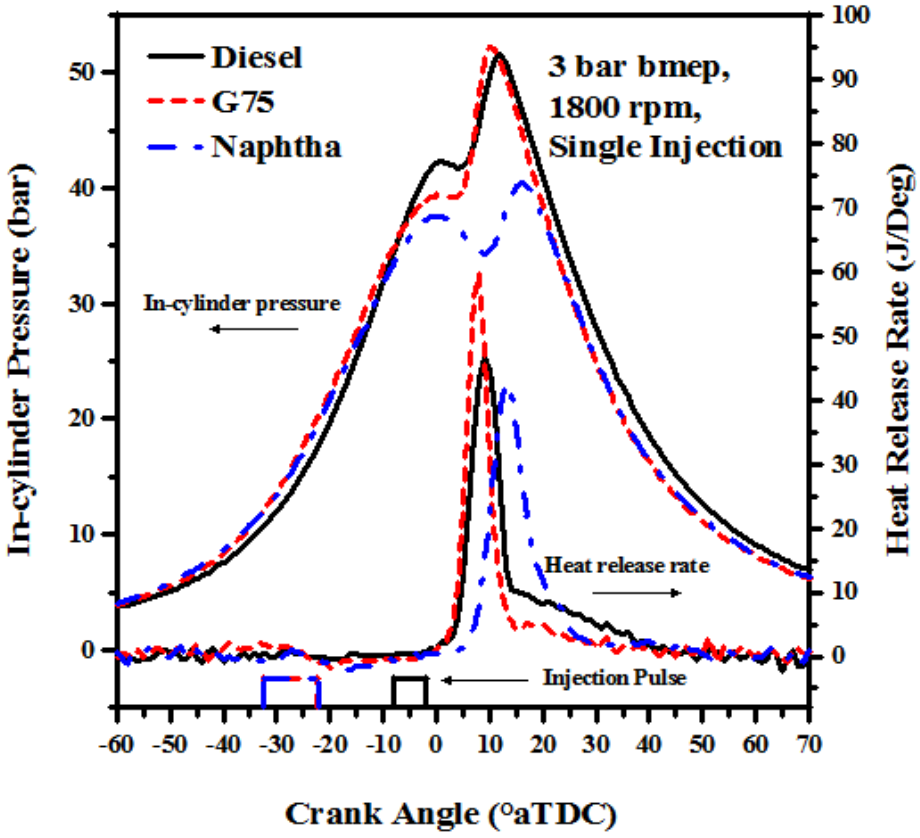
5.2 Combustion Performance

5.2.1 Heat Release Rate Analysis

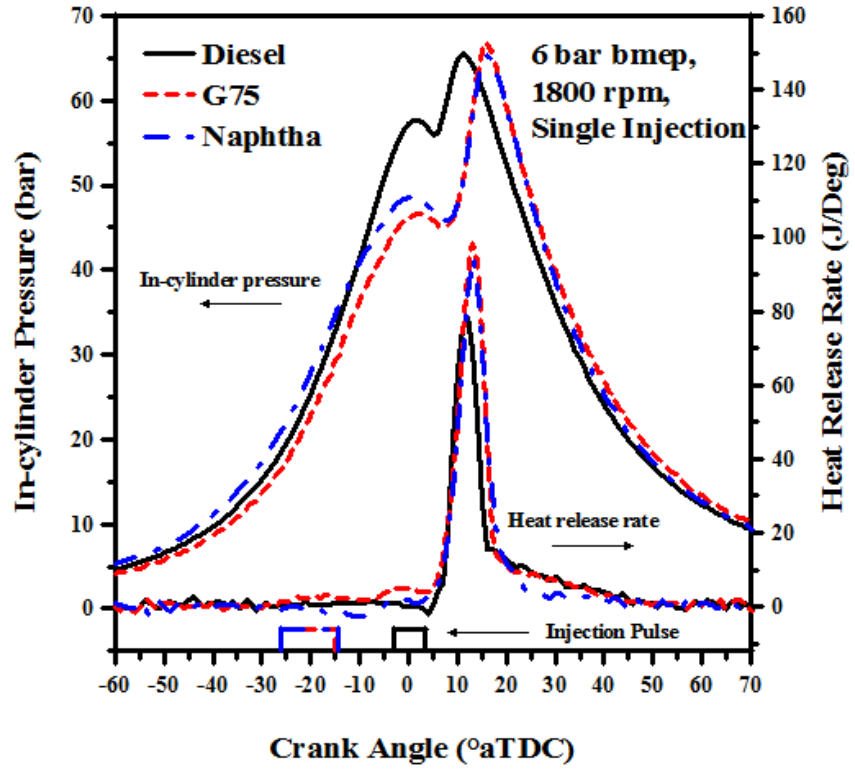
The heat release rate, injection pulses, and in-cylinder pressure of the three fuels using single injection at four different loads and at a fixed speed of 1800 rpm are plotted against the crank angle degree (CAD), as shown in Figure 5.1. The maximum in-cylinder pressure and heat release rate for all fuels at different engine loads are presented in Figure 5.2. At low load 1.5 bar BMEP, it was observed that after the end of the fuel injection event, the high heat release rate for all three fuels began, as shown in Figure 5.1 (a). A similar observation was made when the load was increased from 1.5 to 6 bar BMEP: the high heat release rate started after the end of the fuel injection event and two fuels – G75 and naphtha – had a higher HRR compared to diesel at all loads, as shown in Figure 5.2. This observation indicates that the combustion was in a premixed compression ignition (PCI) mode. At low load 1.5 bar BMEP, the separation between the start of combustion and the end of the fuel injection event was attributed to the usage of a high EGR level. It was noticed that G75 and naphtha fuels have a higher heat release rate compared to diesel, except in the case of naphtha fuel at 3 bar BMEP, which was very low compared to the other fuels. The drop of heat release at 3 bar BMEP is also matched with the drop in the brake thermal efficiency (BTE) and MPRR, as shown in Figure 5.4 (a, b). The load was not stable while logging the data at 3 bar BMEP.


Diesel
G75
Naphtha
1.5 bar bmep,
1800 rpm
Single Injection
In-cylinder pressure
Heat release rate
Injection Pulse
In-cylinder Pressure (bar)
Heat Release Rate (J/Deg)
Crank Angle (°aTDC)

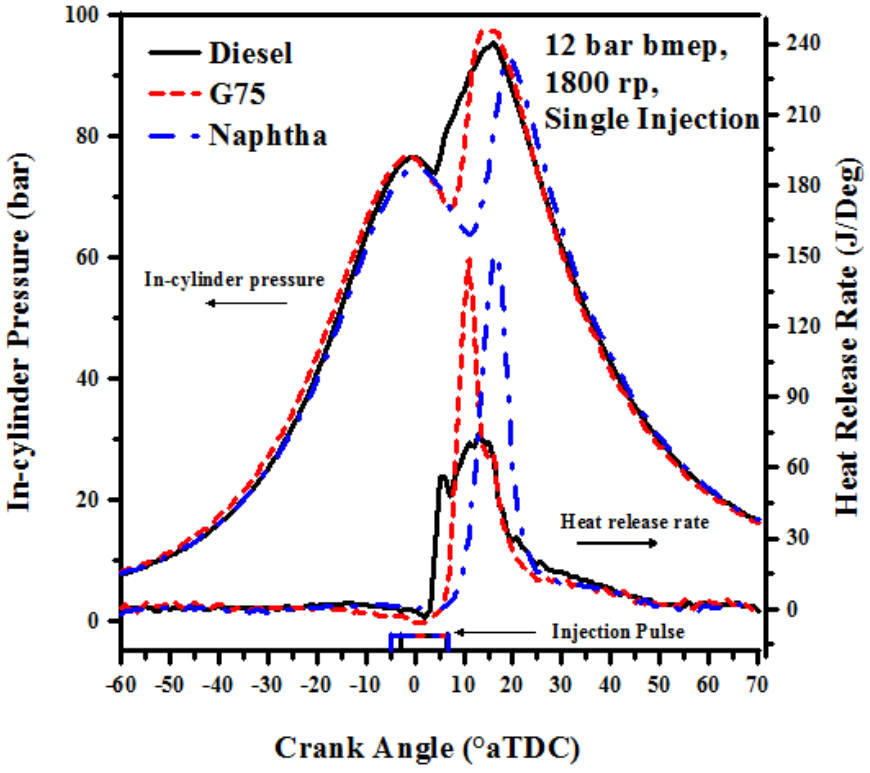
(a)


Diesel
G75
Naphtha
3 bar bmep,
1800 rpm,
Single Injection
In-cylinder pressure
Heat release rate
Injection Pulse
In-cylinder Pressure (bar)
Heat Release Rate (J/Deg)
Crank Angle (°aTDC)

(b)



(C)



(d)

Figure 5.1: In-cylinder pressure and heat release rate of diesel, G75 and naphtha fuels with single injection versus crank angle: (a) 1.5, (b) 3, (c) 6, (d)12 bar BMEP

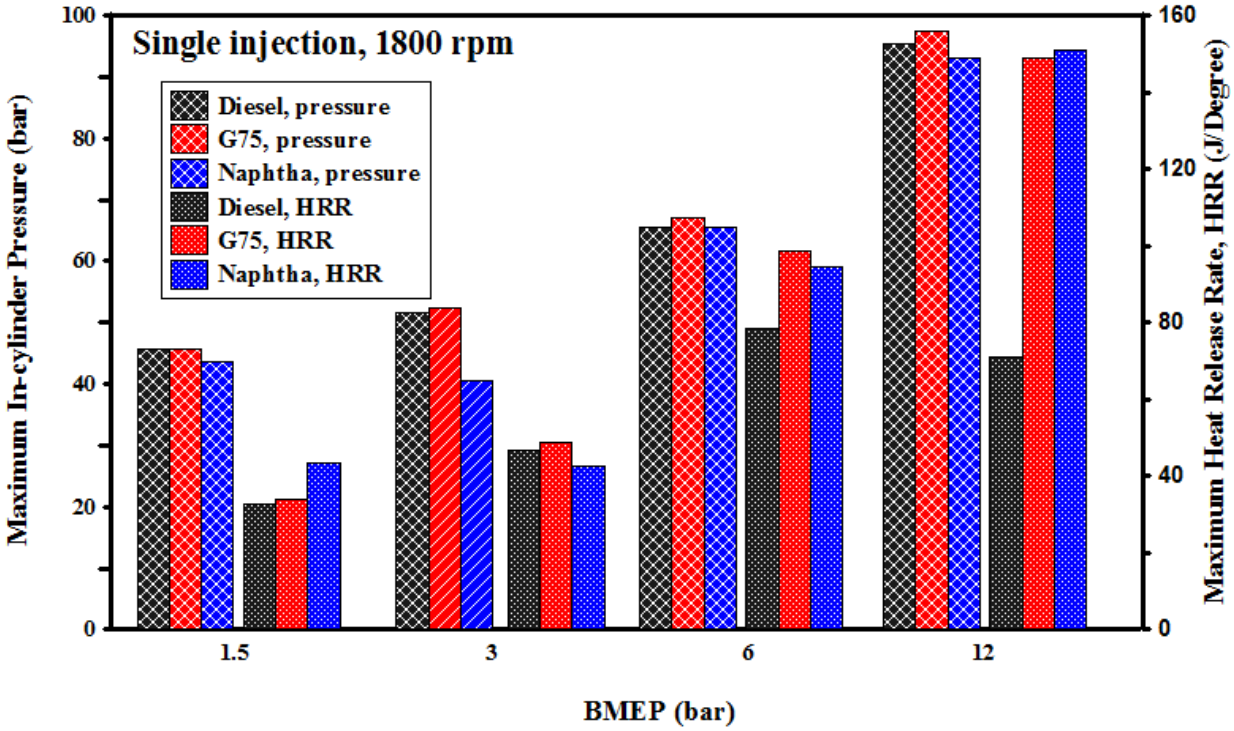
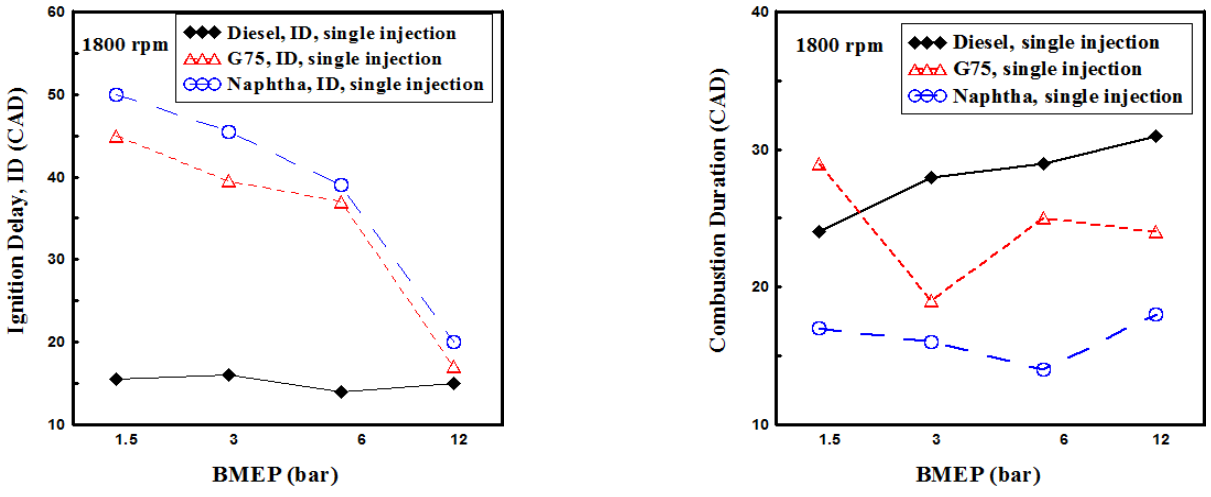


Figure 5.2:Maximum incyline pressure and heat release rate of diesel, G75 and naphtha fuels with single injection versus engine loads.

G75 and naphtha fuels have a longer ignition delay; naphtha fuel has the longer, as shown in Figure 5.3. A longer ignition delay provides more time for the fuel to mix more fully with the surrounding air. At load 6 bar BMEP, the peaks of the heat release of G75 and naphtha were single and coincided; the onset of the diesel fuel combustion was closer to the end of the fuel injection event. When the load was increased to 12 bar BMEP, the start of combustion and the end of the fuel injection event for the diesel fuel overlapped, resulting in a lower heat release peak. For G75 and naphtha fuels, the combustion process with a high heat release rate began closer to the end of the fuel injection event. It was also observed that in terms of the peaks of the rate of heat release with the naphtha fuel, most cases were retarded compared to the diesel and G75 fuel. This is due to the longer ignition delay, as shown in Figure 5.3.

5.2.2 Ignition Delay

Ignition delay (ID) is defined as the difference between the start of the fuel injection event and 50% of the cumulative apparent heat release AHR50, as shown in Figure 5.3 (a) for three fuels at four different loads. It has been proven by Kalghatgi, et al. (2010) that the ID is a good indicator when seeking to understand the effect of fuel on the combustion performance of CI engines. Longer ID results in more time for fuel to be well mixed with the surrounding air. In Figure 5.3(a), at a load of 1.5 bar BMEP, G75 and naphtha fuels have a longer ID compared to diesel fuel. The ID of G75 fuel was 33 CA degrees longer than diesel fuel, while naphtha fuel was 39 CA degrees. The ID of naphtha fuel was 5 CA degrees longer than G75 fuel. The reasons for the long ID delay of both G75 and naphtha fuels compared to diesel fuel are the high volatility and low cetane number (CN); naphtha fuel, however, has the highest ID compared to the other two, since the ID was 39 CA degrees.



(a) (b)

Figure 5.3: The ignition delay (a), the combustion duration (b) of three fuels at four different loads

Increasing the load decreased the ID for fuels and became smaller at the high load 12 bar BMEP. This is attributed to the decrease in EGR level, and to the fact that the cylinder wall

and piston became hotter, which this helps with fuel autoignition. For diesel fuel, the decrease of ID was very small compared to low load 1.5 bar BMEP. The decrease was about 1.5CA degrees.

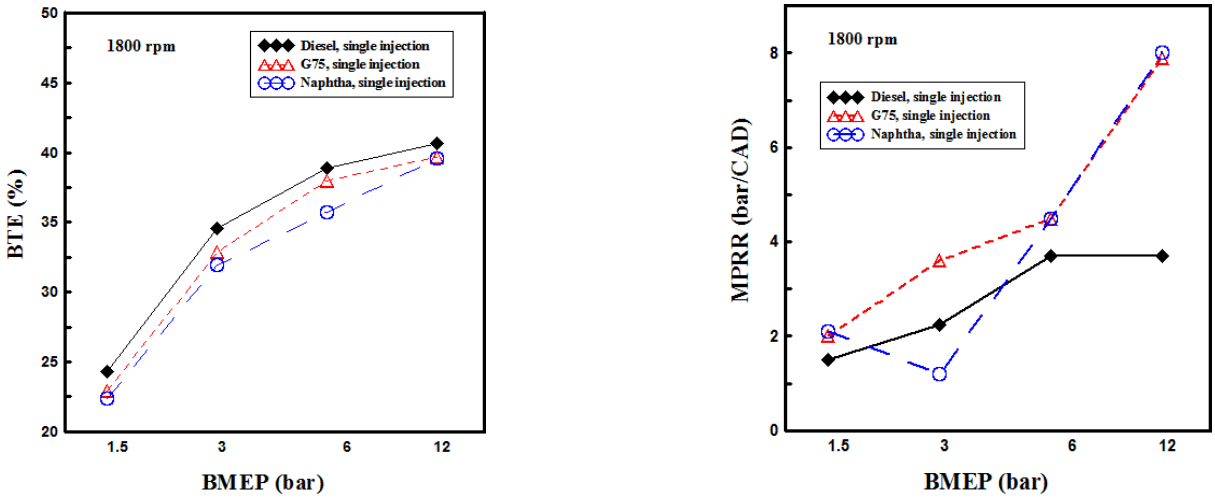
The combustion duration as shown in Figure 5.3 (a) is defined as the difference between the crank angle of 10% mass fraction burn (MFB 10) and 90 % mass fraction burn (MFB 90). G75 fuel has a longer combustion duration at load 1.50 bar BMEP compared to diesel and naphtha fuels, while diesel fuel has a longer combustion duration compared to G75 and naphtha fuels when the load increased from 3 bar BMEP to 12 bar BMEP. It could be said that before the combustion of G75 fuel at load 1.50 bar BMEP began, the local mixture was in some regions over-lean, resulting in a longer combustion duration with a low burning rate. From load 3 bar to 12 bar BMEP, the combustion duration of G75 was shorter than that of diesel fuel, while naphtha fuel was considered to be the shortest at all loads. The burning rate at these loads was high since the local mixture was close to a stoichiometric condition.

5.2.3 Brake Thermal Efficiency

In Figure 5.4 (a), the brake thermal efficiency (BTE) of diesel, G75, and naphtha fuels is plotted against the load variations. It was noted that the BTE of all fuels increased with the increase in engine loads. Increasing the load leads to an increase in the in-cylinder temperature. High in-cylinder temperatures produced fewer emissions of BSHC and BSCO, and the BTE increased as a result. At low load 1.50 bar BMEP, G75 and naphtha fuels were around 1.36% and 1.93% (absolute value) respectively, which was lower than diesel fuel. When the load was increased to 6 bar BMEP, the BTE of G75 and naphtha fuels was lower than diesel fuel by 0.88% and 3.11% (absolute value) respectively. At high load 12 bar

BMEP, both fuels G75 and naphtha were lower than diesel by 0.94% and 1.01% (absolute value) respectively.

The maximum pressure rise rate (MPRR), which could provide insight into combustion noise induction, is plotted against the load variation as shown in Figure 5.4 (b). It is evident that diesel fuel maintains low noise levels while the load is increased: the short ID of diesel reduces the burning rate. For G75 and naphtha fuels, it was observed that the combustion noise was higher compared to diesel when the load increased, except in the case of naphtha fuel at load 3 bar BMEP. The naphtha fuel was quieter compared to diesel and G75 fuels, which was also observed in Figure 5.1 (b), where the combustion phasing of naphtha fuel at 3 bar BMEP was retarded with a lower in-cylinder pressure and heat release rate. This could be related to the local air-fuel ratio where the mixture was leaner, which resulted in a lower burning rate, since at high load the burning rate was high and the MPPR increased.



(a) (b)

Figure 5.4: The brake thermal efficiency (a) and maximum pressure rise rate (b)

5.2.4 Regulated Emissions

Figure 5.5 presents smoke emissions and the three normalized types of emission – nitrogen oxides (NO_x), hydrocarbons (HC), and carbon monoxide (CO) – at four different loads with single injection. It was noted that at low load up to 6 bar BMEP, G75 fuel produced low NOx compared to diesel fuel, as shown in Figure 5.5 (a). Also, naphtha fuel produced low NOx at 1.50 and 6 bar BMEP compared to diesel fuel, but at 3 bar BMEP it produced a similar amount.

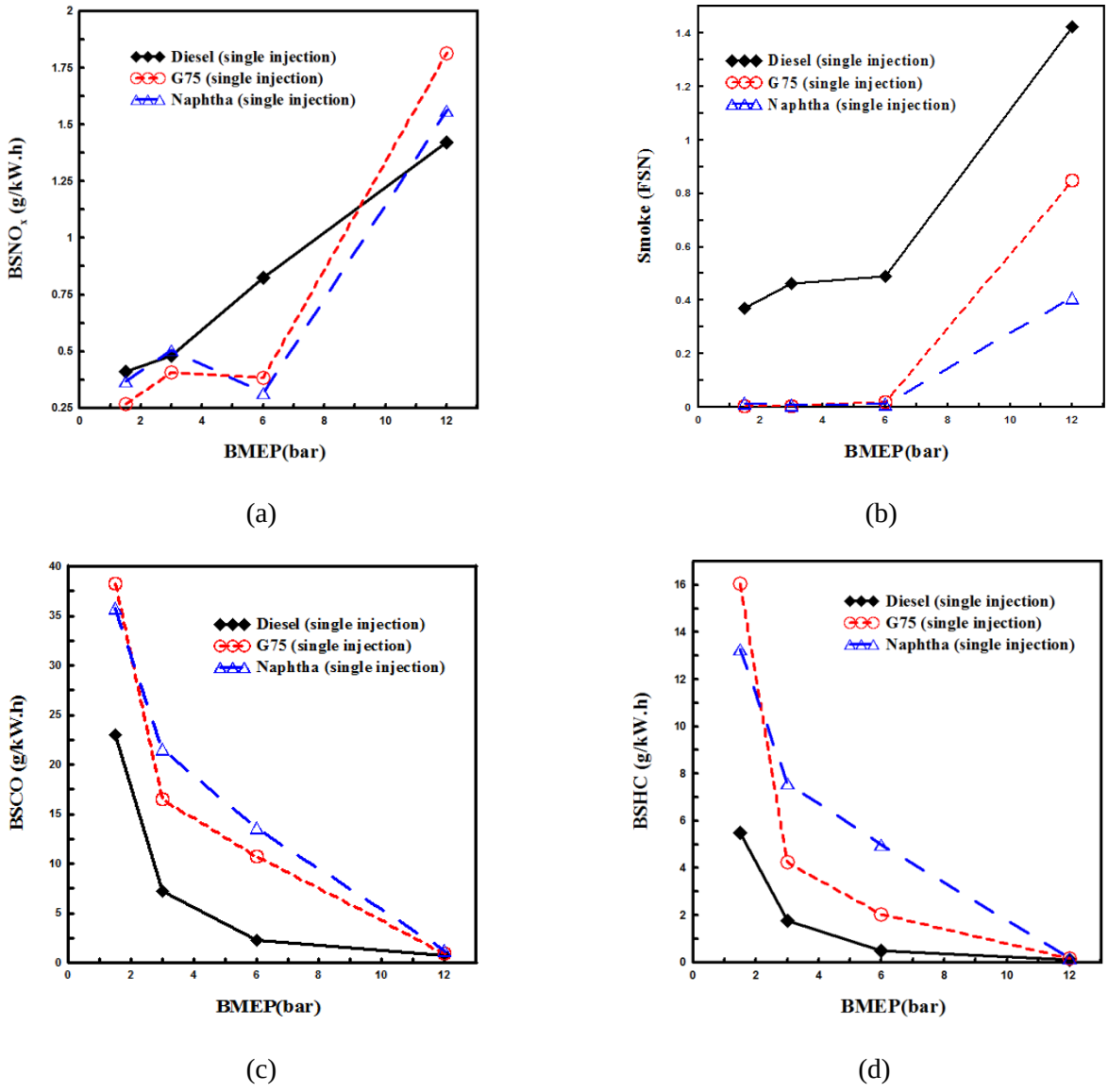


Figure 5.5: BSNOx (a), Smoke (b), BSHC (c), BSCO (d) emissions at four loads with single injection

At low loads, the EGR ratio was used in large amounts, and the onset of the combustion processes of G75 and naphtha fuels were separated from the end of the fuel injection event, which resulted in low-temperature combustion and a reduction in NO_x. As the load increased, NO_x emissions increased for all fuels, but G75 and naphtha fuels produced more NO_x compared to diesel fuel. At high load 12 bar BMEP, the EGR level was decreased, and the start of combustion and the end of the fuel injection event overlapped for the diesel fuel; this resulted in a low heat release peak. Furthermore, the combustion process of G75 and naphtha fuels became closer to the end of the fuel injection event, as shown in Figure 5.1 (d).

The G75 and naphtha fuels produced a very low amount of smoke, as shown in Figure 5.5 (b). They produced smoke lower than FSN 0.03 up to a load of 6 bar BMEP compared to diesel fuel. When the load was increased to 12 bar BMEP, the smoke emissions increased sharply, but G75 and naphtha fuels still maintained their low levels of smoke emission (FSN < 0.85) compared to the diesel fuel. At low loads, with the usage of a high EGR ratio and a short duration of fuel injection, the combustion processes for the three fuels were separated from the fuel injection event. As a result, a low in-cylinder temperature and improved fuel-air mixture were obtained; these are considered to create a demotivating environment for soot formation. Soot favours a high temperature and a fuel-rich region for formation (Glassman, 1989).

As presented in Figure 5.5 (c, d), G75 and naphtha fuels produced high amounts of HC and CO at low loads compared to the diesel fuel; these amounts started decreasing when the load was increased. At high load 12 bar BMEP, all three fuels produced similar amounts of HC and CO. At low loads, the larger amounts of CO and HC for G75 and naphtha fuel could be attributed to the incomplete combustion that resulted from the over-lean mixture in some regions. As the load increased, the ID decreased (as shown in Figure 5.3) and this resulted in

an increase of gas temperature and the production of local mixtures near to the stoichiometric mixture. Therefore, less HC and CO was emitted.

5.3 Effect of Engine Load on Particle Size Distribution

Particle size–number distributions were initially measured per unit of volume by using the DMS. The particle size and number distribution exhibited a slight change under test repetitions. For accuracy, the test was repeated four times and the results were averaged. Subsequently, the standard and uncertainties were reported and presented in the figures. The measured particle size number distributions have been normalized to part per kilowatt hour (kWh) at four engine loads – 1.50, 3, 6 and 12 bar BMEP – maintaining speed at 1800 rpm and lambda. The test operating conditions are presented in Table 5.1. The measurements were obtained after thermal stabilization of each test condition. Figures 5.5 and 5.6 illustrate the distribution of the particle size-number and the variation of particle number concentration in nucleation and accumulation modes for diesel, dieseline G75 and naphtha fuels at different operating conditions. In order to maximize the visibility of the particle size number distributions of G75 and naphtha, separate figures have been merged with the main figures.

5.3.1 Particle Size-Number Distribution

The process of soot formation is strongly influenced by engine operating conditions such as load, injection pressure, localized temperature, air/fuel ratio and injection timing. The variation of any parameters, namely the air/fuel ratio and localized temperature, can affect the soot formation and release rates. In fuel-rich zones, the soot formation rate dominates the soot oxidation rate. In lean zones, the rate of soot oxidation is greater than the soot formation, and therefore soot concentrations are reduced in these zones.

For diesel fuel at 500 bar injection pressure and at low load 1.50 bar BMEP as shown in Figure 5.6 (a), with EGR 60%, and injection timing of (9.5°bTDC), the peak of the high particle number concentration was $1.20x10^{15}$ (part.kWh^{-1}). The total particle number concentration was $8.25x10^{14}$ (part.kWh^{-1}), while the particle number concentrations of the nucleation mode and accumulation mode were 3.91E14 and 3.80E14 (part.kWh^{-1}) respectively, as shown in Figure 5.7 (a, b). The high particle number concentration is also matched with high smoke emissions compared to other fuels in that load, as shown in Figure 5.5 (b). This increase is due to the short ignition delay of diesel fuel as shown in Figure 5.3, and to the usage of a large amount of EGR which reduced the oxygen concentration inside the combustion chamber. Therefore, the soot oxidation process was ceased.

G75 and naphtha fuels produced very low particle numbers at load 1.50 bar BMEP compared to diesel fuel, but G75 fuel (at injection pressure of 150 bar, EGR 51% and injection timing (40°bTDC)) produced the lowest numbers compared to other fuels, as shown in Figure 5.7 (a). The low PN was also confirmed with low $BSNO_x$ and smoke, as shown in Figure 5.5 (a,b). A lean mixture region was generated inside the cylinder, promoting the soot oxidation process over soot formation and making the rate of oxidation greater. Therefore, the particle

number concentration and CMD were reduced significantly compared to diesel fuel. The total particle number concentration of G75 was reduced by 98.60%; the particle number concentration in the nucleation and accumulation modes was reduced by 97% and 99.9% respectively, as shown in Figure 5.7 (b). Additionally, the CMD was reduced from 38 nm to 12 nm, as shown in Figure 5.7 (a).

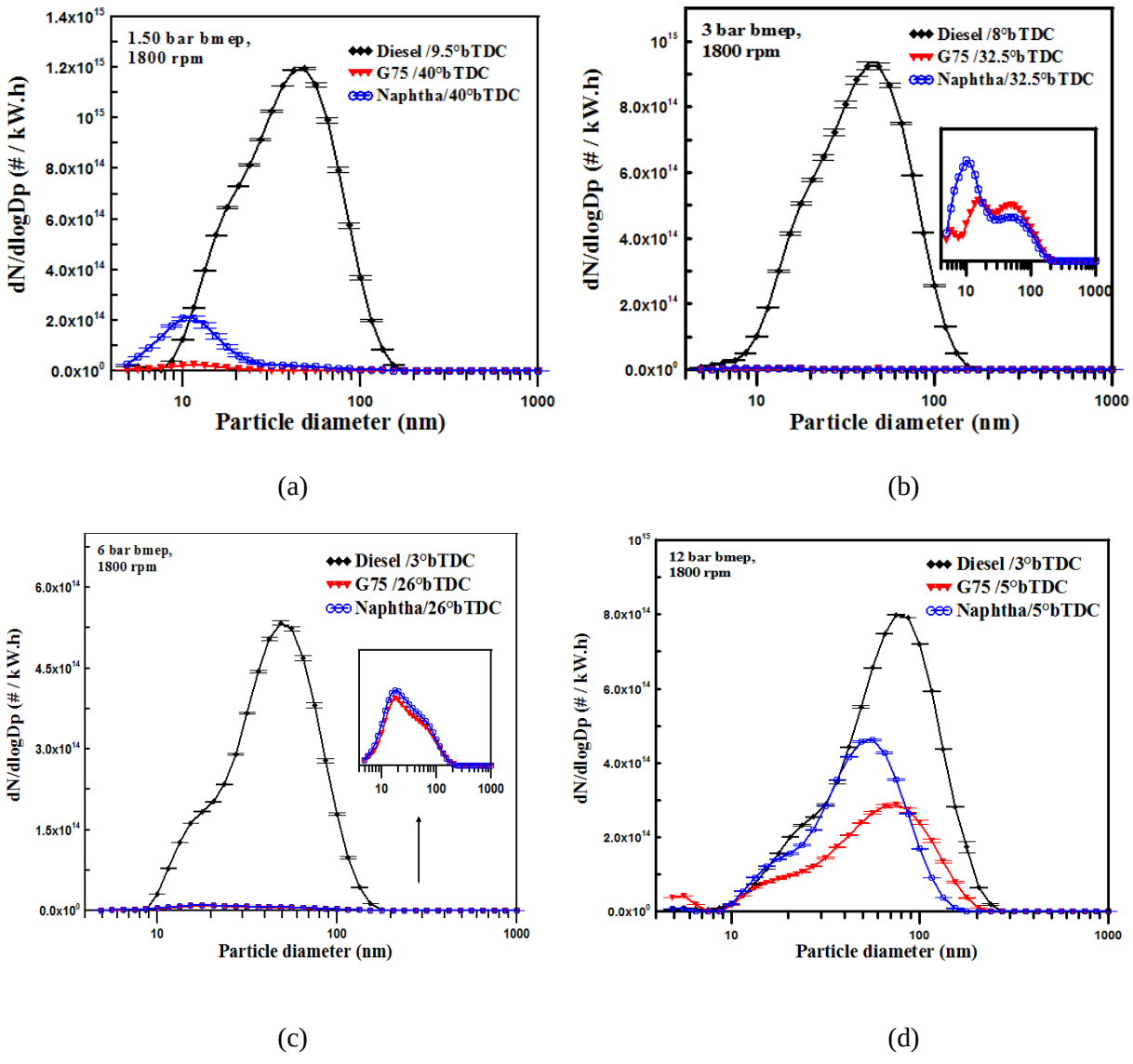


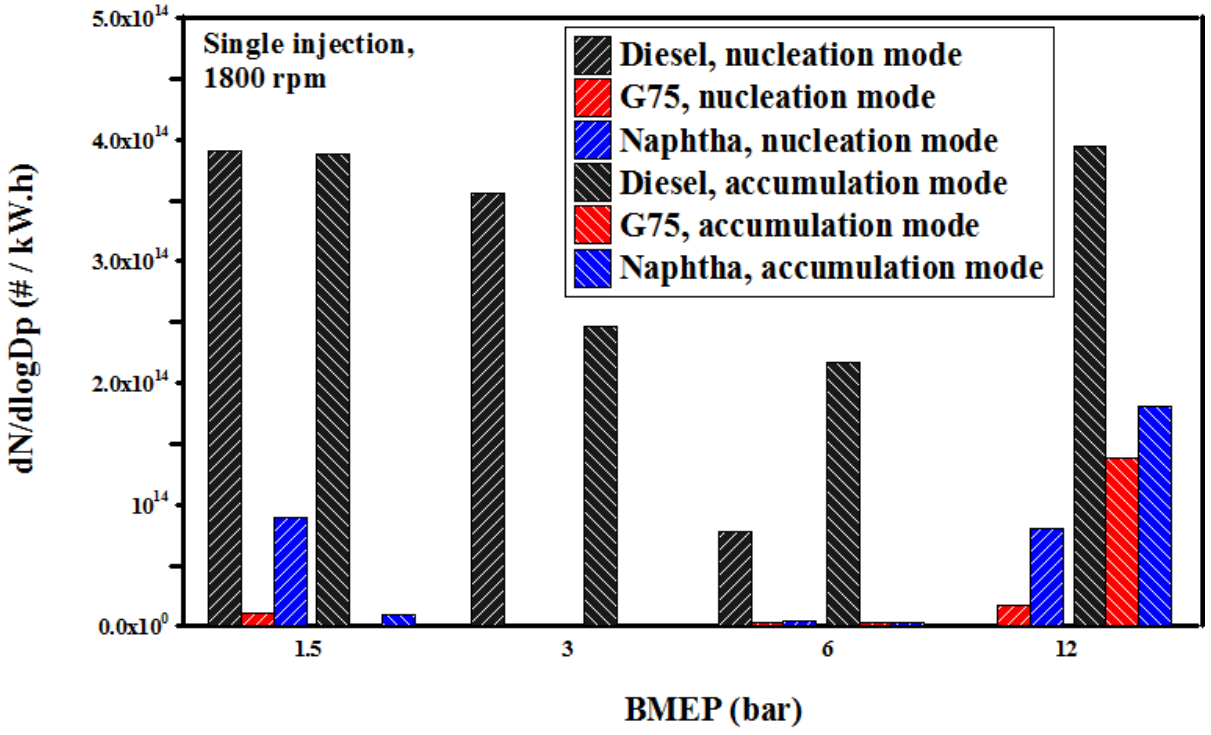
Figure 5.6: Particle size- number distributions at four loads(a) 1.50, (b) 3 , (c) 6, (d) 12 bar BMEP

Naphtha fuel also produced low PN compared to diesel fuel. The total particle number concertation was reduced by 88.50%, while the particle number concentration in both nucleation and accumulation modes was reduced by 77% and 97.50% respectively. CMD was reduced from 38 nm to 11 nm compared to diesel fuel. When increasing the load for diesel fuel from 1.50 up to 6 bar BMEP, the peak of the high particle number concentration decreased and CMD was reduced, as shown in Figure 5.6 (a, b) and Figure 5.7 (a). The decrease could be related to two factors; the first factor is the fuel atomization, since the injection pressure was higher than it was at low load. The second factor is the increased oxygen concentration inside the chamber, since the EGR level was lower than it was at low load. Reducing the EGR level increases the oxygen level, helping to oxidize soot. When the load was increased to 12 bar BMEP, the total particle number concentration increased a little, and the increase was matched with smoke, as shown Figure 5.5 (b). The fuel was injected in high quantities near TDC and at high in-cylinder temperature and so there was insufficient time for the mixture to be well mixed, resulting in an increase in PN emissions. The overlap between the start of combustion and the end of the injection event as shown in Figure 5.1 (d) is considered to be evident.

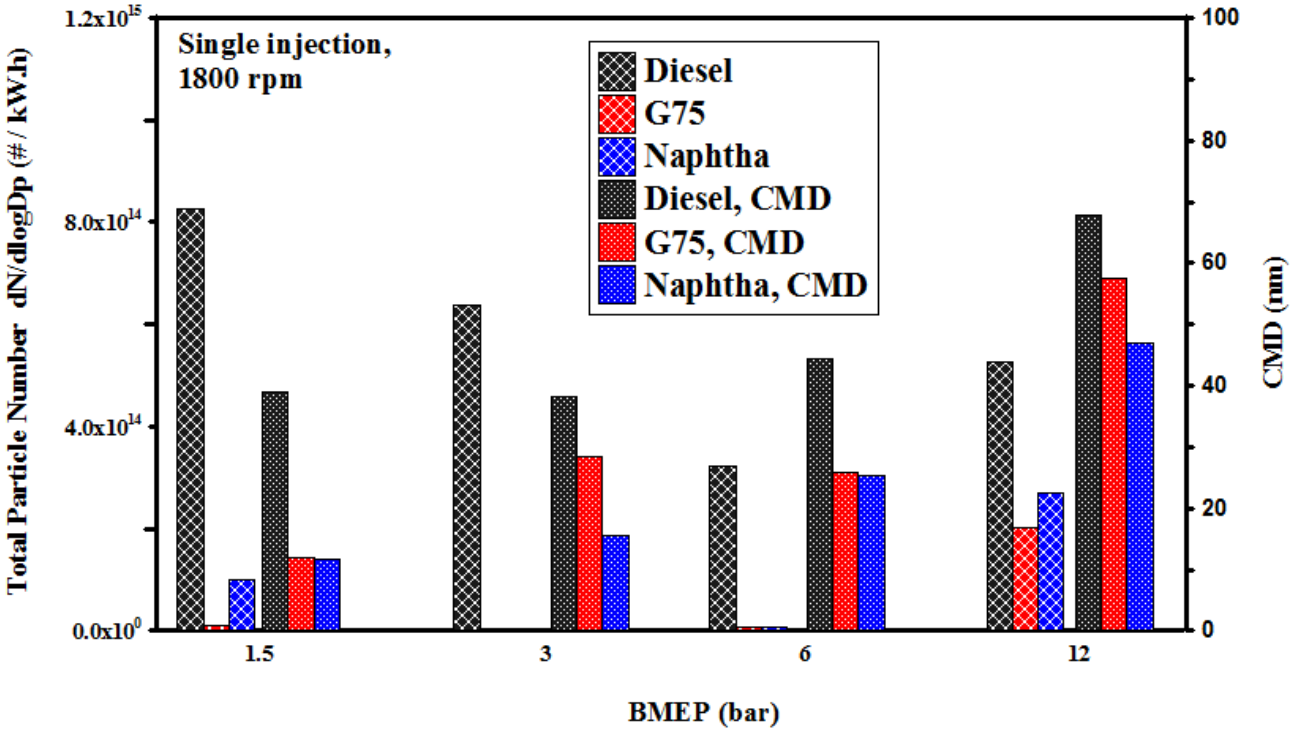
Increasing the load for G75 and naphtha fuels from 1.50 to 6 bar BMEP, the total particle number concentrations and CMD decreased, but they began increasing a little when the load was increased to 12 bar BMEP, as shown in Figure 5.6 (a, b, c, d). There are multiple possible reasons for the decrease of the total particle number concentration and CMD at low loads; the first cause is the injection pressure, as it was increased at 6 bar BEMP to 500 bar. That pressure helps to atomize the fuel and decreases the size of the droplets. The second reason is related to the fuels' properties, where both fuels have high volatility and low cetane numbers (CN), and the fuel was injected early. These creates a longer time for the small fuel droplets to mix more fully with air. Also, the EGR level was lower than at load 1.50 bar BMEP, and may

have led to an increase in the oxygen concentration inside the cylinder, which in turn promotes soot oxidation. The G75 fuel produced less PN compared to naphtha fuel, which could be due to the combustion duration. G75 took longer than naphtha fuel, as shown Figure 5.3(b), where the burning rate was slow and there was more time for soot to be oxidized.

When the load for G75 and naphtha fuels was increased from 6 to 12 bar BMEP, the total particle number concentrations and CMD increased correspondingly. At a high load, the cylinder wall temperature will be high, which provides assistance to the fuel auto ignition, resulting in incomplete combustion and increased soot emission, as shown in Figure 5.5 (b). Therefore, the peaks of high particle number concentrations shift towards larger size particles, as shown in Figure 5.6 (d).



(a)



(b)

Figure 5.7: (a) Total particle number concentration and CMD (b) nucleation and accumulation mode particles

Moreover, the fuels were injected near the top dead centre in high quantities and the ignition delay was short, not giving enough time for the mixture to be well mixed, which resulted in rich regions where the soot formation rate and agglomeration processes dominated the soot oxidation rate.

The percentages of the reduction of the total particle number concentration and CMD compared to diesel fuel were high. For example, at load 3 bar BMEP and injection pressure 350 bar, with EGR 43% and injection timing 32.5°bTDC, the total particle number concentration of G75 fuel was reduced by 99.60% compared to diesel (at injection pressure 700 bar, injection timing 8°bTDC, EGR 49%). Also, the particle numbers in the nucleation and accumulation modes were reduced by 99.7% and 99.60% respectively. The CMD was reduced from 38 nm to 28 nm. For naphtha fuel, the total particle number concentration was reduced by 99.50% compared to diesel, while the nucleation and accumulation modes'

particle numbers were reduced by 99.48% and 99.58%, and the CMD from 38 nm to 15 nm respectively. At 6 bar BMEP, injection pressure 500 bar, injection timing 26°bTDC and EGR 29.5%, G75 and naphtha fuels produced a very low particle number compared to the diesel fuel (at injection pressure 1200 bar, injection timing 3°bTDC, EGR 28%). The reduction of the total particle number concentration was about 99.74% and 97.4%, while the CMD for both fuels was reduced from 44 nm to 25 nm respectively, as shown in Figure 5.7 (a). The nucleation and accumulation mode particles also reduced by 95.40% and 98.5% respectively.

At a higher load of 12 bar BMEP as shown in Figure 5.7 (a), an injection pressure 1000 bar, injection timing 5°bTDC, and EGR 16.4% for G75 fuel and EGR 8% for naphtha fuel, the total particle number concentration decreased by 61.50% and 48.8% respectively, compared to diesel at injection pressure 1200 bar, EGR 16.8%, injection timing 3°bTDC. For the diesel fuel, all the particles were in the accumulation mode region since the diesel fuel did not emit particles in the small sized region or nucleation modes. The reduction in large sized particles of both G75 and naphtha was 53.50% compared to diesel fuel, and the CMD, as shown in Figure 5.7 (a), was reduced from 67 nm to 57 nm for G75 and to 46 nm for naphtha.

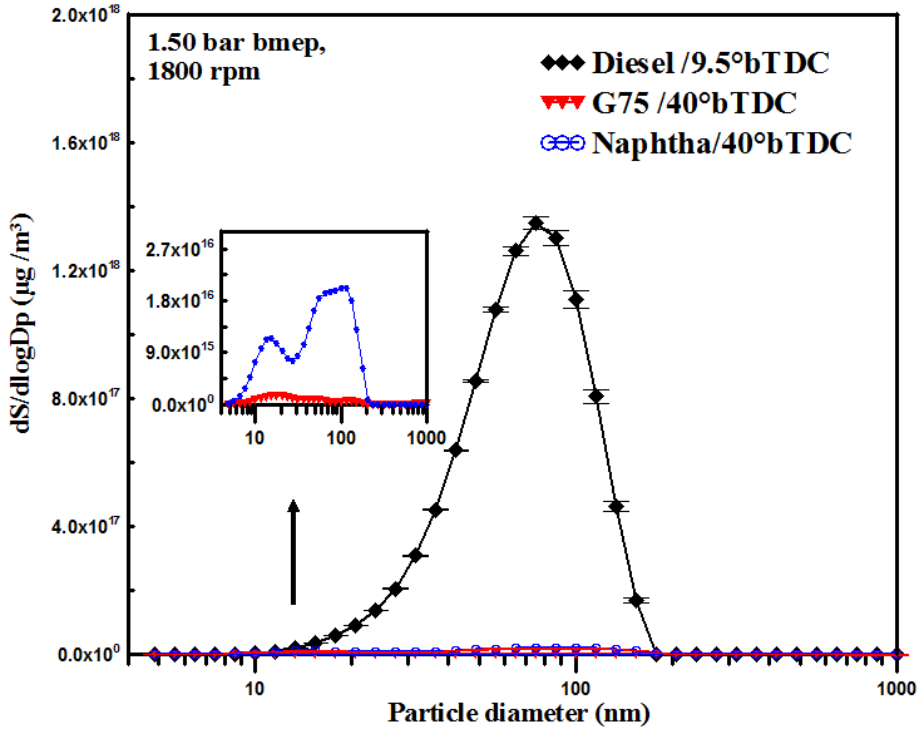
5.3.2 Particle Size-Surface Area Distribution

An individual nucleus encompassing the agglomerates has a surface area that creates a site for the absorption or condensation of toxic gases. For the surface area of diesel particles, the size of individual nuclei in agglomerates is more representative than the size of the agglomerates themselves (Kittelson, 1998). In the atmosphere, there are other constituents apart from engines' exhaust constituents. Therefore, the atmospheric constituents may compete for this

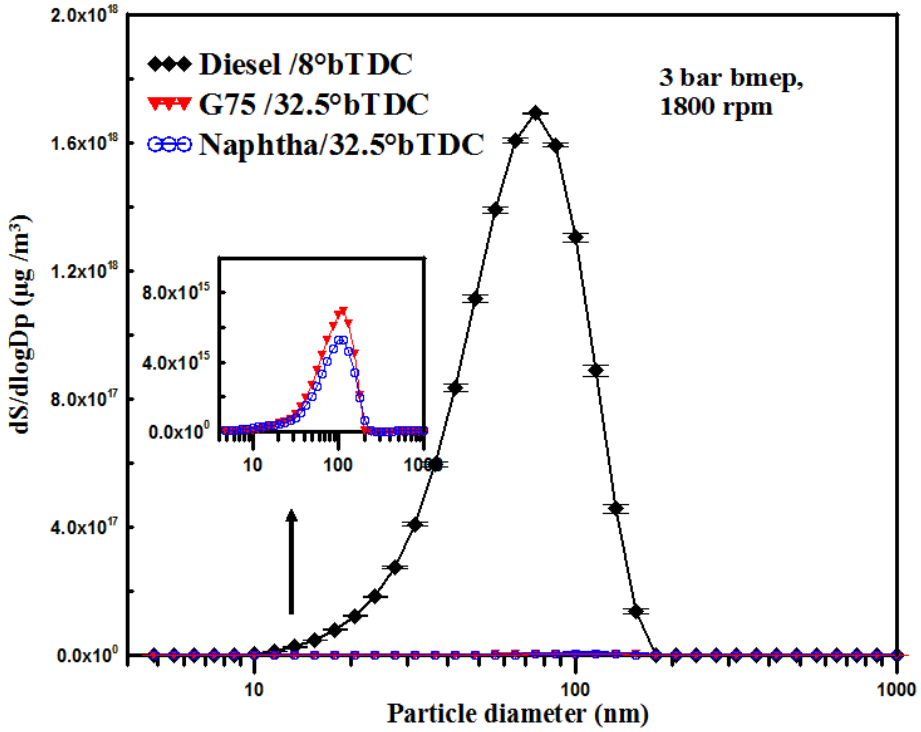
surface area before the exhausts' constituents. Per unit of particle mass, the surface area of smaller particles is higher than larger particles. Therefore, the higher surface area provides room for toxins such as poly aromatic hydrocarbons (PAHs) and volatile organic carbons (VOCs) to absorb or condense in these surface areas. In other words, for human health, smaller particles are more dangerous than larger particles. Figure 5.8 shows the particle size–surface area distributions for diesel, G75, and naphtha fuels at the same speed but with different injection pressures, timing, and EGR levels in each load (1.5, 3, 6, and 12 bar BMEP).

In order to maximize the visibility of particle size–surface area distributions of G75 and naphtha, separate figures have been merged with the main figures. In Figure 5.8 (a, b, c), it has been observed that for diesel fuel, increasing the load up to 6 bar BMEP, the peaks of the high surface area of the particles did not shift and were the dominating size of around 75 nm. At 12 bar, the peak shifted towards larger-sized particles. A similar trend was observed for naphtha fuel, as when increasing the load up to 6 bar BMEP, the peaks of the high surface areas of the particles did not shift and were the dominating size of around 115 nm; they shifted towards larger-sized particles at 12 bar BMEP. For G75 fuel, when the load was increased to 12 bar BMEP, the peaks first shifted towards larger-sized particles from load 1.5 to 3 bar BMEP, and there was no shifting at load 6 bar BMEP. At load 12 bar, however, they shifted towards larger-sized particles.

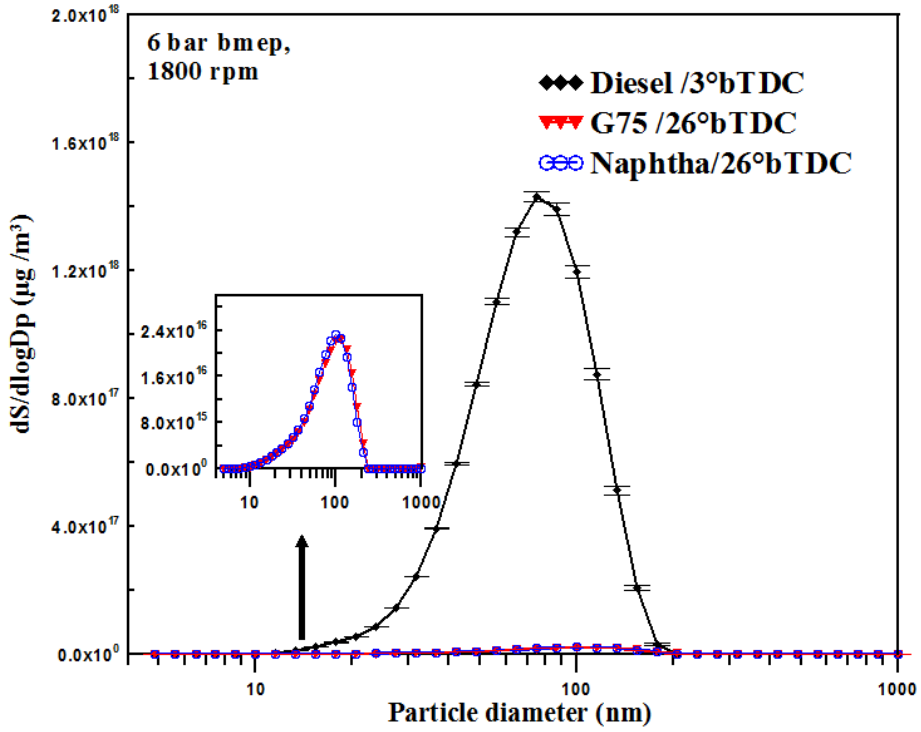
In all loads, G75 and naphtha fuels emit particles with low surface area concentrations since they produce less soot compared to diesel, as discussed earlier in section 5.3.1.


1.50 bar bmep,
1800 rpm
Diesel /9.5°bTDC
G75 /40°bTDC
Naphtha/40°bTDC
dS/dlogDp (µg /m³)
Particle diameter (nm)
2.0x10¹⁸
1.6x10¹⁸
1.2x10¹⁸
8.0x10¹⁷
4.0x10¹⁷
0.0x10⁰
2.7x10¹⁶
1.8x10¹⁶
9.0x10¹⁵
0.0x10⁰
10
100
1000

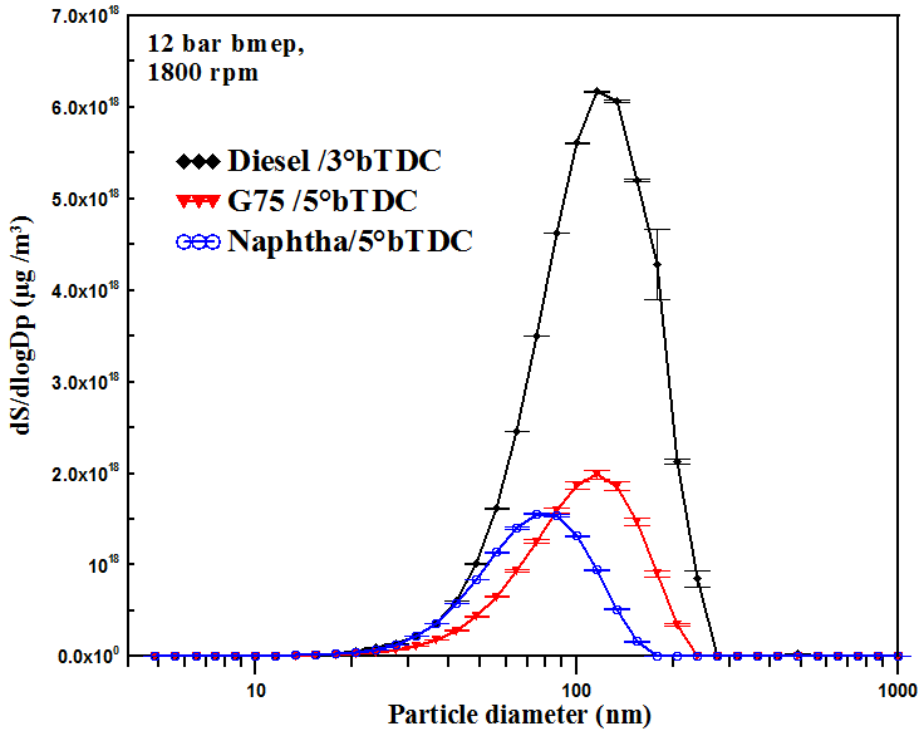
(a)


Diesel /8°bTDC
G75 /32.5°bTDC
Naphtha/32.5°bTDC
3 bar bmep,
1800 rpm
dS/dlogDp (µg /m³)
Particle diameter (nm)
2.0x10¹⁸
1.6x10¹⁸
1.2x10¹⁸
8.0x10¹⁷
4.0x10¹⁷
0.0x10⁰
8.0x10¹⁵
4.0x10¹⁵
0.0x10⁰
10
100
1000

(b)



(c)



(d)

Figure 5.8: Particle size-surface area distribution at loads (a) 1.50, (b) 3, (c) 6, (d) 12 bar BMEP

5.3.3 Total Particle Mass and Particle Number

From the point of view of emissions legislation, the total mass of the particles emitted by engines is very important. Figure 5.9 shows the total particle number concentration per kWh compared to total mass concentration per unit volume at a constant speed and with different operating conditions in each load. It is clear from the figure that the particle number and mass concentrations are dependent on engine operating conditions. As discussed previously, increasing the load for diesel fuel up to 6 bar BMEP decreased the total particle number concentration and increased at 12 bar BMEP, while for G75 and naphtha fuels, the total particle number concentrations decreased when the load increased up to 3 bar BMEP, and then increased when the load increased from 6 to 12 bar BMEP.

.

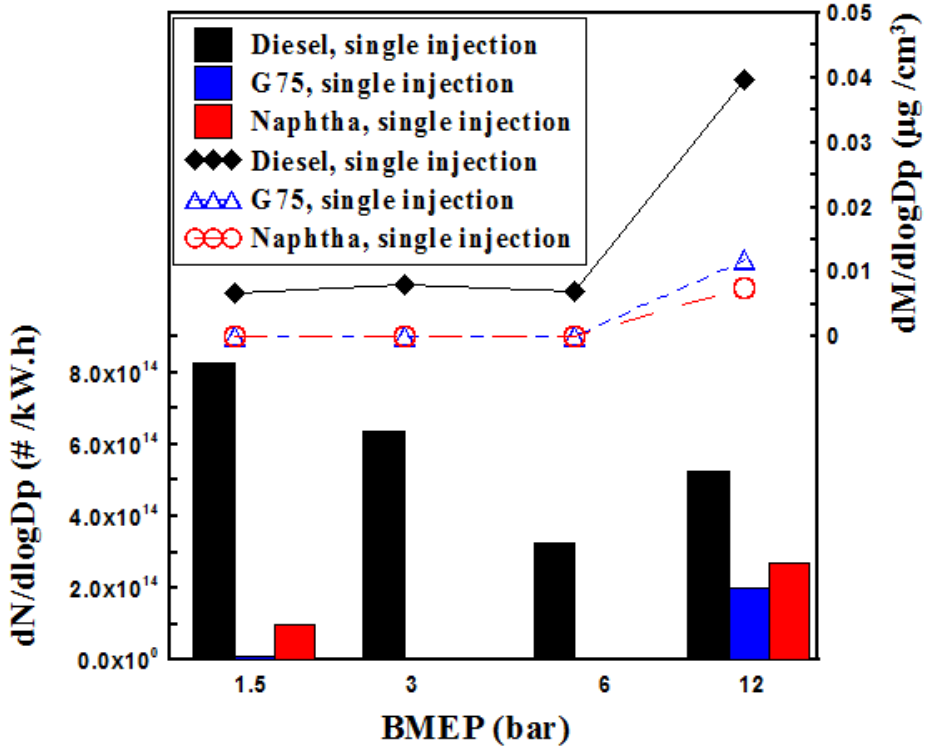
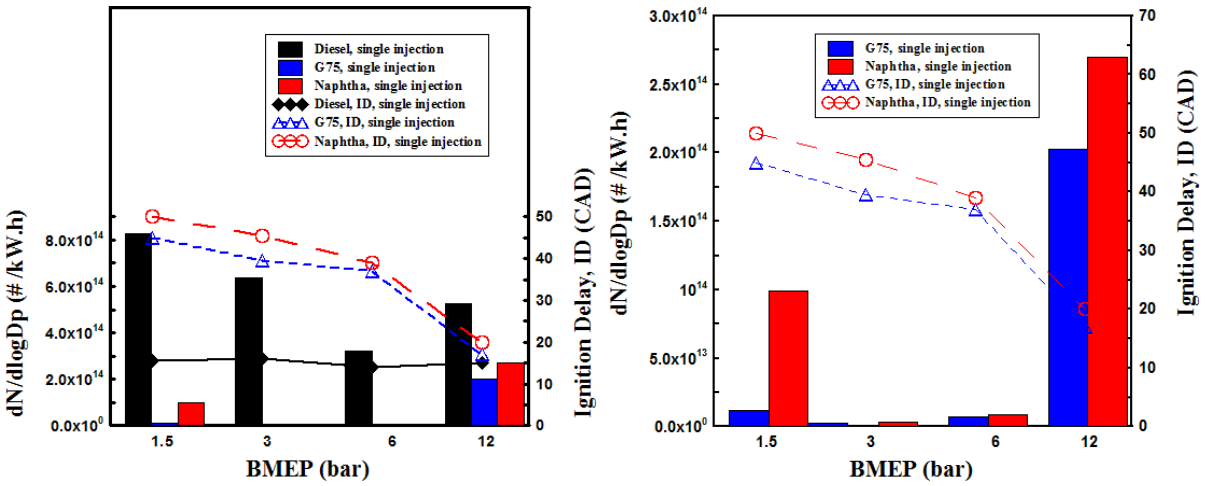


Figure 5.9: Comparison between total particle number concentration and total particle mass at four different loads

The reasons for these variations have been explained in in section 5.3.1. In the case of the total mass concentration, the increased load did not affect the total mass concentration: it kept the concentration very low. The total mass concentrations for all fuels at loads below 12 bar BMEP were dominant in the size range 11nm to 40 nm. At high load 12 bar BMEP, the total mass concentrations increased. At this load, the emitted particles were mainly in the accumulation mode, with sizes around 75 nm, accompanying the domination of soot formation over soot oxidation. G75 and naphtha fuels emit a very low total mass concentration compared to diesel fuel. The high volatility of the fuels, long ignition delays, and EGR levels play a significant role in reducing particle number (PN) and particle mass.

5.3.4 Effect of Ignition Delay on PN

Figure 5.10 shows the comparison between the total particle number concentrations per kWh with ignition delay. In order to maximize the visibility of the trends of the G75 and naphtha fuels, a separate figure has been plotted. It was observed that an increase in loads decreased the ignition delay for all fuels, becoming smaller at high load 12 bar BMEP. As discussed previously in section 5.3.1, the total particle number concentration for diesel fuel decreased with an increasing load, and increased at high load 12 bar BMEP, as shown in Figure 5.10 (a). For G75 and naphtha fuels in Figure 5.10 (b), a similar trend was observed when the load increased: the total particle number concentration decreased and then increased at high load



(a) (b)

Figure 5.10: Comparison between total particle number concentration and Ignition delay at four different loads (a) all fuels (b) G75 and naphtha fuels

It was observed that an increase in total particle number concentration corresponded to a short ignition delay. The cylinder wall and piston became hotter at high load, promoting the fuel auto-ignition. For G75 and naphtha fuels, it was noted that the ignition delay was longer at low load 1.5 bar BMEP, but the total concentrations of both fuels increased, as shown in Figure 5.10 (b). This increase could be attributed to the increase of the EGR level, where the oxygen level is decreased and oxygen is considered as a soot oxidizer. Also, it could be due to fuel impingement in the cylinder wall, where fractions of fuel leave the combustion chamber unburned, and the increase of HCs was overserved, as shown in Figure 5.5 (d). A similar observation was reported by Zhang (2012), who concluded that the increase of particle number concentration, especially small particles below 50 nm, is related to the increase of unburned hydrocarbons.

5.4 Chemical Characterization of PM

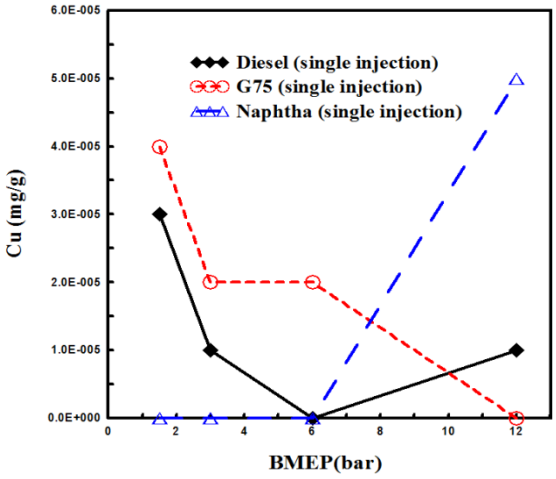
5.4.1 Metal Concentration in PM

The metals emitted from CI engines are considered to have a major effect on the environment and on human health. Fuel, lubricating oil, and material disintegration and wear from the engine are considered to be the main source of these metals. The concentration of metals in fuels depends on various aspects: specifically, the type of crude oil that was used in the production of the fuels, and the refining processes that were used to refine the crude oil. Metals are characterized as anthropogenic emissions – pollutants originated by human activities – and Ca, Fe, Pb, and Cr are considered as the major metal emissions. For example, breathing or inhaling a high concentration of chromium (Cr) can cause nose ulcers, asthma, or shortness of breath, while skin contact can cause allergic reactions or skin irritation. Long-term exposure can cause dysfunction of the human kidney or liver. Lead (Pb) and iron (Fe) are also carcinogenic, and long-term exposure can also cause brain, liver, and kidney damage (Perlingieri, 2003). There have been many studies about metals emitted from diesel engines, which show that metals containing particulates can easily penetrate deep into the human body, and can affect the activity of the cell structure by increasing the level of the reactive oxygen species (ROS). this causes an elevation in oxidative stress (Agarwal, et al., 2015; Donaldson, et al., 2005; Baulig, et al., 2003).

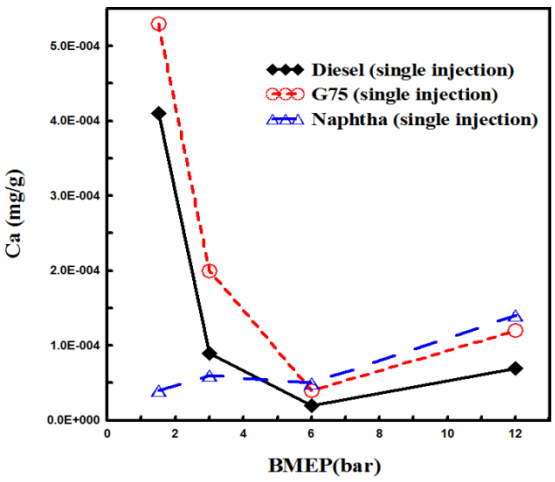
Filter papers (Whatman, Quartz, 47 mm in diameter) were placed in a filter holder assembly which was installed with TSI diluter model 3302A with a dilution ratio 35±5:1. The flow rate was 10 l/min. After running the engine with the desired operating conditions and collecting a

sample for a predetermined time (30 mins), the filter papers were removed from the holder assembly and were prepared for analysis of the metals in the particulates using ICP-OES. More information on the sample extraction and analysis is discussed in the section on analytical procedure, which can be found in sections 3.2.6.1 and 3.3.2 in Chapter Three.

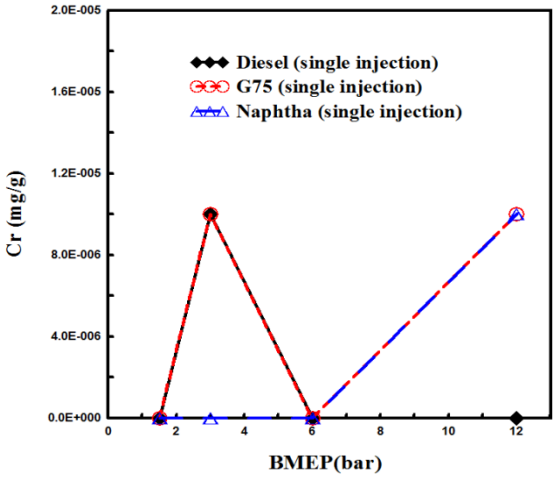
Figure 5.11 shows the concentrations of copper (Cu), calcium (Ca), chromium (Cr), lead (Pb), nickel (Ni), zinc (Zn), and iron (Fe) in milligram per gram. Measurements were taken at a constant speed of 1800 rpm and with different loads; each load had different injection timings and pressure (see Table 5.1).



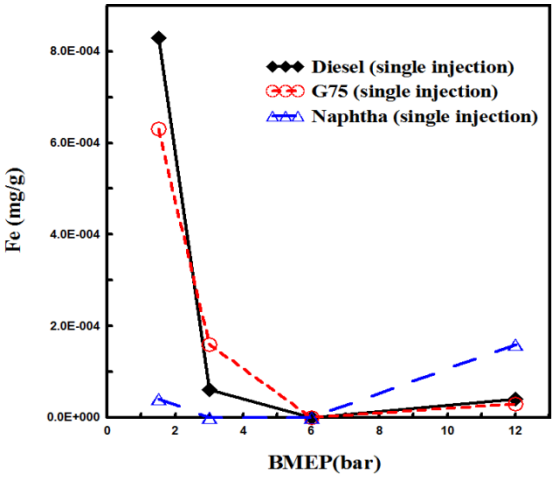
(a)



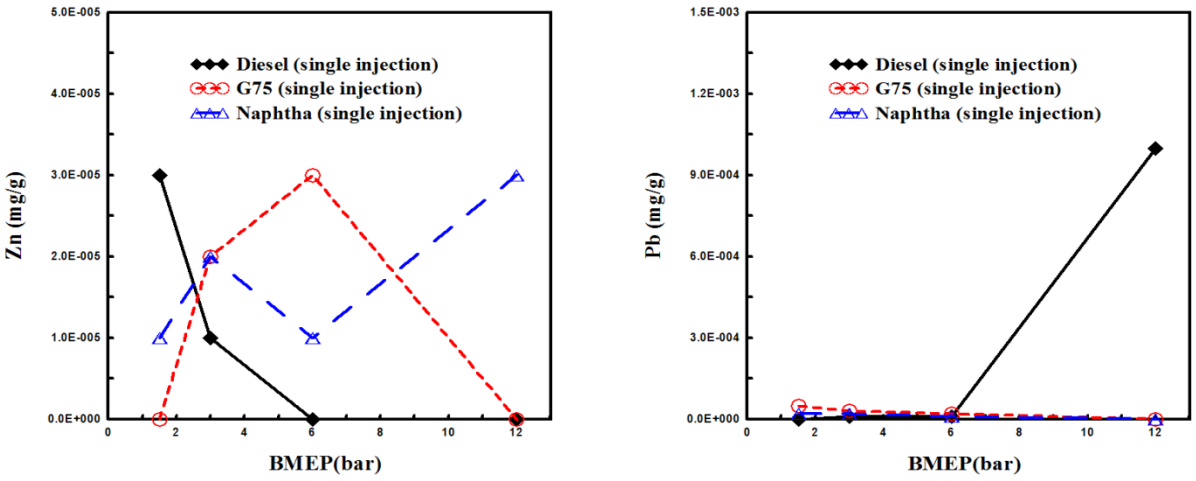
(b)



(c)

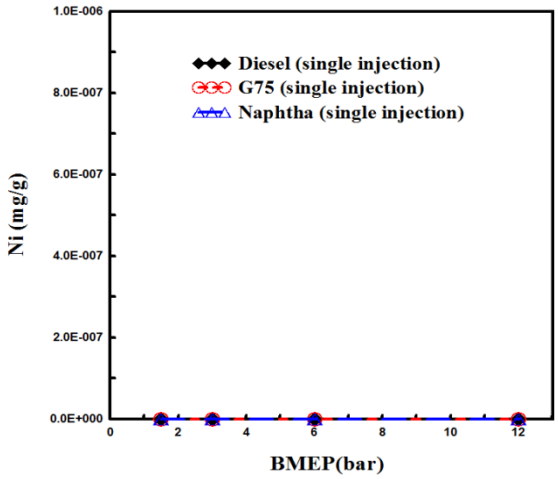


(d)



(e)

(f)



(g)

Figure 5.11: Concentrations of trace metals in diesel, G75 and naphtha particulates at four different loads (a) Cu, (b) Ca, (c) Cr, (d) Fe, (e) Zn, (f) Pb, (g) Ni

There is no specific trend pertaining to trace metals with an increasing load, as some research has stated that the presence of trace metals in a diesel particulate is mostly dependent on fuel and engine oil compositions, engine wear, and the conditions at a sampling point (Gangwar, et al., 2012; Agarwal, et al., 2015). Figure 5.11 (a) shows the concentration of copper (Cu) at different loads. There was no specific trend observed for the concentration of Cu for all three fuels, but naphtha fuel at 12 bar BMEP produced the highest concentration. Agarwal[b], et al.

(2013) reported that the presence of Cu in a diesel particulate originates from engine lube oil and engine wear. It appears at high loads and in that condition only, when more lube oil is mixed with fuel during combustion, or along with more engine wear. It is also possible that there are some traces of Cu in naphtha fuel components, so at high loads more fuel is injected, resulting in some fractions of fuel leaving the combustion chamber without burning and being deposited into the filter paper.

Figure 5.11 (b, d) shows the concentration of calcium (Ca) and iron (Fe) at different loads. It was observed that when increasing loads for G75 and diesel fuels to 6 bar BMEP, the concentration of Ca significantly decreased, but increased a little at high loads. Ca can originate from fuel or engine oil, while Fe can originate from fuel or engine wear, as reported by Gangwar, et al. (2012). At low loads, it was hypothesised that both Ca and Fe originated from fuel where the in-cylinder temperature was low, and that some fractions of fuel escaped the combustion chamber without burning and were deposited into the filter paper. It also caused an increase of BSHC, as shown in Figure 5.5 (d), but the slight increase of Ca concentrations at high loads could be explained by its presence in engine oil, while Fe concentration could be explained by engine wear. The low concentration of naphtha fuel at low loads could be attributed to the conditions at the sampling point, where some fractions of Ca and Fe did not deposit into the filter paper as they managed to escape from the exhaust system in gas form.

Figure 5.11 (c) shows the content of chromium (Cr) in particulates at different loads. It was noted that nearly the same concentration of Cr was emitted by the diesel and G75 fuels at 3 bar BMEP, and by G75 and naphtha fuels at 12 bar BMEP. It was reported that the presence of Cr in a diesel particulate can be attributed to the wear of the piston rings, which are chrome-plated (Agarwal, et al., 2015).

Figure 5.11 (e) shows the concentration of Zn at different loads. Zinc di-alkyl-di-thio-phosphate (ZDDP) is normally found in engine lubricating oil as an additive. When engine lubricating oil is heated to a temperature above 100°C in the presence of oxygen, zinc polyphosphate is formed via a thermo-oxidative decomposition of ZDDP. In the combustion chamber, a reaction occurs between zinc polyphosphate and iron oxide to produce ZnO. Zn is formed as a trace metal via a redox reaction of ZnO in a high temperature environment (Agarwal[b] et al., 2013). The presence of high concentrations of Zn for all fuels at different loads originates from engine oil, while low concentrations could be explained by the discussion above.

Figure 5.11 (f) shows the concentration of lead (Pb) at different loads. Diesel fuel emitted high concentrations of Pb at high loads, while G75 and naphtha fuels emitted almost zero concentration of Pb in all loads. It was hypothesized that very small traces of Pb is present in all fuels components, but both G75 and naphtha have fewer traces than diesel fuel. It can be seen from Figure 5.1 (d) that there was an overlap between the end of the injection event and the start of the high peak of heat release, which may in very small fractions of fuel escaping from the combustion chamber unburned and condensing into the filter paper.

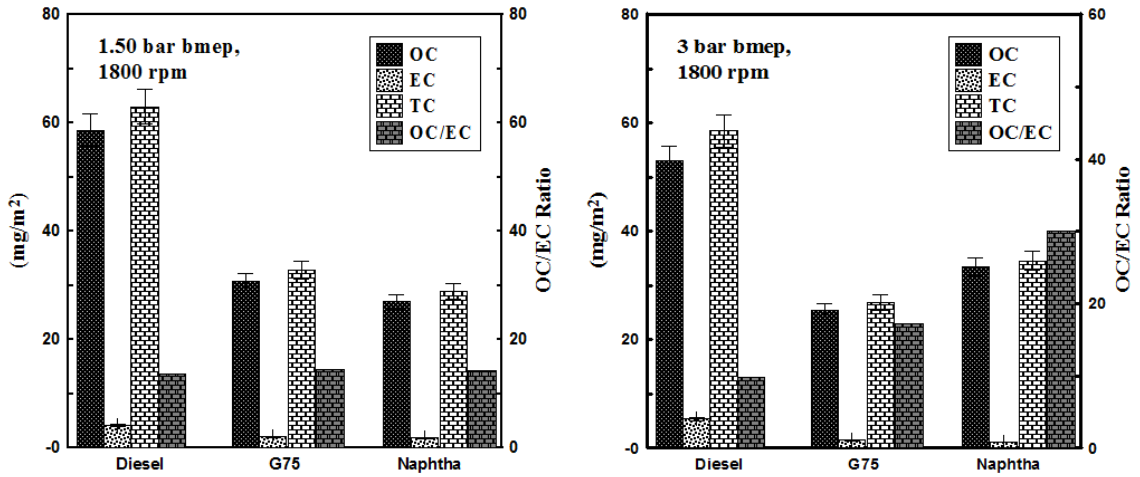
Figure 5.11 (g) shows the concentration of nickel (Ni) at different loads. It was noted that all fuels in all loads do not show any trace of Ni in the exhaust, which could be due to the absence of Ni in the fuels and engine oil.

To summarize, fuel components, lubricating oil components, and operating conditions play a significant role in determining the presence of trace metals in the exhaust system. Some metals are abundant in fuel or engine oil. Some of the fuel droplets hit the cylinder liner wall where there could be a film of lubricating oil. The fuel droplets mix with the lubricating oil, generating a high level of metals. Also, the disintegration of the metal of the engine piston

increases the level of metals. The low concentration of metals is attributed to the escape of metals from the exhaust system in a gas phase, as fractions of them did not deposit into the filter paper.

5.4.2 OC, EC and TC in PM

Elemental carbon (EC) and organic carbon (OC) are the main components of exhaust gas emitted from CI engines. The process of the formation of EC and OC is explained in Chapter 4, section 4.4.1. EC and OC were initially measured as milligram per square metre and were averaged for repetition; their anomalies have been reported and presented in the figures. Furthermore, the procedures and equipment used to analyse EC and OC can be found in Chapter 3, section 3.3.1. Figure 5.12 (a, b) presents the EC, OC, TC, and OC/EC ratio for diesel, G75, and naphtha fuels at two different loads: 1.50 and 3 bar BMEP.



(a) (b)

Figure 5.12: Elemental carbon EC, organic carbon OC, total carbon TC and OC/EC ratios of diesel, G75 and Naphtha fuels at two loads: (a) 1.50 bar BMEP, (b) 3bar BMEP

From Figure 5.12(a), it is clear that G75 and naphtha fuels emitted a low concentration of EC, OC, and TC compared to the diesel fuel at both loads. Both fuels were injected earlier compared to diesel fuel, increasing the chance of the fuel being well mixed before the combustion started, as shown in Figure 5.3 (a). At low loads, the low temperature combustion prevents the extensive pyrolytic reaction that eventually generates soot. The total carbon (TC), however, was reduced for naphtha and G75 fuels by 54% and 47.80% respectively, compared to diesel fuel.

When increasing the load to 3 bar BMEP, as shown in Figure 5.12 (b), the EC, OC, and TC for diesel and G75 fuels decreased compared to the load 1.50 bar BMEP; while they increased for naphtha fuel. The decrease was a result of the increase in combustion temperature, which caused the re-burning of the organic species and formation of elemental carbon. For naphtha fuel, the increase of the TC and OC/EC ratio at load 3 bar BMEP could be related to fuel impingement in the cylinder wall and piston top land crevice, which led to an increase in unburned fuel that could participate in the nucleation mode. Also, naphtha fuel has a short combustion duration with a high burning rate compared to other fuels, as shown in Figure 5.3 (b), and so there may not be enough time to burn the organic carbons that are formed.

5.4.3 Poly Aromatic Hydrocarbons (PAHs) in PM

Regulated emissions of fuels have been widely investigated, but emissions such as PAHs are less regulated in the wider range of research. Recently, widespread attention has been given to PAHs from vehicle emissions, since they are considered to be carcinogenic and mutagenic (Riddle, et al., 2007). PAHs are complex organic compounds that consist of two or more fused benzene rings, containing hydrogen and carbon atoms (Rhead and Hardy, 2003). They

are ubiquitous in the environment and they mainly originate from incomplete combustion scenarios, including unburned lubricating oil (Richter and Howard, 2000). The US EPA has identified and prioritised 16 PAH compounds, which are shown in Figure 2.8 in Chapter 2.

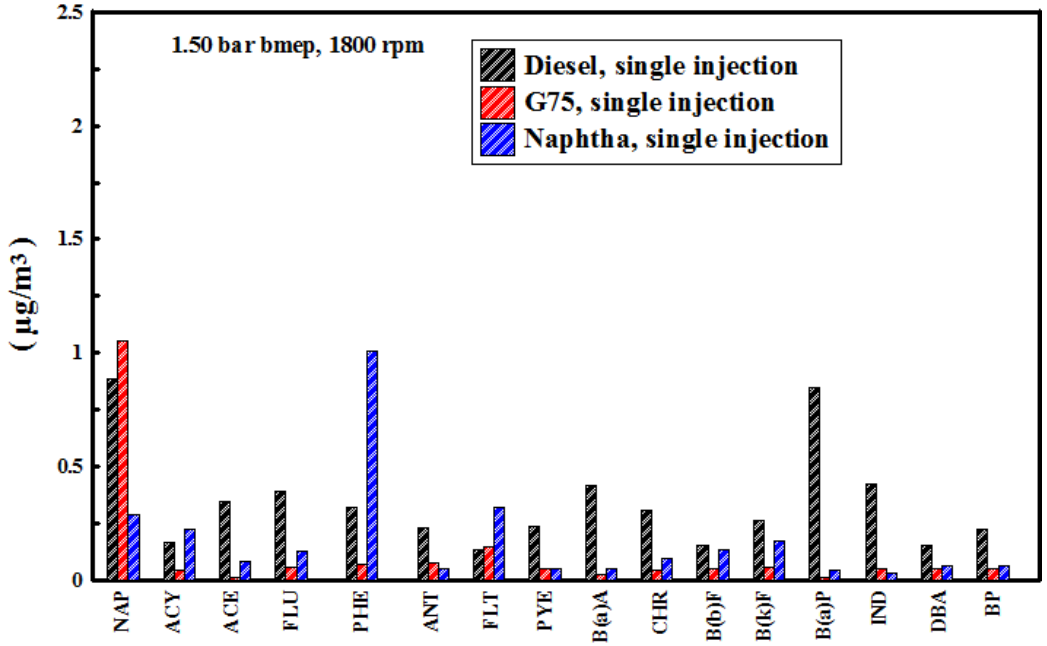
In this study, 16 PAH compounds were identified and quantified from particulate samples collected from the diesel engine running on diesel, G75 and naphtha fuels at different operating conditions. The samples were collected on quartz filter substrates (Whatman, 47 mm) using a filter holder assembly which was downstream of a modified TSI diluter (model 3302A) with a dilution ratio of 35±5:1 and a flow rate of 10 L/min. After running the engine under the desired operating conditions, the samples were collected for 30 mins in order to ensure a sufficient deposit for offline analysis. The filter substrate was removed from the filter holder and was prepared for analysis of the PAH compounds in the particulate phase using gas chromatography – mass spectrometry (GC-MS). Information about this technique is discussed in Chapter 3 in sections 3.2.6.2 and 3.3.3. The chemical properties of the identified PAH compounds are listed in Table 5.2.

Figures 5.13 (a, b, c, d) illustrate the concentrations of the 16 PAH compounds in the particulate phase for diesel, G75 and naphtha fuels at 1.5, 3, 6, and 12 bar BMEP loads respectively. The total and individual concentrations of the 16 PAH compounds, together with their emitted differences when using different fuels, is demonstrated in Table 5.3. Figure 5.13 shows that the low molecular weight (LMW) PAH compounds are present in higher concentrations compared to the high molecular weight (HMW) compounds in all loads. It is hypothesized that these compounds are originally present in the fuel, as it was also reported by Liang, et al. (2005) that LMW compounds in diesel fuel are found in higher concentrations than HMW compounds.

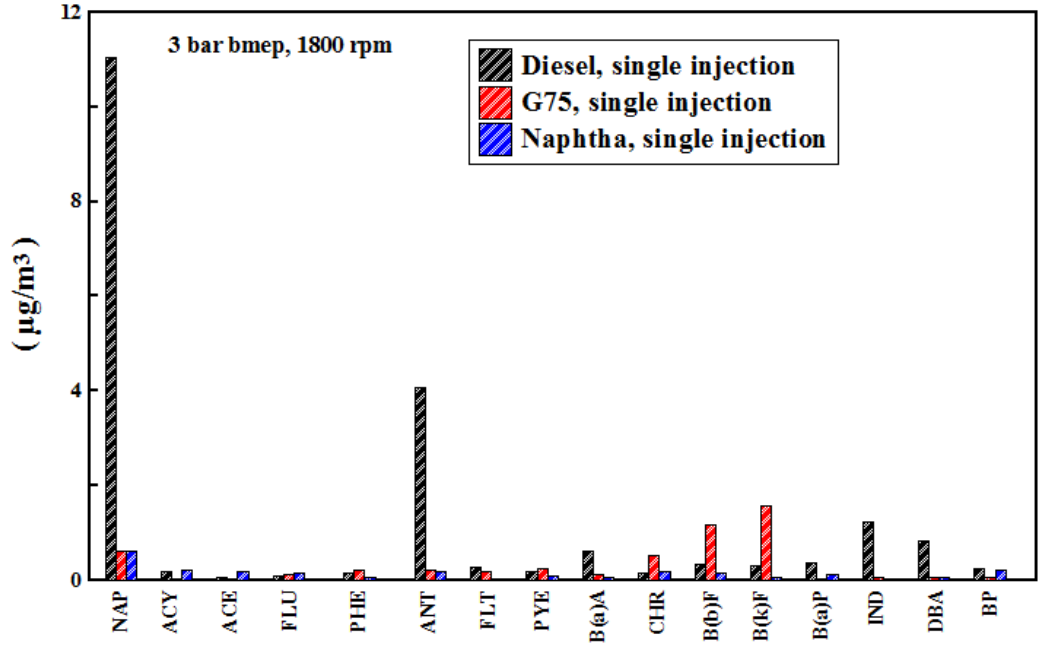
Table 5.2: the chemical properties of 16 PAHs identified in this study (Matar, S., & Hatch, L. F. 2001)

PAH	Abbreviation	Formula	Number of rings	Molecular Weight (MW)	Molecular weight category
Naphthalene	NAP	$C_{10}H_8$	2	128	LMW
Acenaphthylene	ACY	$C_{12}H_8$	3	152	LMW
Acenaphthene	ACE	$C_{12}H_{10}$	3	154	LMW
Fluorene	FLU	$C_{13}H_{10}$	3	166	LMW
Phenanthrene	PHE	$C_{14}H_{10}$	3	178	LMW
Anthracene	ANT	$C_{14}H_{10}$	3	178	LMW
Fluoranthrene	FLT	$C_{16}H_{10}$	4	202	LMW
Pyrene	PYE	$C_{16}H_{10}$	4	202	LMW
Benzo(a)anthracene	B(a)A	$C_{18}H_{12}$	4	228	LMW
Chrysene	CHR	$C_{18}H_{12}$	4	228	LMW
Benzo(b)fluoranthene	B(b)F	$C_{20}H_{12}$	5	252	HMW
Benzo(k)fluoranthene	B(k)F	$C_{20}H_{12}$	5	252	HMW
Benzo(a)pyrene	B(a)P	$C_{20}H_{12}$	5	252	HMW
Indeno(1,2,3-CD)pyrene	IND	$C_{22}H_{12}$	6	276	HMW
Dibenz(a, h)anthracene	DBA	$C_{22}H_{14}$	5	278	HMW
Benzo(g,h,i)perylene	BP	$C_{22}H_{12}$	6	276	HMW

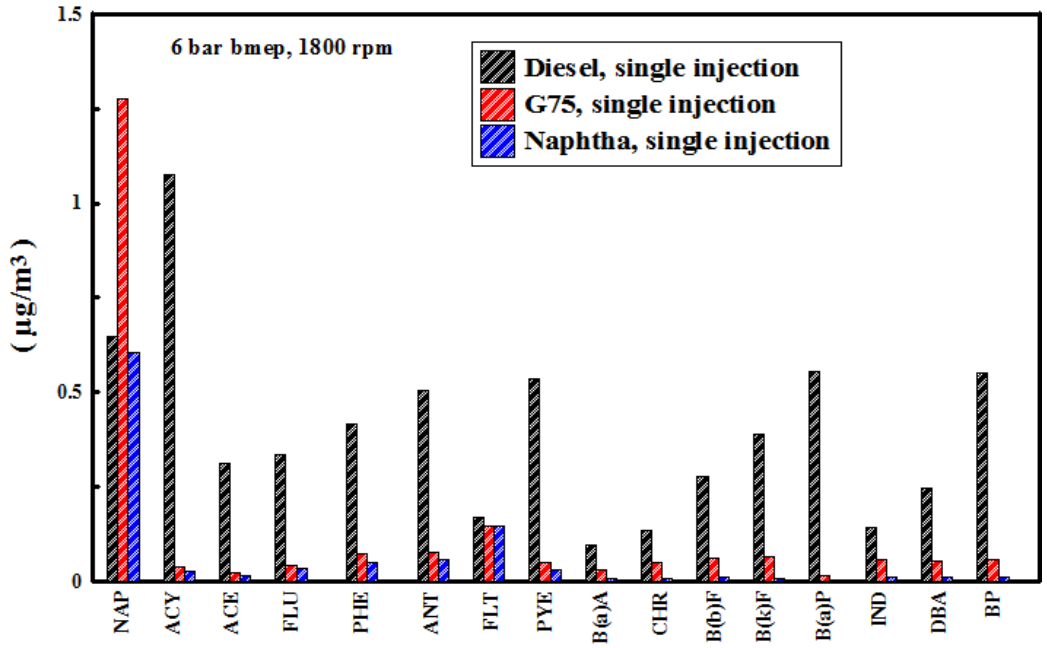
At load 1.50 bar BMEP, G75 fuel emitted the highest concentrations of NAP (1.05 μgm^{-3}) in comparison to other fuels, as shown in Figures 5.13 (a) and Table 5.3. For G75 fuel, the incomplete combustion that resulted from the over-lean mixture in some regions was considered to be a source of the presence of PAHs in PM. At load 1.50 bar BMEP, the HCs were high for G75 fuel, as shown in Figure 5.5 (d); therefore, the unburned fuel escaped from the combustion chamber and was deposited into the filter paper. G75 fuel also produced the lowest concentration of Benzo(a)pyrene (B(a)P) (0.012 μgm^{-3}) compared to the other fuels. It was suggested that this low concentration is related to some part of the (B(a)P) failing to condense on the filter paper and escaping in gas form (Agarwal, et al., 2011; Abdul-Khalek, et al., 1999).


1.50 bar bmep, 1800 rpm
Diesel, single injection
G75, single injection
Naphtha, single injection
(µg/m³)
2.5
2
1.5
1
0.5
0
NAP
ACY
ACE
FLU
PHE
ANT
FLT
PYE
B(a)A
CHR
B(b)F
B(k)F
B(a)P
IND
DBA
BP

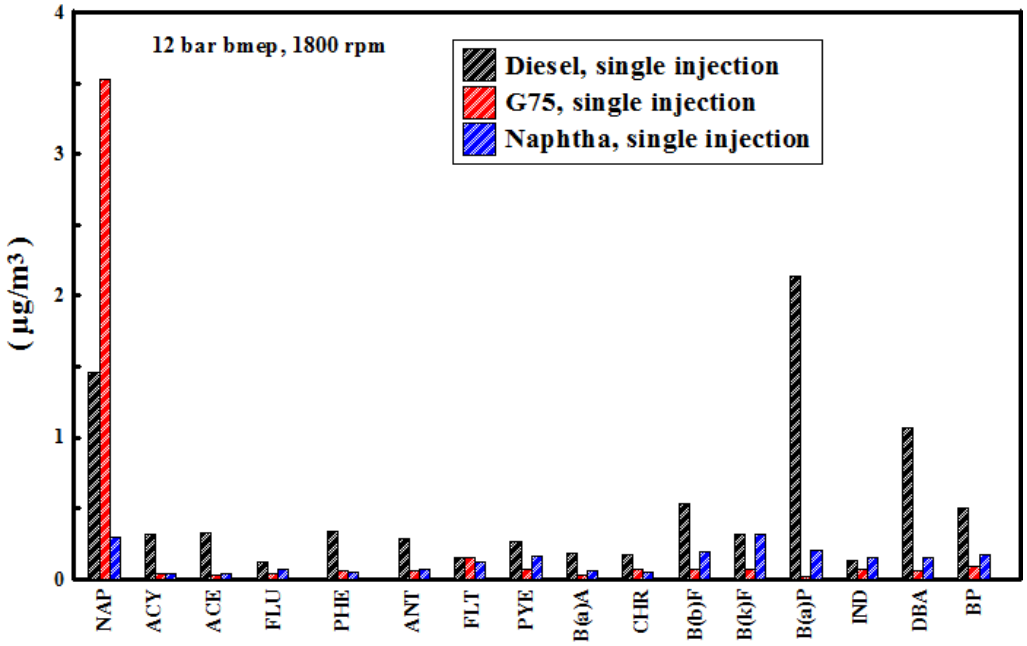
(a)


3 bar bmep, 1800 rpm
Diesel, single injection
G75, single injection
Naphtha, single injection
(µg/m³)
12
8
4
0
NAP
ACY
ACE
FLU
PHE
ANT
FLT
PYE
B(a)A
CHR
B(b)F
B(k)F
B(a)P
IND
DBA
BP

(b)



(c)



(d)

Figure 5.13: The concentrations of identified 16 PAHs for diesel, G75 and naphtha fuels at four loads (a) 1.50 , (b)3 , (c) 6, (d) 12 bar BMEP

When the load was increased to 3 bar BMEP, diesel fuel produced the highest concentration of NAP (11.05 μgm^{-3}) compared to other fuels, while the lowest concentration was observed from G75 fuel (the observed concentration of ACY was 0.029 μgm^{-3}). It was hypothesized that a high concentration of NAP is originally presents in the diesel fuel, and survives during the combustion process, leaving the exhaust system without burning. Another possible reason is that the compound was synthesized by partial combustion of the fuel, or the presence of the compound in the lubricating oil could be volatilized in the exhaust system. A further possible reason is that the compound was initiated from the deposits of the engine and/or exhaust system (Agarwal, et al., 2011).

When the load was increased from 3 to 12 bar BMEP, it was observed that both fuels G75 and naphtha reduced the total PAH compounds by more than 84% compared to diesel, as shown in Figure 5.13 and Table 5.3. Increasing the load increased the gas temperature and also produced local mixtures comparable to a stoichiometric mixture, and therefore less unburned fuel left the combustion chamber, resulting in less PAH deposition into the filter. It was also noted that naphtha fuel produced a lower concentration of total PAH compared to the other fuels. This suggests that PAH compounds were originally present in low concentrations.

Table 5.3: PAHs concentrations in particulates of diesel, G75 and naphtha fuels at four different loads with single injection * The concentration increased compared to diesel fuel

PAH	Diesel Conc (μgm^{-3})	G75 Conc (μgm^{-3})	Naphtha Conc (μgm^{-3})	G75 Reduction (%)	Naphtha Reduction (%)
1.50 bar BMEP					
Naphthalene (NAP)	0.89	1.05	0.29	18% >*	0.67%
Acenaphthylene(ACY)	0.17	0.04	0.23	75%	33.5% >
Acenaphthene (ACE)	0.35	0.01	0.08	96%	77%
Fluorene (FLU)	0.39	0.05	0.12	86%	67%
Phenanthrene (PHE)	0.32	0.07	1.01	78%	100% >
Anthracene (ANT)	0.23	0.08	0.05	67%	79%
Fluoranthrene (FLT)	0.14	0.15	0.32	7.5% >	100% >
Pyrene (PYE)	0.23	0.05	0.05	79%	80%
Benzo(a)anthracene (B(a)A)	0.41	0.02	0.05	95%	88%
Chrysene (CHR)	0.31	0.05	0.09	85%	69%
Benzo(b)fluoranthene (B(b)F)	0.15	0.05	0.13	67%	12%
Benzo(k) fluoranthene (B(k)F)	0.26	0.06	0.17	79%	33%
Benzo(a) pyrene (B(a)P)	0.85	0.01	0.04	99%	95%
Indeno(1,2,3-CD)pyrene(IND)	0.42	0.05	0.03	89%	93%
Dibenz(a,h) anthracene (DBA)	0.15	0.05	0.06	67%	61%
Benzo (g, h, i) perylene (BP)	0.22	0.05	0.07	78%	71%
Total	*5.49*	*1.84*	*2.79*	*67%*	*49%*
3 bar BMEP					
Naphthalene (NAP)	11.06	0.62	0.61	94%	95
Acenaphthylene(ACY)	0.18	0.03	0.22	84%	19% >
Acenaphthene (ACE)	0.06	0.03	0.17	43%	100% >
Fluorene (FLU)	0.07	0.10	0.13	34% >	79% >
Phenanthrene (PHE)	0.16	0.22	0.05	35% >	67%
Anthracene (ANT)	4.06	0.22	0.19	95%	95%
Fluoranthrene (FLT)	0.27	0.16	0.03	39%	87%
Pyrene (PYE)	0.17	0.25	0.08	46% >	56%
Benzo(a)anthracene (B(a)A)	0.61	0.13	0.06	79%	90%
Chrysene (CHR)	0.15	0.51	0.18	100% >	20% >
Benzo(b)fluoranthene (B(b)F)	0.32	1.17	0.15	100% >	54%
Benzo(k) fluoranthene (B(k)F)	0.30	1.55	0.07	100% >	78%
Benzo(a) pyrene (B(a)P)	0.35	0.01	0.10	98%	71%
Indeno(1,2,3-CD)pyrene(IND)	1.22	0.05	0.02	96%	98%
Dibenz(a,h) anthracene (DBA)	0.84	0.05	0.04	94%	95%
Benzo (g, h, i) perylene (BP)	0.23	0.05	0.19	79%	16%
Total	*20.05*	*5.15*	*2.30*	*74%*	*89%*

(Table 5.3) continued

PAH	Diesel Conc (μgm^{-3})	G75 Conc (μgm^{-3})	Naphtha Conc (μgm^{-3})	G75 Reduction (%)	Naphtha Reduction (%)
6 bar BMEP					
Naphthalene (NAP)	0.65	1.28	0.60	96% >	07%
Acenaphthylene(ACY)	1.07	0.04	0.02	96%	98%
Acenaphthene (ACE)	0.31	0.02	0.01	93%	95%
Fluorene (FLU)	0.34	0.04	0.03	88%	90%
Phenanthrene (PHE)	0.42	0.07	0.05	82%	88%
Anthracene (ANT)	0.50	0.08	0.06	85%	89%
Fluoranthrene (FLT)	0.17	0.15	0.15	14%	14%
Pyrene (PYE)	0.53	0.05	0.03	91%	95%
Benzo(a)anthracene (B(a)A)	0.09	0.03	0.01	70%	94%
Chrysene (CHR)	0.13	0.05	0.01	65%	94%
Benzo(b)fluoranthene (B(b)F)	0.28	0.06	0.01	78%	97%
Benzo(k) fluoranthene (B(k)F)	0.39	0.06	0.01	84%	98%
Benzo(a) pyrene (B(a)P)	0.55	0.01	0.00	98%	99%
Indeno(1,2,3-CD)pyrene(IND)	0.14	0.06	0.01	59%	93%
Dibenz(a,h) anthracene (DBA)	0.24	0.05	0.01	78%	96%
Benzo (g, h, i) perylene (BP)	0.55	0.06	0.01	90%	98%
Total	*6.38*	*2.10*	*1.02*	*67%*	*84%*
12 bar BMEP					
Naphthalene (NAP)	1.46	3.52	0.30	100% >	80%
Acenaphthylene(ACY)	0.32	0.04	0.04	87%	87%
Acenaphthene (ACE)	0.33	0.03	0.04	92%	88%
Fluorene (FLU)	0.12	0.04	0.06	66%	45%
Phenanthrene (PHE)	0.33	0.06	0.05	83%	85%
Anthracene (ANT)	0.29	0.06	0.07	79%	77%
Fluoranthrene (FLT)	0.15	0.15	0.12	0.05%	22%
Pyrene (PYE)	0.27	0.07	0.17	73%	38%
Benzo(a)anthracene (B(a)A)	0.18	0.03	0.06	83%	69%
Chrysene (CHR)	0.17	0.06	0.05	62%	69%
Benzo(b)fluoranthene (B(b)F)	0.53	0.07	0.19	87%	64%
Benzo(k) fluoranthene (B(k)F)	0.32	0.07	0.32	79%	0.01%
Benzo(a) pyrene (B(a)P)	2.13	0.02	0.20	99%	91%
Indeno(1,2,3-CD)pyrene(IND)	0.13	0.07	0.15	47%	11.5% >
Dibenz(a,h) anthracene (DBA)	1.06	0.06	0.15	95%	86%
Benzo (g, h, i) perylene (BP)	0.50	0.09	0.17	82%	66%
Total	*8.31*	*4.44*	*2.13*	*47%*	*74%*

5.5 Summary

The study was conducted to investigate the effect of a single injection of diesel, G75, and naphtha fuels on the particle size distributions and chemical characterizations of PM. The investigation was carried out with an EGR cooler modification (deactivating the EGR cooler) and with a constant speed of 1800 rpm and λ. The following are the observations:

Particle Size and Number Distributions

- At low and medium loads, the total particle number concentration of both G75 and naphtha was significantly lower than that of diesel fuel. A lean mixture region was generated inside the cylinder, promoting soot oxidation processes over soot formation, and increasing the rate of oxidation. Also, both G75 and naphtha have a high volatility and low cetane number CN. The fuels were injected earlier than the diesel fuel, which provided a longer time for the small fuel droplets to mix with air before the combustion started. Therefore, the total particle number concentration and CMD were reduced significantly, by around 99%. In addition, smoke was reduced and stayed below 0.01 FSN, where the lowest smoke emission was observed for G75 fuel: 0.003 FSN at load 1.50 bar BMEP. It was also observed that G75 fuel produced lower PN emissions than naphtha fuel, which could be related to the combustion duration as G75 has longer combustion duration than naphtha fuel. This longer combustion duration makes the burning rate of the mixture very slow, which may help to provide time for the soot to be oxidized. The usage of large amounts of EGR helped to lower the combustion temperature, and $BSNO_x$ emissions of both G75 and naphtha decreased compared to diesel fuel. Low emissions were observed at load 1.50 bar BMEP. The emissions of $BSNO_x$ from G75 fuel were (0.27 g/kWh), and from naphtha fuel were (0.37 g/kWh).

- Although the PN emissions of G75 and naphtha fuel were reduced significantly compared to diesel fuel, the downsides are brake thermal efficiency (BTE), BSHC, and BSCO emissions. The BTE was reduced for both G75 and naphtha fuels compared to diesel fuel. It was observed that at load 6 bar BMEP, the BTE of diesel fuel was 38.87%; for G75 fuel it was 37.99% and for naphtha it was 35.76%. The drop is 0.88% in absolute value for G75 fuel and 3.11% in absolute value for naphtha fuel, compared to diesel. In the case of BSHC and BSCO emissions, it was observed that high emissions were found at load 1.50 bar BMEP; BSHC increased for G75 fuel from 5.5 to 16 g/kWh, and for naphtha fuel from 5 to 13 g/kWh. Compared to diesel fuel, BSCO emissions increased from 23 to 38 g/kWh for G75 fuel and from 23 to 35 g/kWh for naphtha fuel. The incomplete combustion that resulted from the over-lean mixture in some regions increased BSHC and BSCO emissions.

Trace Metals

There is no specific trend for trace metals when increasing the load for all three fuels; this corresponded with other researchers' conclusions, as they reported that the presence of trace metals in a diesel particulate are mostly dependent on fuel and engine oil composition, engine wear, the conditions of the sampling point, and in-cylinder temperature. Metal particulates originate either from engine oil (in the case of Zn and Cu), from fuel (in the case of Fe, Ca, and Pb), or from engine wear (in the case of Cr).

EC, OC and PAH Concentrations

- It was observed that at load 3 bar BMEP, the G75 fuel produced low total carbon (TC) – a reduction of over 54% – compared to the other fuels. Also, the reduction was correlated with a reduction of PN. It was hypothesized that at low loads, low temperature combustion prevents the extensive pyrolytic reaction that eventually generates soot, and so the soot oxidation process was motivated. At load 6 bar BMEP, the naphtha fuel emitted the lowest concentration of PAH compounds ($1.08 \mu g m^{-3}$) compared to the other fuels in all loads. Increasing the load increased the gas temperature and also produced local mixtures near to a stoichiometric mixture, and therefore, with less unburned fuel leaving the combustion chamber, there was less PAH deposition into the filter. It was also noted that naphtha fuel produced a lower concentration of total PAH compared to other fuels. It was hypothesized that naphtha fuel is composed of PAH compounds in low concentration.

CHAPTER 6

PM CHARACTERISTICS OF DIESELINE AND NAPHTHA FUELLED PCI WITH DOUBLE INJECTION

6.1 Introduction

As discussed earlier in section 4.3.3 of chapter 4, PCI combustion can be attained by using high EGR ratios and injection timing advancement. The injection timing and combustion phasing are important parameters in achieving the PCI combustion mode. In other words, injecting fuel too early or late may shift the combustion phasing to before TDC, resulting in a high maximum pressure rise rate MPRR, and in a drop in the BTE. If the injection timing is left too late, high smoke emissions are the result as the ignition delay will be short.

A new approach to PCI, which starts by using a double or split injections strategy, has been introduced; this involves early direct injection followed by late direct injection (pulsed at compression stroke). The early or first injection creates a homogenous fuel/air mixture and the second injection timing controls the combustion phasing. The use of high EGR provides a longer ignition delay, which in turn promotes fuel/air mixing. This results in fewer fuel-rich packets followed by low temperature combustion, which reduces soot and NO_x levels (Imtenan, et al., 2014; Inagaki, et al., 2006).

A study conducted at the University of Birmingham examined light duty diesel engines (2.2 litre-four cylinder run on dieseline with 50% gasoline and 50% diesel) and PCI. The split

injections were investigated and it was concluded that larger-sized particles were reduced by 90%, and the particles' mean diameter was reduced by 23.8 nm (Rezaei, et al., 2013).

This chapter discusses the investigation of the effects of double injection on combustion performance, particle size, number distribution, and chemical characterization of the PM of diesel-, G75-, and naphtha-fuelled premixed compression ignition PCI engines at three loads (1.50, 3, and 6 bar BMEP). Also, trace metals, PAHs, and semi-volatile organic compounds (SVOCs) are investigated.

6.1.1 Research Objective

Using a double injection strategy, the study was conducted to investigate the effect of load variation on the particle size and number distribution and chemical characterization of the PM of a diesel-, G75-, and naphtha-fuelled PCI engine. The pertinent points were collected under conditions comparable to diesel fuel in terms of BTE, NO_x, soot, and PN.

6.1.2 The Engine and Test Conditions

The experimental setup is the same as that discussed in section 5.1.2 of Chapter 5, but here double injections have been utilized and the studied loads were up to 6 bar BMEP, since higher loads produced massive smoke emissions compared to single injection. The engine speed was fixed at 1800 rpm and overall lambda ($\lambda \sim 1.23$). The first injection timings were fixed for all fuels at each load. The second injection timing was obtained based on the operating conditions that produce lower smoke, NO_x, and PN emissions. It was found that

fixing the injection quantity of the first injection timing at 30% and of the second injection timing at 70% produced low smoke and NO_x emissions, with a comparable BTE to single injection. Table 6.1 demonstrates the operating conditions of the double injections strategy.

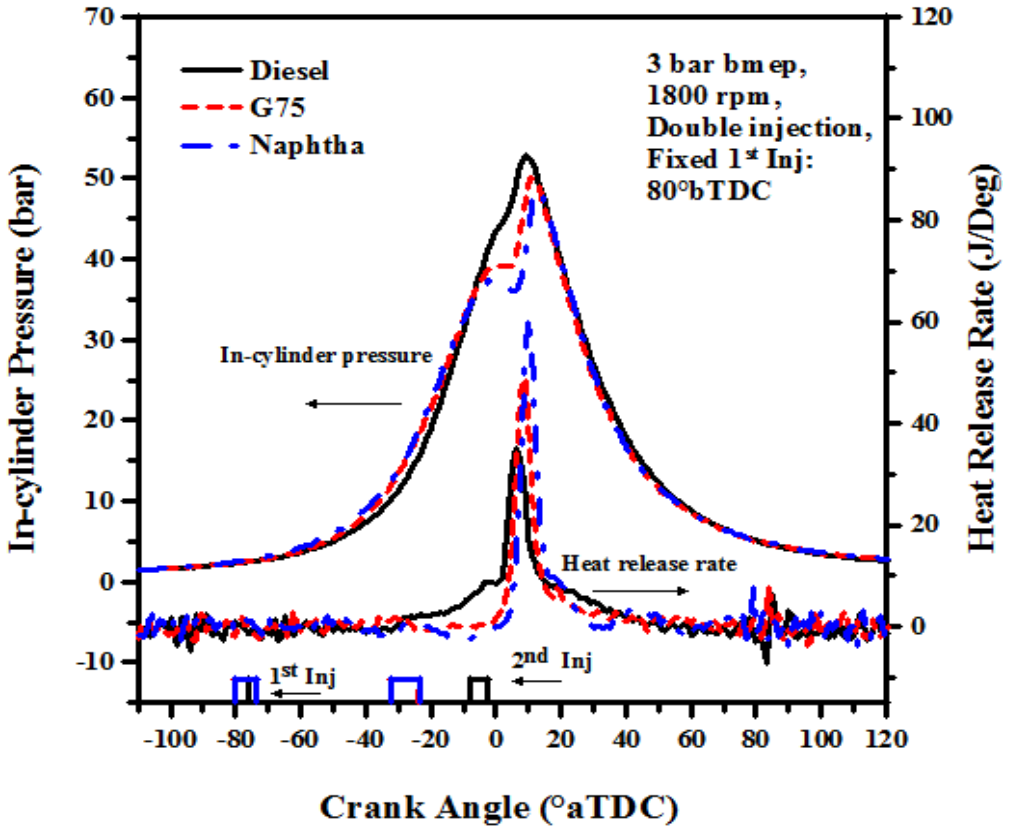
Table 6.1: Test conditions at four different loads for diesel, G75 and naphtha fuels with double injection

Speed	**1800 rpm**			**Fuel**
Load (bar bmep)	**1.50**	**3**	**6**	
Injection Pressure (bar)	500	700	1200	
1st Injection Timing (°bTDC)	100	80	60	
2nd Injection Timing (°bTDC)	9.5	8	3	
1st Injection Quantity (%)	30%			
2nd Injection Quantity (%)	70%			**Diesel**
EGR Ratio (%)	59.40	49.50	28	
NOx (g.kWh^{-1})	0.37	0.48	0.79	
Smoke (FSN)	0.39	1.365	3.75	
BTE (%)	21.98	31.48	35.75	
Injection Pressure (bar)	150	350	500	
1st Injection Timing (°bTDC)	100	80	60	
2nd Injection Timing (°bTDC)	40	32.5	26	
1st Injection Quantity (%)	30%			
2nd Injection Quantity (%)	70%			**G75**
EGR Ratio (%)	51	43	29.5	
NOx (g.kWh^{-1})	0.21	0.22	0.33	
Smoke (FSN)	0.008	0.004	0.011	
BTE (%)	22.40	31.23	36.94	
Injection Pressure (bar)	150	350	500	
1st Injection Timing (°bTDC)	100	80	60	
2nd Injection Timing (°bTDC)	40	32.5	26	
1st Injection Quantity (%)	30%			
2nd Injection Quantity (%)	70%			**Naphtha**
EGR Ratio (%)	44.50	32.70	30	
NOx (g.kWh^{-1})	0.324	0.421	0.34	
Smoke (FSN)	0.009	0.002	0.008	
BTE (%)	22.50	29.84	36.42	

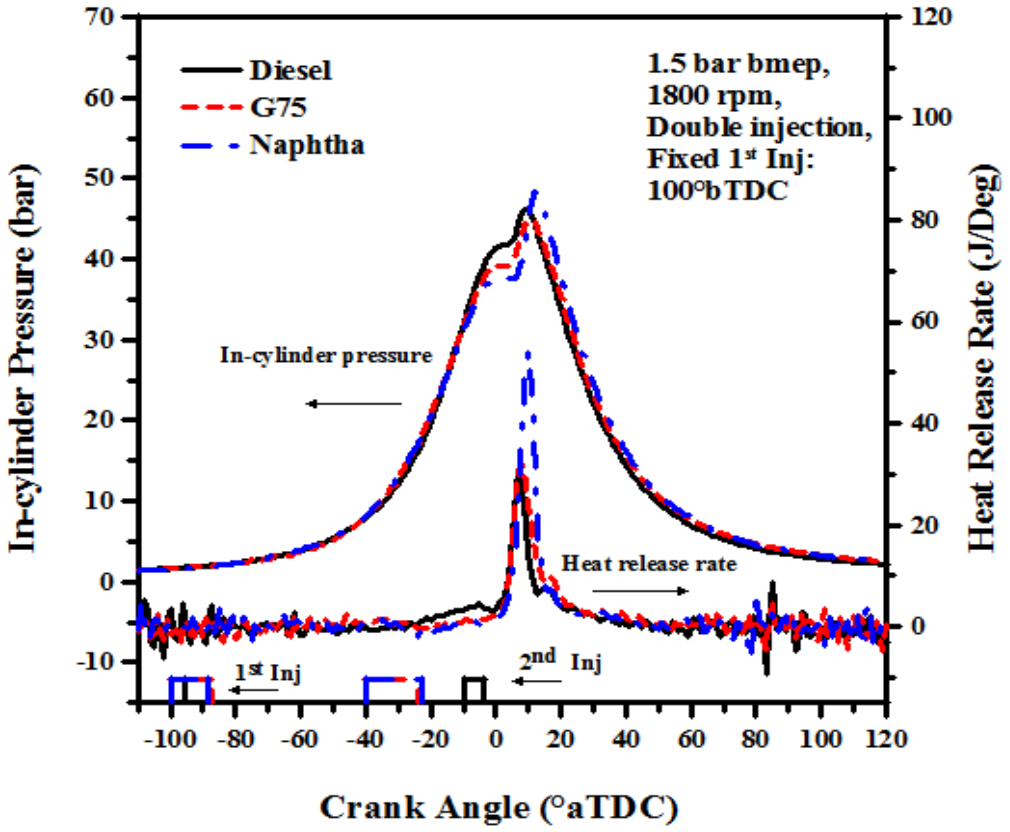
6.2 Combustion Performance

6.2.1 Heat Release Rate Analysis

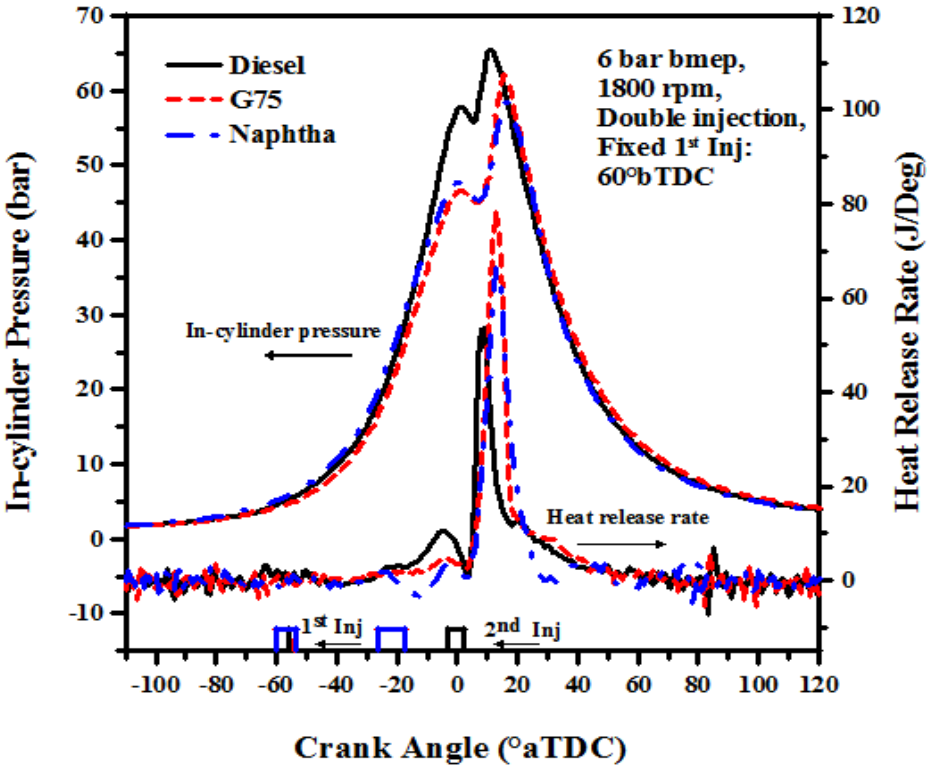
The heat release rate, injection pulses, and in-cylinder pressure of the three fuels with double injection at three different loads are plotted against the crank angle degree (CAD), as shown in Figure 6.1 and 6.2. Increasing the load from 1.50 to 6 bar BMEP, it was observed that after the end of the second fuel injection event, the first peak heat release for G75 and naphtha fuels started. There was an overlap between the end of the second injection timing and the start of the first peak heat release for diesel fuel, as shown in Figure 6.1 (a, b, c). Naphtha fuel has the highest HRR at both loads 1.50 and 3 bar BMEP, as shown in Figure 6.2. The overlap with the diesel fuel is explained by the ignition delay, as the first stage of the injected fuel has a shorter ignition delay, and so the first peak of the HRR commenced before the start of the second fuel injection. G75 and naphtha fuels exhibited a longer ignition delay, which, coupled with sufficient time for the fuel to mix with air, leads to a lean mixture. The disappearance of the overlap is an indication that the combustion was in premixed compression ignition (PCI) mode.


Diesel
G75
Naphtha
3 bar bmep,
1800 rpm,
Double injection,
Fixed 1st Inj:
80°bTDC
In-cylinder pressure
Heat release rate
1st Inj
2nd Inj
In-cylinder Pressure (bar)
Heat Release Rate (J/Deg)
Crank Angle (°aTDC)

(a)


Diesel
G75
Naphtha
1.5 bar bmep,
1800 rpm,
Double injection,
Fixed 1st Inj:
100°bTDC
In-cylinder pressure
Heat release rate
1st Inj
2nd Inj
In-cylinder Pressure (bar)
Heat Release Rate (J/Deg)
Crank Angle (°aTDC)

(b)



(c)

Figure 6.1: In-cylinder and heat release rate of diesel, G75 and naphtha fuels with double injection vs. crank angle: (a) 1.5 ,(b) 3 , (c) 6 bar BMEP

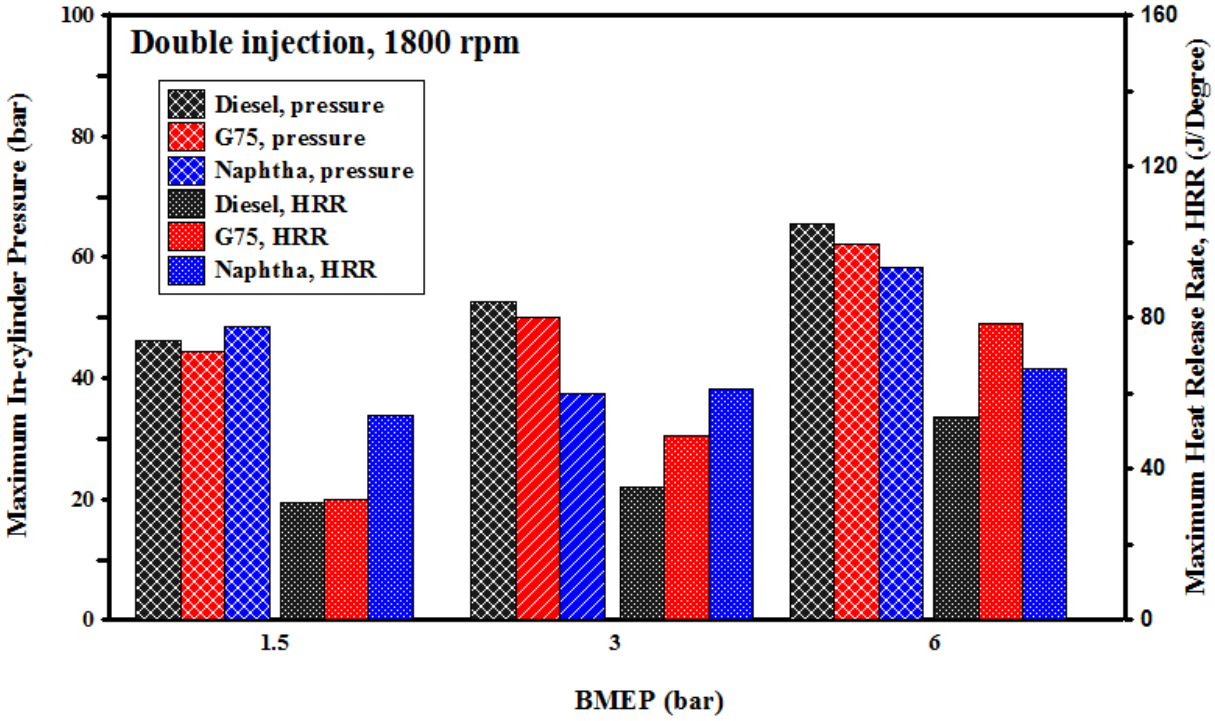
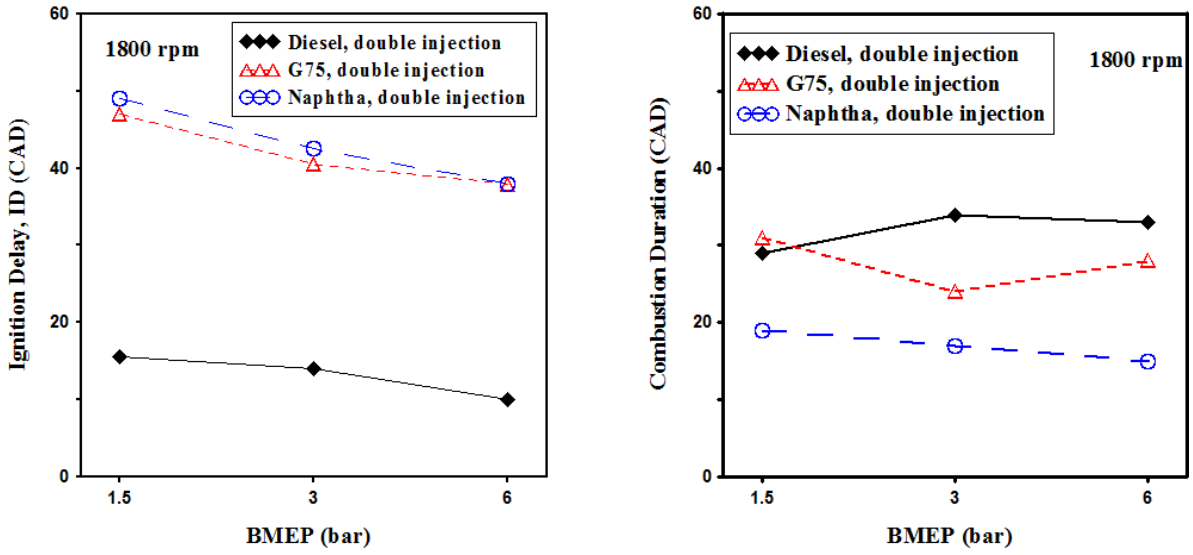


Figure 6.2: Maximum incyline pressure and heat release rate of diesel, G75 and naphtha fuels with double injection versus engine loads

The ignition delay (ID) of the double injection was defined as the difference between the start of the second injection fuel event and AHR50 of the total heat release rate, as shown in Figure 6.3 (a).

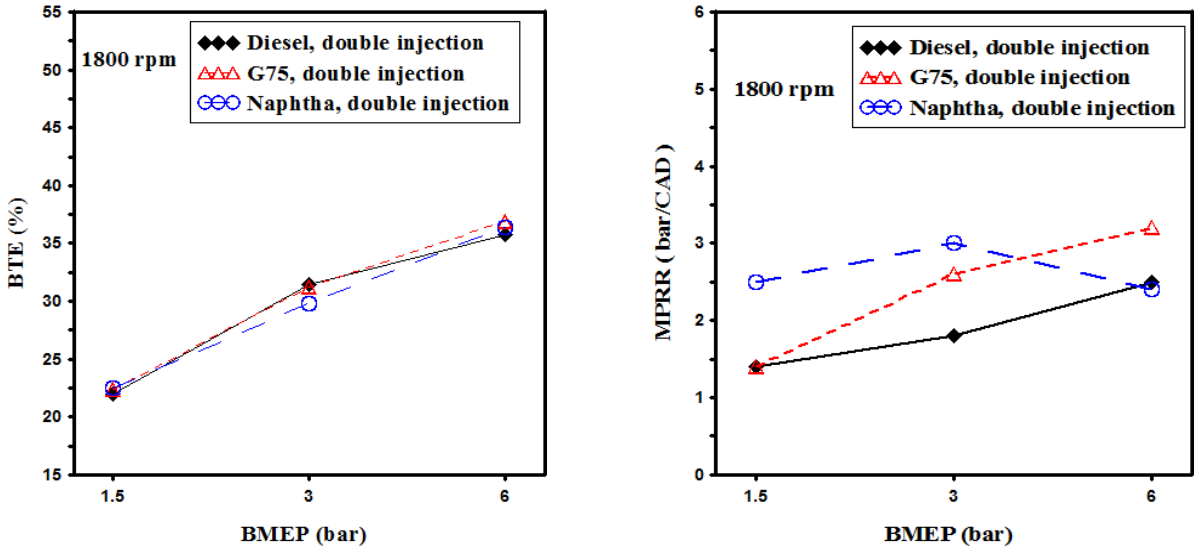
The combustion duration shown in Figure 6.3 (b) is defined as the difference between the crank angle of 10% mass fraction burn (MFB 10) and 90 % mass fraction burn (MFB 90). G75 fuel has a longer combustion duration at load 1.50 bar BMEP compared to diesel and naphtha fuels, while diesel fuel has a longer combustion duration compared to G75 and naphtha fuels when the load increased from 3 bar BMEP to 6 bar BMEP. It could be said that before the combustion of G75 fuel at load 1.50 bar BMEP began, the over-lean mixture generated from the first stage injection timing made the burning rate very slow, resulting in a long combustion duration. It was noted that when increasing the load from 1.50 to 6 bar BMEP, naphtha fuel had the shortest combustion duration. When the second stage injection timing happened, the local mixture was close to stoichiometric conditions, where the burning rate was high.

The BTE increased as the load increased, as shown in Figure 6.4 (a). The first injection timing was influential in the BTE variation. In other words, the charge with less premixed fuel can produce fewer emissions of BSCO and BSHC, as shown in Figure 6.5 (c, d). As a result, higher BTE was produced (Rezaei, et al., 2013). At low load 1.50 bar BMEP, the BTE of G75 and naphtha fuels was 0.42 and 0.52% respectively higher than diesel fuel (absolute values). When the load was increased to 3 bar BMEP, the BTE of G75 and naphtha fuels was lower than diesel fuel by 0.25% and 1.64% respectively (absolute values). At load 6 bar BMEP, both fuels were higher than diesel by 1.19% and 0.67% respectively (absolute values). G75 fuel has a higher MPRR at load 6 bar BMEP compared to other fuels, as shown in Figure 6.4 (b). It could be said that MPRR is linked to the second injection timing, where it can control the combustion phase.



(a) (b)

Figure 6.3: Ignition delay (a) combustion duration (b) for diesel, G75 and naphtha fuels at three different loads with double injection



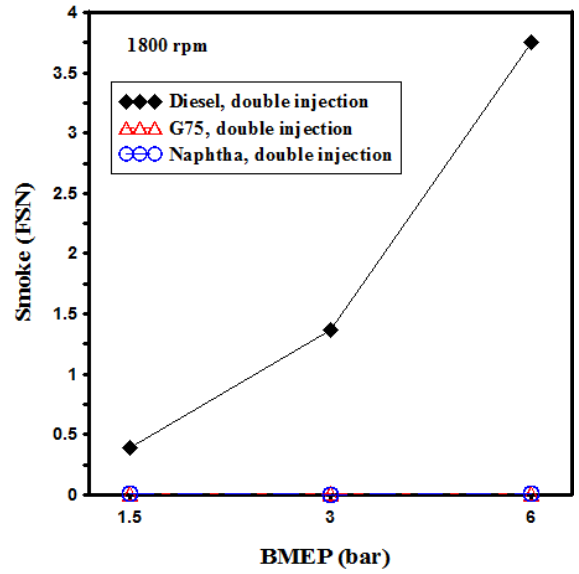
(a) (b)

Figure 6.4: The brake thermal efficiency (a) and maximum pressure rise rate (b) of three fuels at three loads

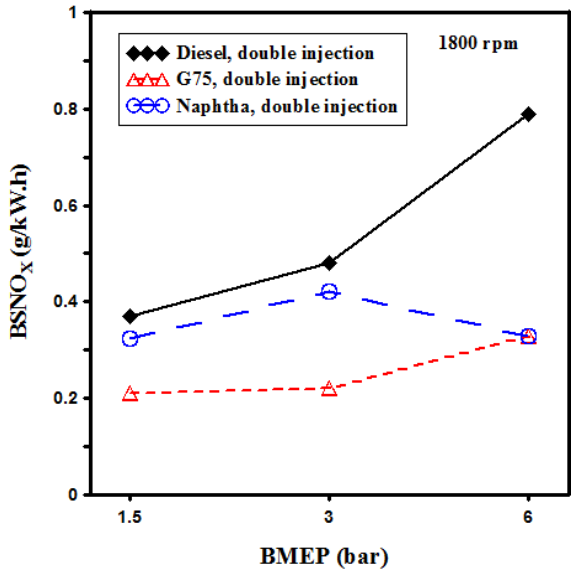
6.2.2 Regulated Emissions

Increasing the load increased smoke emissions for diesel fuel to around 3.8 FSN as shown in Figure 6.5 (a). When the second stage injection began, there was insufficient time to remove the fuel-rich zones, and so smoke was produced. Conversely, increasing the load maintained the smoke emissions of both G75 and naphtha fuels below 0.01 FSN. The less rich zones kept the smoke very low. Moreover, the first injection quantity ratio and second injection timing were considered to be the dominant parameters in varying smoke emission (Rezaei, et al., 2013).

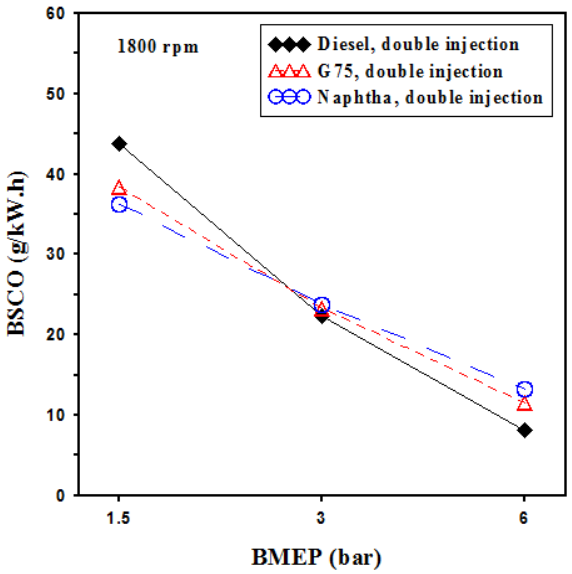
The $BSNO_x$ increased with an increasing load for all fuels except for the naphtha fuel, where the $BSNO_x$ decreased at 6 bar BMEP. The increase of $BSNO_x$ is attributed to low levels of EGR; high combustion temperatures occurred, leading to an increase in $BSNO_x$ emissions. It was also observed that at 6 bar BMEP, both G75 and naphtha exhibited the same emissions of $BSNO_x$. The same ignition delay, as shown in Figure 6.3 (a), leads to the production of the same $BSNO_x$ levels (Kalghatgi, 2014). Increasing the load decreased the BSHC and BSCO emissions, except in the case of BSCO emissions for naphtha fuel at load 3 bar BMEP, as shown in Figure 6.5 (c, d). The less premixed charge generated by the first injection timing reduced the emissions of BSHC and BSCO. The sudden increase in BSCO of the naphtha fuel at load 3 bar BMEP could be due to fuel wall impingement.



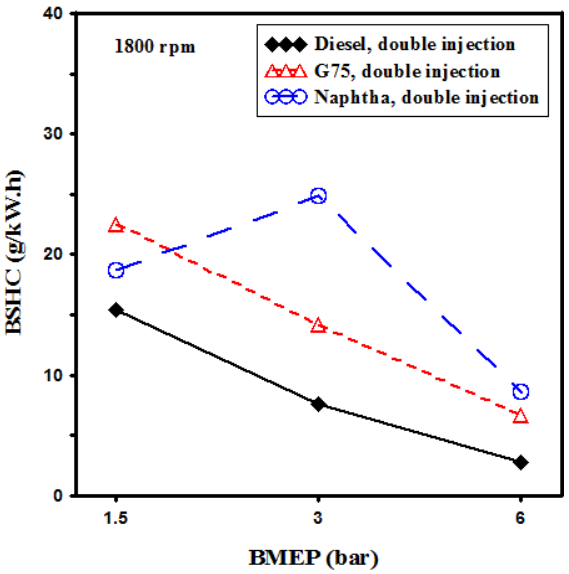
(a)



(b)



(c)



(d)

Figure 6.5: The emissions of three fuels at three loads: (a) Smoke, (b) BSNOx (c) BSCO, (d) BSHC

6.3 Particle Size-number Distribution with Double Injection

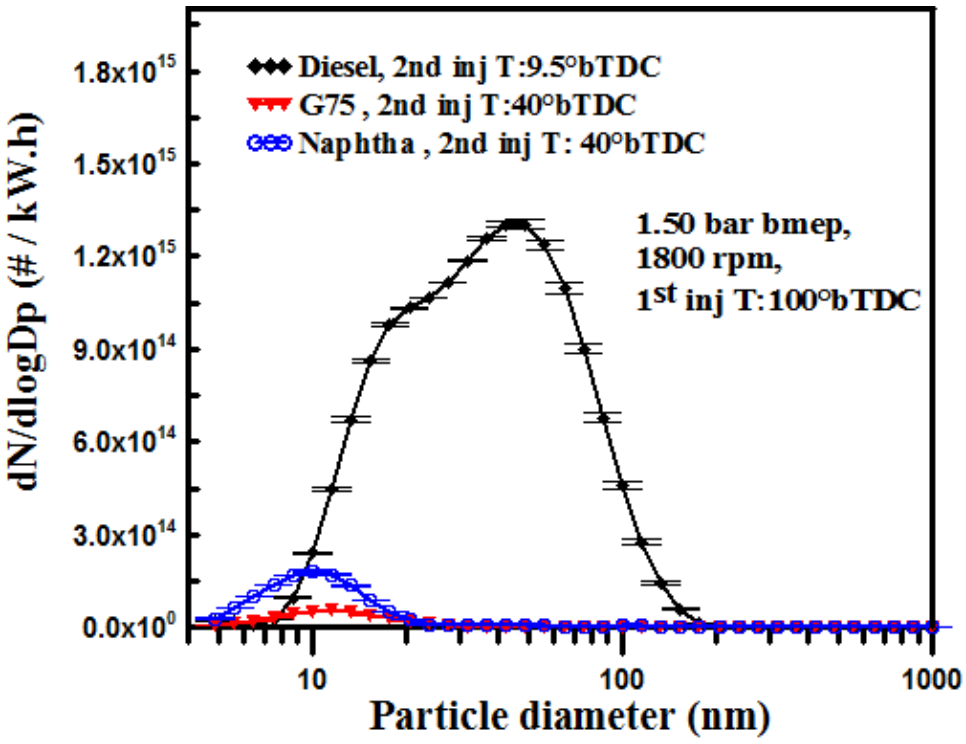
Particle size–number distributions were initially obtained after thermal stabilization of each test condition, and measurements were taken per unit of volume and averaged for four times of repetition. The standard and uncertainties have been reported and presented in the figures. The measured particle size number distributions have been normalized to part per kilowatt hour (kWh) at three engine loads: 1.50, 3, and 6 bar BMEP, while maintaining the speed at 1800 rpm and ($\lambda \sim 1.23$). Figures 6.6 and 6.7 illustrate the distribution of the particle size-number and the variation in particle number concentrations in nucleation and accumulation modes for diesel, G75 and naphtha fuels at different operating conditions. In order to maximize the visibility of the particle size number distributions of G75 and naphtha fuels, separated figures have been merged with the main figures.

6.3.1 Effect of Engine Load on Particle Size-Number Distribution

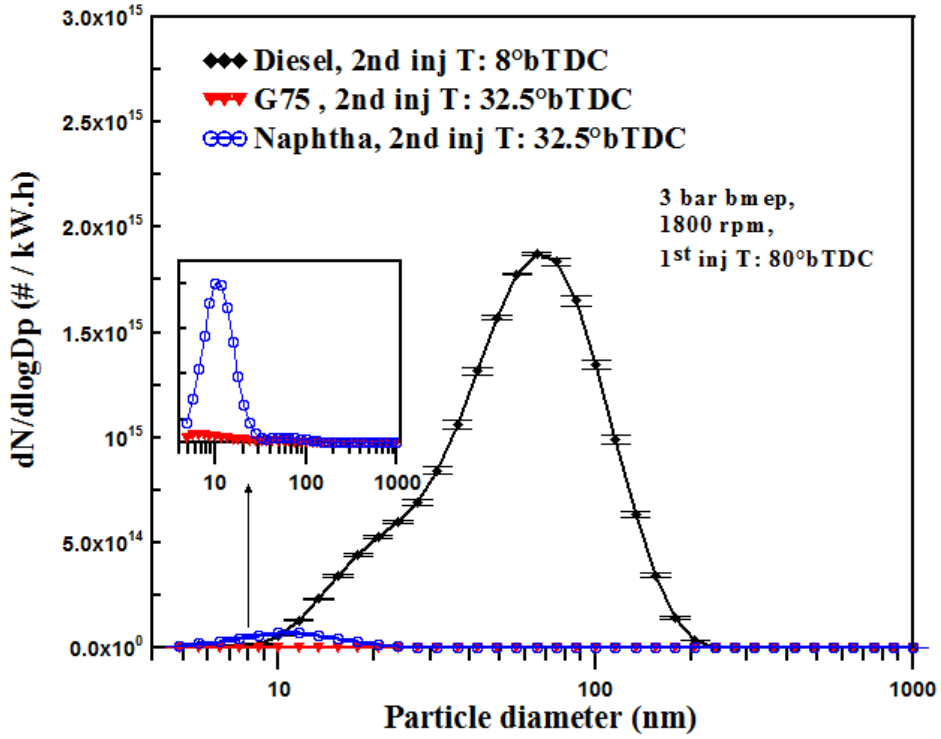
From Figure 6.6 and 6.7 (a), it was noted that as the load for diesel fuel was increased, the total particle number concentration and CMD increased, while for G75 and naphtha fuels the levels decreased, as did smoke emissions. The increase in the total particle number concentration of diesel fuel is due to insufficient time to remove the fuel-rich zones when the second injection timing started. The overlap between the start of the first heat release peak and the end of the second fuel injection event as shown in Figure 6.1 (c) is evident. For G75 and naphtha fuels, the local lean mixture produced by the first injection timing kept the PN emissions low. Additionally, both G75 and naphtha had sufficient time to mix fully with air

before combustion started, as shown in Figure 6.1, where the first peak of heat release began after the end of the second injection.

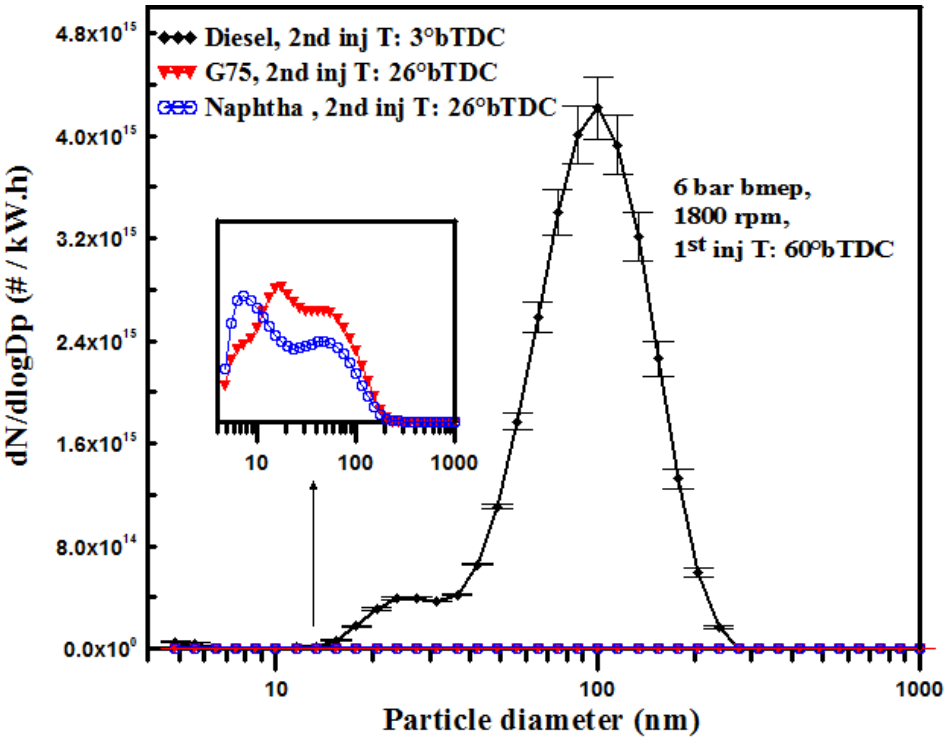
The PN and CMD of both G75 and naphtha fuels were reduced significantly compared to diesel fuel. For example, at low load of 1.50 bar BMEP, it was observed that the G75 fuel emitted the lowest total particle number concentration, as shown in Figure 6.7 (a). The reduction was 97.7%, while the reduction of nucleation and accumulation mode particles compared to diesel were 95% and 99.9% respectively, as shown in Figure 6.7 (b). Compared to diesel, naphtha fuel also displayed a reduction of 92.5% in the total particle number concentration, and a reduction of the nucleation and accumulation mode particles by 84.5% and 99% respectively. CMD, as shown in Figure 6,7 (a), was reduced from 35 nm to 11 nm for G75 fuel, and to 10 nm for naphtha fuel.



(a)

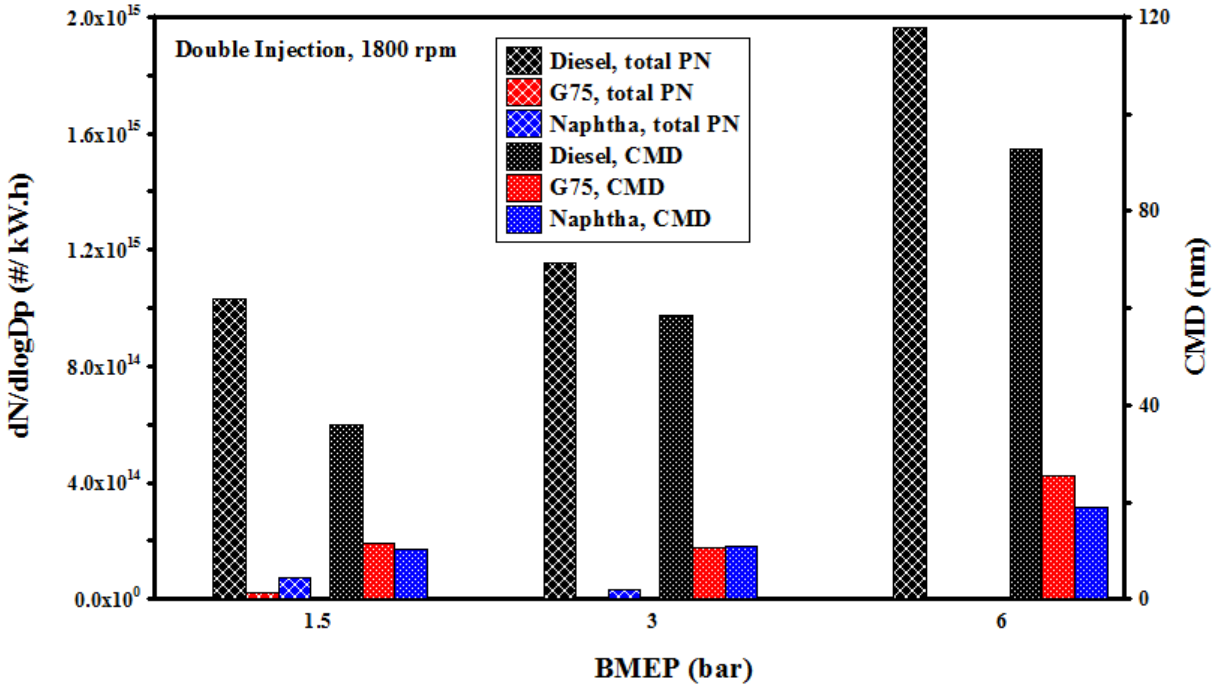


(b)

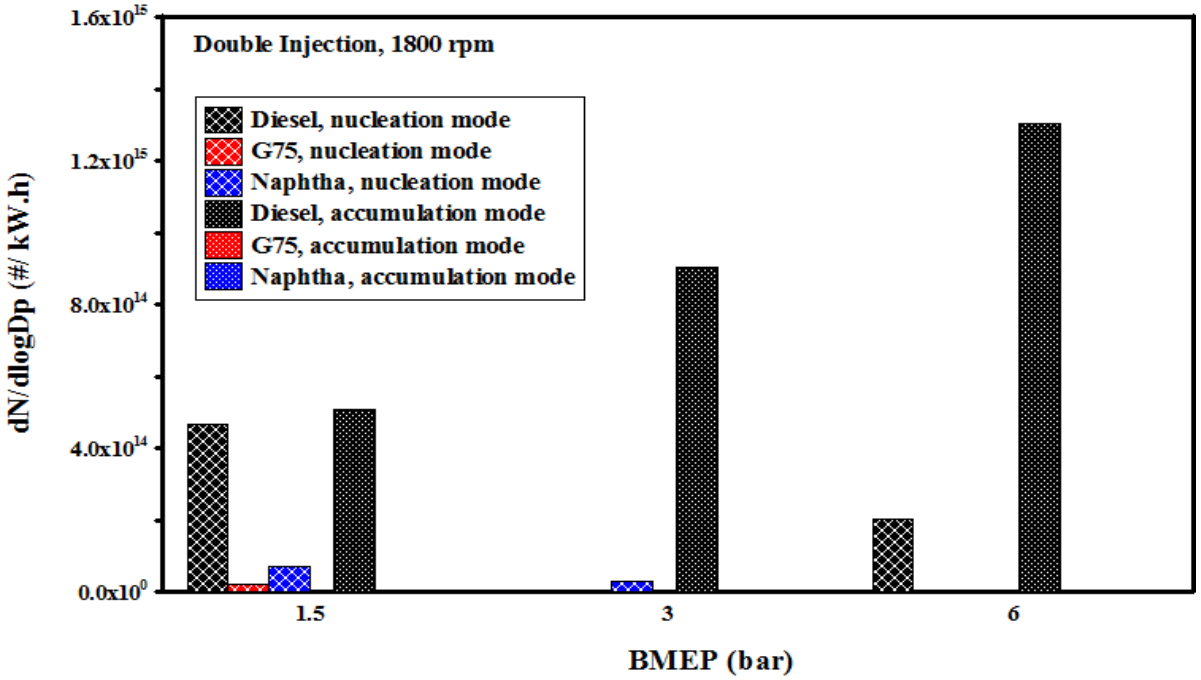


(c)

Figure 6.6: The particle size-number distribution of diesel, G75 and naphtha fuels with double injection at three loads: (a) 1.50 bar BMEP, (b) 3 bar BMEP (c) 6 bar BMEP



(a)



(b)

Figure 6.7: The particle number concentrations of diesel, G75 and naphtha fuels with double injection at three loads: (a) total PN, (b) total PN of nucleation and accumulation modes

At load 3 bar BMEP, as shown in Figure 6.7, it was observed that the total particle number concentration of G75 and naphtha decreased by 99.8% and 97% respectively. For the accumulation mode particles, the G75 fuel emitted zero compared to naphtha and diesel fuels, but the accumulation mode particles in the naphtha fuel decreased by 99.9% compared to the diesel fuel. The CMD for both G75 and naphtha fuels at 3 bar BMEP decreased from 58 nm to 10 nm. At load 6 bar BMEP, as shown in Figure 6.7, the total particle number concentrations of both fuels G75 and naphtha decreased significantly by 99.9%; even the nucleation and accumulation mode particles were reduced by 99.9% compared to diesel fuel. Both G75 and naphtha have the same combustion phases, as shown in Figure 6.1 (c), and the same ignition delay, as shown in Figure 6.3 (a).

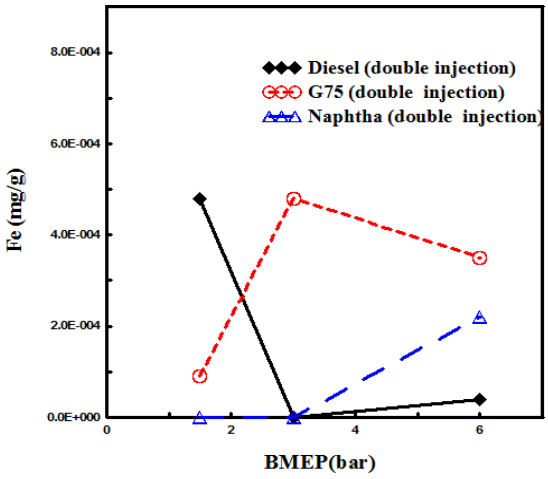
6.3.2 Metal Concentration in Particulates with Double Injection

This section investigates the concentration of metals in the particulates for double injection, as shown in Figure 6.8. It was noted that in all loads and all fuels there was no presence of Ni in the particulates, as shown in Figure 6.8 (g). This is also the case for single injection. It could be hypothesized, therefore, that all fuels do not contain any traces of Ni in either fuel or engine oil. Another similarity with single injection is that the concentration of Pb in diesel particulates was high compared to that in the other fuels, as shown in Figure 6.8 (b). As discussed earlier, there were very small traces of Pb present in diesel fuel, while G75 and naphtha fuels had almost zero concentration. Also, it can be seen from Figure 6.1(c) that at 6 bar BMEP, there was an overlap between the first peak of the heat release rate and the end of the second injection timing. It could be said that some fractions of fuel escaped from the combustion chamber unburned, and condensed into the filter.

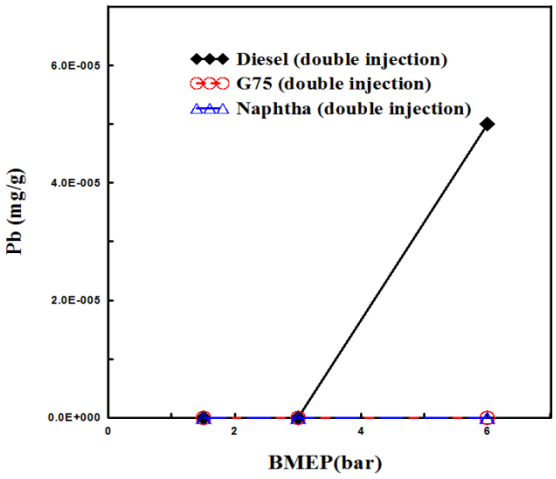
From the figures, it is clear that there is no specific trend regarding trace metals in the case of double injection; this is also the case with single injection. Double injection also confirmed

the other researchers' findings, as it has been reported that metals in diesel particulates are mostly dependent on fuel, engine oil compositions, engine wear, in-cylinder temperature, and the condition of a sampling point (Gangwar, et al., 2012; Agarwal, et al., 2015). Therefore, it could be said that the presence of Fe and Ca metals, as shown in Figure 6.8 (a,d), originates from fuel where the in-cylinder temperature was low, and where some fractions of fuel escaped the combustion chamber without burning and were deposited into the filter paper.

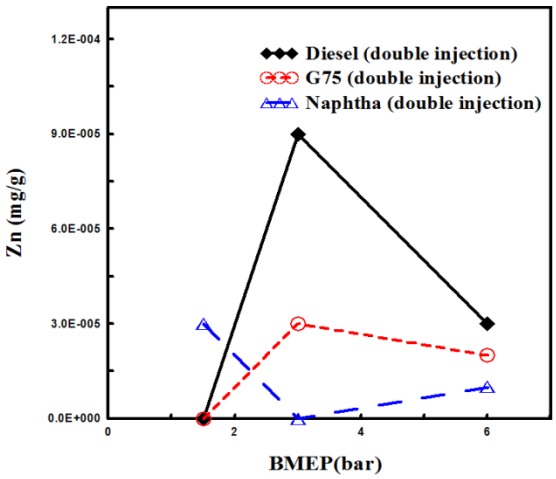
For copper (Cu), as shown in Figure 6.8 (e), it could be argued that the presence of a high concentration of Cu in G75 particulates originates from engine oil, which was mixed with fuel during combustion. Another possible reason is that G75 fuel contains some traces of Cu, and during combustion very small fractions of fuel managed to leave the exhaust system without burning. Then, at the dilution system, these fractions were diluted with air and their temperature decreased, and so the fractions were condensed onto the filter paper. For Zn metal, as shown in Figure 6.8 (c), it was observed that high concentrations were produced from diesel fuel at load 3 bar BMEP. It could be said that at that load, some fractions of engine oil mixed with fuel, and given the low in-cylinder temperature, the fraction escaped without burning and was deposited into filter paper.



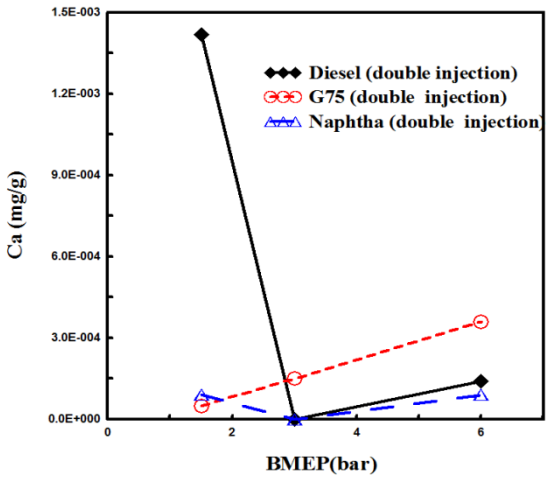
(a)



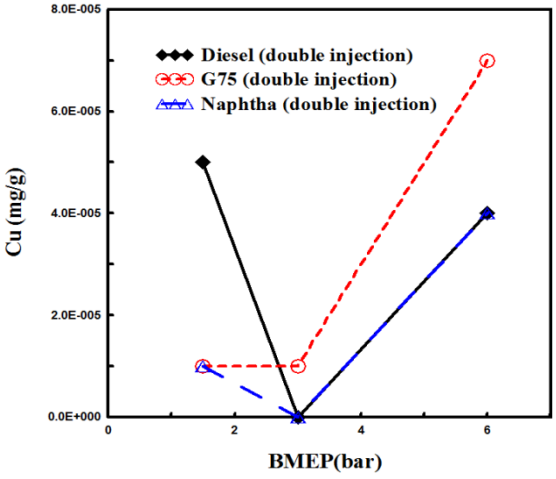
(b)



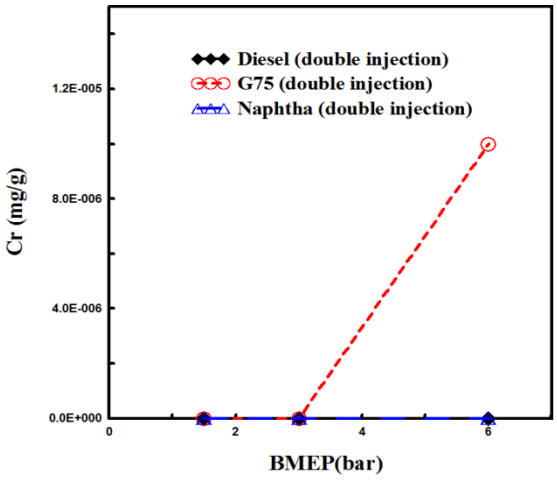
(c)



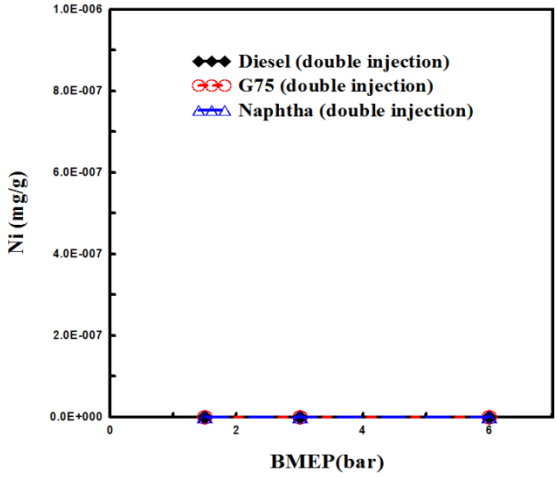
(d)



(e)



(f)



(g)

Figure 6.8: Concentrations of trace metals in diesel, G75 and naphtha particulates at three different loads with double injection (a) Fe, (b) Pb, (c) Zn, (d) Ca, (e) Cu, (f) Cr, (g) Ni

In the case of the Cr metal, as shown in Figure 6.8 (f), G75 fuel produced higher concentrations of Cr than the other fuels. It may be suggested that the presence of Cr in G75 particulates is related to the engine wear. The wear of the chrome-plated piston rings as they mixed with the fuel during combustion may have led to condensation on the filter paper. Single and double injections emit a variable concentration of trace metals. As discussed earlier, this depends on fuel composition, engine oil composition, engine wear, and the condition of the sampling point. For the condition of sampling point, the temperature may not be conducive to condensation of all the emitted trace metals from the exhaust system, and some of the metals therefore escaped from the exhaust in gas form without condensing. This explains why we found very low concentrations of trace metals in some loads (Gangwar, et al., 2012).

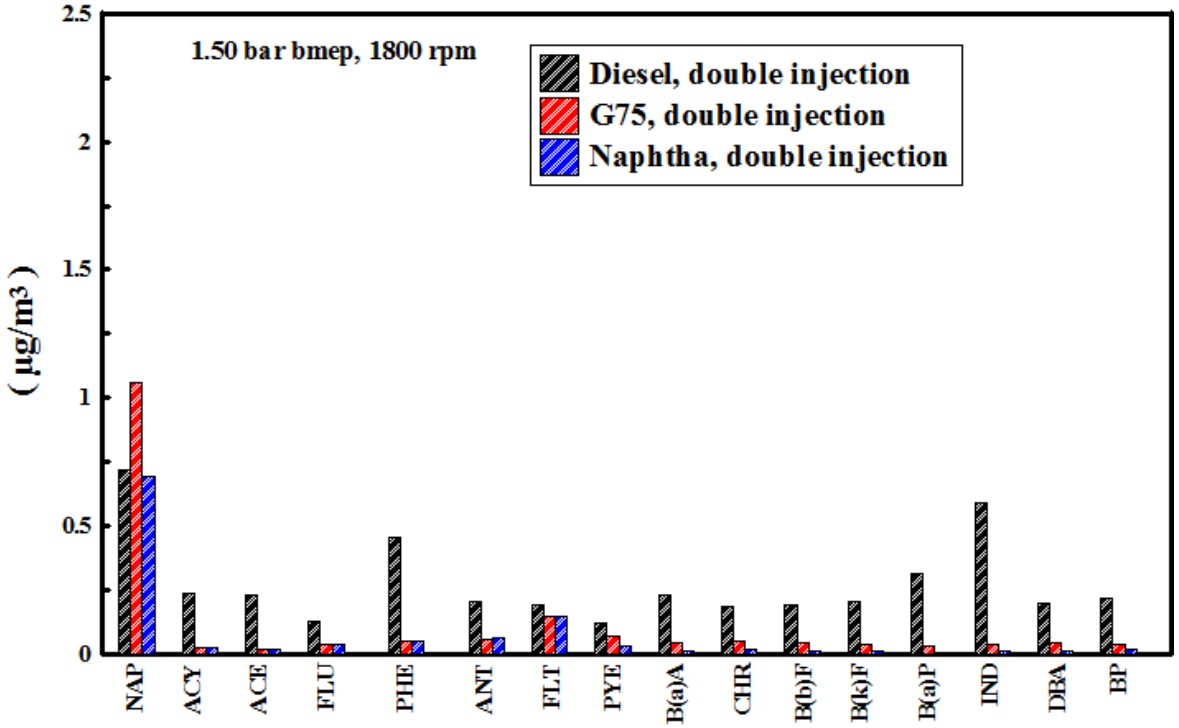
6.3.3 PAHs' Concentrations with Double Injection

Figure 6.9 (a, b, c, d) illustrates the concentrations of the 16 PAH compounds in the particulate phase for diesel, G75 and naphtha fuels at 1.5, 3, and 6 bar BMEP loads respectively. The total and individual concentrations of the 16 PAH compounds, together with their emitted differences when using different fuels with double injection, are demonstrated in Table 6.2. Figure 6.9 shows that the low molecular weight (LMW) PAH compounds are present in higher concentrations than the high molecular weight (HMW) compounds in all loads. This is also the case with single injection, which means that these compounds were originally present in the fuel, as reported by Liang, et al. (2005).

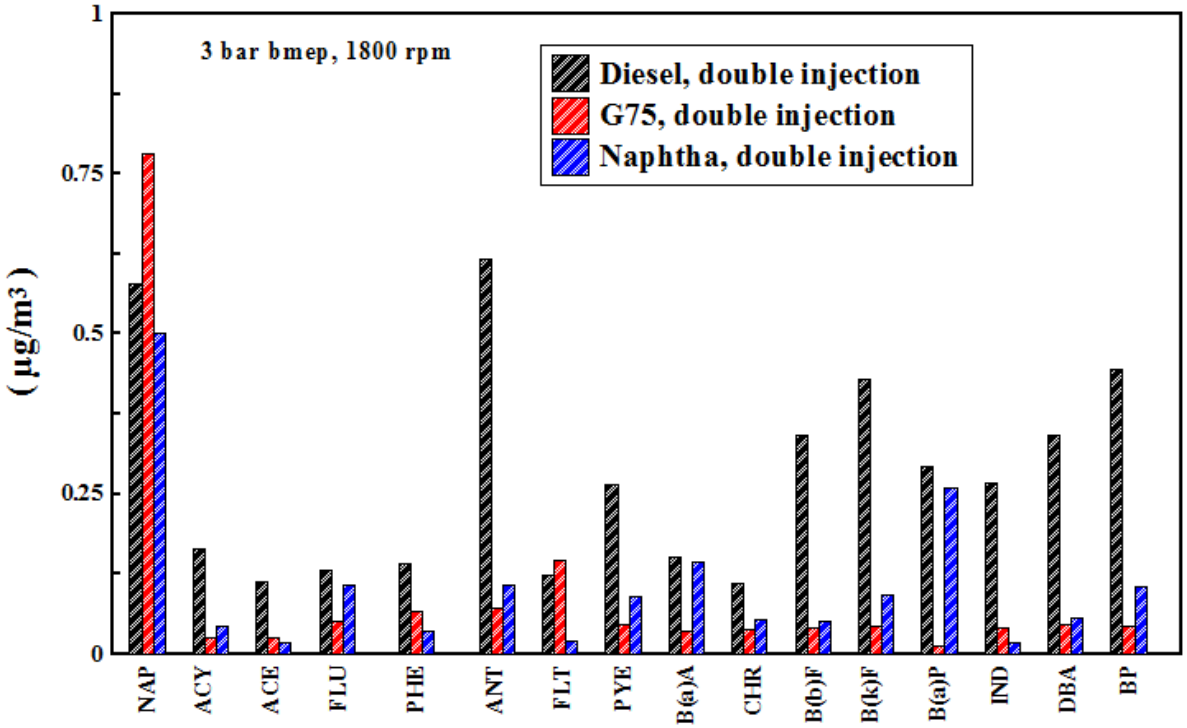
At load 1.50 bar BMEP, G75 fuel emitted the highest concentrations of NAP (1.05 μgm^{-3}) in comparison to other fuels, as shown in Figure 6.9 (a) and Table 6.2. The increase in NAP

concentration is consistent with the high emissions of BSHC when using G75 fuel as opposed to diesel and naphtha fuels. The lean mixture generated by the first injection timing resulted in some unburned fuel leaving the exhaust system. The lowest concentration of PAH compounds (e.g. the observed concentration of benzo (a) pyrene (B(a)P) was 0.004 μgm^{-3}) was emitted from the naphtha fuel. It was hypothesized that this low concentration is related to some form of (B(a)P) which failed to condense on the filter paper and escaped in gas form (Agarwal, et al., 2011).

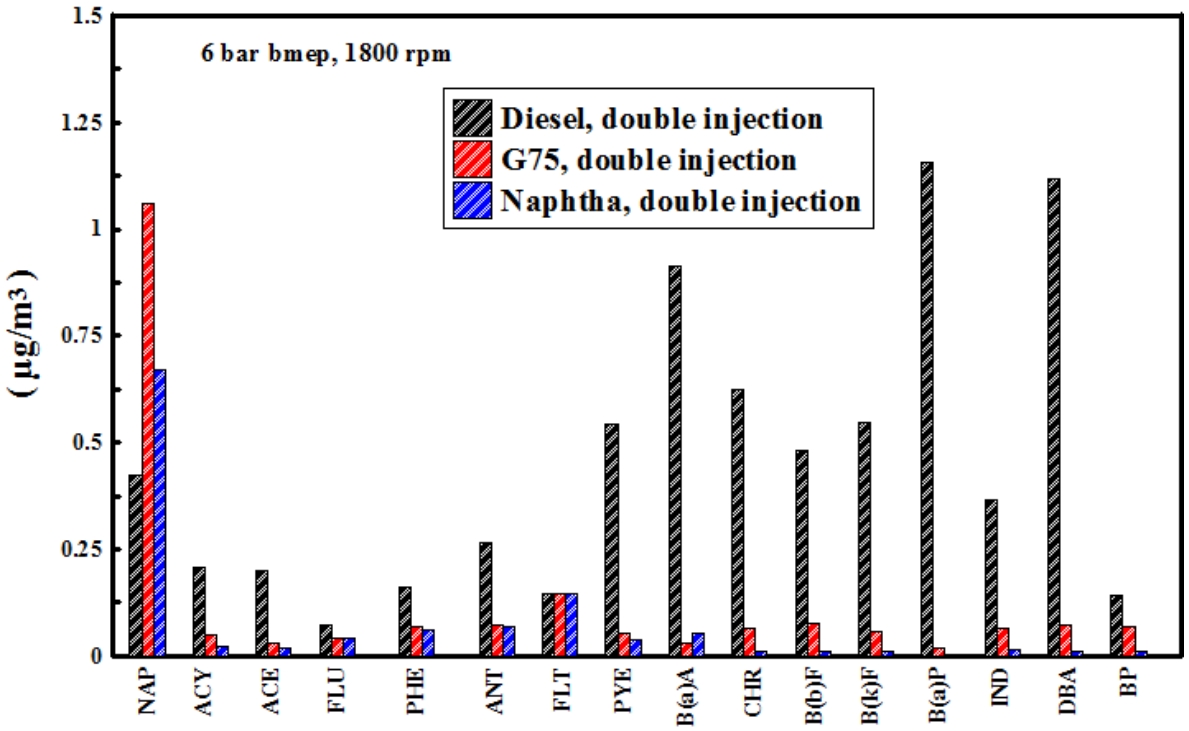
When the load was increased from 1.50 to 6 bar BMEP, as shown in Table 6.2, it was observed that the total PAH compounds of both G75 and naphtha decreased significantly compared to diesel fuel, by around 84%. An exception was naphtha fuel at load 3 bar BMEP, where the total of PAH compounds increased a little. The trend is also consistent with BSHC and PN emissions, as shown in Figures 6.5 (d) and 6.6 (b). The first injection timing of G75 and naphtha fuels with a low fuel quantity ratio produced a local lean mixture and kept the PAH emissions low. It was also observed that naphtha fuel produced a lower concentration of total PAH compounds compared to the other fuels. Similar observations were made with the single injection method, which supports our hypothesis that PAH compounds in naphtha fuel are originally present in lower concentrations. The increase in the PAH compounds of naphtha fuel at load 3 bar BMEP was also confirmed by the increase of BSHC and PN emissions. This could be attributed to fuel wall impingement, as the fuel was injected at low in-cylinder pressure, so the fuel could hit the piston head and form a film.


1.50 bar bmep, 1800 rpm
Diesel, double injection
G75, double injection
Naphtha, double injection
(µg/m³)
2.5
2
1.5
1
0.5
0
NAP
ACY
ACE
FLU
PHE
ANT
FLT
PYE
B(a)A
CHR
B(b)F
B(k)F
B(a)P
IND
DBA
BP

(a)


3 bar bmep, 1800 rpm
Diesel, double injection
G75, double injection
Naphtha, double injection
(µg/m³)
1
0.75
0.5
0.25
0
NAP
ACY
ACE
FLU
PHE
ANT
FLT
PYE
B(a)A
CHR
B(b)F
B(k)F
B(a)P
IND
DBA
BP

(b)



(c)

Figure 6.9: Concentrations of PAH compounds in diesel, G75 and naphtha particulates at three different loads with double injection (a) 1.50 bar BMEP, (b) 3 bar BMEP, (c) 6 bar BMEP

Table 6.2: PAHs concentrations in particulates of diesel, G75 and naphtha fuels at three different loads with double injection, * The concentration increased compared to diesel fuel

PAH	Diesel Conc (μgm^{-3})	G75 Conc (μgm^{-3})	Naphtha Conc (μgm^{-3})	G75 Reduction (%)	Naphtha Reduction (%)
1.50 bar BMEP					
Naphthalene (NAP)	0.72	1.06	0.69	46.5 % >*	4%
Acenaphthylene(ACY)	0.24	0.02	0.02	90%	91%
Acenaphthene (ACE)	0.23	0.02	0.02	93%	93%
Fluorene (FLU)	0.13	0.03	0.04	73%	71%
Phenanthrene (PHE)	0.46	0.05	0.05	89%	89%
Anthracene (ANT)	0.20	0.06	0.06	73%	70%
Fluoranthrene (FLT)	0.19	0.15	0.15	23%	23%
Pyrene (PYE)	0.12	0.07	0.03	43%	74%
Benzo(a)anthracene (B(a)A)	0.23	0.04	0.01	82%	95%
Chrysene (CHR)	0.18	0.05	0.02	74%	91%
Benzo(b)fluoranthene (B(b)F)	0.19	0.04	0.01	78%	94%
Benzo(k) fluoranthene (B(k)F)	0.20	0.04	0.01	82%	94%
Benzo(a) pyrene (B(a)P)	0.31	0.03	0.00	90%	99%
Indeno(1,2,3-CD)pyrene(IND)	0.59	0.04	0.01	94%	98%
Dibenz(a,h) anthracene (DBA)	0.20	0.04	0.01	79%	95%
Benzo (g, h, i) perylene (BP)	0.22	0.04	0.02	83%	91%
Total	4.41	*1.77*	1.16	60%	73%
3 bar BMEP					
Naphthalene (NAP)	0.58	0.78	0.50	35% >	13%
Acenaphthylene(ACY)	0.16	0.03	0.04	84%	74%
Acenaphthene (ACE)	0.11	0.02	0.02	78%	84%
Fluorene (FLU)	0.13	0.05	0.11	62%	18%
Phenanthrene (PHE)	0.14	0.07	0.03	52%	75%
Anthracene (ANT)	0.62	0.07	0.11	89%	83%
Fluoranthrene (FLT)	0.12	0.15	0.02	19% >	83%
Pyrene (PYE)	0.26	0.04	0.09	83%	66%
Benzo(a)anthracene (B(a)A)	0.15	0.03	0.14	77%	5%
Chrysene (CHR)	0.11	0.04	0.05	65%	52%
Benzo(b)fluoranthene (B(b)F)	0.34	0.04	0.05	88%	8500%
Benzo(k) fluoranthene (B(k)F)	0.43	0.04	0.09	90%	78%
Benzo(a) pyrene (B(a)P)	0.29	0.01	0.26	96%	11%
Indeno(1,2,3-CD) pyrene(IND)	0.27	0.04	0.02	85%	94%
Dibenz(a,h) anthracene (DBA)	0.34	0.05	0.06	87%	84%
Benzo (g, h, i) perylene (BP)	0.44	0.04	0.10	90%	77%
Total	*4.50*	*1.51*	*1.70*	*67%*	*62%*

(Table 6.2) continued

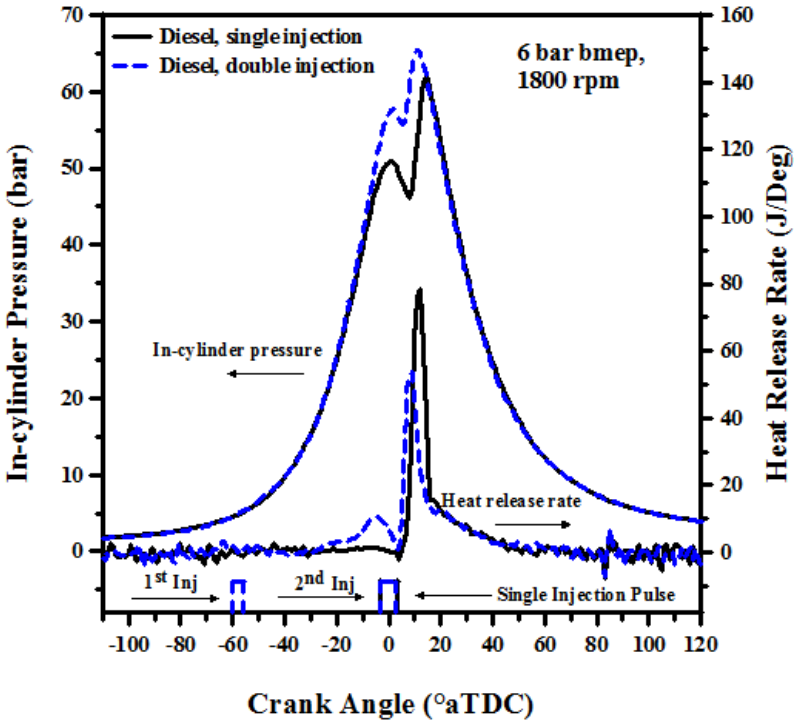
PAH	Diesel Conc (μgm^{-3})	G75 Conc (μgm^{-3})	Naphtha Conc (μgm^{-3})	G75 Reduction (%)	Naphtha Reduction (%)
6 bar BMEP					
Naphthalene (NAP)	0.42	1.06	0.67	100% >	58% >
Acenaphthylene(ACY)	0.21	0.05	0.02	76%	89%
Acenaphthene (ACE)	0.20	0.03	0.02	86%	90%
Fluorene (FLU)	0.07	0.04	0.04	42%	40%
Phenanthrene (PHE)	0.16	0.07	0.06	58%	63%
Anthracene (ANT)	0.26	0.07	0.07	73%	75%
Fluoranthrene (FLT)	0.15	0.15	0.15	0%	0%
Pyrene (PYE)	0.54	0.05	0.04	90%	93%
Benzo(a)anthracene (B(a)A)	0.91	0.03	0.05	97%	94%
Chrysene (CHR)	0.62	0.07	0.01	90%	98%
Benzo(b)fluoranthene (B(b)F)	0.48	0.07	0.01	85%	97%
Benzo(k) fluoranthene (B(k)F)	0.55	0.06	0.01	89%	98%
Benzo(a) pyrene (B(a)P)	1.16	0.02	0.00	98%	100%
Indeno(1,2,3-CD)pyrene(IND)	0.37	0.07	0.01	82%	96%
Dibenz(a,h) anthracene (DBA)	1.12	0.07	0.01	94%	99%
Benzo (g, h, i) perylene (BP)	0.14	0.07	0.01	51%	91%
Total	*7.37*	*1.98*	*1.19*	*73%*	*84%*

6.4 Single Injection versus Double Injection

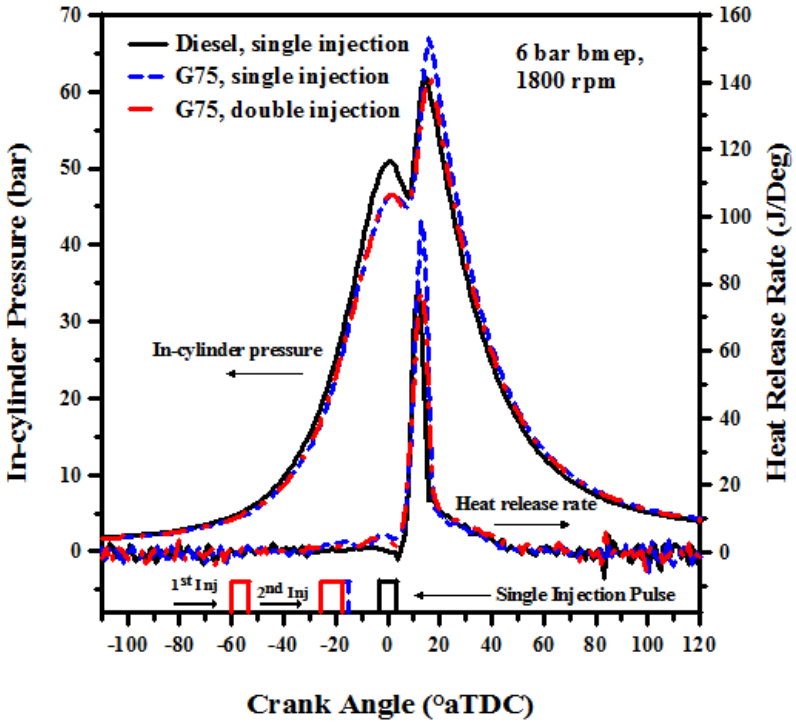
6.4.1 Heat Release Analysis

The heat release rate, injection pulses, and in-cylinder pressure of diesel-, G75-, and naphtha-fuelled PCI with single and double injection at 6 bar BMEP are plotted against the crank angle degree (CAD), as shown in Figure 6.10 (a, b, c). It was observed that the double injection strategy had a lower peak in heat release rate compared to the single injection

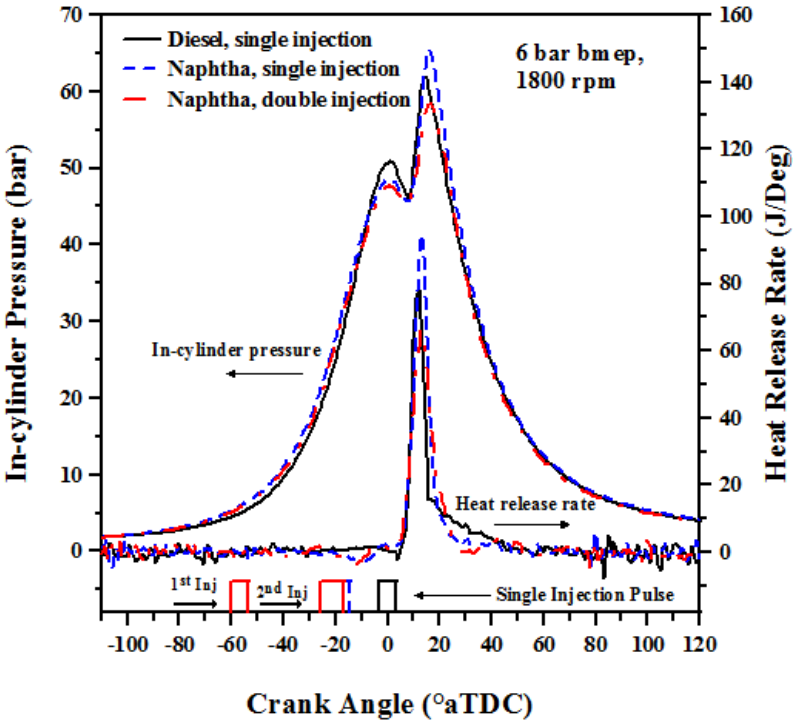
strategy for all three fuels, as shown in Figures 6.10 and 6.11. The ignition delay of the double injection was shorter than the single injection, as shown in Figure 6.12 (a). The low combustion temperature of the first injection significantly shortens the ignition delay of the double injection. In addition, the over-lean mixture generated from first stage injection timing made the burning rate very slow, resulting in a long combustion duration compared to single injection, as shown in Figure 6.12 (b). The brake thermal efficiency (BTE) and maximum pressure rise rate (MPRR) for the single and double injection strategies are illustrated in Figure 6.12 (c, d). The lower emissions of BSHC and BSCO in single injection are shown in Figure 6.13 (c, d); this led to higher BTE compared to double injection, as shown in Figure 6.12 (c).



(a)

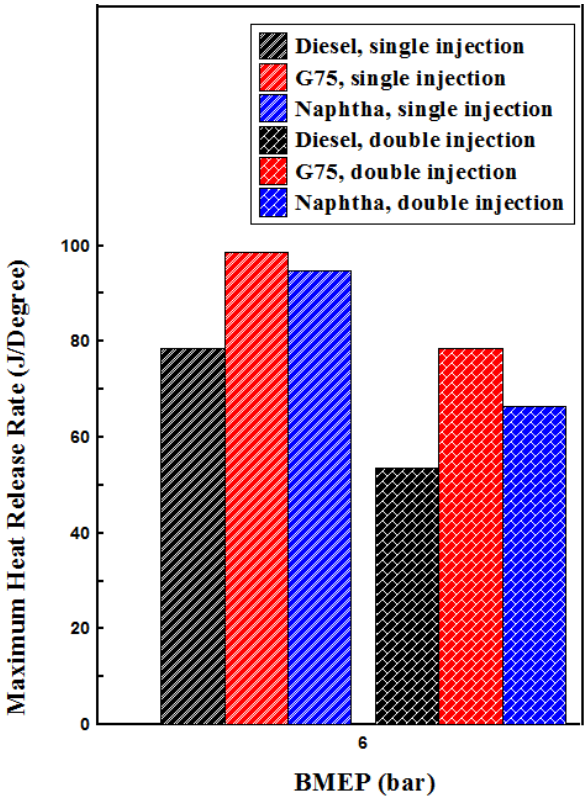


(b)

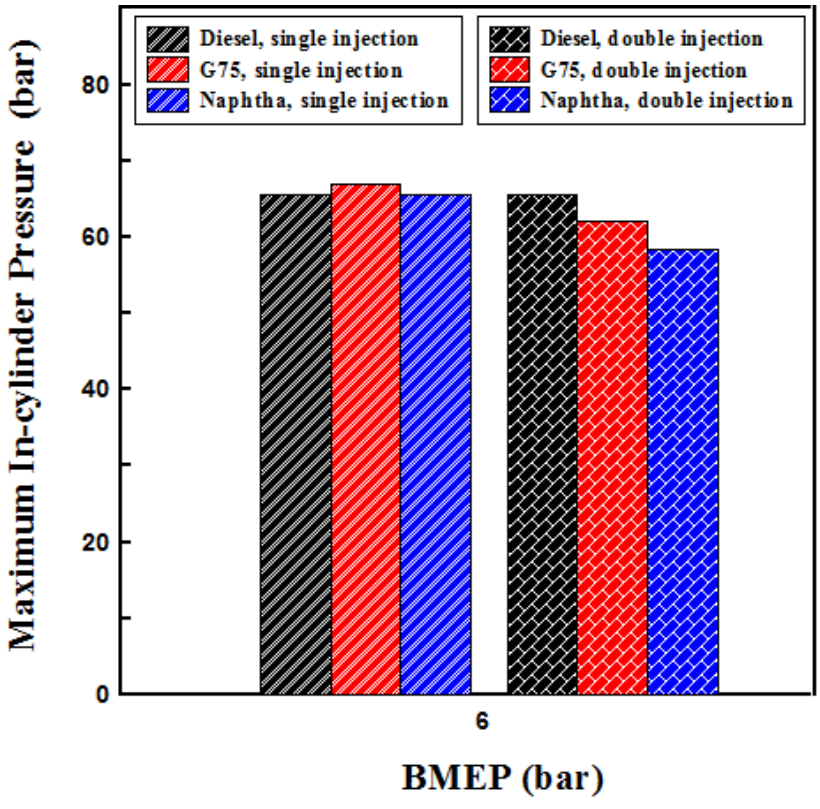


(c)

Figure 6.10: In-cylinder pressure and heat release rate comparision between single and double injections of (a) diesel fuel , (b) G75 fuel , and (c) and naphtha fuel at 6 bar BMEP



(a)



(b)

Figure 6.11: Maximum heat release rate and in-cylinder pressure comparision between single and double injections of (a) diesel fuel , (b) G75 fuel , and (c) and naphtha fuel at 6 bar BMEP

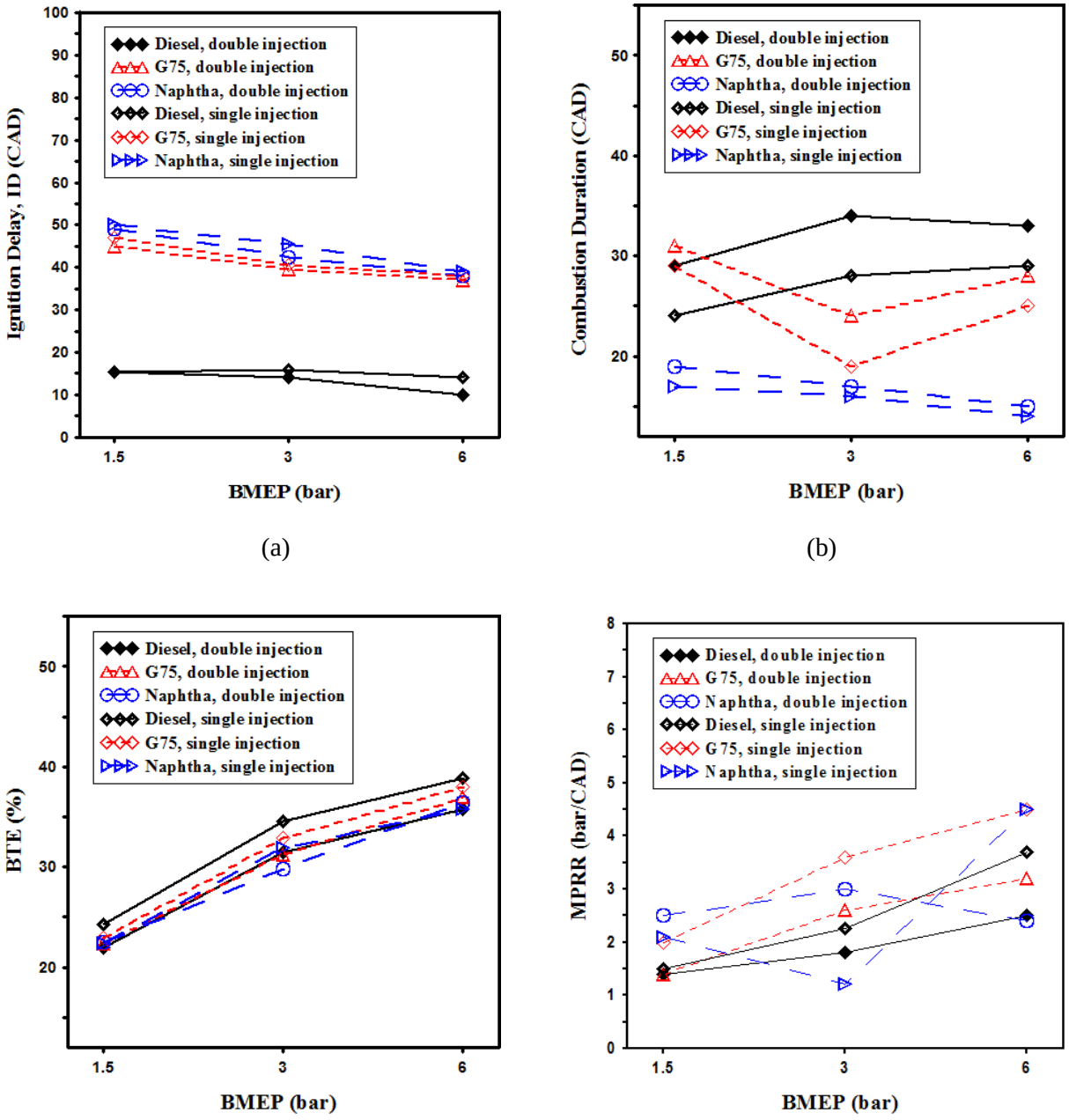


Figure 6.12: The comparison between single and double injection of three fuels at three loads: (a) ignition delay, (b) combustion duration, (c) BTE and (d) MPRR

The MPRR observed for diesel and G75 fuel was lower in double injection compared to single injection, as shown in Figure 6.12 (d). Second injection timing played a significant role

in controlling the combustion phase, and so could vary the MPRR. For naphtha fuel, the drop in MPRR, especially at load 3 bar BMEP, is most likely related to load stability.

6.4.2 Regulated Emissions

The smoke, $BSNO_x$, BSCO, and BSHC emissions for single and double injection strategies are illustrated in Figure 6.13 (a, b, c, d). It was observed that both G75 and naphtha produced very low smoke (FSN < 0.01) in both injection strategies compared to diesel fuel, but the double injection strategy reduced smoke more compared to single injection, as shown in Figure 6.13(a). The longer ignition delay of both fuels and the sufficient time for the fuel to mix with air in the first injection timing produced a local lean mixture. In the case of diesel fuel, it was noted that the double injection method produced more smoke compared to single injection when the load was increased. The ignition delay of the second injection was short and did not allow time for the fuel-rich region to dissipate; therefore, a high level of smoke was produced, as shown in in Figure 6.13(a).

Double injection reduced the level of $BSNO_x$ compared to single injection, as shown in in Figure 6.13(b). The low combustion temperature of the first injection timing with a high EGR level contributed to reduced $BSNO_x$. It was also observed that at load 6 bar BMEP, the single injection of both naphtha and G75 fuels produced almost similar amounts of $BSNO_x$; this was attributed to their both having the same ignition delay. Furthermore, single injection of naphtha fuel at load 6 bar BMEP produced almost similar amounts of $BSNO_x$ as with the double injection method, which is explained by the same ignition delay shown in Figure 6.12(a).

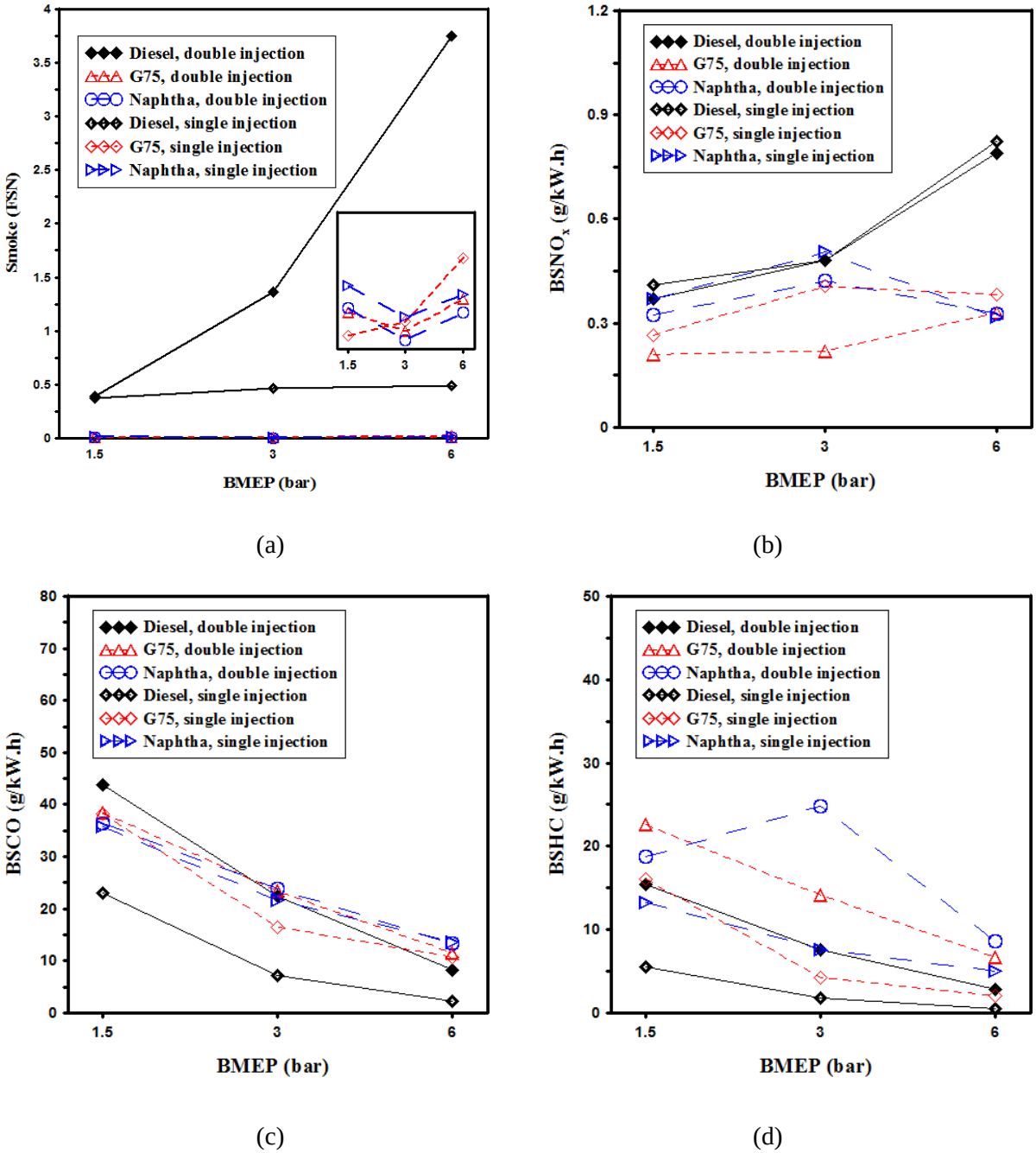


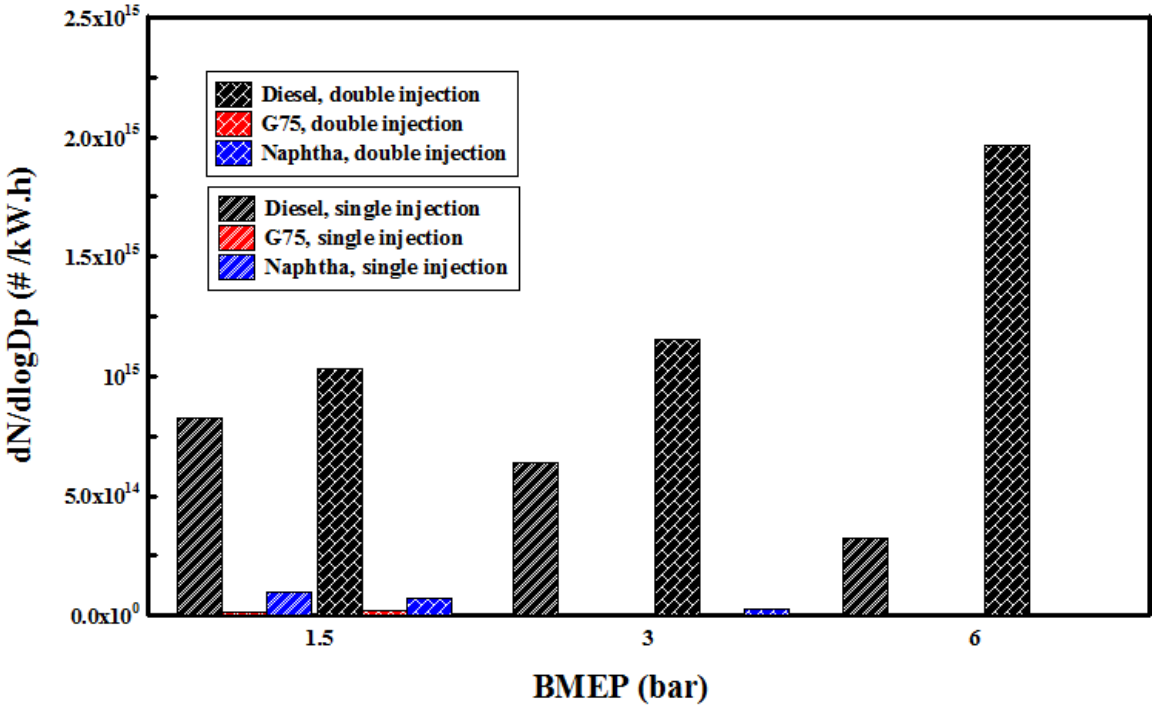
Figure 6.13: The comparison between single and double injection of three fuels at three loads: (a) smoke, (b) $BSNO_x$, (c) BSCO, and (d) BSHC

Double injection increased the emissions of BSHC and BSCO compared to single injection, as shown in Figure 6.13 (c, d). This is due to the low gas temperature generated by the double injection; more emissions of HC and CO were the result.

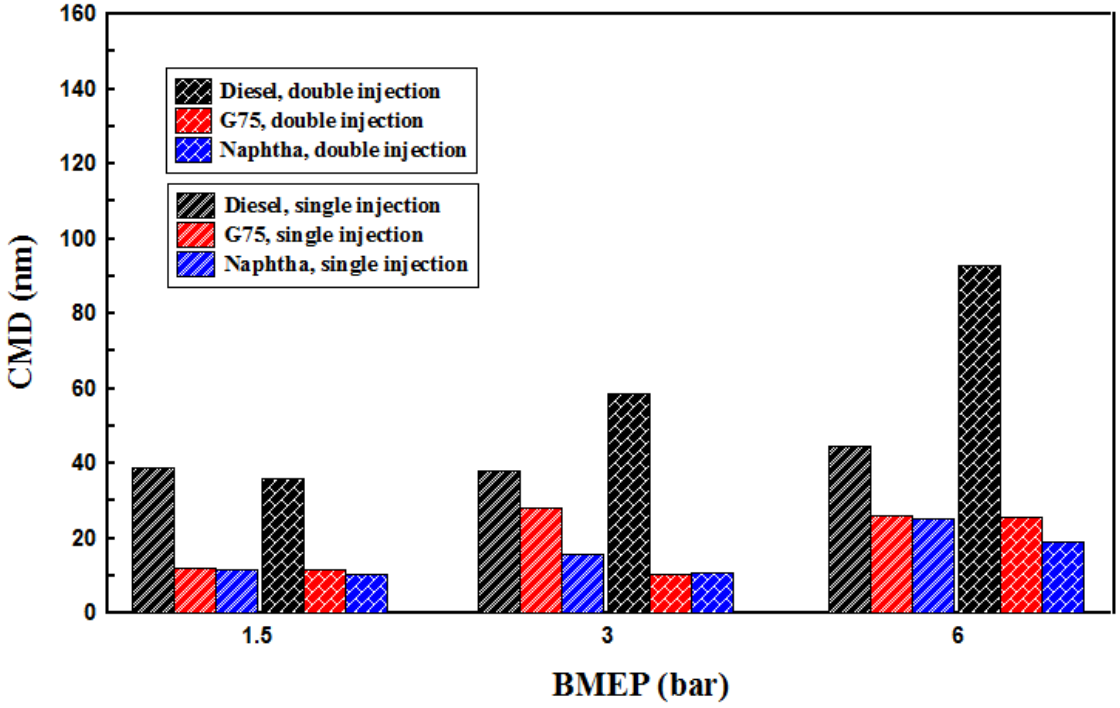
6.4.3 Total Particle Number Concentrations

This section discusses the comparison between the particle number concentrations and CMD of diesel, G75, and naphtha fuels in single and double injections at three different loads: 1.50, 3, and 6 bar BMEP. It was observed that for diesel fuel, as shown in Figure 6.14 (a,b), the double injection strategy increased the total particle number concentration by around 90% at high loads, and CMD ~ 90 nm compared to single injection. The increase corresponded with an increase in smoke, BSHC, and BSCO emissions. It could be said that when the second stage injection timing started, there was insufficient time to remove the fuel-rich zones, and therefore PN emissions increased, especially at high loads where the in-cylinder temperature is high. Conversely, double injection of G75 and naphtha fuels reduced the particle number concentration by around 99.70% and CMD ~ 18 nm, which is due to the long ID that generated a local lean mixture in the first injection timing.

The decrease of the total particle number concentration of G75 fuel at 1.50 bar BMEP was 97%; at 3 bar BMEP it was 99.70%; at 6 bar BMEP it was 98.90%. For naphtha fuel, at 1.50 bar BMEP the decrease was 91%; at 3 bar BMEP it was 95%; and at 6 bar BMEP it was 99%. To compare this with single injected G75 and naphtha fuels, the total particle number concentration was reduced by around 20% at low loads and by around 65% at medium loads.



(a)



(b)

Figure 6.14: The comparison between single and double injection of total particle number and CMD of three fuels at three loads (a) PN, (b) CMD

6.4.4 PAHs' Concentration

This section examines the comparison between the single and double injections and their effect on the total PAH compounds from diesel, G75 and naphtha fuels at three different loads: 1.50, 3, and 6 bar BMEP. From Figure 6.15, the double injection decreased the total PAH compounds for all fuels in all operating conditions except for the case of diesel fuel at 6 bar BMEP. The local lean mixture and low combustion temperature created by the first injection timing could prevent some PAH compounds from being formed inside the combustion chamber, and so the total concentration of PAH compounds was reduced. The increase of PAH compounds for diesel fuel at 6 bar BMEP was also linked with the increase of smoke as shown in in Figure 6.12(a). It could be said that the second injection timing was coupled with less time available to remove fuel-rich regions, and so some unburned fuel escaped and condensed on the filter. Another possible reason could be that some of the PAH compounds found a motivated environment to be synthesized inside the combustion chamber, resulting in an increase in the total amount of PAH compounds. Compared to single injected diesel fuel, G75 and naphtha fuels with double injection reduced total PAH compounds by more than 90%, and the concentrations remained below 1.90 $\mu g/m^{-3}$. Also, it was noted that naphtha fuel produced the lowest concentration, which supported the hypothesis that naphtha fuel originally has low concentrations of PAH compounds.

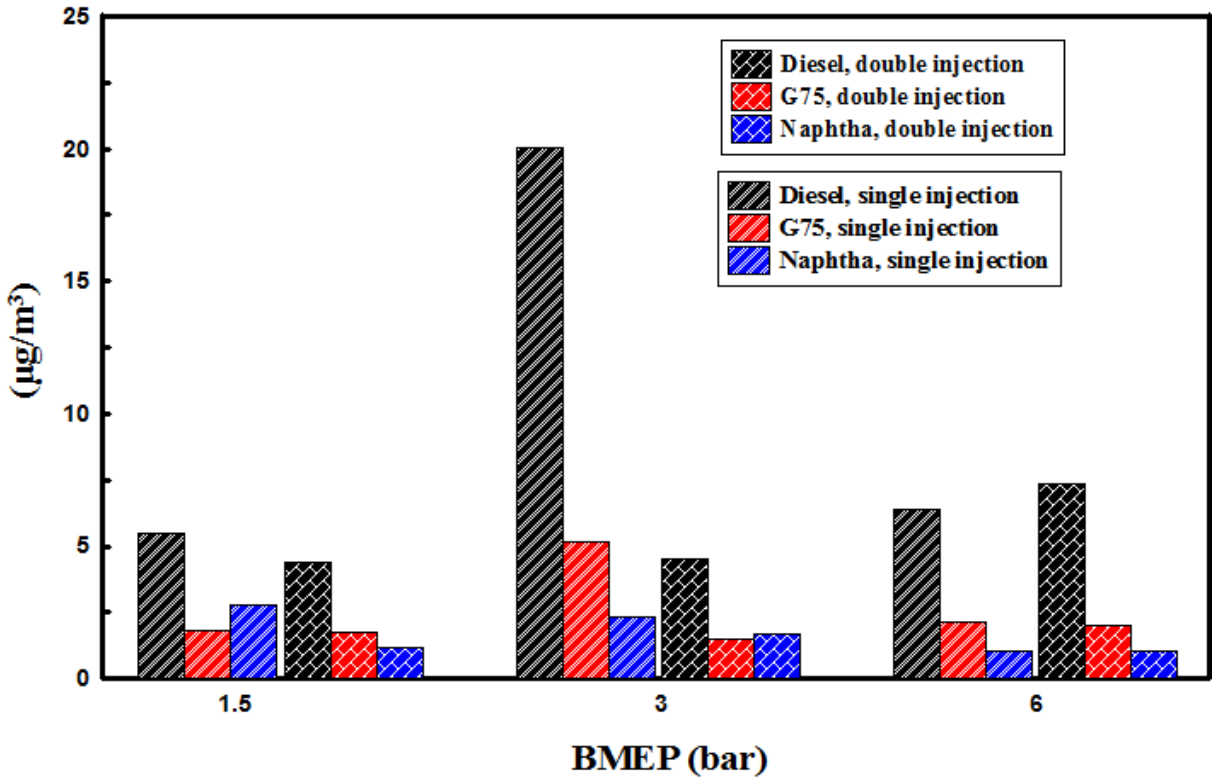


Figure 6.15: The comparison of PAHs concentration between single and double injection of three fuels at three loads

6.4.5 C-alkanes and C-cycloalkanes' Concentrations

The hydrocarbons with the carbon range C_{10}-C_{25} are not characterized widely due to the limitation of the instruments, and cannot be resolved by traditional gas chromatography. They appear in the chromatogram as Unresolved Complex Mixture (UCM) (Alam[a], et al., 2016).

In this section, the two-dimensional gas-chromatography time of flight mass-spectrometry (GCXGC-ToF-MS) discussed in section 3.3.4 was used to characterize and quantify the composition of SVOCs (e.g. C-alkanes, C-cycloalkanes) in diesel, G75, and naphtha particulates emitted from a diesel engine. The engine was running at 6 bar BMEP with a constant speed and lambda λ, and at two different injection strategies: single and double injections. For diesel fuel, the injection pressure was 1200 bar while for G75 and naphtha

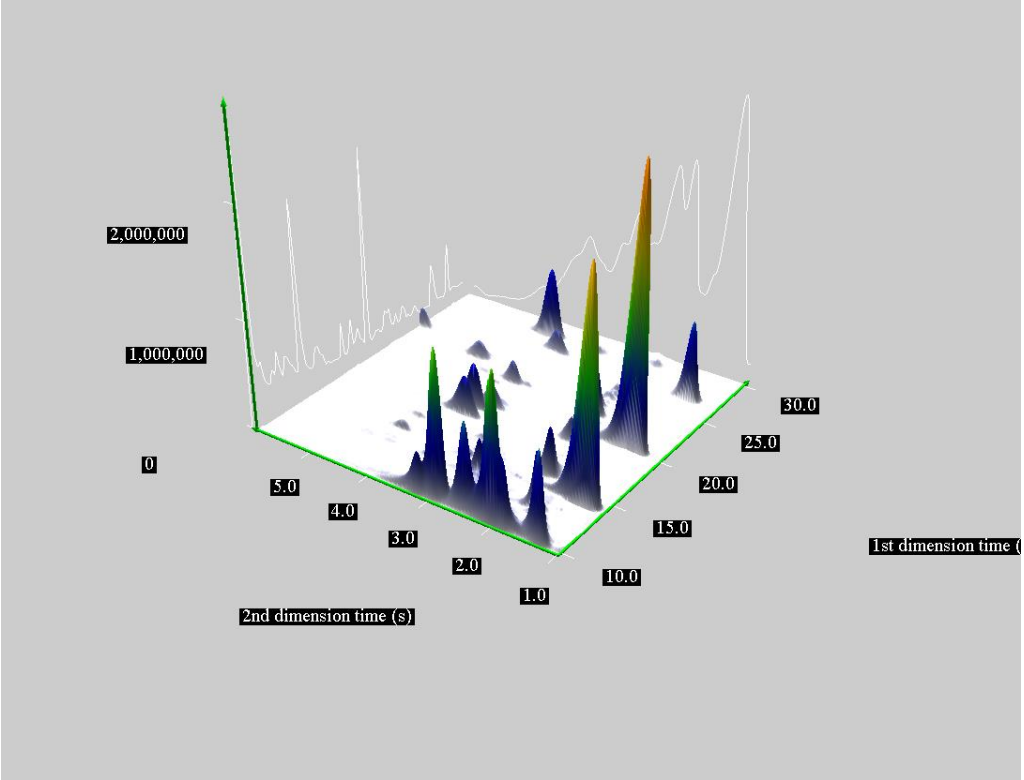
fuels it was 500 bar. The EGR ratios were fixed for diesel, G75 and naphtha fuels at 28%, 29.5%, and 30% respectively. The samples were collected on quartz filter paper (47 mm) before the DOC in a predetermined time (30 mins), with a dilution ratio of 35 ±5:1 and with a fixed flow rate of 10 l/min. The diluter that was used is discussed in section 3.2.4 of Chapter 3. The samples were collected at a temperature below < 52°C and the extraction procedures are discussed in section 3.2.6.2 of Chapter 3. The extracts then were analysed using GCXGC-ToF-MS, as discussed in section 3.3.4 of Chapter 3.

Figure 6.16 (a, b, c, d) demonstrates an example of a contour plot or a two-dimensional separation for G75 fuel, engine lubricating oil, and diesel fuel. The first dimension (x-axis) represents the separation of the compounds by volatility in minutes, while the second dimension (y-axis) represents the separation by polarity in seconds. From the National Institute of Standards and Technology's (NIST) library, the peaks of individual species were identified based on the retention keys and mass spectral data, as shown in Figure 6.16 (a).

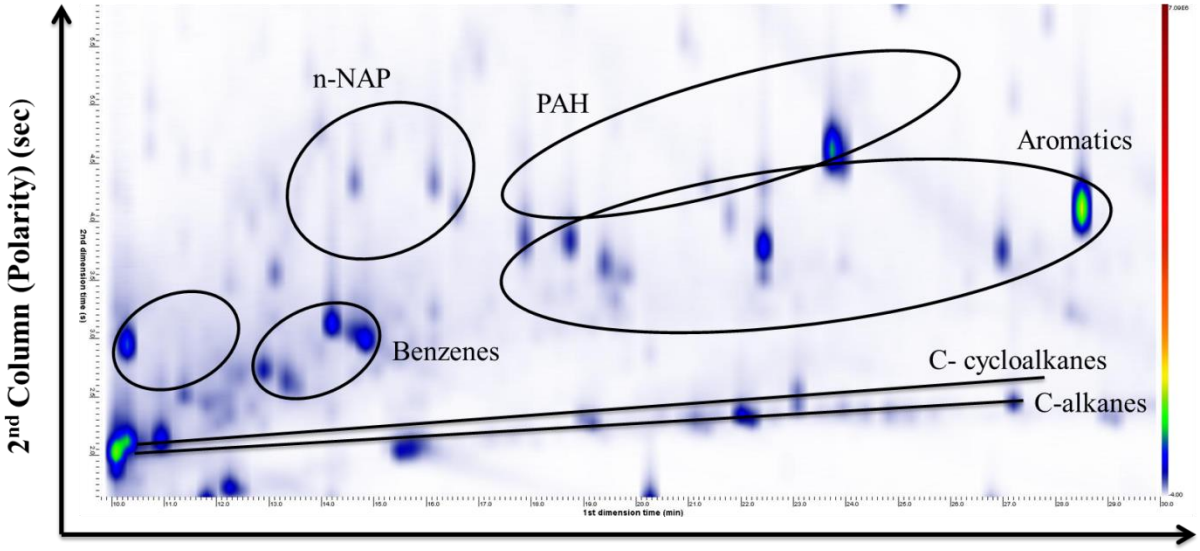
Various compound groups were also identified, such as PAHs, alkanes, cycloalkanes, aromatics, and benzenes, as shown in Figure 6.16 (b). The coloured spots in the figure represent the intensity of the individual species with its corresponding full mass spectrum. The red spot represents more abundant peaks, while the blue stands for less abundant peaks. It shows that diesel fuel contains carbons up to C_{20}, while engine lubrication oil contains carbons in the range of C_{18}-C_{36}, as shown in Figure 6.16 (c, d). Carbons in the range of C_{18}-C_{20} have an overlap between fuel and engine oil, but in this range both fuel and engine oil are present only in small fractions (Alam[a], et al., 2016).

The carbons' numbers were positioned in the counter plot in order to discover the origin of the compounds present in the filters; they are either derived from fuel or from engine oil. The distribution of the c-alkanes of diesel, G75, and naphtha fuels with single and double

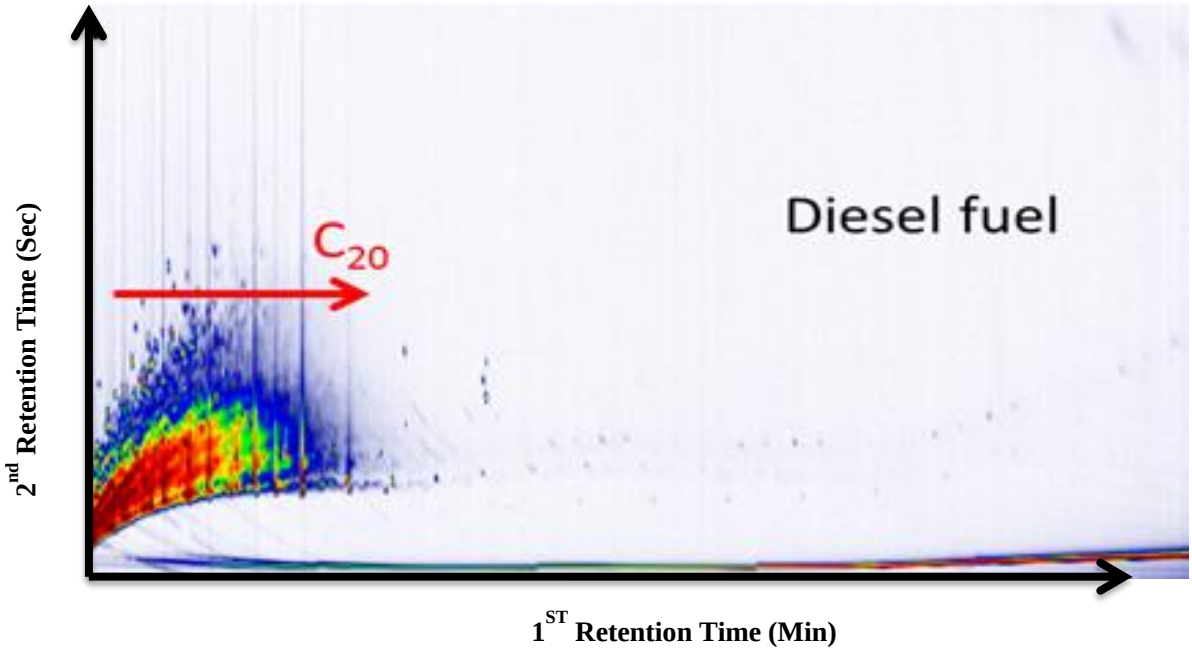
injections at load 6 bar BMEP is presented in Figure 6.17 (a, b). Table 6.3 presents the concentration of the individual compounds for the tested fuels, and the percentage difference of G75 and naphtha fuels compared to diesel fuel. The identified compounds shown in Figure 6.17 (a) are alkanes including straight and branched (C_{12}-C_{38}). Some other carbons are classified as not detected (Nd) (see Table 6.3).



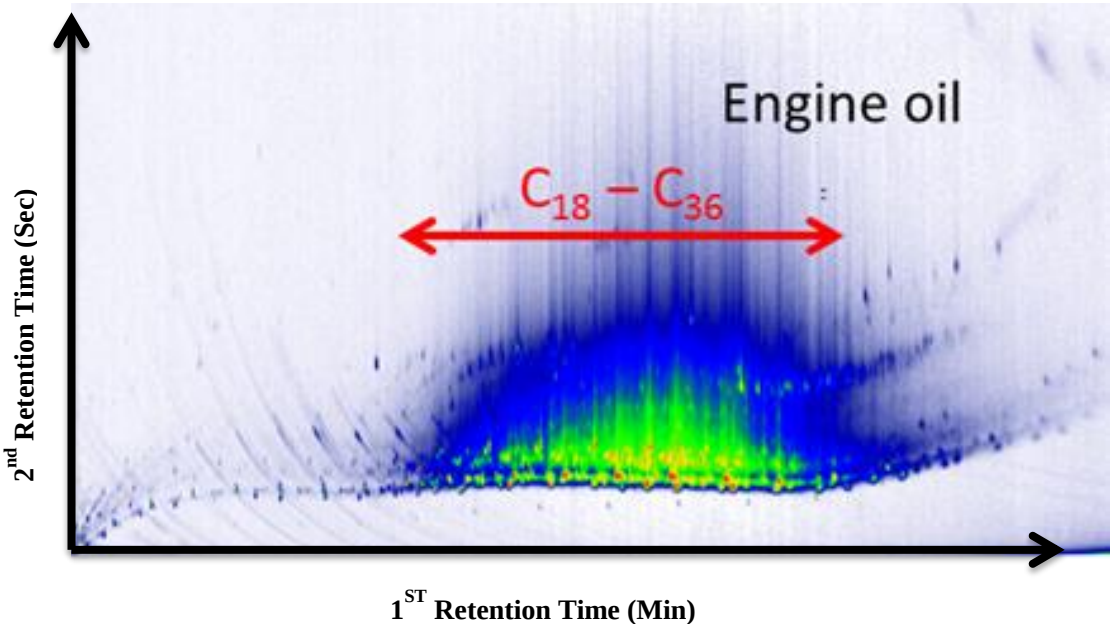
(a)


n-NAP
PAH
Aromatics
Benzenes
C- cycloalkanes
C-alkanes
2nd Column (Polarity) (sec)
1st Column Separation (Volatility) (min)

(b)

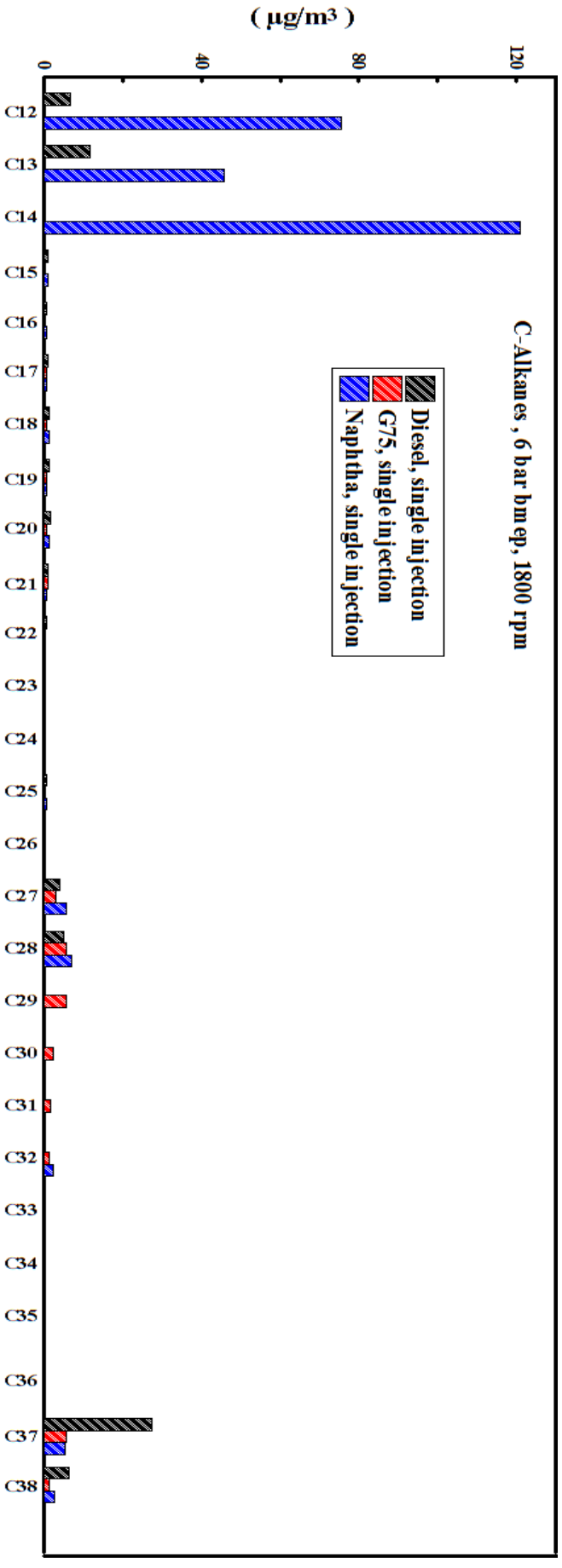

Diesel fuel
C20
2nd Retention Time (Sec)
1ST Retention Time (Min)

(c)

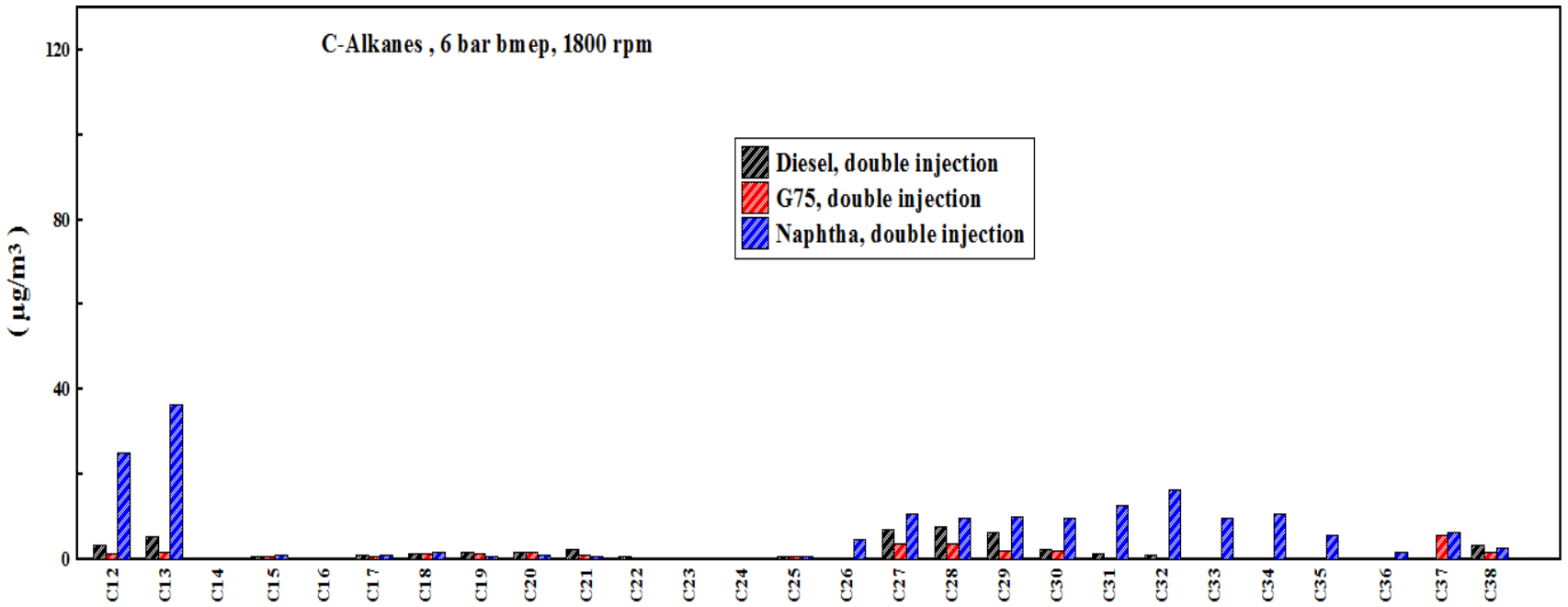


(d)

Figure 6.16: A two dimensional separation (a) G75 contour plot in 3D (b) G75 contour plot, (c) diesel fuel contour plot*, (d) engine oil contour plot* (*Alam[b], et al., 2016)


(µg/m³)
0
40
80
120
C12
C13
C14
C15
C16
C17
C18
C19
C20
C21
C22
C23
C24
C25
C26
C27
C28
C29
C30
C31
C32
C33
C34
C35
C36
C37
C38
C-Alkanes , 6 bar bmep, 1800 rpm
Diesel, single injection
G75, single injection
Naphtha, single injection

(a)



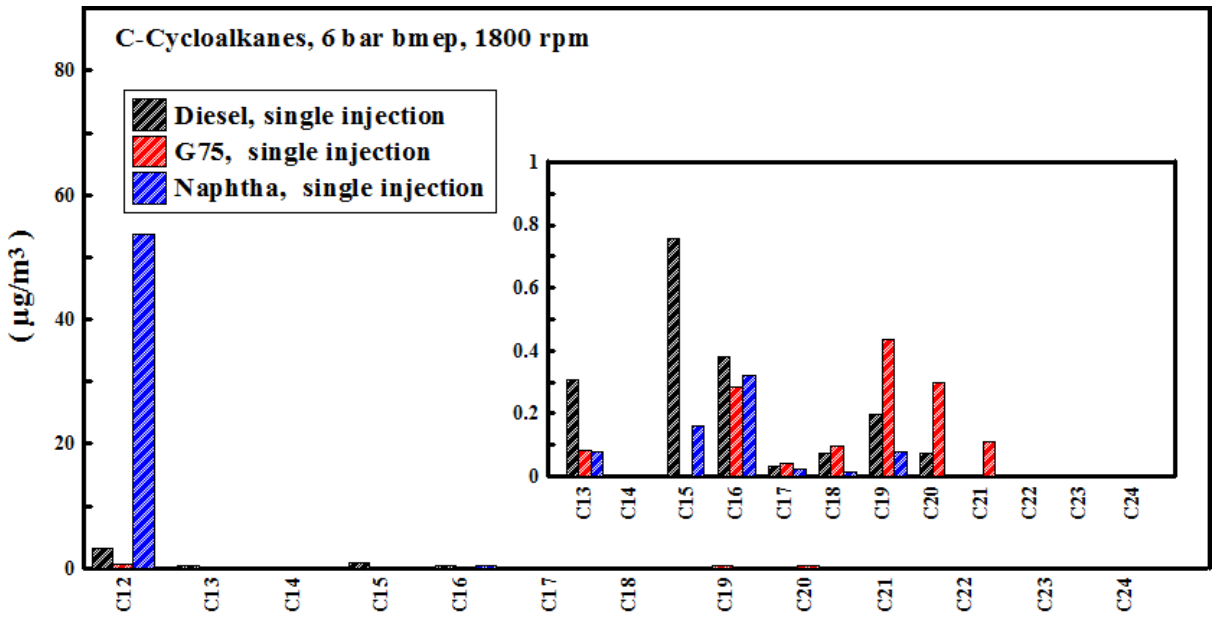
(b)

Figure 6.17: C-Alkanes distribution with carbon number (a) single injection, and (b) double injection

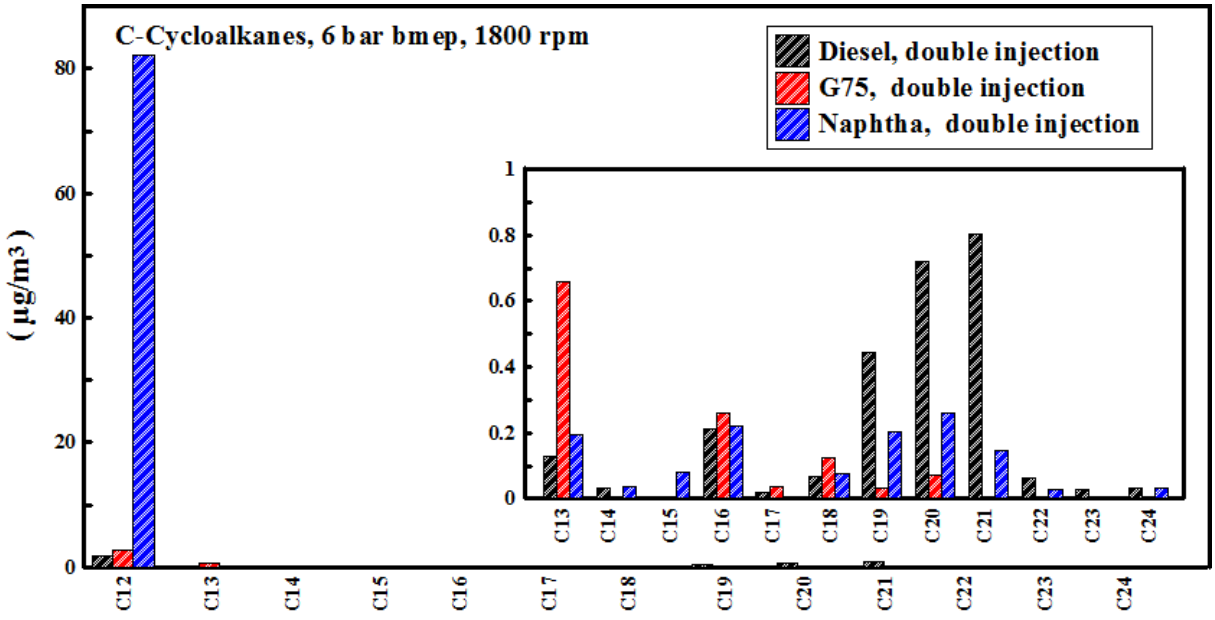
From Figures (6.17–6.19), It can be observed that naphtha fuel in both injection strategies was more pronounced in producing more alkanes and cycloalkanes originating from fuel ($<C_{20}$) compared to diesel and G75 fuels. This is because naphtha fuel is originally composed of large fractions of normal and branched alkanes (Matar and Hatch, 2001). For alkanes, it was noted that double injection reduced the concentration of alkanes (C_{12} - C_{14}) compared to single-injected naphtha fuel. The first injection timing of the double injection created a low temperature combustion, so there were more BSHC emissions, as shown in Figure 6.13 (d). It was hypothesized that the low temperature combustion may not have motivated the synthesis or formation of C_{12} - C_{14} inside the chamber. Therefore, the high in-cylinder temperature with single injection may form more alkanes (C_{14} ~121 μgm^{-3}) during combustion (Li, et al., 2008; Schauer, et al., 1999).

It was also noted that in the case of diesel and G75 fuels, double injection reduced the alkanes, as shown in Figure 6.19 (a). It was observed that double-injected G75 fuel produced the lowest concentration of total alkanes (28 μgm^{-3}, reduced by 60%) compared to single-injected diesel and naphtha fuels.

As discussed earlier, a lean mixture and a low temperature combustion was produced by double injection. The low concentration of alkanes produced by G75 fuel can be explained by the low concentrations present in the fuel.

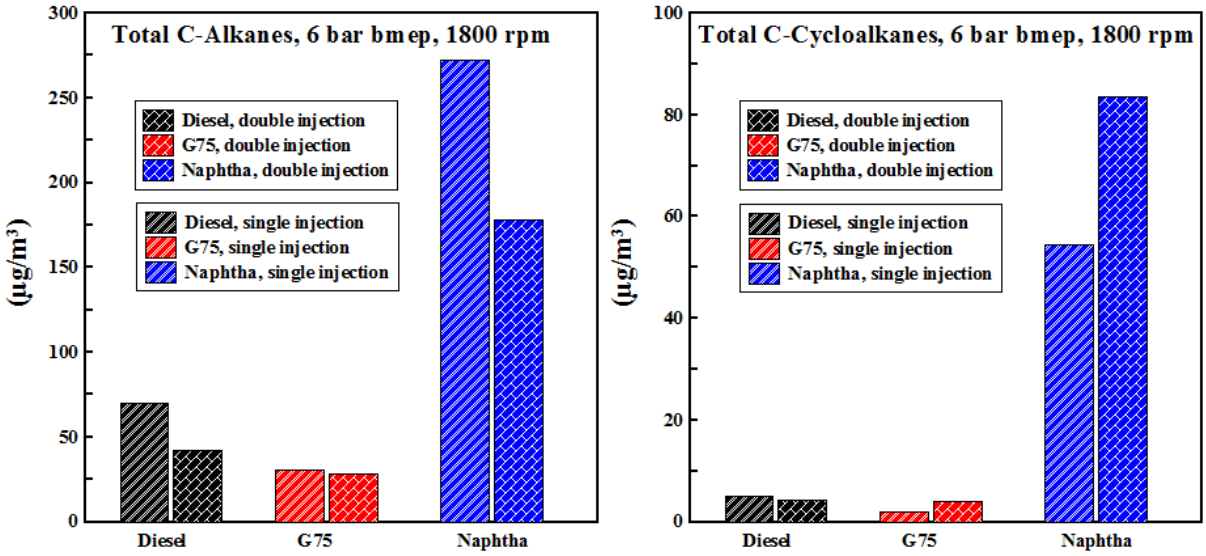


(a)



(b)

Figure 6.18: C-Cycloalkanes distribution with carbon number (a) single injection, and (b) double injection



(a) (b)

Figure 6.19: Total concentration at single and double injections: (a) C-alkanes, (b) C-cycloalkanes

As shown in Figure 6.18 (a, b), it was observed that the cycloalkanes emitted from the fuels were in the range (C_{12}-C_{24}), since some of the cycloalkanes were not detected. Double injection produced more cycloalkanes (C_{12}-C_{24}) originating from fuel and engine oil compared to single injection for G75 and naphtha fuels. In other words, single injection reduced the total concentration of cycloalkanes, as shown in Figure 6.19 (b). This was consonant with the BSHC emissions, shown in Figure 6.13 (d), where double injection produced more compared to single injection. It was hypothesized that the increase of cycloalkanes with double injection is related to the low in-cylinder temperature, which was not high enough to burn the unburned cycloalkanes resulting from the incomplete combustion of fuel and engine oil. It was also noted that with single injection, BHCS emissions were lower; in other words, the high in-cylinder temperature burned the unburned cycloalkanes and reduced them.

Table 6.3: C-alkanes and Cycloalkanes concentrations in particulates of diesel, G75 and naphtha fuels at 6 bar BMEP loads with single and double injections.

Single Injection Load: 6 bar bmep	Diesel Conc (μgm^{-3})	G75 Conc (μgm^{-3})	Naphtha Conc (μgm^{-3})	G75 Reduction (%)	Naphtha Reduction (%)
C-Alkanes					
C_{12}	6.46	0.04	75.49	99%	100% >*
C_{13}	11.65	0.16	45.66	99%	100% >
C_{14}	0.15	0.00	121.15	100%	100% >
C_{15}	0.91	0.31	0.90	66%	1%
C_{16}	0.57	0.21	0.54	63%	4%
C_{17}	0.85	0.46	0.56	46%	33%
C_{18}	1.40	0.44	1.16	69%	17%
C_{19}	1.25	0.68	0.75	45%	40%
C_{20}	1.49	0.65	1.14	56%	23%
C_{21}	1.06	0.81	0.67	24%	37%
C_{22}	0.47	0.13	0.26	73%	45%
C_{23}	0.14	Nd*	0.01	--	90%
C_{24}	0.12	0.00	0.01	100%	90%
C_{25}	0.47	0.03	0.48	93%	3% >
C_{26}	0.13	0.14	0.18	10% >	41% >
C_{27}	4.07	2.94	5.78	28%	42% >
C_{28}	5.11	5.54	6.90	9% >	35% >
C_{29}	Nd	5.64	Nd	--	--
C_{30}	Nd	2.35	Nd	--	--
C_{31}	Nd	1.60	Nd	--	--
C_{32}	Nd	1.34	2.43	--	--
C_{37}	27.22	5.52	5.42	80%	80%
C_{38}	6.24	1.40	2.57	78%	59%
Total	69.75	30.38	272.1	56%	100% >

Single Injection Load: 6 bar bmep	Diesel Conc (μgm^{-3})	G75 Conc (μgm^{-3})	Naphtha Conc (μgm^{-3})	G75 Reduction (%)	Naphtha Reduction (%)
C- Cycloalkanes					
C_{12}	3.28	0.60	53.76	82%	100% >
C_{13}	0.31	0.08	0.08	73%	75%
C_{14}	Nd	0.00	Nd	--	--
C_{15}	0.76	0.00	0.16	100%	78%
C_{16}	0.38	0.28	0.32	25%	15%
C_{17}	0.03	0.04	0.02	30% >	36%
C_{18}	0.07	0.10	0.01	36% >	83%
C_{19}	0.20	0.44	0.08	100% >	60%
C_{20}	0.08	0.30	Nd	100% >	--
C_{21}	Nd	0.11	Nd	--	--
C_{22}	Nd	Nd	Nd	--	--
C_{23}	Nd	Nd	Nd	--	--
C_{24}	Nd	Nd	Nd	--	--
Total	5.11	1.95	54.44	62%	100% >

(Table 6.3) continued

Double Injection Load : 6 bar bmep	Diesel Conc (µgm-3)	G75 Conc (µgm-3)	Naphtha Conc (µgm-3)	G75 Reduction (%)	Naphtha Reduction (%)
C-Alkanes					
C_{12}	3.14	1.11	25.10	65%	100% >
C_{13}	5.24	1.69	36.31	68%	100% >
C_{14}	0.14	0.12	0.21	16%	53% >
C_{15}	0.74	0.70	1.06	4%	43% >
C_{16}	0.26	0.16	0.38	36%	50% >
C_{17}	0.76	0.48	0.79	38%	3% >
C_{18}	1.21	1.32	1.66	9% >	38% >
C_{19}	1.50	1.21	0.72	19%	52%
C_{20}	1.69	1.53	0.92	10%	45%
C_{21}	2.31	1.01	0.72	56%	69%
C_{22}	0.72	0.29	0.13	59%	82%
C_{23}	0.16	0.08	0.11	49%	33%
C_{24}	0.09	0.10	0.07	12% >	19%
C_{25}	0.53	0.45	0.62	16%	18% >
C_{26}	0.31	0.13	4.60	57%	100% >
C_{27}	6.98	3.65	10.53	48%	51% >
C_{28}	7.72	3.49	9.46	55%	23% >
C_{29}	6.29	1.84	10.07	71%	60% >
C_{30}	2.36	1.90	9.76	20%	100% >
C_{31}	1.18	Nd	12.50	--	100% >
C_{32}	0.98	Nd	16.46	--	100% >
C_{33}	Nd	Nd	9.49	--	
C_{34}	Nd	Nd	10.60	--	
C_{35}	Nd	Nd	5.65	--	
C_{36}	Nd	Nd	1.56	--	
C_{37}	Nd	5.47	6.16	--	--
C_{38}	3.37	1.71	2.67	49%	21%
Total	42.15	28.45	178.32	33%	100% >
C- Cycloalkanes					
C_{12}	1.75	2.78	82.20	59% >	100% >
C_{13}	0.13	0.66	0.19	100% >	49% >
C_{14}	0.03	0.00	0.04	100%	8% >
C_{15}	Nd	0.00	0.08	--	--
C_{16}	0.21	0.26	0.22	23% >	3% >
C_{17}	0.02	0.04	0.00	66% >	100%
C_{18}	0.07	0.13	0.08	80% >	13% >
C_{19}	0.45	0.03	0.20	93%	55%
C_{20}	0.72	0.07	0.26	90%	64%

Double Injection Load : 6 bar bmep	Diesel Conc (µgm-3)	G75 Conc (µgm-3)	Naphtha Conc (µgm-3)	G75 Reduction (%)	Naphtha Reduction (%)
C_{21}	0.80	Nd	0.15	--	82%
C_{22}	0.06	Nd	0.03	--	57%
C_{23}	0.03	Nd	Nd	--	--
C_{24}	0.03	Nd	0.03	--	0.34% >
Total	4.31	3.97	83.5	8%	100% >

* The concentration increased compared to diesel fuel

For diesel fuel, the lower concentration of the cycloalkanes with double injection compared to single injection could be explained by a fraction of the cycloalkanes escaping in gas form.

It was also observed that G75 fuel with single injection produced the lowest concentration of total cycloalkanes (3.97 μgm^{-3}, reduced by 54%) compared to single-injected diesel and naphtha fuels. The purpose of this was explained earlier, and the lowest concentration of G75 supports the hypothesis that low concentrations of alkanes and cycloalkanes are originally present in G75 fuel.

6.5 Summary

This study was conducted in order to investigate the effect of double injection of diesel, G75 and naphtha fuels on the particle size and number distribution and chemical characterization of PM. It was carried out with an EGR cooler modification (deactivating EGR cooler) and with a constant speed of 1800 rpm and (λ ~1.24). The following are the observations:

Particle Size and Number Distributions

- The double injection strategy increased the total particle number concentration for diesel fuel, where the increase was up to 90%. This increase is due to the short time allowed for the removal of fuel-rich regions generated by the second injection timing.

- Double injection reduced the total particle number concentration for both G75 and naphtha fuels by around 99.70 % and CMD ~ 18 nm, compared to single-injected diesel fuel at low and medium loads. This is due to the long ignition delay, which provides enough time to generate a local lean mixture in the first injection timing, meaning that PN emissions are reduced. Additionally, smoke emission was reduced by around 99.80% compared to single injected diesel fuel. The observed minimum emission of $BSNO_x$ (0.22 g/kW.h) was from G75 fuel at load 3 bar BMEP. The disadvantages are the drop in BTE and the increase of BSHC and BSCO emissions. Compared to single injected diesel fuel, the drop was recorded at between 1.88% and 3.20% (absolute value) for both fuels G75 and naphtha at low loads, and at around 2.40% at medium load.

Chemical Characterization of PM

Trace Metals

There was no specific trend observed with double injection, which was also the case with single injection. The presence of metals as discussed in Chapter 5 originates from many sources such as fuel, lube oil, and engine wear.

PAH Concentration

- Double injection is more efficient compared to single injection in reducing the total concentration of PAH compounds. The local lean mixture and low combustion temperature created by the first injection timing could prevent some PAH compounds from being formed inside the combustion chamber. The total concentration of PAH compounds in both G75 and naphtha remained below 1.90 $\mu g/m^{-3}$, however, and the

reduction was more than 90% compared to single injected diesel fuel. Naphtha fuel with double injection was considered to be the lowest producer of total PAH compounds. The hypothesis that naphtha fuel has a low concentration of PAHs compared to other fuels was also confirmed with single injection.

Concentrations of C-alkanes and C-cycloalkanes

The investigation of the total concentration of alkanes and cycloalkanes of all three fuel was carried out at load 6 bar BMEP, and led to the following conclusions:

- Double injection reduced the total concentration of alkane compounds for all fuels compared to single injection (a high reduction of 60% was observed for G75 fuel). It was hypothesized that a low temperature inside the combustion chamber was not a motivator for the synthesis or formation alkane compounds, as this increased with single injection.
- Single injection reduced the total concentration of cycloalkane compounds compared to double injection (a high reduction 54% was observed for G75 fuel). There was also a decrease in BSHC emissions, which means that the high in-cylinder temperature burned the unburned cycloalkanes and consequently reduced them. G75 fuel was demonstrated to be the lowest producer of alkanes (28.42 μgm^{-3}) and cycloalkanes (1.95 μgm^{-3}) compared to the other fuels. It was hypothesized that G75 fuel originally has a low concentration of alkanes and cycloalkanes.

CHAPTER 7

SUMMARY, CONCLUSIONS AND FUTURE WORK

7.1 Introduction

This research work mainly focused on the particle size and number distribution and chemical characterization of the particulate matter (PM) of low octane-fuelled PCI (G75 and naphtha) and compared it to that of diesel fuel. Fuels with higher volatility and lower cetane numbers have an advantage over diesel fuel and are considered to be the promising fuels for high efficiency and low emissions from CI engines. This chapter summarizes the conclusions drawn from the experiments which were carried out on a light duty, four-cylinder diesel engine with a preserved compression ratio (as it is in the auto industry), running at a constant speed and lambda λ under a variety of operating conditions. The diesel engine was given a minimum modification by introducing hot EGR via EGR cooler deactivation. The main conclusions and proposals for future work are presented in the following sections.

7.2 Summary and Conclusions

EGR Temperature and Ratio

The deactivation of the EGR cooler in order to introduce hot EGR was proven to be a good technique in significantly reducing the particle number concentration and mean diameter for fuels with a low octane number, such as G75 and naphtha. The cold EGR was not efficient for

G75 and naphtha fuels, as the engine was unable to start. It was hypothesized that the preheated intake temperature with hot EGR leads the quick vaporization of gasoline fractions in the diesel, and allows it to mix well with the surrounding air. Consequently, this enhanced the combustion process, resulting in a significant reduction in PN emissions.

The hot EGR was not efficient in the case of the diesel fuel, as the total particle number concentration was massively increased. Diesel fuel has a high cetane number, and with the introduction of hot EGR the ignition delay became shorter, resulting in an increase in unburned hydrocarbons and particle numbers overall. It was proven that increasing the EGR ratio for both diesel and G75 fuels had significantly increased the total particle number concentrations, by more than 95%. This was attributed to the decrease in oxygen levels affecting the soot oxidation process, and it was also hypothesized that the lower temperature accompanying the increased EGR percentage led to more PN emission.

Injection Pressure and Timing

The particle number concentration and CMD for diesel fuel was reduced by 98.50% when the fuel injection pressure was increased to 1400 bar. The particle number and CMD of G75 fuel, however, could be reduced by 99% with low injection pressure (150 bar) at low loads. The tiny droplet sizes produced by the high injection pressure created a better opportunity for the fuel to mix with air, resulting in reduced PN emission.

At low loads, advancing the injection timing for G75 fuel to 40° bTDC significantly reduced the particle number concentrations of both nucleation and accumulation modes compared to the diesel fuel, by 95% and 99.96% respectively. G75 fuel has a longer ignition delay, which was tied to early fuel injection, and this provided enough time for the fuel to be mixed with air sufficiently before the start of ignition.

Single Injection

At low and medium loads, single injection massively reduced the particle number concentration and mean diameter of both G75 and naphtha fuels by 99% compared to diesel fuel. A lean mixture region was generated inside the cylinder, which promoted soot oxidation over soot formation.

The smoke was reduced and kept below 0.01 FSN at low and medium loads for both G75 and naphtha fuels. The lowest smoke emission (0.003 FSN) was observed for G75 fuel at load 1.50 bar BMEP. With the use of large amounts of EGR, the combustion temperature was lowered and $BSNO_x$ emissions dropped for both G75 and naphtha. Low emissions were observed at load 1.50 bar BMEP. The emissions of BSNOx from G75 fuel were recorded at 0.27 g/kWh, and from naphtha fuel at 0.37 g/kWh.

The disadvantage to this was the reduction in the brake thermal efficiencies (BTE) of both G75 and naphtha fuels, compared to the diesel fuel. The difference of the absolute value of BTE compared to the diesel fuel was between 1.01% and 3% for all loads. The drop in the BTE of both fuels was caused by incomplete combustion, since both fuels emit high levels of HC and CO compared to the diesel fuel.

Single injection also reduced the emissions of total carbon (TC) by over 54% in both G75 and naphtha fuels compared to diesel fuel. There was also a reduction of PN emissions at low loads compared to diesel fuel. It was hypothesized that at low loads, low temperature combustion prevents the extensive pyrolytic reaction that eventually generates soot, and so the soot oxidation process was motivated.

The naphtha fuel produced the lowest concentration of PAHs (1.08µgm$^{-3)}$ compared to the G75 and diesel under all loads. It was hypothesized that PAH compounds in naphtha fuel are originally present in low concentrations.

Double Injection

At low and medium loads, double injection reduced the total particle number concertation by around 99.70% and CMD ~ 18 nm for both G75 and naphtha compared to single-injected diesel fuel. This reduction was attributed to the local lean mixture created by the first injection timing. In contrast, the double injection strategy was not very efficient for the diesel fuel, as the total particle number concentration increased by 90% when the load was increased. The increase of the particle number concentration of the diesel fuel with double injection was attributed to insufficient time to eliminate the fuel-rich regions generated by the second injection timing.

Smoke emission was reduced by around 99.80% compared to single-injected diesel fuel; the lowest smoke emission (0.002 FSN) was recorded with naphtha fuel at load 3 bar BMEP. The observed minimum emission of $BSNO_x$ (0.22 g/kWh) was from G75 fuel at load 3 bar BMEP. The low combustion temperature of the first injection and the consequently over-lean mixture, together with the high EGR level, contributed to the reduction in $BSNO_x$ emissions.

Double injection is more efficient in reducing the total concentration of PAHs (more than 90%) compared to single injection. The local lean mixture and low combustion temperature created by the first injection timing prevented some PAH compounds from being formed inside the combustion chamber. Both G75 and naphtha produced fewer PAHs (below 1.90 µg/m^{-3}) compared to singly injected diesel fuel; naphtha fuel was considered to the lowest

producer of total PAH compounds at all loads. It was hypothesized that the naphtha fuel is composed of fewer PAH compounds, which was also confirmed with single injection.

C-alkanes and C-cycloalkanes

Compared to single-injected diesel fuel at 6 bar BMEP, double injection reduced the total concentration of alkanes for all fuels. It was hypothesized that low temperature combustion was not conducive to the synthesis of alkanes.

Single injection reduced the total concentration of cycloalkane compounds compared to double injection (a high reduction of 54% was observed for G75 fuel), and the reduction was hypothesized to be caused by the high in-cylinder temperature, which resulted in the burning of the unburned cycloalkanes. G75 fuel was the lowest producer of alkanes (28.42 μgm^{-3}) and cycloalkanes (1.95 μgm^{-3}) compared to the other fuels. It was hypothesized that G75 fuel has low a concentration of alkanes and cycloalkanes.

Trace Metals

Both single and double injection strategies demonstrated no specific trends for the trace metals. The metals originated from fuel, engine oil, and engine wear; see sections 5.4.1 and 6.3.2 for more details.

7.3 Future Work

The research work leads to some recommendations, as presented below:

7.3.1 PM Morphology

The current study did not cover all physical characterizations of PM. It only discussed the particle number and size distributions. Due to limitations on resources, a detailed study of PM

morphology is recommended. Such a study could show primary particles with volatile materials condensed on them, and could also show soot agglomeration.

7.3.2 PM Emissions after a DOC

The current study was conducted before the diesel oxidation catalyst (DOC) and at a steady state. A DOC was used to reduce harmful emissions – including CO, HCs, and NO – by oxidizing them. It can also oxidize some soluble organic fractions' (SOF) compounds. A DOC equipped with a diesel particulate filter can also reduce PM by trapping particulates. It is recommended that a study is conducted about PM emissions and their characteristics after DOC.

7.3.3 PM Emissions at Higher Load

The emissions studied from the PCI combustion were achieved at 12 bar BMEP. A higher load was not studied due to the limitations of the test rig. It is suggested that a higher load could be reached by defining the required intake pressure (boosted intake) and EGR level.

7.3.4 G75 and Naphtha Fuels' Spray Characteristics

Fuel distribution and the process of the formation of the mixture can affect combustion performance and emissions. It is recommended that the spray angles, droplet size distributions, spray break-up lengths, and spray tip penetrations of both fuels are studied.

LIST OF REFERENCES

Abdul-Khalek, I., Kittelson, D. and Brear, F. (1999) "The influence of dilution conditions on diesel exhaust particle size distribution measurements". SAE Technical paper.

Agarwal[a], A.K., Gupta, T., Dixit, N., et al. (2013) Assessment of toxic potential of primary and secondary particulates/aerosols from biodiesel vis-a-vis mineral diesel fuelled engine. Inhalation Toxicology, 25: (6): 325-332.

Agarwal, A.K., Gupta, T. and Kothari, A. (2011) Particulate emissions from biodiesel vs diesel fuelled compression ignition engine. Renewable and Sustainable Energy Reviews, 15: (6): 3278-3300.

Agarwal, A.K., Gupta, T., Shukla, P.C., et al. (2015) Particulate emissions from biodiesel fuelled CI engines. Energy Conversion and Management, 94: 311-330.

Agarwal[b], A.K., Singh, A.P., Lukose, J., et al. (2013) Characterization of exhaust particulates from diesel fueled homogenous charge compression ignition combustion engine. Journal of Aerosol Science, 58: 71-85.

Akihama, K., Takatori, Y., Inagaki, K., et al. (2001) "Mechanism of the smokeless rich diesel combustion by reducing temperature". SAE technical paper.

Alam[a], M.S., Stark, C. and Harrison, R.M. (2016) Using Variable Ionization Energy Time-of-Flight Mass Spectrometry with Comprehensive GC× GC To Identify Isomeric Species. Analytical chemistry, 88: (8): 4211-4220.

Alam[b], M.S., Zeraati-Rezaei, S., Stark, C.P., et al. (2016) The characterisation of diesel exhaust particles–composition, size distribution and partitioning. Faraday discussions.

Alam[c], M.S., Delgado-Saborit, J.M., Stark, C., et al. (2014) Investigating PAH relative reactivity using congener profiles, quinone measurements and back trajectories. Atmospheric Chemistry and Physics, 14: (5): 2467-2477.

Alriksson, M. and Denbratt, I. (2006) "Low temperature combustion in a heavy duty diesel engine using high levels of EGR". SAE Technical Paper.

Amann, C.A. and Siegla, D.C. (1981) Diesel particulates—what they are and why. Aerosol Science and Technology, 1: (1): 73-101.

Andrews, L.S. and Snyder, R. (1991) Toxic effects of solvents and vapors. Casarett & Doulls toxilogy: the basic science of poisons, 4: 681-722.

Atkinson, R.W., Fuller, G.W., Anderson, H.R., et al. (2010) Urban ambient particle metrics and health: a time-series analysis. Epidemiology, 21: (4): 501-511.

Bartok, W. and Sarofim, A.F. (1991) Fossil fuel combustion: a source book.

Baulig, A., Garlatti, M., Bonvallot, V., et al. (2003) Involvement of reactive oxygen species in the metabolic pathways triggered by diesel exhaust particles in human airway epithelial cells. American journal of physiology. Lung cellular and molecular physiology, 285: (3): L671-679.

Baumgard, K.J. and Johnson, J.H. (1996) "The effect of fuel and engine design on diesel exhaust particle size distributions". SAE Technical Paper.

Benajes, J., García-Oliver, J.M., Novella, R., et al. (2012) Increased particle emissions from early fuel injection timing Diesel low temperature combustion. Fuel, 94: 184-190.

Benajes, J., Novella, R., Arthozoul, S., et al. (2010) Particle size distribution measurements from early to late injection timing low temperature combustion in a heavy duty diesel engine. SAE International Journal of Fuels and Lubricants, 3: (2010-01-1121): 567-581.

Bittle, J., Knight, B. and Jacobs, T. (2010) Investigation into the use of ignition delay as an indicator of low-temperature diesel combustion attainment. Combustion Science and Technology, 183: (2): 138-153.

Bockhorn, H. (2013) Soot formation in combustion: mechanisms and models. Springer Science & Business Media.

Boot, M., Rijk, E., Luijten, C., et al. (2010) "Spray impingement in the early direct injection premixed charge compression ignition regime". SAE Technical Paper.

Bradfoed A. 2014. http://www.livescience.com/37003-global-warming.html

Bruce, C.W., Stromberg, T.F., Gurton, K.P., et al. (1991) Trans-spectral absorption and scattering of electromagnetic radiation by diesel soot. Applied optics, 30: (12): 1537-1546.

Bryce, D., Ladommatos, N., Xiao, Z., et al. (1999) Investigating the effect of oxygenated and aromatic compounds in fuel by comparing laser soot measurements in laminar diffusion flames with diesel-engine emissions. Journal of the Institute of Energy, 72: (493): 150-156.

Burtscher, H. (2001) Literature study on tailpipe particulate emission measurement for diesel engines. Report for Particle Measurement Programme, BUWAL/GRPE.

Cartellieri, W. and Tritthart, P. (1984) "Particulate Analysis of Light Duty Diesel Engines (IDI &DI) With Particular Reference to the Lube Oil Particulate Fraction". SAE Technical Paper.

Cheng, A., Fisher, B.T., Martin, G.C., et al. (2010) Effects of fuel volatility on early direct-injection, low-temperature combustion in an optical diesel engine. Energy & Fuels, 24: (3): 1538-1551.

Chen, Y., Shah, N., Huggins, F., and Huffmen, G. (2005) "Transmission Electron Microscopy Investigation of Ultrafine Coal Fly Ash Particles."

Choi, M., Hamins, A., Mulholland, G.W., et al. (1994) Simultaneous optical measurement of soot volume fraction and temperature in premixed flames. Combustion and flame, 99: (1): 174-186.

Colban, W.F., Miles, P.C. and Oh, S. (2007) "Effect of intake pressure on performance and emissions in an automotive diesel engine operating in low temperature combustion regimes". SAE Technical Paper.

Dec, J.E. (1997) "A conceptual model of DI diesel combustion based on laser-sheet imaging". SAE technical paper.

Desantes, J., Bermúdez, V., García, J., et al. (2005) Effects of current engine strategies on the exhaust aerosol particle size distribution from a heavy-duty diesel engine. Journal of Aerosol Science, 36: (10): 1251-1276.

DMS500 user manual, (2015), http://www.cambustion.com/products/dms500

Donaldson, K., Tran, L., Jimenez, L.A., et al. (2005) Combustion-derived nanoparticles: a review of their toxicology following inhalation exposure. Particle and fibre toxicology, 2: (1): 1.

Eastwood, P. (2008) Particulate emissions from vehicles. John Wiley & Sons.

Engeljehringer, K. (2013) AVL emission testing-Overview and Trends in Worldwide Emission Legislations. AVL List GmbH, Graz.

Fang, T., Coverdill, R.E., Chia-fon, F.L., et al. (2008) Effects of injection angles on combustion processes using multiple injection strategies in an HSDI diesel engine. Fuel, 87: (15): 3232-3239.

Fang, T., Coverdill, R.E., Chia-fon, F.L., et al. (2009) Air–fuel mixing and combustion in a small-bore direct injection optically accessible diesel engine using a retarded single injection strategy. Fuel, 88: (11): 2074-2082.

Frenklach, M., Wang, H. and Bockhorn, H. (1994) Soot formation in combustion. Springer-Verlag, Berlin, 165.

Ford,B.,Bradbury,S., Joy, D. (2011) https://www.britannica.com/technology/transmission-electron-microscope.

Fujita, E.M., Campbell, D.E., Stockwell, W., et al. (2002) Weekend/weekday ozone observations in the South Coast Air Basin Volume II: Analysis of air quality data. Final report prepared for the National Renewable Energy Laboratory, Golden, CO, and the Coordinating Research Council by the Desert Research Institute, Reno, NV, April.

Gangwar, J., Gupta, T. and Agarwal, A.K. (2012) "Comparative Study of PM Mass and Chemical Composition from Diesel and Biodiesel Fuelled CRDI SUV Engine". SAE Technical Paper.

Gary, J.H., Handwerk, G.E. and Kaiser, M.J. (2007) Petroleum refining: technology and economics. CRC press.

Genzale, C.L., Reitz, R.D. and Musculus, M.P. (2009) Effects of spray targeting on mixture development and emissions formation in late-injection low-temperature heavy-duty diesel combustion. Proceedings of the combustion institute, 32: (2): 2767-2774.

Giechaskiel, B., Arndt, M., Schindler, W., et al. (2012) Sampling of non-volatile vehicle exhaust particles: a simplified guide. SAE International Journal of Engines, 5: (2012-01-0443): 379-399.

Glassman, I. (1998, December). Sooting laminar diffusion flames: effect of dilution, additives, pressure, and microgravity. In Symposium (International) on Combustion (Vol. 27, No. 1, pp. 1589-1596). Elsevier.

Glassman, I. 1989. Soot formation in combustion processes. Symposium (International) on Combustion, 22**,** 295-311.

Han, M., Assanis, D.N. and Bohac, S.V. (2009) Sources of hydrocarbon emissions from low-temperature premixed compression ignition combustion from a common rail direct injection diesel engine. Combustion Science and Technology, 181: (3): 496-517.

Hanson, R., Splitter, D. and Reitz, R.D. (2009) "Operating a heavy-duty direct-injection compression-ignition engine with gasoline for low emissions". SAE Technical Paper.

Haynes, B.S. and Wagner, H.G. (1981) Soot formation. Progress in Energy and Combustion Science, 7: (4): 229-273.

Heeb, N.V., Schmid, P., Kohler, M., et al. (2008) Secondary effects of catalytic diesel particulate filters: conversion of PAHs versus formation of nitro-PAHs. Environmental Science & Technology, 42: (10): 3773-3779.

Heywood, J.B. (1988) Internal combustion engine fundamentals. Mcgraw-hill New York.

Hilborn, J. and Still, M. (1990) Canadian perspectives on air pollution. Environment Canada.

Hildingsson, L., Johansson, B., Kalghatgi, G.T., et al. (2010) Some effects of fuel autoignition quality and volatility in premixed compression ignition engines. SAE International Journal of Engines, 3: (2010-01-0607): 440-460.

Hildingsson, L., Kalghatgi, G., Tait, N., et al. (2009) "Fuel octane effects in the partially premixed combustion regime in compression ignition engines". SAE Technical Paper.

Hinds, W.C. (2012) Aerosol technology: properties, behavior, and measurement of airborne particles. John Wiley & Sons.

Horiuchi, M., Saito, K. and Ichihara, S. (1990) "The effects of flow-through type oxidation catalysts on the particulate reduction of 1990's diesel engines". SAE Technical Paper.

Houghton, J., Ding, Y., Griggs, D., et al. (2001) "Climate Change 2001: the scientific basis third assessment report of the intergovernmental panel on climate change". Cambridge: Cambridge University Press.

Houghton, J.T., Ding, Y., Griggs, D.J., et al. (2001) Climate change 2001: the scientific basis.

Hountalas, D., Mavropoulos, G. and Binder, K. (2008) Effect of exhaust gas recirculation (EGR) temperature for various EGR rates on heavy duty DI diesel engine performance and emissions. Energy, 33: (2): 272-283.

ICP-OES manual (2013) https://www.agilent.com/cs/library/usermanuals/Public/2301.pdf

Idicheria, C.A. and Pickett, L.M. (2005) "Soot formation in diesel combustion under high-EGR conditions". SAE Technical Paper.

Imtenan, S., Varman, M., Masjuki, H., et al. (2014) Impact of low temperature combustion attaining strategies on diesel engine emissions for diesel and biodiesels: a review. Energy Conversion and Management, 80: 329-356.

Inagaki, K., Fuyuto, T., Nishikawa, K., et al. (2006) Combustion system with premixture-controlled compression ignition. R&D Review of Toyota CRDL, 41: (3): 35-46.

Institute, M.D.W.G.H.E. and Green, G.M. (1995) Diesel exhaust: A critical analysis of emissions, exposure, and health effects. HEI (Health Effects Institute).

Jacobs, T.J. and Assanis, D.N. (2007) The attainment of premixed compression ignition low-temperature combustion in a compression ignition direct injection engine. Proceedings of the combustion institute, 31: (2): 2913-2920.

Kagawa, J. (2002) Health effects of diesel exhaust emissions—a mixture of air pollutants of worldwide concern. Toxicology, 181: 349-353.

Kalghatgi, G., Hildingsson, L. and Johansson, B. (2010) Low NOx and low smoke operation of a diesel engine using gasolinelike fuels. Journal of Engineering for Gas Turbines and Power, 132: (9): 092803.

Kalghatgi, G.T. (2005) "Auto-ignition quality of practical fuels and implications for fuel requirements of future SI and HCCI engines". SAE Technical Paper.

Kalghatgi, G.T., Risberg, P. and Angstrom, H.-E. (2007) "Partially pre-mixed auto-ignition of gasoline to attain low smoke and low NOx at high load in a compression ignition engine and comparison with a diesel fuel". SAE Technical Paper.

Kalghatgi, G.T., Risberg, P. and Ångström, H.-E. (2006) "Advantages of fuels with high resistance to auto-ignition in late-injection, low-temperature, compression ignition combustion". SAE Technical Paper.

Kalghatgi, G. T. (2014). Fuel/engine interactions, 08-21.

Kawamoto, K., Araki, T., Shinzawa, M., et al. (2004) "Combination of combustion concept and fuel property for ultra-clean DI diesel". SAE Technical Paper.

Kittelson, D., Watts, W. and Johnson, J. (2002) Diesel aerosol sampling methodology-CRC E-43. Final report, Coordinating Research Council.

Kittelson, D.B. (1998) Engines and nanoparticles: a review. Journal of Aerosol Science, 29: (5): 575-588.

Kittelson, D.B., Arnold, M. and Watts, W.F. (1999) Review of diesel particulate matter sampling methods: Final Report. University of Minnesota, Department of Mechanical Engineering, Center for Diesel Research Minneapolis, MN.

Kittleson, D.B., Abdul-Khalek, I.S., Graskow, B.R., et al. (1998) Diesel Exhaust Particle Size: Measurement Issues and Trends.

Kolodziej, C., Wirojsakunchai, E., Foster, D.E., et al. (2007) "Comprehensive characterization of particulate emissions from advanced diesel combustion". SAE Technical Paper.

Kolodziej, C., Wissink, M., Splitter, D., et al. (2013) "Particle Size and Number Emissions from RCCI with Direct Injections of Two Fuels". SAE Technical Paper.

Kook, S. and Bae, C. (2004) "Combustion control using two-stage diesel fuel injection in a single-cylinder PCCI engine". SAE Technical Paper.

Krivoshto, I.N., Richards, J.R., Albertson, T.E., et al. (2008) The toxicity of diesel exhaust: implications for primary care. The Journal of the American Board of Family Medicine, 21: (1): 55-62.

kumar Agrawal, A., Singh, S.K., Sinha, S., et al. (2004) Effect of EGR on the exhaust gas temperature and exhaust opacity in compression ignition engines. Sadhana, 29: (3): 275-284.

Labecki, L. and Ganippa, L. (2012) Effects of injection parameters and EGR on combustion and emission characteristics of rapeseed oil and its blends in diesel engines. Fuel, 98: 15-28.

Ladommatos, N. and Zhao, H. (1994) "A Guide to Measurement of Flame Temperature and Soot Concentration in Diesel Engines Using the Two-Colour Method Part I: Principles". SAE Technical Paper.

Lee, K.O., Cole, R., Sekar, R., et al. (2001) "Detailed characterization of morphology and dimensions of diesel particulates via thermophoretic sampling". SAE Technical Paper.

Levine, M.D. and Gresham, C. (2009) Toxicity, hydrocarbons. Emergency Medicine.

Li, H., Lea-Langton, A., Andrews, G.E., et al. (2008) "Comparison of exhaust emissions and particulate size distribution for diesel, biodiesel and cooking oil from a heavy duty DI diesel engine". SAE Technical Paper.

Liang, F., Lu, M., Keener, T.C., et al. (2005) The organic composition of diesel particulate matter, diesel fuel and engine oil of a non-road diesel generator. Journal of Environmental Monitoring, 7: (10): 983-988.

Liang, F., Lu, M., Keener, T.C., et al. (2005) The organic composition of diesel particulate matter, diesel fuel and engine oil of a non-road diesel generator. Journal of Environmental Monitoring, 7: (10): 983-988.

Lilik, G.K. and Boehman, A.L. (2011) Advanced diesel combustion of a high cetane number fuel with low hydrocarbon and carbon monoxide emissions. Energy & Fuels, 25: (4): 1444-1456.

Liu, Z.G., Berg, D.R., Vasys, V.N., et al. (2010) Analysis of C 1, C 2, and C 10 through C 33 particle-phase and semi-volatile organic compound emissions from heavy-duty diesel engines. Atmospheric Environment, 44: (8): 1108-1115.

Lu, T., Huang, Z., Cheung, C.S., et al. (2012) Size distribution of EC, OC and particle-phase PAHs emissions from a diesel engine fueled with three fuels. Science of the Total Environment, 438: 33-41.

Lu, X., Han, D. and Huang, Z. (2011) Fuel design and management for the control of advanced compression-ignition combustion modes. Progress in Energy and Combustion Science, 37: (6): 741-783.

Majewski, W.A. and Khair, M.K. (2006) Diesel emissions and their control. Society of Automotive Engineers.

Manente, V., Johansson, B. and Tunestal, P. (2009) "Partially premixed combustion at high load using gasoline and ethanol, a comparison with diesel". SAE Technical Paper.

Matar, S. and Hatch, L.F. (2001) Chemistry of petrochemical processes. Gulf Professional Publishing.

Merkisz, J. and Pielecha, J. (2015) Nanoparticle emissions from combustion engines. Springer.

Miet, K., Le Menach, K., Flaud, P.-M., et al. (2009) Heterogeneous reactivity of pyrene and 1-nitropyrene with NO 2: kinetics, product yields and mechanism. Atmospheric Environment, 43: (4): 837-843.

Miller, J.A. and Melius, C.F. (1992) Kinetic and thermodynamic issues in the formation of aromatic compounds in flames of aliphatic fuels. Combustion and flame, 91: (1): 21-39.

Najt, P.M. and Foster, D.E. (1983) "Compression-ignited homogeneous charge combustion". SAE Technical paper.

Noehre, C., Andersson, M., Johansson, B., et al. (2006) "Characterization of partially premixed combustion". SAE Technical Paper.

Onishi, S., Jo, S.H., Shoda, K., et al. (1979) "Active thermo-atmosphere combustion (ATAC)-a new combustion process for internal combustion engines". SAE Technical paper.

Outlook, A.E. (2007) with Projections to 2030. US Energy Information Administration.

Pagán, J. (2000) National air toxics program the integrated urban strategy, report to Congress. DIANE Publishing.

Parks, J.E., Prikhodko, V., Storey, J.M., et al. (2010) Emissions from premixed charge compression ignition (PCCI) combustion and affect on emission control devices. Catalysis Today, 151: (3): 278-284.

Payri, F., Benajes, J., Novella, R., et al. (2011) Effect of intake oxygen concentration on particle size distribution measurements from diesel low temperature combustion. SAE International Journal of Engines, 4: (2011-01-1355): 1888-1902.

Payri, R., García, A., Domenech, V., et al. (2012) An experimental study of gasoline effects on injection rate, momentum flux and spray characteristics using a common rail diesel injection system. Fuel, 97: 390-399.

Penney, D.G. (1996) Carbon monoxide. CRC Press.

Perez, J., Hills, F., Schuetzle, D., et al. (1980) "Informational report on the measurement and characterization of diesel exhaust emissions". Coordinating Research Council, Inc., Atlanta, GA (USA).

Perlingieri, I.S. Chemtrails: The Consequences of Toxic Metals and Chemical Aerosols on Human Health–Part I.

Peterson, J.S. and Cairns, C. (2003) "Toxicity, nitrous dioxide".

Pfefferle, L.D., Bermudez, G. and Boyle, J. (1994) "Benzene and higher hydrocarbon formation during allene pyrolysis". Soot Formation in Combustion. Springer 25-49.

Pinson, J.A., Ni, T. and Litzinger, T.A. (1994) "Quantitative imaging study of the effects of intake air temperature on soot evolution in an optically-accessible DI diesel engine". SAE Technical Paper.

Pi-Innovov generic diesel strategies user guide, http://pi-innovo.com/downloads/, 2013

Pope III, C.A. and Dockery, D.W. (2006) Health effects of fine particulate air pollution: lines that connect. Journal of the Air & Waste Management Association, 56: (6): 709-742.

Prikhodko, V.Y., Curran, S.J., Barone, T.L., et al. (2010) Emission characteristics of a diesel engine operating with in-cylinder gasoline and diesel fuel blending. SAE International Journal of Fuels and Lubricants, 3: (2010-01-2266): 946-955.

Prikhodko, V. Y., Curran, S. J., Barone, T. L., Lewis, S. A., Storey, J. M., Cho, K., ... & Parks, J. E. (2011, January). Diesel oxidation catalyst control of hydrocarbon aerosols from reactivity controlled compression ignition combustion. In ASME 2011 international mechanical engineering congress and exposition (pp. 273-278). American Society of Mechanical Engineers

Pulkrabek, W. W. (2004). Engineering fundamentals of the internal combustion engine (Vol. 249). New Jersey: Pearson Prentice Hall.

Ra, Y., Loeper, P., Andrie, M., et al. (2012) Gasoline DICI engine operation in the LTC regime using triple-pulse injection. SAE International Journal of Engines, 5: (2012-01-1131): 1109-1132.

Ra, Y., Loeper, P., Reitz, R.D., et al. (2011) Study of high speed gasoline direct injection compression ignition (GDICI) engine operation in the LTC regime. SAE International Journal of Engines, 4: (2011-01-1182): 1412-1430.

Raatz, T. and Mueller, E. (2001) "Examination of particle size distribution of homogeneous and conventional diesel combustion". SAE Technical Paper.

Ramadhas, A.S. (2016) Alternative fuels for transportation. CRC Press.

Ravindra, K., Sokhi, R. and Van Grieken, R. (2008) Atmospheric polycyclic aromatic hydrocarbons: source attribution, emission factors and regulation. Atmospheric Environment, 42: (13): 2895-2921.

Rezaei, S.Z., Zhang, F., Xu, H., et al. (2013) Investigation of two-stage split-injection strategies for a Dieseline fuelled PPCI engine. Fuel, 107: 299-308.

Rhead, M. and Hardy, S. (2003) The sources of polycyclic aromatic compounds in diesel engine emissions☆. Fuel, 82: (4): 385-393.

Richter, H. and Howard, J.B. (2000) Formation of polycyclic aromatic hydrocarbons and their growth to soot—a review of chemical reaction pathways. Progress in Energy and Combustion Science, 26: (4): 565-608.

Riddle, S.G., Jakober, C.A., Robert, M.A., et al. (2007) Large PAHs detected in fine particulate matter emitted from light-duty gasoline vehicles. Atmospheric Environment, 41: (38): 8658-8668.

Ris, C. (2007) US EPA health assessment for diesel engine exhaust: a review. Inhalation Toxicology, 19: (sup1): 229-239.

Rosenbaum, A.S., Axelrad, D.A., Woodruff, T.J., et al. (1999) National estimates of outdoor air toxics concentrations. Journal of the Air & Waste Management Association, 49: (10): 1138-1152.

Seong, H., Lee, K.O., Choi, S., et al. (2012) "Characterization of particulate morphology, nanostructures, and sizes in low-temperature combustion with biofuels". SAE Technical Paper.

Schauer, J.J., Kleeman, M.J., Cass, G.R., et al. (1999) Measurement of emissions from air pollution sources. 2. C1 through C30 organic compounds from medium duty diesel trucks. Environmental Science & Technology, 33: (10): 1578-1587.

Schauer, J.J., Kleeman, M.J., Cass, G.R., et al. (2002) Measurement of emissions from air pollution sources. 4. C1-C27 organic compounds from cooking with seed oils. Environmental Science & Technology, 36: (4): 567-575.

Seinfeld, J. and Pandis, S. (1986) Atmospheric chemistry and air pollution. Wiley Intersci. Publ., New York.

Sellnau, M., Sinnamon, J., Hoyer, K., et al. (2011) Gasoline direct injection compression ignition (GDCI)-diesel-like efficiency with low CO2 emissions. SAE International Journal of Engines, 4: (2011-01-1386): 2010-2022.

Sellnau, M.C., Sinnamon, J., Hoyer, K., et al. (2012) Full-Time Gasoline Direct-Injection Compression Ignition (GDCI) for High Efficiency and Low NOx and PM. SAE International Journal of Engines, 5: (2012-01-0384): 300-314.

Sher, E. (1998) Environmental aspects of air pollution. Handbook of Air Pollution from Internal Combustion Engines, Academic Press Inc, London, 27-41.

Sher, E. (1998) Handbook of air pollution from internal combustion engines: pollutant formation and control. Academic Press.

Shi, Y. and Reitz, R.D. (2010) Optimization of a heavy-duty compression–ignition engine fueled with diesel and gasoline-like fuels. Fuel, 89: (11): 3416-3430.

Singh, S., Reitz, R.D., Musculus, M.P., et al. (2007) Simultaneous optical diagnostic imaging of low-temperature, double-injection combustion in a heavy-duty DI diesel engine. Combustion Science and Technology, 179: (11): 2381-2414.

Smith, O.I. (1981) Fundamentals of soot formation in flames with application to diesel engine particulate emissions. Progress in Energy and Combustion Science, 7: (4): 275-291.

Soloiu, V., Duggan, M., Ochieng, H., et al. (2013) Investigation of Low Temperature Combustion Regimes of Biodiesel With n-Butanol Injected in the Intake Manifold of a Compression Ignition Engine. Journal of Energy Resources Technology, 135: (4): 041101.

Sunset Laboratory operational manual, http://www.sunlab.com/

Tree, D.R. and Foster, D.E. (1994) "Optical measurements of soot particle size, number density, and temperature in a direct injection diesel engine as a function of speed and load". SAE Technical Paper.

Tree, D.R. and Svensson, K.I. (2007) Soot processes in compression ignition engines. Progress in Energy and Combustion Science, 33: (3): 272-309.

Ullman, T.L. (1989) "Investigation of the effects of fuel composition on heavy-duty diesel engine emissions". SAE Technical Paper.

UKESSAYS (2003), https://www.ukessays.com/essays/biology/dioxin-and-dioxin-like-compounds-biology-essay.php?&session-id=c4f7bc2d1db049e7bcaa94b9318b1fd1

Valentino, G., Corcione, F.E., Iannuzzi, S.E., et al. (2012) Experimental study on performance and emissions of a high speed diesel engine fuelled with n-butanol diesel blends under premixed low temperature combustion. Fuel, 92: (1): 295-307.

Vander Wal, R.L., Ticich, T.M. and Stephens, A.B. (1999) Can soot primary particle size be determined using laser-induced incandescence? Combustion and flame, 116: (1): 291-296.

Vegburner, (http://vegburner.co.uk/DIcombustion.html).

Wang, H. and Frenklach, M. (1997) A detailed kinetic modeling study of aromatics formation in laminar premixed acetylene and ethylene flames. Combustion and flame, 110: (1): 173-221.

Wayne, E. (2007). Innovative approaches to improving engine efficiency. In Diesel Engine-Efficiency and Emissions Research (DEER) Conference. Detroit: is. n (p. r3).

Zelenyuk, A., Reitz, P., Stewart, M., et al. (2014) Detailed characterization of particulates emitted by pre-commercial single-cylinder gasoline compression ignition engine. Combustion and flame, 161: (8): 2151-2164.

Zhang, F., Xu, H., Rezaei, S.Z., et al. (2012) "Combustion and emission characteristics of a PPCI engine fuelled with dieseline". SAE Technical Paper.

Zhang, X., Tennison, P., Yi, J., et al. (2013) "Design Optimization of an Emissions Sample Probe Using a 3D Computational Fluid Dynamics Tool". SAE Technical Paper.

Zhang, J. (2011) Particle matter emission control and related issues for Diesel engines. University of Birmingham.

Zielinska, B. (2005) Atmospheric transformation of diesel emissions. Experimental and Toxicologic Pathology, 57: 31-42.

Yazicioglua, A. G., Megaridis, C. M., Campbell, A., Lee,K.-O., and Choi, M. Y.,(2001)"Measurement of Fractal Propertiesof Soot Agglomerates in Laminar Coflow Diffusion FlamesUsing Thermophoretic Sampling in Conjunction withTransmission Electron Microscopy and Image Processing,"*Combust. Sci. and Tech.*, Vol. 171, pp. 71-87.